



Faculty of Maritime Studies  
University of Rijeka, Croatia



Royal Institute of Navigation  
Science Technology Practice



The University of  
Nottingham



# 6<sup>th</sup> GNSS Vulnerabilities and Solutions Conference

## PROCEEDINGS

Baška, Krk Island, Croatia  
21 – 24 May 2012



Faculty of Maritime Studies  
University of Rijeka, Croatia



Royal Institute of Navigation  
Science Technology Practice



The University of  
Nottingham

# 6<sup>th</sup> GNSS Vulnerabilities and Solutions Conference

## PROCEEDINGS

Baška, Krk Island, Croatia  
21 – 24 May 2012

**Published by:**

University of Rijeka, Faculty of Maritime Studies Rijeka, Rijeka, Croatia

The Royal Institute of Navigation, London, UK

The Nottingham Geospatial Institute, University of Nottingham, UK

**For the Publisher:**

Full Professor Serdjo Kos, Ph. D., FRIN, Faculty of Maritime Studies Rijeka

**Publishing Associates:**

Colin Beatty, President, The Royal Institute of Navigation

Capt. Peter Chapman-Andrews, LVO MBE RN, Director, The Royal Institute of Navigation

Full Professor Terry Moore, Ph. D., FRIN, The Nottingham Geospatial Institute

**Editor-in-Chief:**

Full Professor Serdjo Kos, Ph. D., FRIN, Faculty of Maritime Studies Rijeka

Associate Professor Renato Filjar, Ph. D., FRIN, Faculty of Maritime Studies, Rijeka

**Associate Editor:**

Full Professor Axel Luttenberger, Ph. D., Faculty of Maritime Studies Rijeka

**Executive Editor:**

Marija Šimić Hlača B. Sc., Faculty of Maritime Studies Rijeka

**Front-page photo credits:**

Michael Felux, Ph. D. Candidate

**Text Formatting:**

Tempora, Rijeka

**Print:**

AKD, Zagreb

**Address:**

Faculty of Maritime Studies Rijeka

Studentska 2

51000 Rijeka

Croatia

Tel: ++3895 (0)51 338411

Fax: ++385 (0)51 336755

URL: <http://www.pfri.uniri.hr/>

E-mail: [dekanat@pfri.hr](mailto:dekanat@pfri.hr)

CIP zapis dostupan u računalnom katalogu Sveučilišne knjižnice Rijeka

pod brojem 130128021

ISBN 978-953-165-109-7

## CONTENTS

|  |     |
|--|-----|
| David Brčić, Renato Filjar, Serdjo Kos .....   | 7   |
| IONOSPHERIC MONITORING BY CORRELATION BETWEEN<br>GPS POSITIONING PERFORMANCE AND SID MONITOR                         |     |
| David Brčić, Serdjo Kos, Renato Filjar .....   | 23  |
| A CASE OF DEGRADED GPS PERFORMANCE DURING A<br>SHORT-TERM IONOSPHERIC DISTURBANCE IN NORTHERN<br>ADRIATIC            |     |
| Ljiljana R. Cander.....  | 37  |
| TOTAL ELECTRON CONTENT MODELLING FOR SPACE<br>WEATHER APPLICATIONS   |     |
| Marija Cokrljic, K. Wezka, R. Galas, N. Jakowski .....   | 53  |
| IONOSPHERIC SCINTILLATION MONITORING IN A SINGLE<br>STATION MODE   |     |
| Renato Filjar, Serdjo Kos, Tomislav Kos.....   | 63  |
| A THEORETICAL FRAMEWORK FOR UNDERSTANDING<br>RELATIONSHIP BETWEEN SPACE WEATHER INDICES AND<br>GPS IONOSPHERIC DELAY |     |
| Renato Filjar, Axel Luttenberger, Serdjo Kos .....   | 77  |
| A PROPOSAL FOR A GNSS FAILURE LEGAL LIABILITIES<br>SCHEME  |     |
| Peter Kieft .....  | 89  |
| SCINTILLATION ASSESSMENT TOOLS<br><i>Tools to assess the influence of scintillation on positioning quality</i>       |     |
| Martina Kunštović, Krešimir Malarić, Dragan Roša .....   | 103 |
| INFLUENCE OF SUDDEN IONOSPHERE DISTURBANCES ON<br>VLF COMMUNICATIONS   |     |
| Pavel Najman, Tomislav Kos, Norbert Jakowski .....   | 115 |
| COMPARISON OF TEC MODELS   |     |
| S. Priyadarshi, A.W. Wernik .....  | 127 |
| VARIATION IN THE IONOSPHERIC SCINTILLATION INDEX<br>WITH ELEVATION ANGLE   |     |

|   |     |
|---|-----|
| Jyri Rajamäki, Jouni Viitanen .....   | 135 |
| LAW ENFORCEMENT AUTHORITIES' SPECIAL REQUIREMENTS<br>FOR GNSS                                     |     |
| Tomislav Ratajec, Renato Filjar, Hrvoje Gold, Zoran Vrhovski.....                                 | 149 |
| EFFECTS OF GNSS PERFORMANCE DETERIORATION ON<br>PRECISION AGRICULTURE                             |     |
| Melania Susi, M. Andreotti, M. Aquino, A. Dodson .....  | 159 |
| IONOSPHERIC SCINTILLATION EFFECTS ON THE TRACKING<br>LOOP OF A GPS SOFTWARE RECEIVER              |     |
| Josip Vuković, Tomislav Kos, Pavel Najman .....   | 171 |
| GPS RECEIVER POSITIONING PERFORMANCE  |     |
| Jingnong Weng, Jun Lu, Dongkai Yang, Min Zhang.....   | 179 |
| PROGRESS OF BEIDOU NAVIGATION SATELLITE SYSTEM<br>AND GNSS EDUCATION                              |     |
| Liubov Yankiv-Vitkovska, Oksana Grynshyna-Poliuga .....   | 191 |
| MODELLING OF THE DYNAMIC CHANGES OF COORDINATES<br>GPS-STATION TO PREDICT THE IONOSPHERIC EFFECTS |     |



Faculty of Maritime Studies  
University of Rijeka, Croatia



Royal Institute of Navigation  
Science Technology Practice



The University of  
Nottingham

**6<sup>th</sup> GNSS**  
Vulnerabilities  
and Solutions  
Conference

**PROCEEDINGS**





Faculty of Maritime Studies  
University of Rijeka, Croatia



Royal Institute of Navigation  
Science Technology Practice



The University of  
Nottingham

**6<sup>th</sup> GNSS**  
Vulnerabilities  
and Solutions  
Conference

# IONOSPHERIC MONITORING BY CORRELATION BETWEEN GPS POSITIONING PERFORMANCE AND SID MONITOR OBSERVABLES

**David Brčić, Renato Filjar, Serdjo Kos**

Faculty of Maritime Studies, University of Rijeka, Croatia  
Studentska ulica 2, 51000 Rijeka, Croatia  
E-mail: brcic@pfri.hr

**ABSTRACT.** *Understanding the ionospheric disturbances is the key factor in mitigation of the space weather-induced effects on GNSS (Global Navigation Satellite System) positioning performance. This can be reversed in favour of the GPS (Global Positioning System) receiver to become an ionospheric condition sensor. In addition, the Sudden Ionospheric Disturbances (SID) monitor, a low-cost sensor of lower ionosphere activity recently introduced to scientific community by Stanford University group, offers a good perspective for continuous monitoring of the ionospheric activity, especially in its lower layers.*

*Here we present a concept of the local ionospheric monitoring through correlation between the time series of SID monitor observables and the GPS positioning errors. Assuming the ionospheric disturbances have the key impact on GPS positioning performance, and with reducing the impact of the other sources of GPS positioning errors, the concept offers a prospect for fast identification of the approaching, sudden ionospheric disturbances. Timely identification of these disturbances allows for forecasting of possible disruptions and degradations of GPS positioning service in local area, as well as potential effects on the other technological, social and economic systems. Proposed concept is to be validated through the analysis of continuously collected observables at GNSS laboratory, Faculty of Maritime Studies, University of Rijeka, Croatia.*

**KEY WORDS:** *ionospheric monitoring, GPS positioning error, SID monitors, navigational GNSS space weather laboratory*



changes are mostly manifested as nuisances, leading to deterioration of satellite positioning performance. Figure 1 shows common navigation system frequencies and their relation to the ionosphere.

During increased solar activity, the ionospheric layers may become additionally ionised, affecting the propagation of radio signals. The strength of VLF radio signals will experience raise in signal level, as the ionosphere becomes thicker and more energy-charged. The length of VLF waves, along with the low operating frequency improves the propagation at increased distances, bouncing off the ionospheric layers and the ground.

As the ionisation process reaches the Earth shortly after appropriate solar event – the energy and charged particles expelled from the Sun, travelling at the speed of light – VLF system signal strength changes can be considered as (fast) identification of approaching Sudden Ionospheric Disturbances. Involved operating frequencies are describing the state of the lower layers of the ionosphere. Figure 2 shows the behavior of VLF radio waves with regards to the ionisation process.

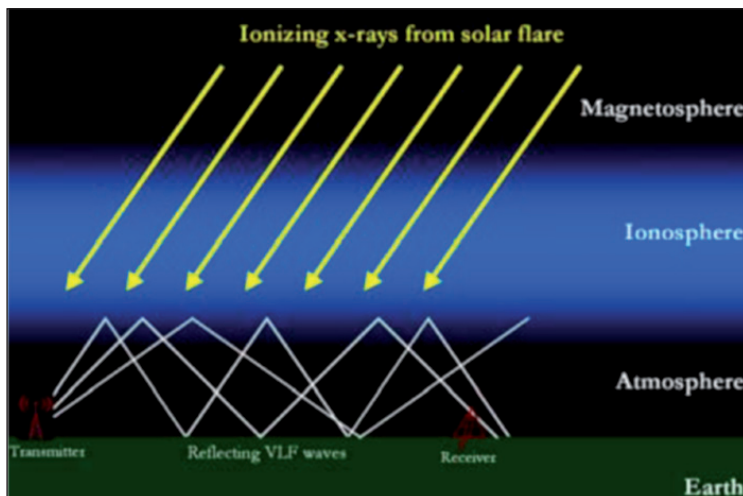


**Figure 2**  
Reflection of the VLF radio waves due to ionising x-rays. Retrieved from the (SuperSID Manual, 2009)

The mentioned processes affect the GNSS signals more inconveniently, given that the signal propagates through the ionosphere reaching the receivers on Earth. The signal reflects from free electrons and ions in the ionospheric layers, which are decelerating the signals and causing delays (Goodman, 2005). Ionospheric delay presents a major single cause of GNSS positioning error. This is explained by the interaction of the emitted signal with the Total Electron Content (TEC) along the propagation path. TEC is defined as the amount of free

electrons encountered along an equivalent column having a cross section of one square meter from the satellite to the receiver (Kintner and Ledvina, 2004, Klobuchar, 1988):

$$\text{TEC} = \int_{\text{receiver}}^{\text{satellite}} N(h)dh \quad (1)$$

where:  $N(h)$ ... vertical distribution of the free electron density over the height  $h$  above the surface of the Earth

The equation (2) describes direct relation between GPS ionospheric delay and the number of free electrons (Kintner and Ledvina, 2004, Klobuchar, 1988):

$$\Delta t = \frac{40.3}{c \cdot f^2} \text{TEC} \quad (2)$$

where:  $\Delta t$ ... GPS ionospheric delay

$f$ ... frequency of radio signal

Increased ionisation of the Earth's ionosphere can be viewed as a potential cause of GPS positioning performance degradation. By monitoring the behavior of the VLF radio waves during sudden solar disturbances, a correlation could be made with the behavior of GPS/UHF<sup>1</sup> signals during the same events with their origin in the activity of the Sun.

### 3 NAVIGATIONAL GNSS SPACE WEATHER LABORATORY

This chapter describes the current laboratory set-up involved in the Navigational GNSS Space Weather Laboratory (NGL) at the Faculty of Maritime Studies, University of Rijeka.

#### 3.1 Space Weather (SID) Monitors

The aim of Very Low Frequency, SID Monitors is to detect the changes in the Earth's ionosphere caused by solar flares and other disturbances (SuperSID Manual, 2009). Sudden Ionospheric Disturbances will manifest as the increase in received VLF signal strength. The VLF stations around the globe (SID

---

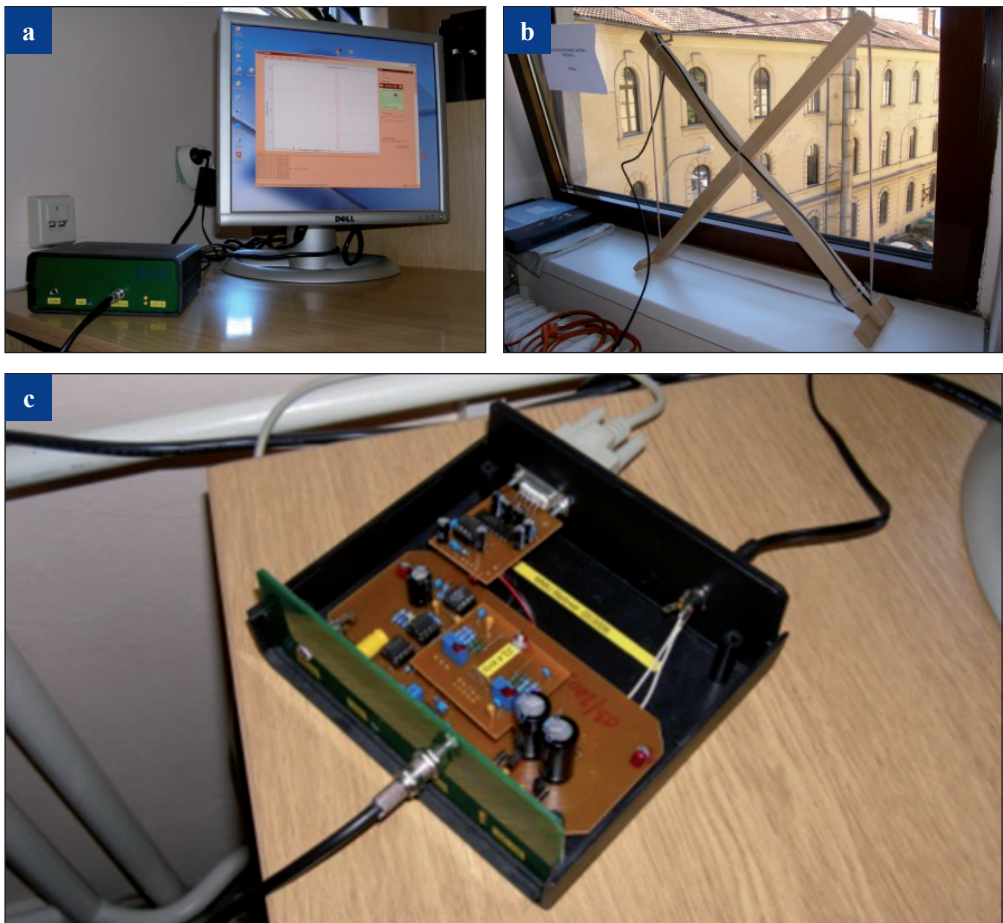
<sup>1</sup> Ultra High Frequency

Monitoring Station, 2010) transmitting the signals are used for the communication purposes with submarines, as well as for time signal provision. Communication messages are not a subject of this research, but the strength of the emitted signal. Currently, the Laboratory employs two generations of SID Monitors: the original SID Monitors, and SuperSID Monitors, enhanced, more powerful and upgraded instrument. The first, SID Monitor, is presented on Figure 3. It consists of a receiver tuned to specific frequency, the antenna and the computer. With appropriate software, the observations are stored as time series data of the received VLF signals.

With two SID devices, two stations are constantly monitored: Rhauderfehn (Germany), which operates/transmits at 23400 Hz frequency, and the Rosnay

**Figure 3**

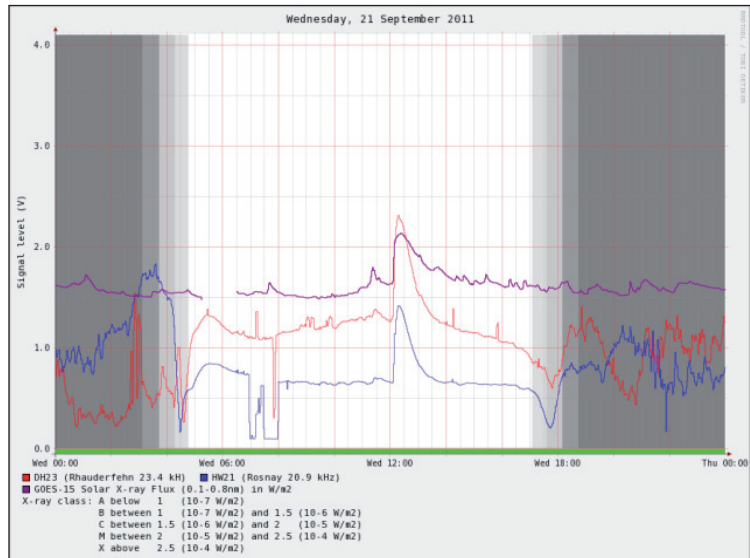
SID Monitor components: the receiver (a and c figure) and the antenna (b).



(France), transmitting at 20900 Hz frequency. Operating network of SID reference stations generates diagrams showing received VLF signal strength during the observed period, with the possible solar x-ray flux time series representation on the same diagram (Figure 4), as monitored by the GOES satellites (NOAA, 2012). In the case of sudden solar event (e.g. storm) and the relevant ionisation process in the layers, the VLF signal strength level will encounter the abrupt change, reaching higher values than usual. If the event takes place during the daytime, all of three curves (both VLF signals and x-ray flux) should follow the same path of the signal level.

**Figure 4**

Current SID monitoring (upper figure). Legend (lower figure): blue curve – Rosnay station (call sign: HWU), France, transmitting frequency 20900 Hz; red curve – Rhauderfehn station (call sign: DHO), Germany, transmitting frequency 23400 Hz; purple curve: Solar x-ray flux (0.1 – 0.8 nm passband), measured by the GOES satellite.



SuperSID monitors are working on somewhat different principle, although providing same information and operating at the same frequency spectrum, as well as receiving the signals from same VLF stations. Here, the receiver is actually a PC sound card, and the monitor is the preamplifier of the signal received with the antenna, identical as for the original SID Monitor (SuperSID Manual, 2009).

Monitor components are presented on Figure 5. The Laboratory employs four SuperSIDs with accompanying equipment. Four stations can be monitored, whose locations can be seen on the Fig 6. Monitors are designed to receive signals from two VLF stations already known to the reader (Rhauderfehn and Rosnay), as well as from Isola di Tavolara (Sardinia, Italy, call sign: ICV,

### Figure 5

Components of SuperSID Monitor:

The antenna (a), the preamplifier (b) and the receiver – PC High Definition Sound Card (c).

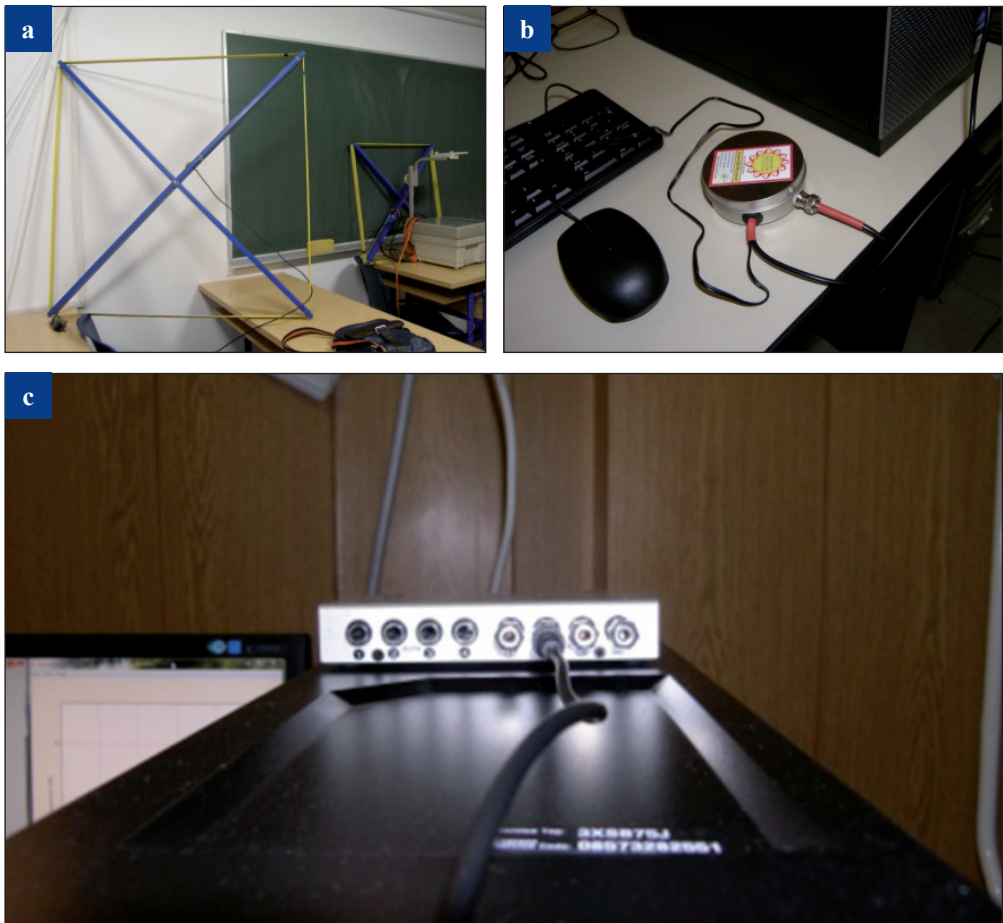
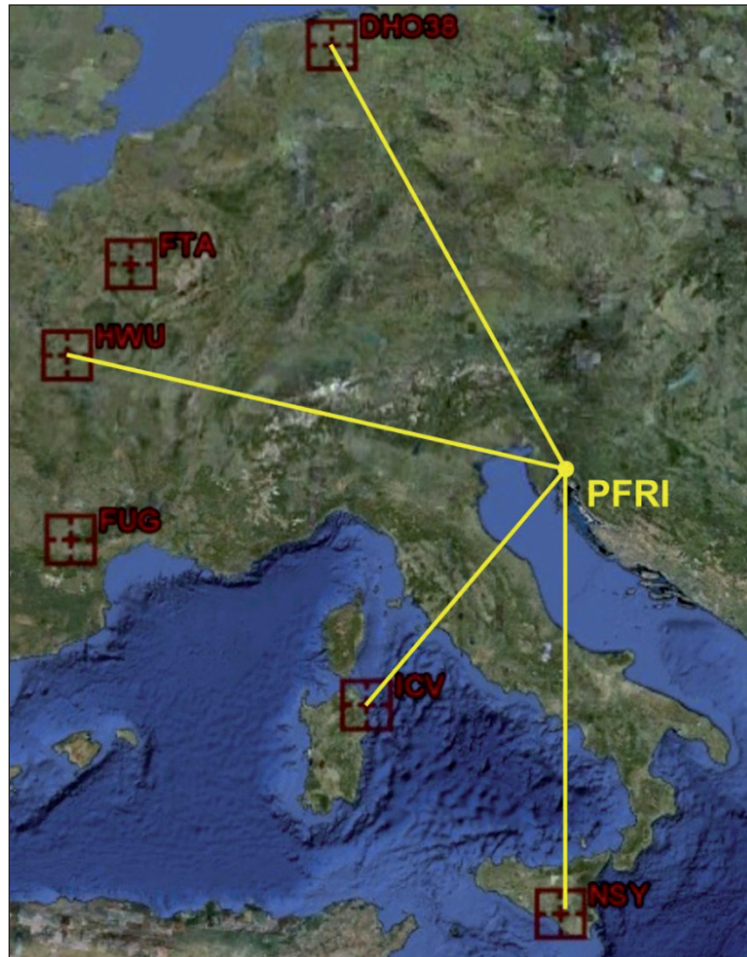


**Figure 6**  
 SuperSID Monitoring  
 Stations:  
 Rhauderfehn (DHO),  
 Rosnay (HWU), Isola  
 di Tavolara (ICV) and  
 Niscemi (NSY).



transmitting on 20270 Hz), and Niscemi (Sicily, Italy, call sign: NSY, transmitting on 45900 Hz). Using the above-mentioned methodology and laboratory equipment set-up, the western part of the horizon is completely covered and thus can be monitored for sudden events in the lower ionosphere.

These monitors are upgraded originals with additional features. Signal strength data are stored in the *comma separated values* (CSV) format, making data more suitable for the automated analysis. In addition, the daily plot format made with the SuperSID software is provided as a graphical representation of collected observables. The plots are showing time series of VLF signal strength from corresponding sites. Four signals – each from a different station – can be plotted on a single graph. Additionally, one graph can contain observables from several days and from all stations. During the day period, the monitor collects signal

strength data for each of the stations and it calculates the power spectrum density, displaying the spectrum on the main window (SuperSID Manual, 2009). Figure 7 presents main SuperSID and stored (daily plot) signal strength data.

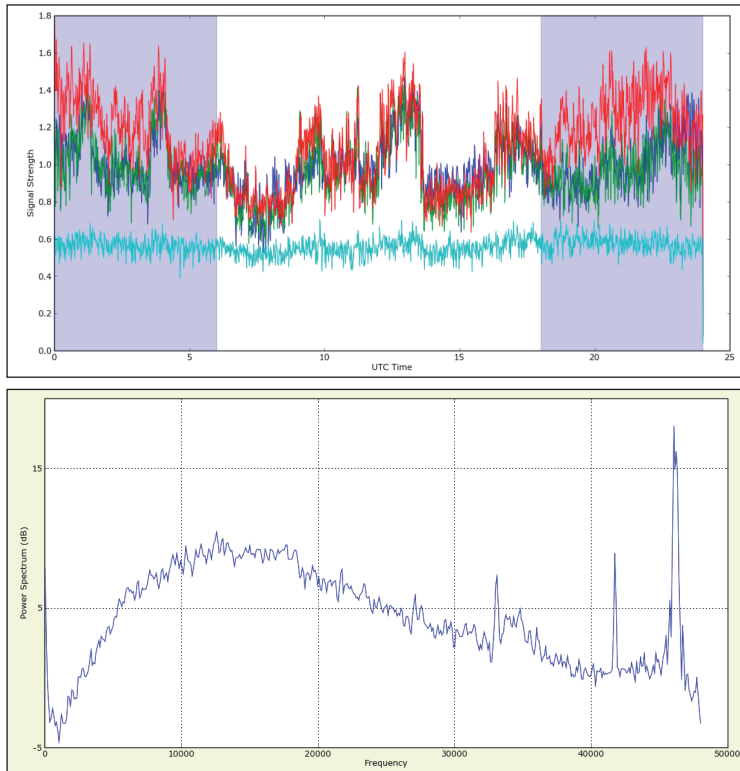


**Figure 7** Daily plot (upper figure) and power spectrum density real-time plot (lower figure) obtained with SuperSID Monitor. Each color on the upper figure represents daily signal strength from stations observed (red – DHO station, blue – HWU station, green – ICV station, cyan – NSY station), while the peaks on the lower graph represent the working frequencies of observed stations, or monitored stations, respectively.

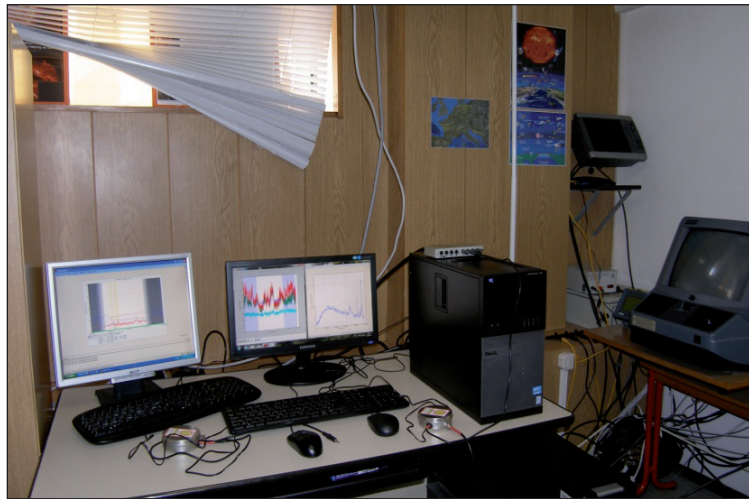
### 3.2 GPS receiver

Connected to the computer, a single-frequency GPS receiver (Garmin GPSMap 4010) records position estimates in real-time period and stores it on a hard disk taking advantage of the serial GPS-to-PC communication. The receiver's antenna is positioned on the roof of the faculty building, thus reducing the multipath effect and geometric dilution of precision. Data collection is conducted using the serial GPS-to-PC communication managed by VisualGPS© open source software. Apart from essential position estimation data (latitude, longitude and height above the sea level), the software collects the other relevant GNSS information (geometric dilution of precision – GDOP, number of visible satellites etc.) using the standardised NMEA<sup>2</sup> format. Besides the NMEA format, data are presented graphically, allowing real-time observations and recordings.

<sup>2</sup> NMEA stands for National Marine Electronics Association

In 2011, the position of the GPS antenna has been determined by the separate high-accuracy geodetic method, with horizontal positioning accuracy of  $\pm 0.01$  metre. The high-quality estimation of the GPS receiver's aerial allows for referring GPS position estimates to the referenced position, thus allowing for the analysis of the components of positioning error patterns. Figure 8 shows the GNSS Space Weather Laboratory in Rijeka.

**Figure 8**  
Snapshot of the  
Navigational GNSS  
Space Weather  
Laboratory inner part,  
Faculty of Maritime  
Studies in Rijeka,  
Croatia.



## 4 DISCUSSION

Continuous and significant observables of ionospheric dynamics can be taken, regarding described equipment. The UV (UltraViolet) and x-ray energy emitted from the Sun will react with atoms in the ionosphere, releasing the electrons and charging the ionospheric layers. The lower frequency/SID signals will respond abruptly on the energy erupted from the solar flare or other similar event, as a result of ionisation, increasing in signal strength. The wavelengths of observed VLF radio signals (with order of magnitude of 10 km) indicate the commotion and changes in lower ionospheric layers. The question is how, when, and in which extent those processes will affect high-frequency, satellite signals, which, in order to reach the ground receivers, have to penetrate through the same ionospheric layers. It is assumed that the ionospheric disturbances have the major impact on GPS positioning performance. By constant collection and analysis of observables both from the VLF and UHF part of the frequency spectrum, GPS positioning degradation forecasting models can be established.

The following figures are showing the observables of both GPS and VLF data in the late September 2011, when one of sudden solar events took place. Strong

solar flares that occurred on September 22nd and 24th have been observed and recorded with SID monitors. Solar activity caused geomagnetic storm on September 26th.

It is still early to state whether these, two day SID events have credit for the storm that followed or not. In other words, there is no valid evidence that the signal peaks predicted the upcoming event. However, the fact is that, with the solar flare that occurred on September 24th (Figure 9, lower plot), a Coronal Mass Ejection (CME) left the same active Sun region as the flare, reaching the

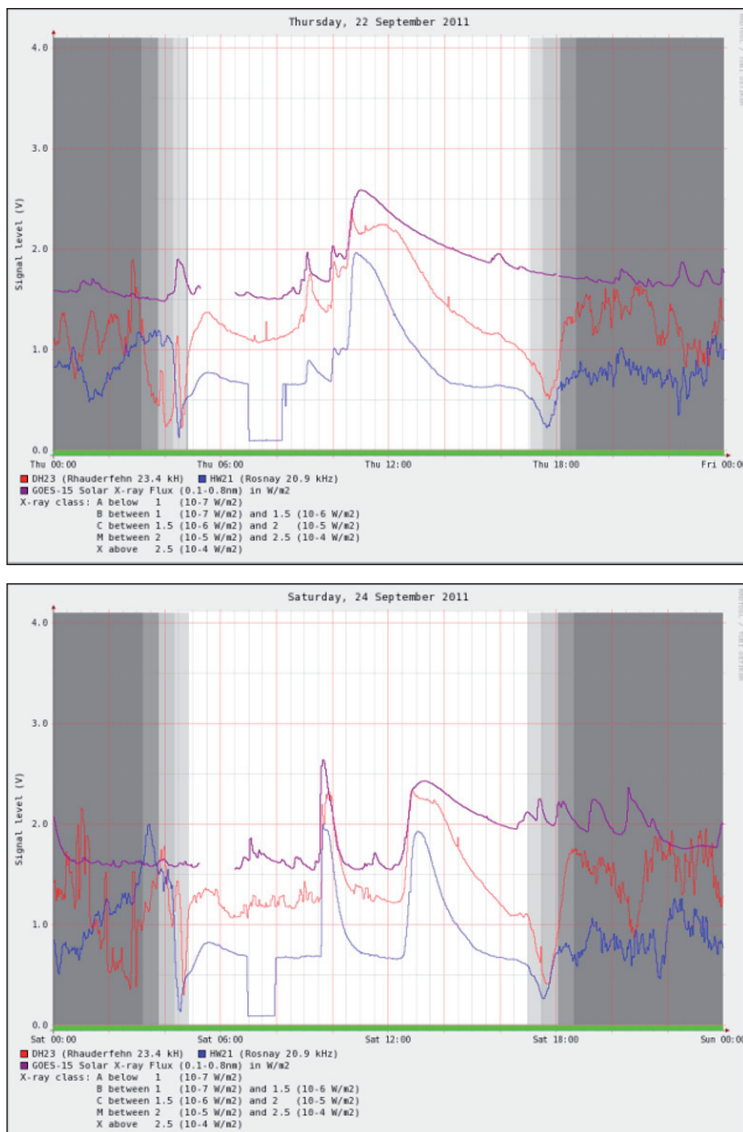
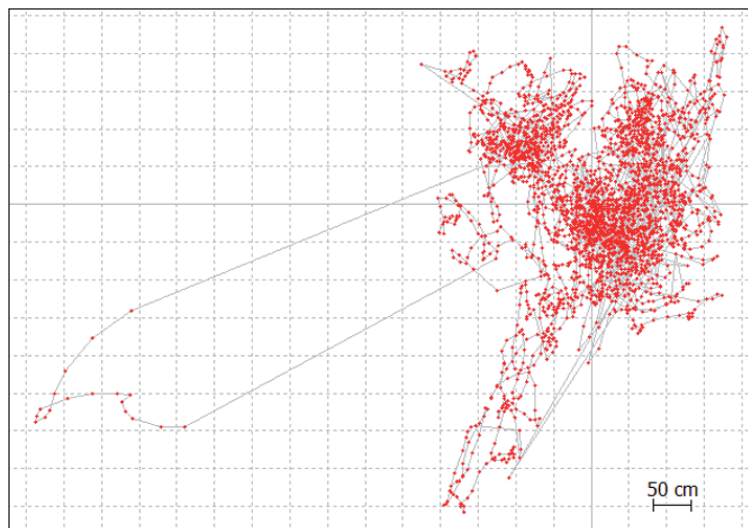
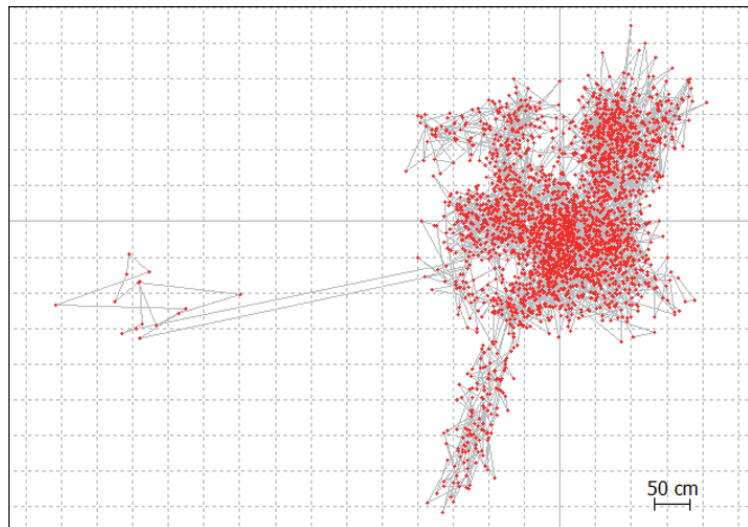


**Figure 9**  
Solar flares as observed with SID monitors on September 22<sup>nd</sup> (upper figure) and 24<sup>th</sup> (lower figure) 2011.

Earth on September 26th and causing geomagnetic disturbance classified as G3 severe storm (NOAA 2011, USGS 2011).

Solar flares and CMEs are closely related phenomena and are thought to be different manifestations of the same magnetic process (Harrison, 2006). However, they do not cause nor exclude one another. It has been found that CME association rate obviously increases with the flare's peak flux, fluence and duration (Yashiro and Gopalswamy, 2009). Therefore, as in the discussed case, the flares – SID monitor signal peaks can serve as good indicators of upcoming events with emphasis on satellite navigation system signals impact.

**Figure 10**  
GPS positioning performance on September 26<sup>th</sup> 2011, reference stations Dubrovnik, Croatia (upper) and Graz, Austria (lower). Made by the authors using ©RTKLIB software and (IGS data, 2011)



In order to present the GPS positioning performance on the day of the storm, four reference GNSS stations with their locations close to the Laboratory have been chosen. Data have been taken from the official International GNSS Service (IGS, 2011) webpage. The following figures are showing GPS positioning Ground Track horizontal pattern in the 24-hours period – of the respective day at reference stations Dubrovnik (Croatia), Graz (Austria), Osijek (Croatia) and Padova (Italia).

It can be seen that, two days after last solar flare observed, solar activity resulted in geomagnetic storm which further affected the GPS positioning. Along with

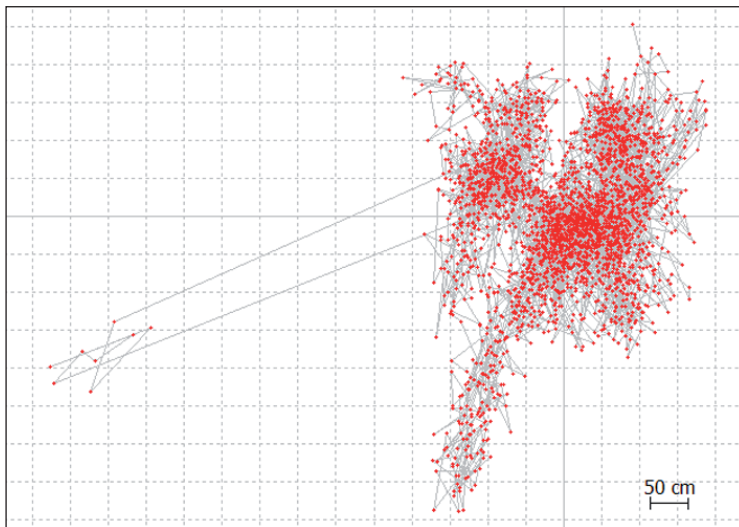
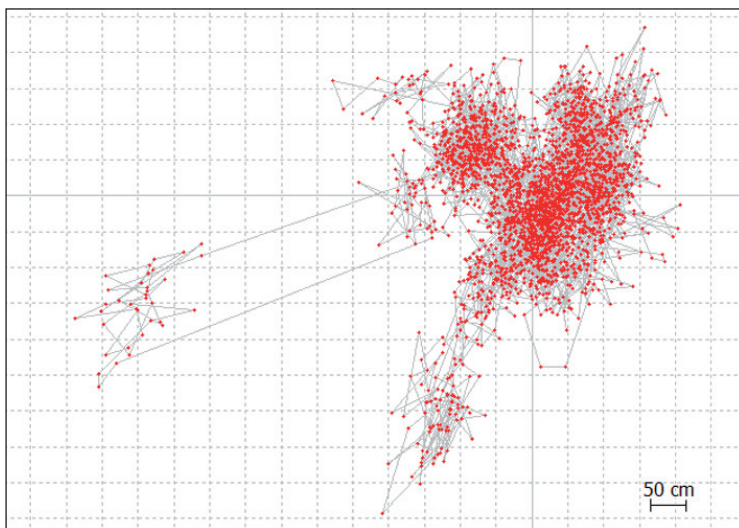


**Figure 11**  
GPS positioning performance on September 26th 2011, reference stations Osijek, Croatia (upper) and Padova, Italia (lower). Made by the authors using ©RTKLIB software and (IGS data, 2011)



flare/energy, matter in the form of CME erupted and, in certain time after the energy reached the Earth, causing geomagnetic disturbances. However, the impact on Earth caused by the solar activity can be manifested in two other ways, that are Solar Radiation Storms and Radio Blackouts, which to a greater or lesser extent affect the GNSS signal (NOAA, 2011). Here, SID observables as indices can be used again, especially in radio blackout conditions. But that remains the subject of further research.

## 5 CONCLUSION AND FURTHER WORK

The paper presented the research procedure in the Navigational GNSS Space Weather Laboratory at the Faculty of Maritime Studies in Rijeka, Croatia. The laboratory equipment has been described, as well as the research methodology. It has been shown that the sudden ionospheric disturbances can be observed promptly by low frequency radio systems, given that the energy emitted from the Sun reaches the Earth in the period of app. 8 minutes. The signal levels from VLF transmitting stations will raise with the level of ionisation. Manifestation of SIDs can take different forms, affecting variety of technological systems on Earth. As for satellite navigation systems, the produced activity can lead to degradation of GNSS positioning, as presented in the final part of the paper. The aim and the further work of the Laboratory is to facilitate and perform continuous monitoring and analysis of ionospheric disturbances in order to investigate the correlation between these disturbances and degradation of the GNSS performance. Moreover, it is planned to introduce additional radio systems (operating both on low and high frequencies), thus additionally complementing the observed image. The proposed concept can provide an insight in diurnal, seasonal, solar cycle and storm time ionospheric dynamics which are prevailing. Bringing the observables into correlation, that are measured SID data (time series of VLF signal strength with emphasis on sudden signal strength changes – which represents disturbed lower ionospheric layers) and measured GPS data (with emphasis on local GPS position deviation in all axis – time series data), the ionospheric patterns for this, local area can be described, especially the impact on satellite positioning navigation systems, depending of nature, intensity and the strength of particular solar event.

## ACKNOWLEDGMENTS

Research activities presented in this paper were conducted under the research projects “Research into the correlation of maritime-transport elements in marine traffic” and “Environment for Satellite Positioning” supported by the Ministry of Science, Education and Sports, Republic of Croatia. Authors admire development of the RTKLIB open-source program package for GNSS positioning. The authors appreciate and support the work and the

provision of SuperSID Monitors, donated by the Stanford Solar Center (Mrs. Deborah Scherrer) and Society of Amateur Radio Astronomers (Mr. William and Mrs. Melinda Lord).

## REFERENCES

- [1] Goodman, J.M. (2005). *Space Weather & Telecommunications*. Springer Science+Business Media, Inc. New York, USA.
- [2] Harrison, R. (2006). *Bursting the solar bubble: The flare-coronal mass ejection relationship*. Geophysical Monograph Series (165).
- [3] IGS (2011). *International GNSS Service, GPS pseudorange observables in RINEX format*, available at: <http://igsceb.jpl.nasa.gov/>
- [4] Kunches, J. (1995). *Space Environment Topics: Navigation*. National Oceanic and Atmospheric Administration (NOAA), Space Environment Laboratory. Boulder, Colorado, USA. Available at: <http://sec.noaa.gov>
- [5] Kintner, P.M. and Ledvina, B.M. (2004). *The Ionosphere, Radio Navigation and Global Navigation Satellite Systems. Proc. of the 7<sup>th</sup> Latin-American Conference on Geophysics*, Sao Jose dos Campos, Brasil.
- [6] Klobuchar, J.A. (1988). *Ionospheric Corrections for Timing Applications*. Ionospheric Physics Division, Air Force Geophysics Laboratory. Hanscom AFB, Maryland, USA.
- [7] Love, J.J. and Gannon, J.L. (2011). *Magnetic Storm 26 September 2011*. USGS Geomagnetism program. Available at: <http://geomag.usgs.gov/storms/>
- [8] NOAA Space Weather Prediction Center (2012). *GOES Solar x-ray flux*. Boulder, Colorado, USA. Available at: [http://www.swpc.noaa.gov/rt\\_plots/xray\\_5m.html](http://www.swpc.noaa.gov/rt_plots/xray_5m.html)
- [9] NOAA Space Weather Prediction Center (2012). *Space Weather Scales*. Boulder, Colorado, USA. Available at: <http://www.swpc.noaa.gov/NOAAAscales/>
- [10] SID Monitoring Station (2010). *VLF Stations List*. Available at: <http://sidstation.loudet.org/stations-list-en.xhtml>
- [11] SuperSID Manual (2009). Stanford Solar Center, Stanford University. Stanford, USA. Available at: [http://solar-center.stanford.edu/SID/Distribution/SuperSID/supersid\\_v1\\_1/Doc/SuperSIDManual\\_v1.pdf](http://solar-center.stanford.edu/SID/Distribution/SuperSID/supersid_v1_1/Doc/SuperSIDManual_v1.pdf)
- [12] Yashiro, S. & Gopalswamy, N. (2009). *Statistical relationship between solar flares and coronal mass ejections. Proc. of the 2008 IAU Symposium on Universal Heliophysical Processes No. 257*, Ionina, Greece.





Faculty of Maritime Studies  
University of Rijeka, Croatia



Royal Institute of Navigation  
Science Technology Practice



The University of  
Nottingham

**6<sup>th</sup> GNSS**  
Vulnerabilities  
and Solutions  
Conference

# A CASE OF DEGRADED GPS PERFORMANCE DURING A SHORT-TERM IONOSPHERIC DISTURBANCE IN NORTHERN ADRIATIC

**David Brčić, Serdjo Kos, Renato Filjar**

Faculty of Maritime Studies, University of Rijeka, Rijeka, Croatia  
Studentska ulica 2, 51000 Rijeka, Croatia  
E-mail: brcic@pfri.hr

**ABSTRACT.** *Ionospheric disturbances are the proven cause of degradation of the GNSS performance. Resulting from the space weather processes, ionospheric disturbances modify the vertical ionospheric profile, thus changing the Total Electron Content (TEC) encountered by satellites' rays on their way towards the GNSS receiver. Here we report a case of the short-lived ionospheric disturbance, detected by SID monitor located at the GNSS laboratory, Faculty of Maritime Studies in Rijeka, Croatia, and the effects it causes to the GPS positioning performance, as observed by the single-frequency maritime GPS receiver situated at the same venue. Observed correlation between GPS and SID monitor observables points to perspective of establishing a model for the ionospheric disturbances identification, which is to be examined further in the mid-term research.*

**KEY WORDS:** *ionospheric disturbances, geomagnetic storm, GPS positioning error*

## 1 INTRODUCTION

The paper presents results and analysis of observations at the Navigational GNSS Laboratory during solar event which took place in first half of March 2012 (days 63 – 74 in 2012). The observations were obtained by employing the Laboratory equipment, that are Sudden Ionospheric Disturbance (SID) monitors, and a single frequency GPS receiver. The following text gives an insight to the state of the ionospheric lower layers during the event/s, as well as the performance of satellite positioning throughout the occurrence. Dynamics of satellite positioning performance are shown, pointing out the correlation in both systems signal response to the mentioned activity, with all effects that followed. Using different frequencies of radio propagation, the image of solar activity event through observed period was reconstructed.

## 2 BACKGROUND

Beside their primary purpose, GNSS receivers can also act as space weather sensors, displaying the state of the ionospheric vertical profile by displaying their own performance. Ionospheric disturbances will affect the satellite's signals by means of a prolonged propagation time, causing positioning errors in a greater or lesser extent. This occurrences are explained by the increased amount of charged particles in ionospheric layers, emerging as a result of solar events, that is the energy ejected from the Sun. At the same time, lower-frequency signals (i.e. VLF) will respond promptly to mentioned disturbances in a form of increased signal strength, given that these signals propagation characteristics depend exactly of ionized layers. The ionosphere represents a sort of natural waveguide for certain parts of the frequency spectrum signals. Long, VLF waves (their sky component, precisely) are traveling through the ionosphere which refracts the signals enabling their propagation over great distances. On the sunlit side of the Earth, additional ionospheric layers are generated, the ionosphere descends in height and it becomes more solid.

During an solar event, the energy (e.g. x-rays), traveling at the speed of light, reaches the Earth's atmosphere first. The layers become additionally ionized, proportionally with the solar energy absorbed. In case of VLF waves, the changes in signal propagation will manifest as a changes in the lower layers of the ionosphere. By the ionisation of lower ionosphere, the signal strength raises immediately after energy absorption. In this way, receivers operating on VLF part of the spectrum can be employed as detectors of the lower ionosphere dynamics.

Opposite to long waves, the GNSS signals will experience nuisances across the propagation path, given that the amount of charged particles increases and interferes with the satellite signal, causing signal's delay. Thus, the GNSS receiver will behave as a sensing system for the ionosphere, measuring the amount of the Total Electron Content (Kintner and Ledvina, 2004).

Mentioned devices are the equipment of the Navigational GNSS Laboratory (NGL); the GPS/GNSS receiver at fixed, differentially determined position and VLF SID space weather monitors. With these, long-wave, low-frequency monitors, signals from two transmitters are received and tracked, both app. 1000 km distant, mutually  $50^\circ$  apart. With the direct GOES (Geostationary Operational Environment Satellite) solar x-ray flux measurement added, daily observables gave a vivid picture of the solar activity, and the ionospheric response to it, respectively. In the following figure signals from both transmitting stations and GOES x-ray flux are presented, in a standard, daily plot.

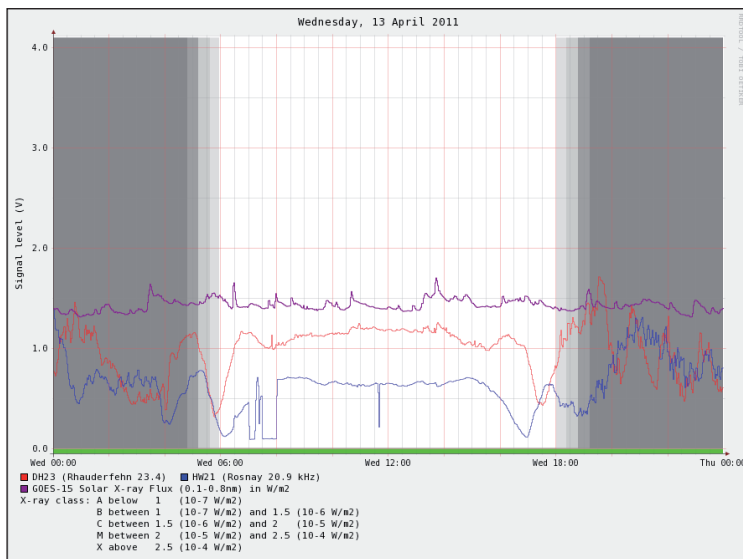


**Figure 1**

SID/GOES signal monitoring.

Legend: blue curve – Rosnay station (HWU), France, transmitting frequency 20900 Hz; red curve – Rhauderfehn station (DHO), Germany, transmitting frequency 23400 Hz; purple curve: Solar x-ray flux, measured by the GOES satellite.

The ejected matter from the Sun reaches the Earth after much longer period given that the speed of travelling particles from app. 300 to 1000 km/s. These particles affect the Earth's magnetosphere, producing disturbances in Earth's magnetic field and generating geomagnetic storms. Other disturbances generated from the Sun beside ionospheric disturbances are manifested as elevated levels of radiation due to the increasment of energetic particles. The duration of every such an event influences the strength and intensity of consenquential effects

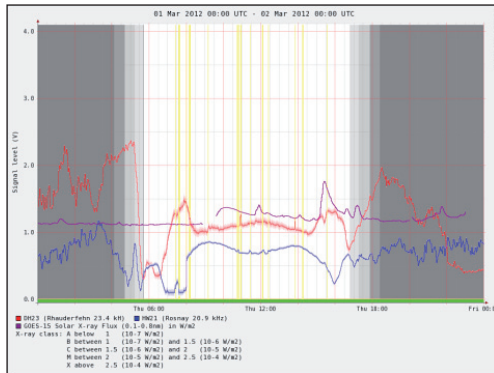
which take place on several systems (NOAA, 2012). Here, the emphasis is placed on the influence on satellite positioning performance during an event of increased and sudden solar activity through several days. This period has been studied in order to monitor the solar activity and, consequently, the performance of GPS positioning.

### 3 METHODOLOGY

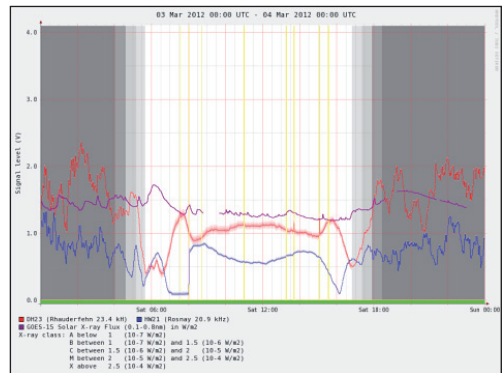
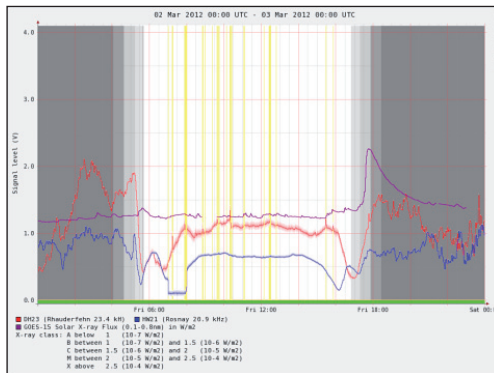
The GPS data have been observed via fixed single frequency GPS receiver with the antenna mounted at the highest point of the building of the Faculty of Maritime Studies, Rijeka. Free from obstacles, the position of the antenna ( $\varphi=45^{\circ}19'49.57105''N$ ;  $\lambda=014^{\circ}26'11.00265''E$ , 37.896 meters above the sea level) was differentially determined (Geodetic Institute, 2011). Data were subsequently collected, recorded and graphically displayed with ©VisualGPS open source software in standardised NMEA sentences format. Data post-processing were enabled with the usage of ©RTKLIB (Takasu, 2007) software. Geomagnetic environment indices were retrieved from the SWPC official website (NOAA, 2012). For the modelling and graphical presentation of dynamical satellite performance results the R Statistical software package has been used.

### 4 THE EVENT

According to observations, march 2012 started with relatively low solar activity, with solar x-ray flux not exceeding class C (NGL, 2012) and Kp geomagnetic activity index hardly exceeding the value of 3 (NOAA, 2012). With the appearance of large sunspot (Active Region 1429) on the Sun's eastern limb, the solar activity started to increase, raising the level of radiation, emitting M and X class solar flares and ejecting matter (CME). This intensified activity period lasted until the observed sunspot moved across the northwestern limb to the far side of the Sun, on March 15<sup>th</sup>.

**Figure 2**

SID plots of first three days in March, 2012 (days 61-62-63), as observed with SID monitors at the NGL.

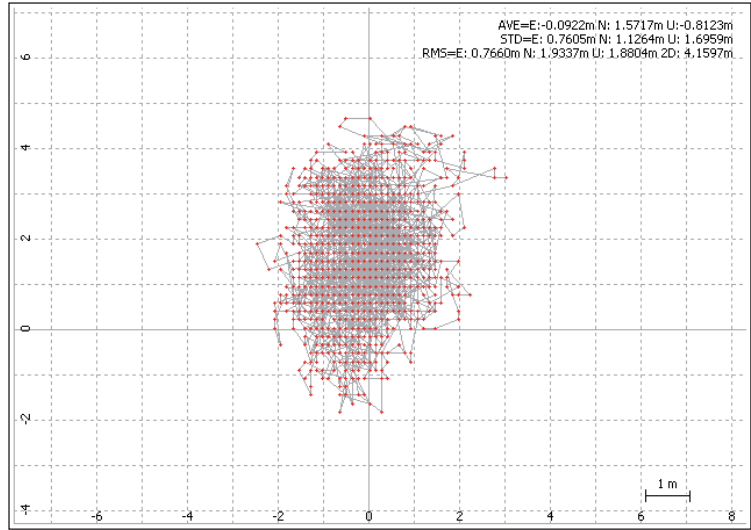


Increased activity has been recorded on each day of the observed period, producing amplifications in GOES x-ray flux measurements, as shown on Figures 2, 4, 6, 8 and 10. Additionally, when sudden solar energy bursts occurred during the daytime (Figure 4 – March 4th and March 6th, Figure 10 – March 14th and 15th), the signal strength increases from two VLF stations closely followed the direct x-ray measurements, indicating ionization of lower ionospheric layers.

Figures 3, 5, 7, 9 and 11 are showing the GPS positioning performance in the observed period. The plots represent the 24-hours GPS positioning pattern and position deviations in north-south and east-west directions. Height deviations are not shown in these plots, however the values of height error component are taken into consideration and elaborated in further chapters, along with other two directions/components.

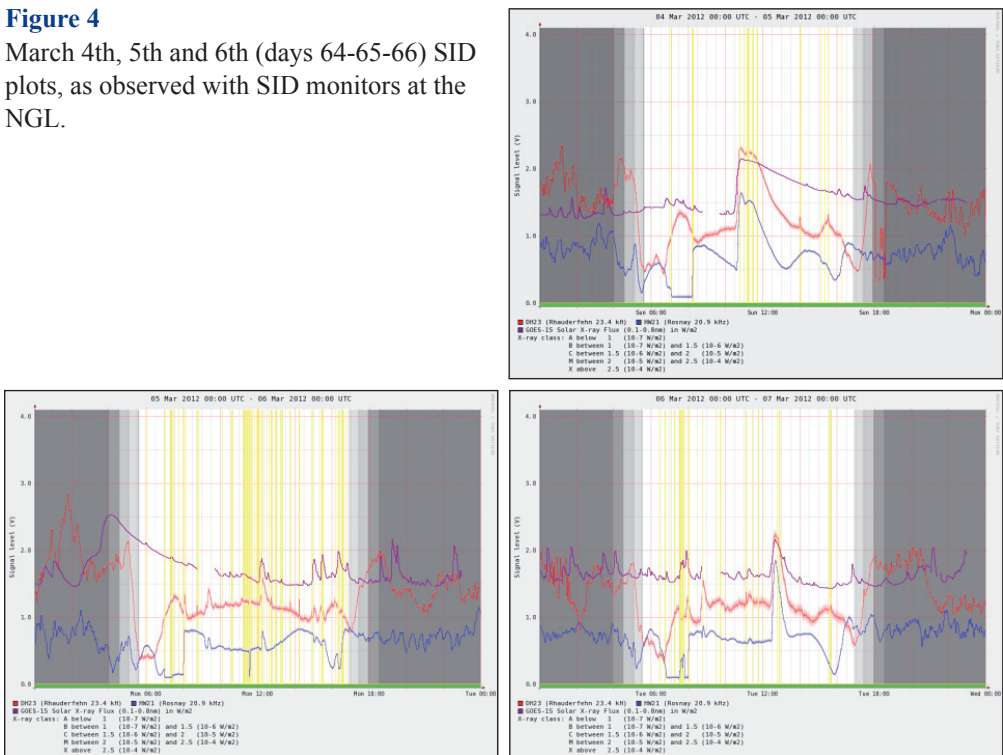
As the day 64 (March 4th) solar flare occurred, both VLF signals followed the x-rays with identical pattern, after which their strength returned to usual values. X-ray flux, however, returned at lower levels in milder way and in longer period

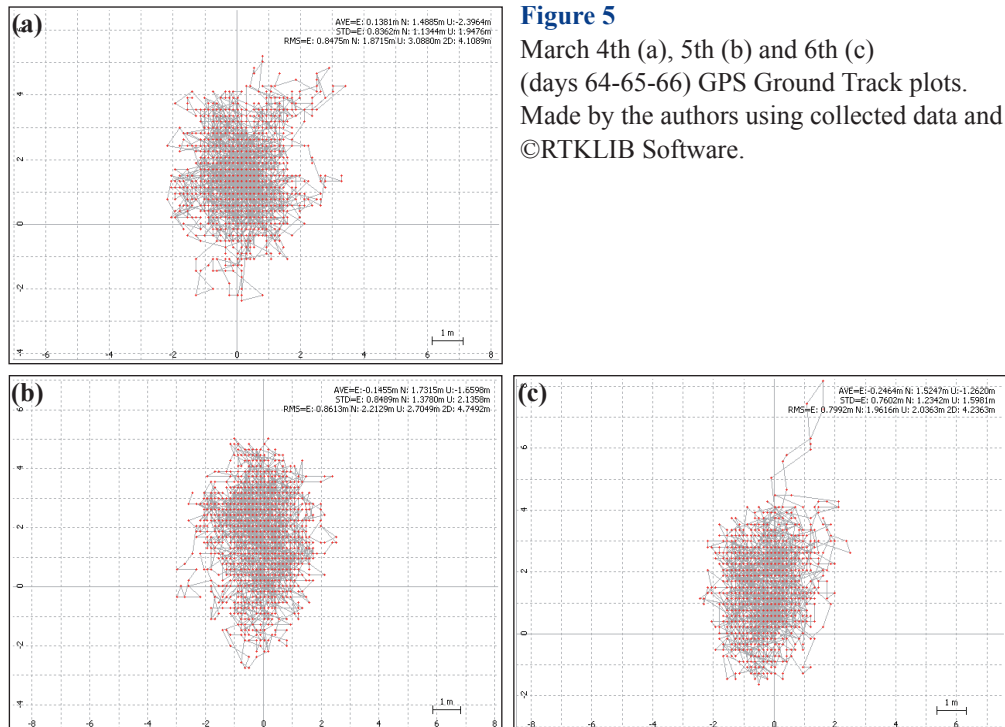
**Figure 3**  
GPS Ground Track plot, March 3rd (day 63).  
Made by the authors using collected data and ©RTKLIB Software.



than the previous two. At contrary, the March 6th flare generated sharper spike and more abrupt decline of all three signals, which all followed the same pattern (Figure 4).

**Figure 4**  
March 4th, 5th and 6th (days 64-65-66) SID plots, as observed with SID monitors at the NGL.





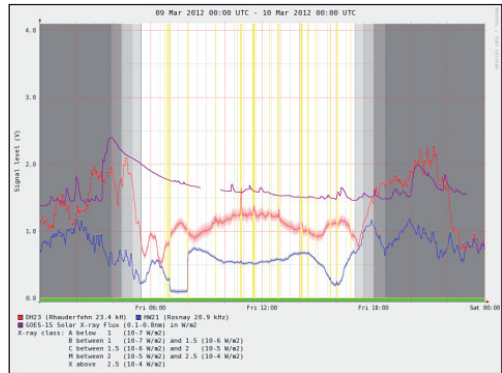
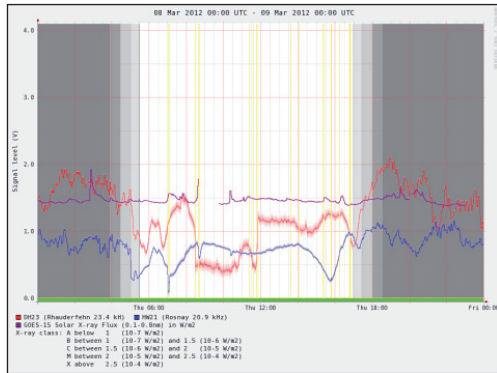
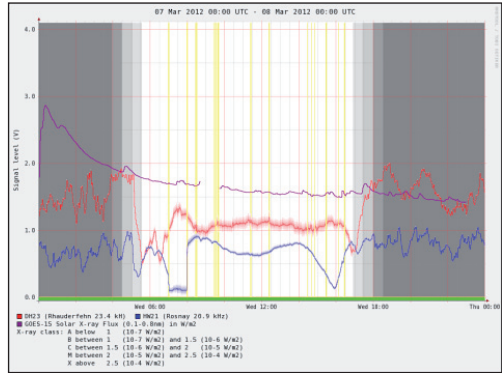
Gradually rising, the solar activity reached its peak on 7th day of march (day 67) in after-midnight hour, releasing the largest amount of energy in the observed period (Figure 6).

The solar activity events resulted in moderate to high geomagnetic storm on days 67, 68 and 69 (March 7th, 8th and 9th, 2012). The greatest daily GPS positioning degradation – north-south and east west direction position scattering was observed on day 69, as shown on Figure 7.

Geomagnetic storm subsided after its highest value ( $K_p=7$ ) on march 9th. The solar activity began to decline in general, but the flares continued to occur occasionally on days 70, 73, 74 and 75 and disturbing the geomagnetic field, bringing another, but less severe storm, as can be seen on corresponding figures.

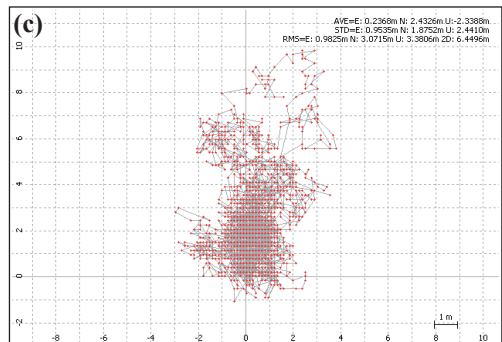
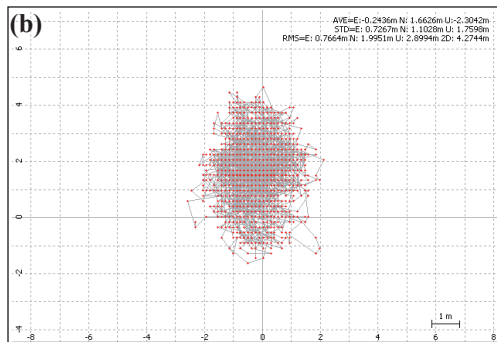
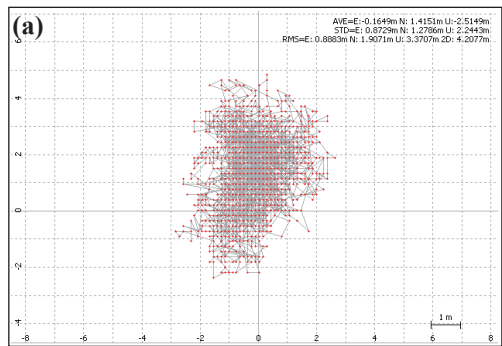
**Figure 6**

March 7th, 8th and 9th (days 67-68-69)  
SID plots, as observed with SID monitors  
at the NGL.



**Figure 7**

March 7th (a), 8th (b) and 9th (c)  
(days 67-68-69) GPS Ground Track plots.  
Made by the authors using collected data and  
©RTKLIB Software.



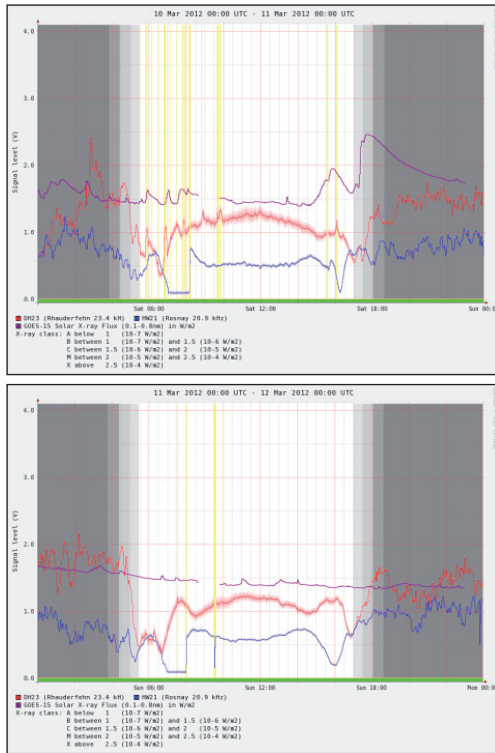


**Figure 8**  
 March 10th, 11th and 12th (days 70-71-72)  
 SID plots, as observed with SID monitors  
 at the NGL.

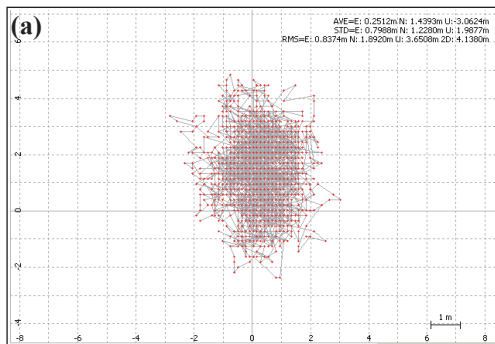
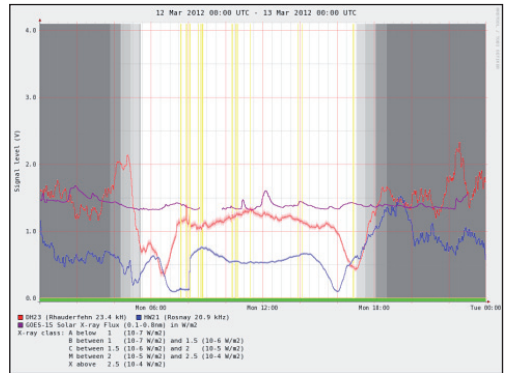


**Figure 9**  
 March 10th (a), 11th (b) and 12th (c)  
 (days 70-71-72) GPS Ground Track plots.  
 Made by the authors using collected data and  
 ©RTKLIB Software.

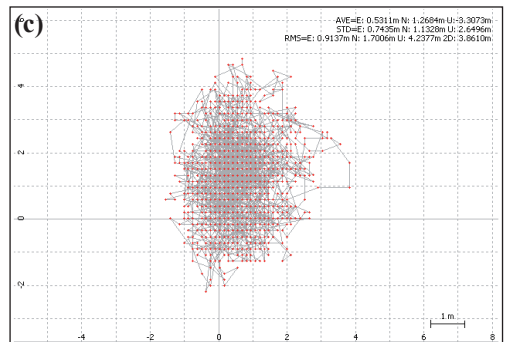
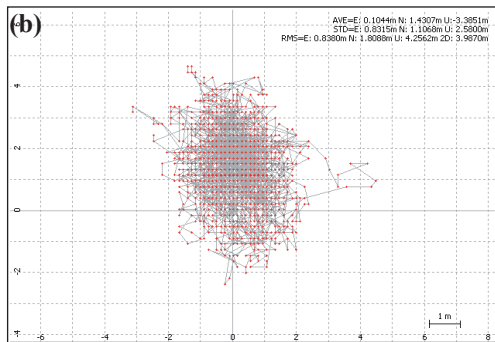


**Figure 10**

March 13th, 14th and 15th (days 73-74-75) SID plots, as observed with SID monitors at the NGL.

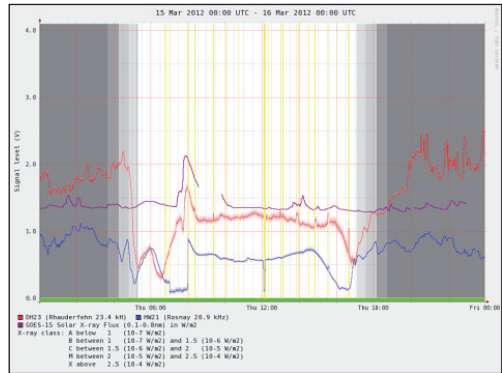
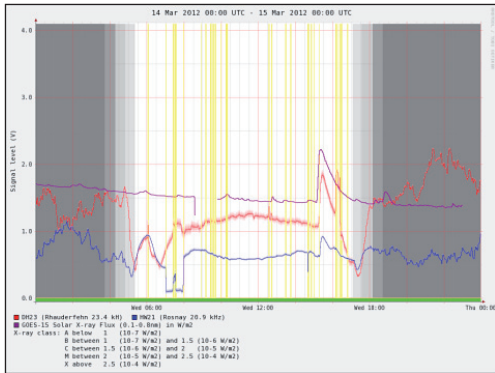
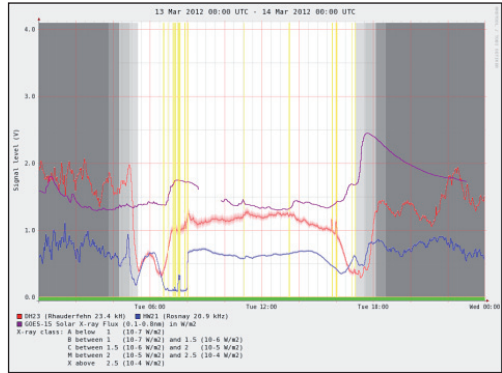
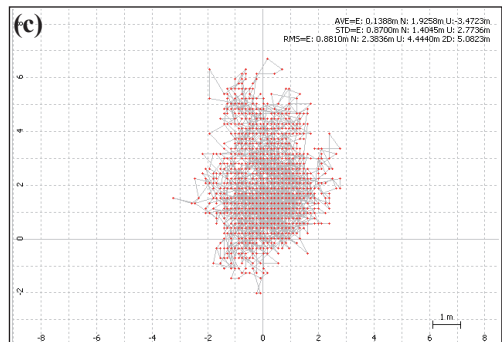
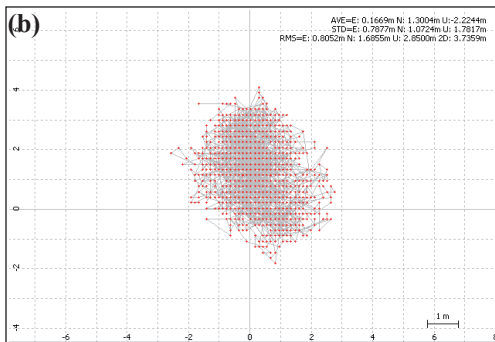
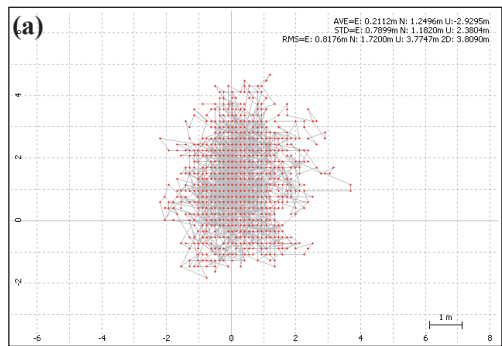


**Figure 11**

March 13th (a), 14th (b) and 15th (c) (days 73-74-75) GPS Ground Track plots. Made by the authors using collected data and ©RTKLIB Software.



## 5 DISCUSSION

The GPS positioning performance was statistically analysed, providing indices (average, standard deviation and root mean square error) for each day of the observed period, with regards to the northing, easting and height GPS positioning deviations. GPS performance analysis have shown the following results, which are graphically presented on figure 13. Figure 12 graphically presents the changes in geomagnetic activity through the observed period (march 03th-14th/days 63-74).

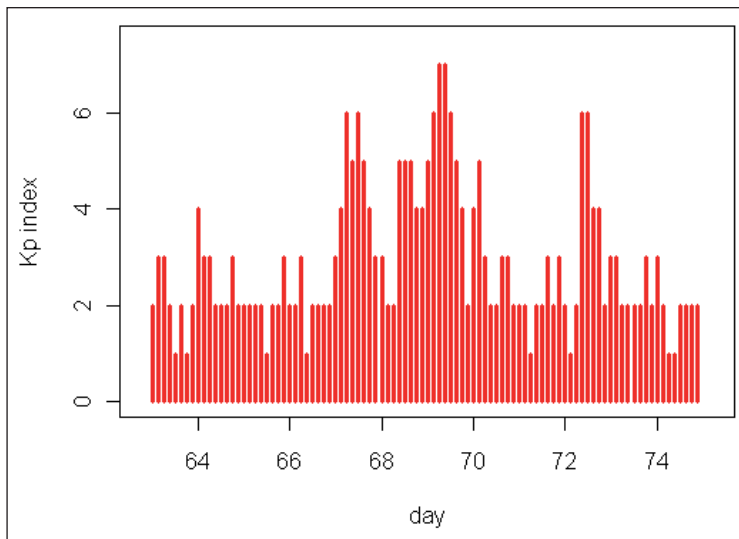


**Figure 12**

Kp index for days 63 to 74 (March 3th to 14th, 2012). Made by the authors using (NOAA/SWPC data, 2012) and R programmable environment.

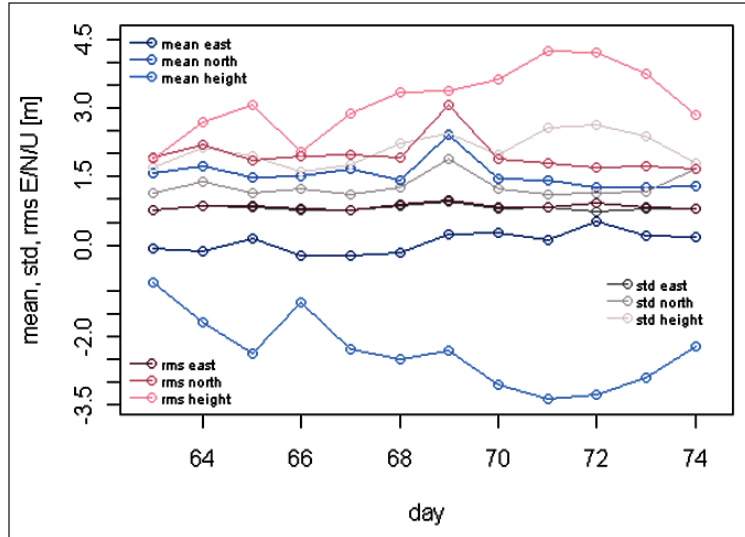
During the event, the significant impact on positional accuracy in the east-west direction was not observed, not even at the time of strongest disturbance on day 69. The easting root mean square error has not exceeded the value of 1 m.

The northing deviations were more pronounced. The lowest observed RMS value was 1.6855 meters, while the highest value exceeded 3 meters on the day of greatest geomagnetic disturbance.

The greatest impact on positional accuracy degradation was observed in the GPS positioning vertical component. Heighting deviations varied more than positions' northing and easting component through the entire observed period, as shown on Figure 13. Furthermore, after the geomagnetic disturbance on day 69, vertical root mean square error exceeded the value of 3.3806 meters, reaching the highest value of 4.2562 meters on day 71, and not decreasing until the end of the observed event. In other words, vertical error component retained the increased degradation trend for several days after the northing and easting component returned to their standard values.

**Figure 13**

Statistics of GPS positioning dynamics through the observed period. Made by the authors using R programmable environment.



## 6 CONCLUSION

The paper presented the ionospheric disturbance event and the GPS performance during the observed period of March 3rd – 14th in 2012. For each day of the event observables were taken; the low-frequency, long-wave signals and the higher frequency, GPS signal propagation characteristics. The GPS positioning accuracy was analysed during changes in geomagnetic activity and disturbances in the lower ionosphere. The most significant positioning error occurred on the day of greatest geomagnetic activity. It has been shown that, considering GPS positioning performance, the most pronounced effect was observed on the positioning error vertical component. Additionally, while the degradation of northing and easting positioning accuracy reached standard values within the one-day period after the impact, height positioning degradation remained high over the entire observed period.

## ACKNOWLEDGMENTS

Research activities presented in this paper were conducted under the research projects “Research into the correlation of maritime-transport elements in marine traffic” and “Environment for Satellite Positioning” supported by the Ministry of Science, Education and Sports, Republic of Croatia. Authors admire development of the open-source statistics and modeling R programmable environment (R Development Core Team, 2010), RTKLIB open-source program package for GNSS positioning, and VisualGPS open source software for GPS output monitoring.

---

## REFERENCES

- [1] Geodetic Institute (2011). Faculty of Maritime Studies: GPS antenna coordinate determination. Geodetic Study, Rijeka, Croatia.
- [2] Kintner, P.M. and Ledvina, B.M. (2004). *The Ionosphere, Radio Navigation and Global Navigation Satellite Systems. Proc. of the 7<sup>th</sup> Latin-American Conference on Geophysics*, Sao Jose dos Campos, Brasil.
- [3] National Oceanographic and Atmospheric Association: NOAA Space Weather Scales. Available at: <http://www.swpc.noaa.gov/NOAAAscales/>, accessed on 25.03.2012.
- [4] Navigational GNSS Laboratory (2012), Faculty of Maritime Studies, Space Weather Forecasting. Available at: <http://www.ionosphere.hr/arhiva/index.php>, accessed on 01.04.2012.
- [5] RTKLIB (2007). An open-source program package for GNSS Positioning, Copyright © 2007 – 2011 by T. Takasu.
- [6] National Oceanographic and Atmospheric Association: Space Weather Prediction Center. Available at: <http://www.swpc.noaa.gov/ftpmenu/warehouse.html>, accessed on 21.03.2012.
- [7] R Development Core Team (2011). R: A language and environment for statistical computing. R Foundation for Statistical Computing, Vienna, Austria. ISBN 3-900051-07-0.





Faculty of Maritime Studies  
University of Rijeka, Croatia



Royal Institute of Navigation  
Science Technology Practice



The University of  
Nottingham

**6<sup>th</sup> GNSS**

Vulnerabilities  
and Solutions  
Conference

# TOTAL ELECTRON CONTENT MODELLING FOR SPACE WEATHER APPLICATIONS

**Ljiljana R. Cander**

Rutherford Appleton Laboratory  
Chilton, OX11 0QX, UK  
E-mail: ljiljana.cander@stfc.ac.uk

**ABSTRACT.** *As modern society continues to develop a new sophisticated infrastructure, its dependence on the properties and behavior of the Sun-Earth system becomes more and more sensitive. The reliance on space-based technologies for communication, navigation and resource management as well as fast growing commercialization of space increase vulnerability to disruptions caused by space weather events requiring in depth knowledge of the whole solar-terrestrial environment. Understanding, prediction and potential mitigation of space weather impact on our technologically reliant society is by no means straightforward for several more or less known reasons. By presenting a method of the ionospheric vertical total electron content (VTEC) empirical modelling in relation to its simple application in long-term prediction; briefly reviewing the VTEC global, regional and local mapping procedures based on data from the International GNSS Service (IGS) network as the standard means of ionospheric real-time monitoring and now casting; and examining some of the most recent major space weather events, these and other challenges related to the total electron content modelling for space weather applications will be discussed.*

**KEY WORDS:** *TEC ionospheric modelling, space weather, GNSS, GPS*

## 1 INTRODUCTION

Although the main purpose of the Global Positioning System (GPS) was to provide accurate positional location at any point on or above the Earth's surface at all times, for defence and civilian purposes, GPS also had a major impact on ionospheric science during the last decade of the twentieth century. The existing Global Navigation Satellite Systems (GNSS), with unprecedented rates of temporal and spatial sampling on a global scale, could systematically provide values for the ionospheric total electron content (TEC) using dual-frequency code pseudorange and carrier phase data. These values have significantly contributed to efforts in empirical modelling and space weather event analysis, the generation of new accurate global, regional and local ionospheric maps of vertical total electron content (VTEC maps), and will serve for future improvements based on the needs of navigation and other service users (Jakowski, 1996; Kersley et al., 2004; Dow et al., 2009; Hernández-Pajares et al., 2011).

It is very important to emphasize that the study of solar–terrestrial physics is the only means to use measurements of solar-terrestrial environment to predict that environment at the user's defined locations for their technological systems at risk during extreme space weather events. Consequently solar–terrestrial physics is a crucial subject underpinning the study of space weather ultimately concerned with engineering problems – namely the effects on operational systems in their daily activities (Cander, 2008).

As the research community continues to make advances in solar-terrestrial physics and space weather prediction activities, this paper briefly describes: a method of the total electron content empirical modelling in relation to its simple application in ionospheric VTEC long-term prediction (Section 2); GNSS VTEC global, regional and local mapping based on data from the International GNSS Service (IGS) network as the standard means of ionospheric real-time monitoring and now casting (Section 3); some morphological features of ionospheric disturbances as seen by GNSS VTEC data during recent space weather events (Section 4). Section 5 discusses and summarizes the conclusions of the paper.

## 2 GNSS VTEC LONG-TERM PREDICTION

A climatology single location model for the monthly median VTEC, extremely important for the background ionosphere in data assimilation procedures, has been developed and tested during the high solar activity conditions at the high mid-latitude ground-based GPS station HERS (50.9 N, 0.3 E) and the low mid-latitude ground-based GPS station NICO (35.1 N, 33.4 E) in 2000 by using

simple empirical equations from Davies and Smith (2000) in a slightly modify form. In general, total electron content modelling involves a set of procedures to establish a mathematical representation of global TEC, together with its temporal variations. Vertical total electron content (VTEC) varies with the solar cycle, month to month, and day to day. The dominant feature is the approximately 11-year cycle in which sunspot numbers vary from around 0 at absolute solar minimum to around 200 at solar maximum.

According to Davies and Smith (2000) the daytime 12-month smoothed TEC,  $TEC_D(R_{12})$  varies approximately linearly with the smoothed sunspot number  $R_{12}$  according to the equation:

$$TEC_D(R_{12}) = TEC_D(0)[1 + 0.02 R_{12}] \quad (1)$$

The corresponding nighttime relationship is:

$$TEC_N(R_{12}) = TEC_N(0)[1 + 0.01 R_{12}] \quad (2)$$

where  $TEC_D(0)$  and  $TEC_N(0)$  are the day and night vertical total electron content in TEC unit ( $1 \text{ TECU} = 10^{16} \text{ electrons/m}^2$ ), respectively for sunspot number zero.

By using the simple empirical equations (1) and (2) in a slightly modify form, a climatological single location prediction model for monthly median vertical TEC is defined as follows:

$$VTEC_D(R_{12}) = VTEC_D(0)[1 + A_D R_{12}] \quad (3)$$

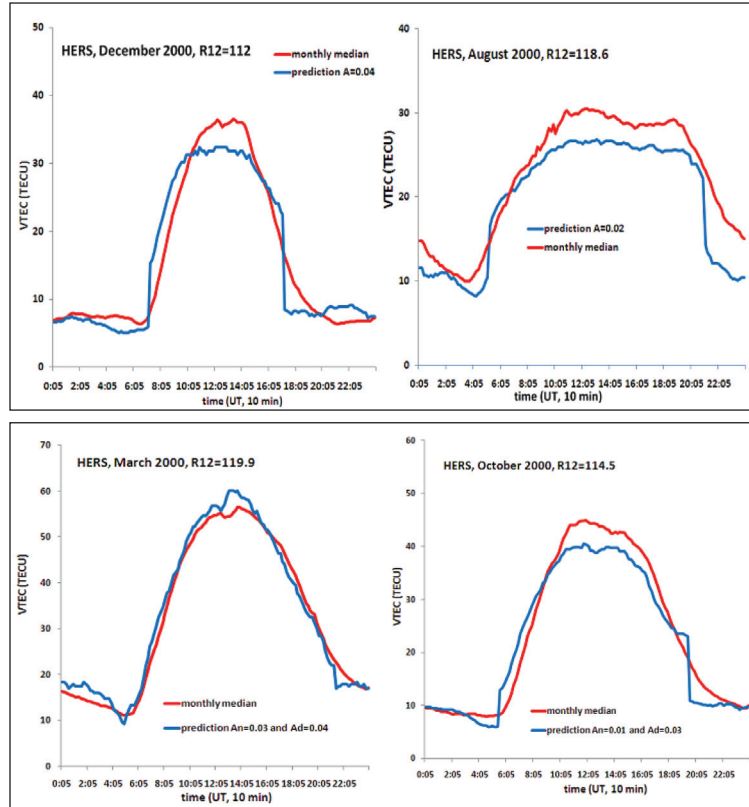
$$VTEC_N(R_{12}) = VTEC_N(0)[1 + A_N R_{12}] \quad (4)$$

where  $A_D$  and  $A_N$  are statistically based daytime and nighttime coefficients, respectively.  $A_D$  and  $A_N$  coefficients are computed from VTEC historical data separately at each ground-based GPS station under consideration.

Testing results during high solar activity conditions in 2000 when  $R_{12} > 100$  during four ionospheric seasons: winter (December), summer (August) and equinox (March and October) at HERS and NICO are shown in Figs. 1 and 2.

**Figure 1**

Comparisons of the observed VTEC monthly median at HERS in 2000 for December (top left), August (top right), March (bottom right), and October (bottom left) with the corresponding predictions.



The estimated  $A_D$  and  $A_N$  coefficient values and exact monthly  $R_{12}$  values are labelled in these figures. Even though the model values tended to under-estimate VTEC by a few TECU during daytime at HERS as seen in Fig. 1, the overall agreement between the observed and predicted monthly medians is very good. Fig. 2 shows that this agreement is particularly convincing for the NICO VTEC monthly median data. These results demonstrate that VTEC ionospheric models are now quite mature, which becomes even more obvious for other much more sophisticated models, like those described by Jakowski et al. (2011).

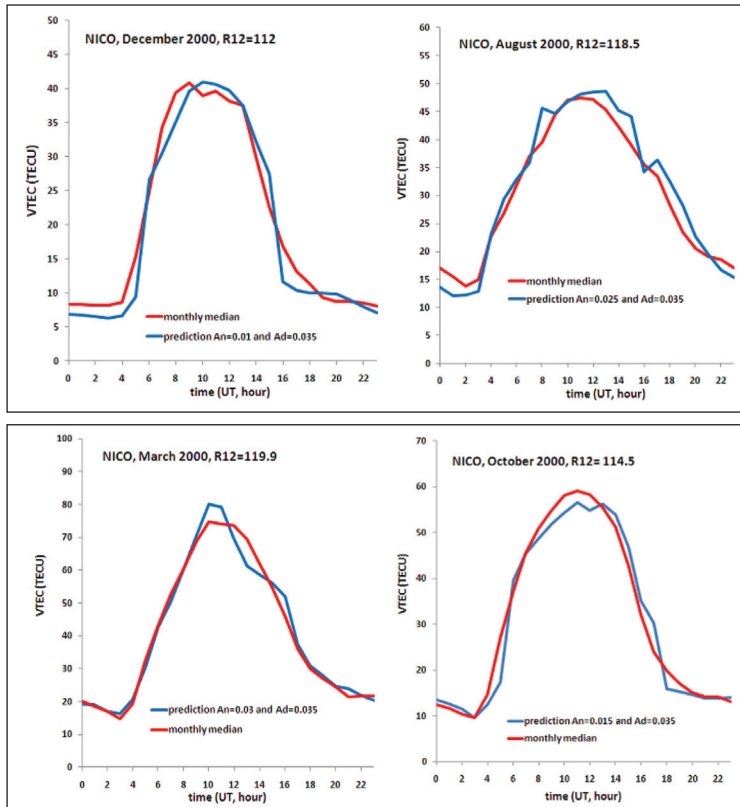


**Figure 2**  
Comparisons of the observed VTEC monthly median at NICO in 2000 for December (top left), August (top right), March (bottom right), and October (bottom left) with the corresponding predictions.

### 3 GNSS VTEC GLOBAL, REGIONAL AND LOCAL AREA MAPPING

The International GNSS Service (IGS), formerly the International GPS Service, is a voluntary federation of more than 200 agencies worldwide that pool resources and permanent GPS & GLONASS stations (Fig. 3) to provide the highest quality data and products, like the standard for Global Navigation Satellite Systems (GNSS) in support of Earth science research, multidisciplinary applications, and education. Consequently the IGS VTEC maps have been generated without interruption since 1998 and have been widely disseminated throughout the research community. In general, a number of global mapping methods currently in use are based on the processing and analysis centre's specific requirements and objectives.

The IGS VTEC maps are generated in the following steps (Hernández-Pajares et al., 2009):



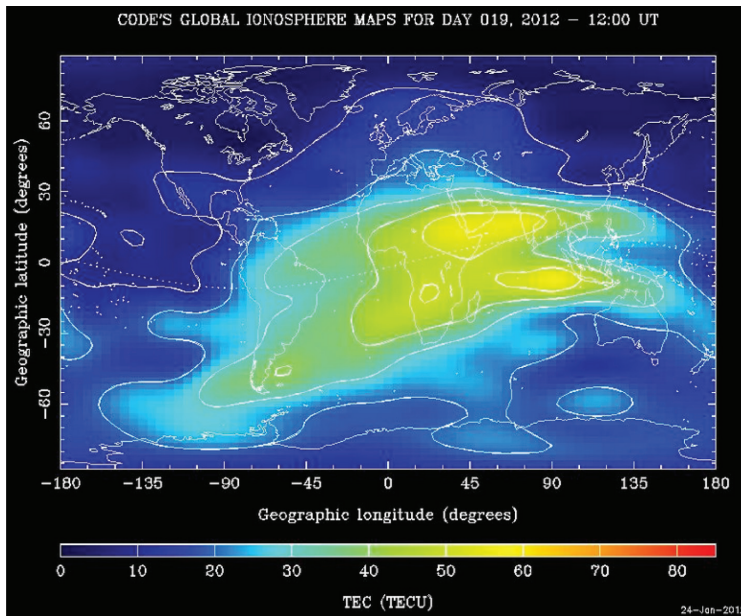


**Figure 4**  
CODE's global ionospheric map for 19 January 2012 at 1200 UT.

monitoring ionospheric behaviour on a near-real-time basis, a regional approach seems more realistic since the majority of receiver locations are within specific areas. In Europe the density of reliable dual-frequency TEC monitoring stations is high, offering the best opportunities to produce creditable maps of TEC (see Fig. 3). A typical map for the European region is shown in Fig. 5 to clearly reveal ionospheric dynamical changes on 8 August 2004 at 1205 UT. This map is obtained by automatically retrieving RINEX (Receiver Independent Exchange Format) data files from the IGS, and converting the 10 minute raw data into

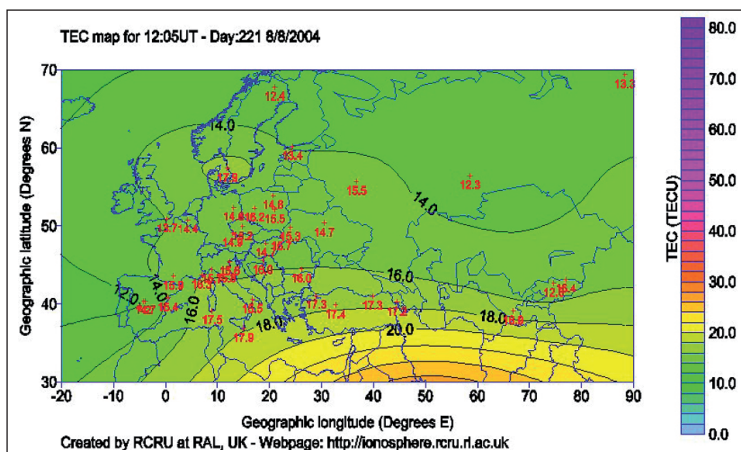


**Figure 5**  
A map of the vertical TEC for the European region. The dots depict the IGS stations and corresponding VTEC values are in red.

vertical TEC using the method developed by Ciruolo (1993) and further explained by Cander and Ciruolo (2010). Then the VTEC data from each station can be redisplayed as contour maps using a numerical Kriging spatial-interpolation technique between IGS stations (Samardjiev et al., 1993).

Similar regional TEC maps are given in Figs. 6 and 7. However, these TEC maps were produced using the NeQuick ionospheric model and the following input parameters (Hochegger et al., 2000 and references therein; Cander, 2003): (i) measured values of foF2 and M(3000)F2 for a near real-time specification (Fig. 6); and (ii) forecast values of foF2 and M(3000)F2 for forecasting TEC maps (Fig. 7). The critical frequency of the layer F<sub>2</sub>, foF2, and propagation factor M(3000)F2 are ionospheric characteristics routinely obtained by world-wide network of ionosondes (Piggot and Rawer, 1972).

**Figure 6**

Regional ionospheric TEC map derived by the NeQuick model using measured values of foF2 and M(3000)F2.

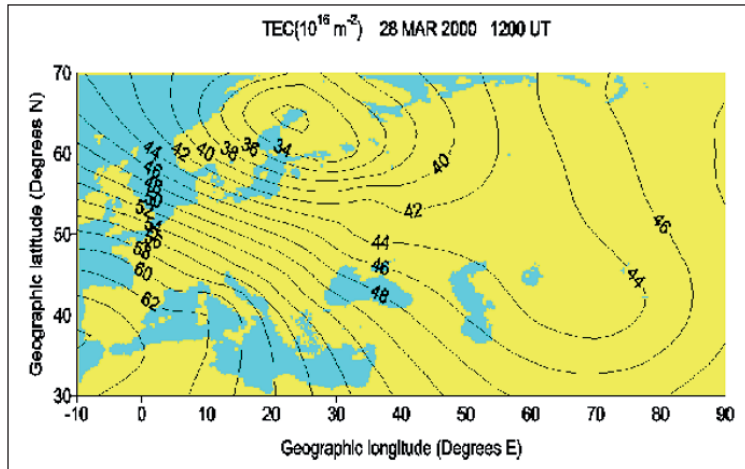
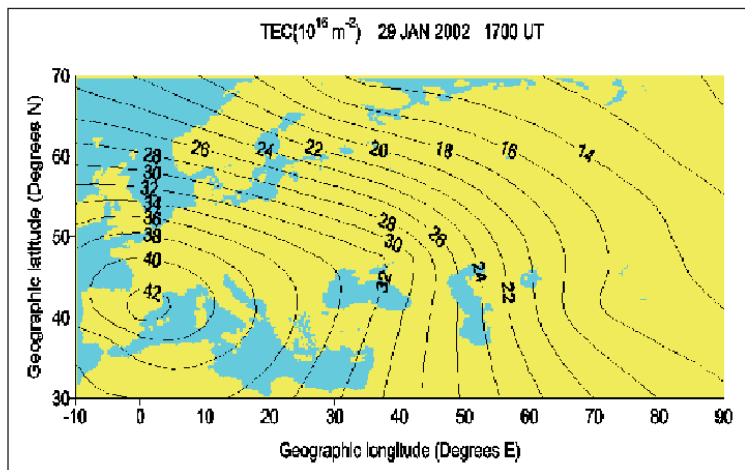


**Figure 7**

Regional ionospheric TEC map derived by the NeQuick model using forecast values of foF2 and M(3000)F2.



Furthermore the advantage of limited area total electron content observations from the local GPS receiver network such as the Ordnance Survey UK (OS) lies in its high spatial and temporal resolution (Fig. 8). An example of an area-centred ionospheric variability study as seen from the OS GPS receiver network is shown in Fig. 9. It further underlines the relationship between regional plasmaspheric-ionospheric structures and associated solar-terrestrial events. Such studies should lead to a regional storm forecasting technique based on continuous rapid measurements over limited areas similar to the OS. It is also very important for determining the required geographical spacing of VTEC monitoring locations for different practical applications.

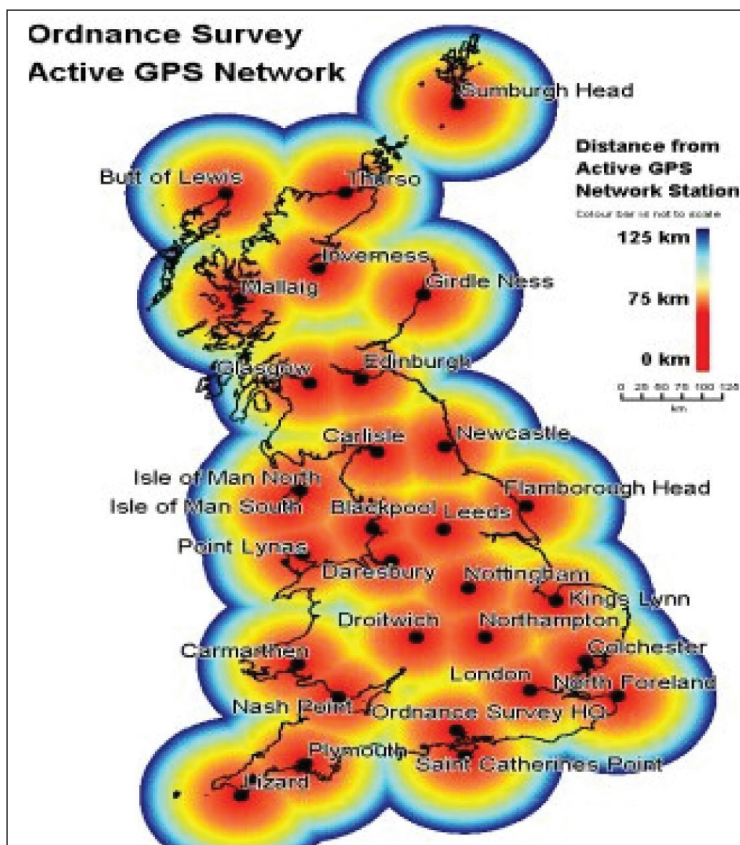
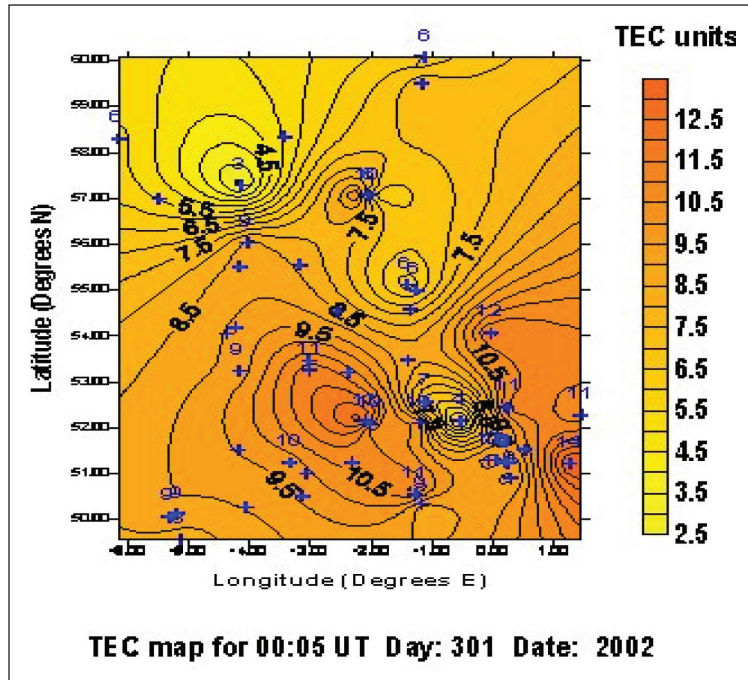


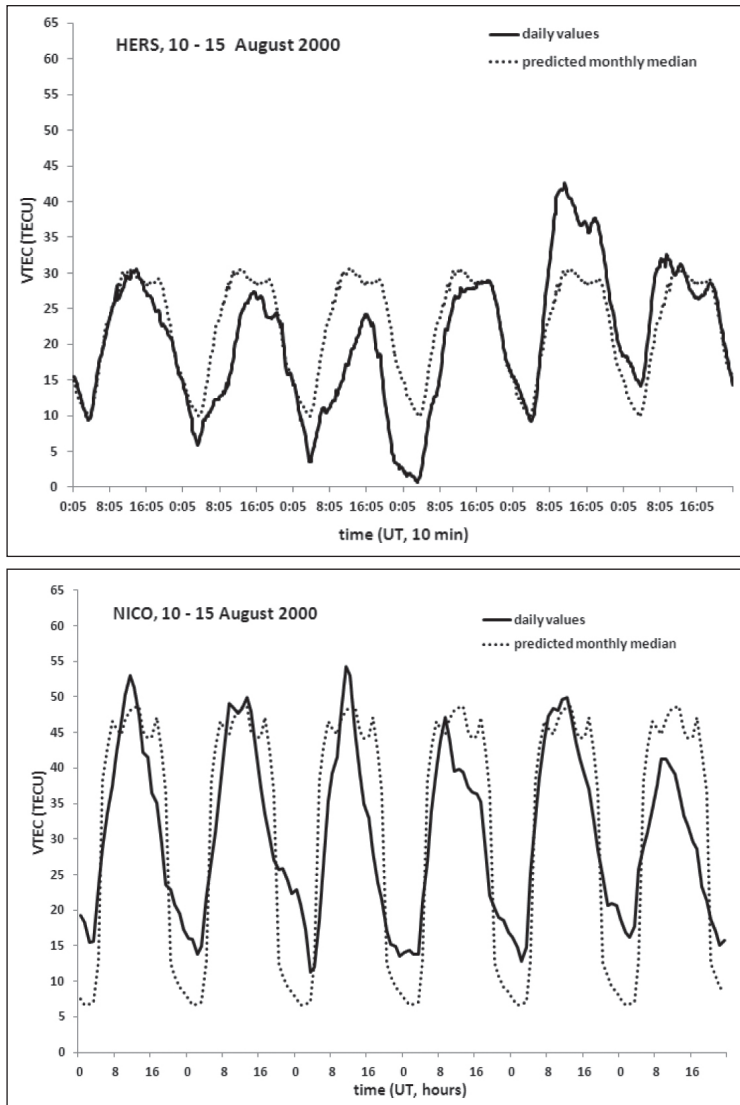
**Figure 8**  
Map of regional GPS receiver network from the Ordnance Survey UK (OS).

It is clear that different models and mapping techniques reproduce ionospheric climatology very well, but as yet cannot reproduce the major ionospheric weather features, shown in Fig. 10 as a simple example. Ground based geomagnetic field measurements show that two sudden commencements started

**Figure 9**  
 Maps showing VTEC  
 over the OS area for  
 28 October 2002  
 generated using the  
 Kriging spatial-  
 interpolation mapping  
 method with data fit  
 for 0005 UT.



on 10 and 11 August 2000 at 0500 UT and 1845 UT, respectively. The maximum Kp value reached magnitudes of 7 and 8 and lasted for a few hours during 12 August when Ap was 123, Ri was 170, and Dst was -235 nT (<http://www.ngdc.noaa.gov/stp/geomag/geoib.html>). These data indicate a major global geomagnetic storm event occurring during the period of high solar activity discussed in Section 2. According to Fig. 10, this global event has a much localized impact on associated ionospheric VTEC variations over the period 10 to 15 August 2000. Daily VTEC values of very different magnitudes understandably do not follow the predicted monthly medians at both HERS (50.9 N, 0.3 E) and NICO (35.1 N, 33.4 E) but more importantly there is a significant difference in the nature of their VTEC responses to the disturbed solar-terrestrial conditions in general and developed ionospheric storm in particular. At the high mid-latitude ground-based GPS station HERS, the ionospheric storm produced a negative phase (daily values well below the monthly median) followed by a clearly defined positive phase (daily values above the monthly median) and then a fast recovery phase, while at the low mid-latitude ground-based GPS station NICO it produced a brief initial positive phase during day time followed by negative phase and then a very slow recovery phase (Prölss, 1995).

**Figure 10**

Daily and predicted monthly median VTEC values at HERS (upper panel) and at NICO (lower panel) during 10 - 15 August 2000.

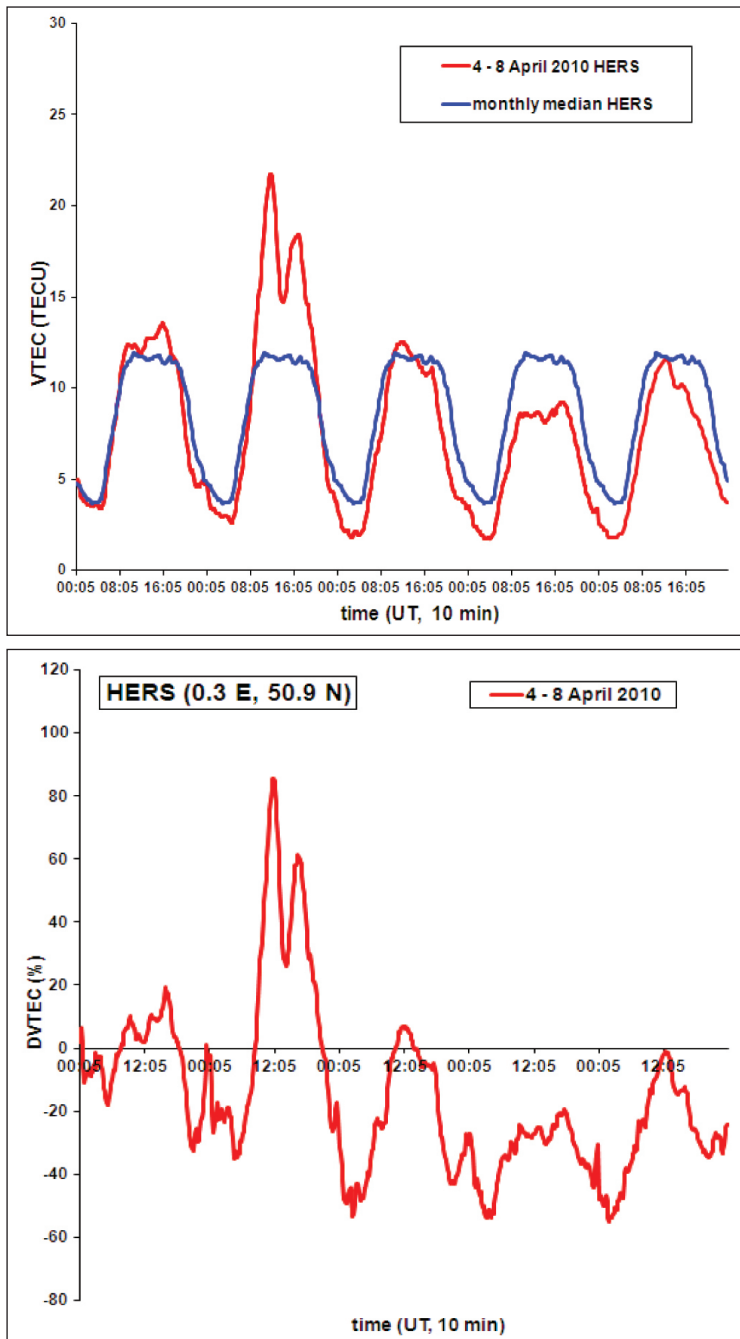
The example shown in Fig. 10 illustrates the complexity of the problems related to ionospheric storm, as one of the most important phenomena of space weather, and the real need for total electron content modelling and mapping on global, regional, and local scales. It is obvious that the spatial evolution of ionospheric storms is best observed from real-time TEC maps generated from GPS reference station data, as provided by services like the IGS. However, these maps require as much observed and/or modelled TEC data as possible in a homogeneous grid in combination with sophisticated and highly accurate numerical mapping techniques.

## 4 GNSS VTEC DURING TWO SPACE WEATHER EVENTS

The last cycle 23/24 solar minimum during the years 2006–2009 has been extraordinarily extended compared to the previous several minima with lack of solar variability and the number of days without sunspots. Although December 2008 signalling the start of solar cycle 24, the first ionospheric storms occurred in 2010. The ground geomagnetic field measurements show that a sudden commencement (Sc) occurred on 5 April 2010 at 0826 UT with the maximum Kp index reaching 8 around noon time and daily Ap index reaching 55 that classify this event as the first major storm ( $A_p > 50$ ) in the 24<sup>th</sup> solar cycle. According to the Royal Observatory of Belgium at <http://www.sidc.be/sunspot-data> the source of such disturbances is a halo CME (Coronal Mass Ejections), which occurred on 3 April 2010. A strong interplanetary shock was observed by the NASA's ACE spacecraft at 0756 UT on 5 April. In addition, a fast solar wind stream linked to a coronal hole quickly followed the arrival of the shock and maintained at active levels an already disturbed situation. Conditions returned to more or less quiet levels after 8 April.

The VTEC data for 5 days (from 4 to 8 April 2010) at HERS are plotted in Fig. 11 as function of universal time (red line at upper panel) with monthly median VTEC for April 2010 as quiet-time reference (blue line at upper panel). The lower panel of Fig. 11 shows the percentage deviation of the daily VTEC from the corresponding monthly median with the same 10-minutes resolution for the period 4-8 April 2010 (red line at lower panel). Fig. 11 confirms that this is an ionospheric storm with a positive phase followed by a negative phase and then a slow recovering phase. A clearly defined positive phase of the ionospheric storm occurred early in the storm development. The negative phase is detected about 14 hours after the storm commencement (Sc) time. It should be noted that VTEC values on 4 April are in a good agreement with the monthly median VTEC values. The first strong increase in VTEC after Sc corresponds to the period (0800-1600 UT) when Kp index was increasing to its maximum value of 8. The maximum VTEC value is approximately 22 TECU ( $1 \text{ TECU} = 10^{16} \text{ electron/m}^2$ ) that is about 85% increase in relation to the quiet time reference. The second pronounced but short lived enhancement (approximately 60%) appears in the evening sector of the same day. The negative phase is prolonged over more than two days but less pronounced in VTEC values at approximately -50% of monthly median values.

Solar activity during the week of 5–11 March 2012 was at high level dominated by sunspot group that produced a numerous X-class, M-class and C-class solar flares. The interplanetary magnetic field (IMF) magnitude increased on March 6, but due

**Figure 11**

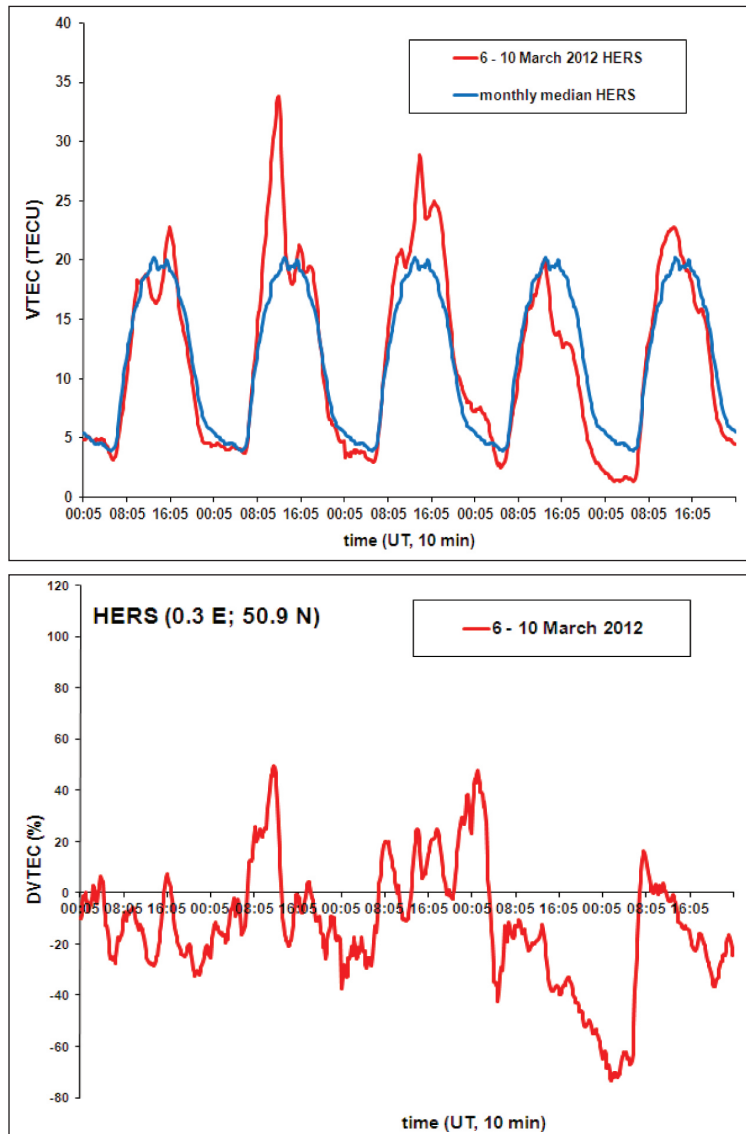
Daily and monthly median VTEC values (upper panel) and daily DVTEC values (lower panel) at HERS during 4-8 April 2010.

to low solar wind speed the geomagnetic conditions remained quiet. However, an interplanetary shock was detected at 0335 UT by ACE and at 0347 by SOHO/CELIAS on 7 March 2012. The ground geomagnetic field measurements show

that the first sudden commencement (Sc) occurred on 7 March at 0420 UT with the maximum Kp index reaching 6 around noon time and daily Ap index reaching 39. Around 0000 UT on March 9, the IMF magnitude in the ICME increased again, and this time the IMF Bz component was directed predominantly southward. This resulted in another geomagnetic storm (Kp = 5-6 as estimated by NOAA). Around 0818 UT the solar wind speed suddenly increased up to around 950 km/s. Together with still negative (southward) IMF Bz component, this led to strengthening the ongoing geomagnetic storm, with Kp reaching 7 during two

**Figure 12**

Daily and monthly median VTEC values (upper panel) and daily DVTEC values (lower panel) at HERS during 6 - 10 March 2012.



intervals and 8 during one interval (<http://www.sidc.be/sunspot-data>). Additionally the daily Ap index reached 87 on 9 March making the storm period 6-10 March 2012 the most disturb one in the current solar cycle.

Fig. 12 shows example of a positive ionospheric storm at HERS during the first geomagnetic storm of 7 March when the storm time VTEC (red line) remains much greater than the monthly median (blue line) particularly during the daytime hours. The second storm on 9 March produced the negative effect with DVTEC values reaching -70%. The strength of both positive and negative ionospheric storms in both cases (April 2010 and March 2012 storms) shows a weak positive correlation with the intensity of the geomagnetic storms expressed by corresponding Kp and Ap indexes, which suggests the large variability of the physical causes of the ionospheric storms. This makes the need to predict the ionospheric storms that can produce serious problems in satellite systems, power supply systems, and satellite navigation and communication even more urgent and detailed observations and modelling approach even more complicated.

## 5 CONCLUSIONS

Over the past decade thousands of ground-based dual frequency GPS receivers have been deployed each of these measures ionospheric total electron content (TEC) continuously in multiple directions. Their observational and modelling studies have been important for revealing the complex seasonal, local time, storm-time, and latitude and longitude effects upon vertical total electron content (VTEC) as shown in previous Sections. Hence, with the standardized formatting of these measurements and their near real-time nature, a unique ionospheric data set exists for significant progress in the development of numerical space weather TEC prediction models. These models of the total electron content vary in complexity, but even state-of-the-art models can normally correct for 70% to 80% of the ionospheric time delay. Therefore, it seems that the best correction for the effects of ionospheric time delay can be made by an actual measurement. Incorporate a near real-time monitoring capability at an observation location is to remove over 90% to 95% of the ionospheric time delay error.

## REFERENCES

- [1] Cander, Lj.R. (2003). Toward forecasting and mapping ionospheric space weather under the COST actions. *Advances in Space Research*, **31**, 957-964.
- [2] Cander, Lj.R. (2008). Ionospheric research and space weather services. *Journal of Atmospheric and Solar–Terrestrial Physics*, **70**, 1870–1878.

- [3] Cander, Lj. R. and Ciruolo, L. (2010). Ionospheric total electron content and critical frequencies over Europe at solar minimum. *Acta Geophysica*, **58**, 468-490.
- [4] Ciruolo, L. (1993). Evaluation of GPS L2-L1 biases and related daily TEC profiles. *Proceedings of the GPS/Ionosphere Workshop*, Neustrelitz, 90-97.
- [5] Davies, K. and Smith, E. K. (2000). Ionospheric effects on land mobile satellite systems. In: Goldhirsh, J., Vogel, W.J. (eds.) A Supplement to "Propagation Effects for Land Mobile Satellite Systems: Overview of Experimental and Modeling Results", NASA, Reference Publication 12, University of Colorado, Boulder.
- [6] Dow, J.M., Neilan, R. E. and Rizos, C. (2009). The International GNSS Service in a changing landscape of Global Navigation Satellite Systems. *Journal of Geodesy*, **83**, 191-198.
- [7] Hernández-Pajares, M., Juan, J. M., Sanz, J., Orus, R., Garcia-Rigo, A., Feltens, J., Komjathy, A., Schaer, S. C. and Krankowski, A. (2009). The IGS VTEC maps: a reliable source of ionospheric information since 1998. *Journal of Geodesy*, **83**, 263-275.
- [8] Hernández-Pajares, M., Miguel Juan, J., Sanz, J., Aragón-Àngel, À., García-Rigo, A., Salazar, D. and Escudero, M. (2011). The ionosphere: effects, GPS modeling and the benefits for space geodetic technique. *Journal of Geodesy*, **85**, 887-907.
- [9] Hochegger, G., Nava, B., Radicella, S.M. and Leitinger, R. (2000). A family of ionospheric models for different uses. *Phys. Chem. Earth (C)*, **25**, 307-310.
- [10] Jakowski, N. (1996). TEC monitoring by using satellite positioning systems. *Modern Ionospheric Science* edited by H. Kohl, R. Ruester, and K. Schlegel, Eur. Geophys. Soc., Katlenburg-Lindau, Germany, 371-390.
- [11] Jakowski, N., Hoque, M. M. and Mayer, C. (2011). A new global TEC model for estimating transionospheric radio wave propagation errors. *Journal of Geodesy*, **85**, 965-974.
- [12] Kersley, L., Malan, D., Pryse, S.E., Cander, Lj.R., Bamford, R., Belehaki, A., Leitinger, R., Radicella, S.M., Mitchel, C.N. and Spencer, P.S.J. (2004). Total electron content - A key parameter in propagation: measurement and use in ionospheric imaging. *Annals of Geophysics*, **47**, 1067-1091.
- [13] Piggot, W.R. and Rawer, K. (1972). U.R.S.I Handbook of Ionogram Interpretation and Reduction. World Data Center A for Solar Terrestrial Physics- Report UAG-23.
- [14] Prölss, G.W. (1995). Ionospheric F-region storms. In: Volland, H. (ed.) *Handbook of Atmospheric Electrodynamics*, CRC Press, Boca Raton, 195-248.
- [15] Samardjiev, T., Bradley, P.A., Cander, Lj.R. and Dick, M.I. (1993). Ionospheric mapping by computer contouring techniques. *Electronics Letters*, **29**, 1794-1975.



Faculty of Maritime Studies  
University of Rijeka, Croatia



Royal Institute of Navigation  
Science · Technology · Practice



The University of  
Nottingham

**6<sup>th</sup> GNSS**  
Vulnerabilities  
and Solutions  
Conference

# IONOSPHERIC SCINTILLATION MONITORING IN A SINGLE STATION MODE

**Marija Cokrljic<sup>1</sup>, K. Wezka<sup>1</sup>, R. Galas<sup>1</sup>, N. Jakowski<sup>2</sup>**

<sup>1</sup> Technische Universitaet Berlin,  
Department for Geodesy and Geoinformation Science  
Straße des 17. Juni 135, 10623 Berlin, Germany  
E-mail: marija.cokrljic@tu-berlin.de

<sup>2</sup> German Aerospace Centre (DLR),  
Institute of Communication and Navigation

**ABSTRACT.** *This paper describes preliminary results of the influence of ionospheric scintillations onto GNSS positioning. The main aims of the study are to investigate the performance of algorithms and software used to determine time series scintillation indices. The investigation is based on GNSS data from a PolaRxS scintillation receiver, which is continuously operating at Navigation Lab of the TU Berlin (TUB). The GNSS observables are processed off-line using software developed at TUB. The scintillation algorithms, software tools and results from the TUB software validation are described.*

**KEY WORDS:** *ionosphere monitoring, scintillation indices, software development*

## 1 INTRODUCTION

Ionosphere is a dispersive medium that has a large influence on the propagation of electromagnetic waves. In GNSS positioning, the signal propagated from the satellite to a user's receiver can be affected by small scale electron density irregularities. These irregularities are visible as rapid amplitude and phase fluctuations and, under some conditions, even in the loss of lock of the signal. They are called ionospheric scintillations. Such phenomena can be described by indices such as S4 amplitude scintillation index and a phase scintillation index known as  $\sigma_\phi$ .

The paper describes selected results of our preliminary studies on amplitude scintillation indices calculated from the In-phase and Quadrature amplitudes. For this purpose, we have used software tools that are under development at the Technische Universität Berlin (TUB). The software tools accept data in receiver dependent formats from various receivers, including Javad and Septentrio. For this study, observables used for the algorithm validation came from Septentrio's PolaRxS scintillation receiver only, which is continuously operating in our Navigation Lab.

## 2 SOFTWARE- AND HARDWARE TEST-BED

The main goal of the research work presented in this paper is to validate the software package used to develop the real- and near-real-time monitoring of ionospheric scintillations. The test-bed comprises two main subunits:

- Station hardware and software for data gathering and distribution to processing centres (field unit), and
- Scintillation processor (main processor).

The main requirements for both the hardware and software are:

- On-site maintenance free continuous operation of our field GNSS monitoring station,
- Processing of observables, e.g. carrier and code phases, I- and Q-amplitudes (correlations), from various types of receivers, and
- Remote maintenance of the field stations by the network operating centre only.

A prototype of an autonomous continuously operating GNSS-station was used for performance tests of our hardware and software solutions. The prototype system was developed in the Navigation Lab (TUB) under the program "Offensive Wissen durch Lernen".

A Septentrio PolaRxS scintillation receiver and a new 3G+C multipath cancelling antenna (Popugaev et al., 2007) developed in Germany were selected for the ionospheric investigations. The PolaRxS was chosen because the receiver includes post-processing software-tools that enables the calculation of scintillation indices. These indices are used as reference values for our own ionospheric software-tools, which also processes data from various GNSS receivers, available from multipurpose real-time reference stations.

## 2.1 GNSS tracing station architecture

The prototype TUB station is based on the Septentrio receiver with a modular hardware and software design, which allows the operation of other off-the-shelf GNSS receivers. The current version of the software-tools supports the Septentrio family as well as Javad and Topcon receivers. The central part of the system is the station computer that runs under a Linux OS (PC-104 board), a power management sub-system with a watch-dog and interfaces for data transmission.



**Figure 2.1**  
Experimental  
TU-Berlin GNSS  
monitoring station.

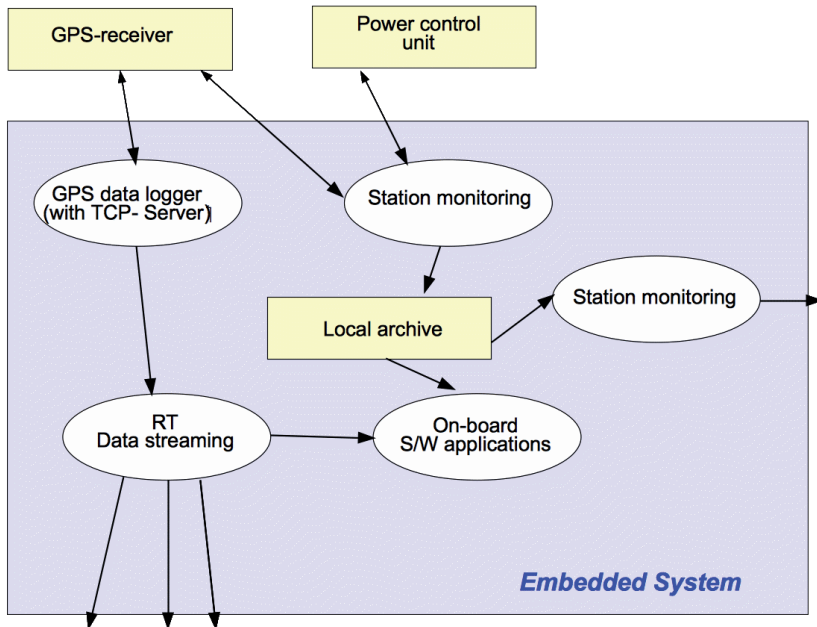
## 2.2 The software architecture

The station software (see Fig. 2.2) is composed of the following modules:

- Station monitoring software tool,
- High-rate data loggers (up to 50 Hz), with serial ports (for lower data sampling rates) and Ethernet interfaces that support Septentrio and Javad/Topcon data protocols,
- Software servers for GNSS data streaming in real-time,

**Figure 2.2**

Software modules and data flow on the prototype field monitoring computer.



- Software-tools for the distribution of observation data files and house-keeping data, and
- Other software modules that are still under development and testing (see conclusions).

The prototype TUB station operates continuously and serves for performance testing of the hardware and the station software. It is also being used to validate the GNSS software package “TUB-NavigationSolutions” currently under development.

### 3 DATA AND ALGORITHMS

The GNSS data processed from the current experiment has been gathered at a high sampling rate (50Hz) during one day of observations at DLR Neustrelitz (Germany).

According to the requirements of the Septentrio scintillation tool “sbf2ismr”, the PolaRxS scintillation receiver was set to record In-phase (I) and Quadrature (Q) correlations (IQCorr for GPS L1CA and L2C) (Septentrio, 2010) every 20 ms, code- and carrier-phase measurements at a lower sampling rate (1 Hz), while the

receiver and channel status were recorded every 10 seconds and the GPS Navigation message was set to *on change*.

After gathering, the GNSS observables, available in the sbf receiver dependent format, the data was converted to our binary data exchange format T-BinEx, which is an extension of the older GFZ-BINEX (Galas and Köhler, 2001) (see also [http://binex.unavco.org/GFZ\\_1999Jan31.html](http://binex.unavco.org/GFZ_1999Jan31.html)). The T-BinEx has been upgraded to include both the I and Q components from the raw Septentrio and Javad messages. This binary data exchange format is our standard input format to the TUB-NavSolutions software.

### 3.1 Algorithm description for evaluation of amplitude scintillation indices

A mathematical model of the bandpass signal  $s(t)$  can be written after (Borre et al., 2007) as:

$$s(t) = s_I + js_Q(t) \quad (1)$$

and

$$s_I(t) = a(t)\cos(\varphi(t)) \quad (2)$$

and

$$s_Q(t) = a(t)\sin(\varphi(t)) \quad (3)$$

are the In-phase (I) and the Quadrature (Q) components, respectively.

From Equations 2 and 3, the amplitude of the signal can be calculated as the square root of the imaginary and real parts of the complex signal,  $s(t)$  (Equation 1):

$$a(t) = \sqrt{s_I^2(t) + s_Q^2(t)} \quad (4)$$

The S4 amplitude scintillation indices is calculated from the signal's power, derived from the measured in-phase (Re) and quadrature (Im) values given by the output of correlators (i.e.  $\tilde{s}_I(t)$  and  $\tilde{s}_Q(t)$ ). Hence:

$$\tilde{s}_I(t) = s_I(t) + \eta_I \quad (5a)$$

$$\tilde{s}_Q(t) = s_Q(t) + \eta_Q \quad (5b)$$

where  $\eta_I$  and  $\eta_Q$  are thermal noise contributions respectively.

### 3.1.1 Calculation of the amplitude scintillation index S4 from signal power

The scintillation index S4 is calculated here after Mushini et al., (2011) using the following formula:

$$S4 = \sqrt{\frac{\langle P^2(N) \rangle - \langle P(N) \rangle^2}{\langle P(N) \rangle^2}} \quad (6)$$

In Equation 6, P is power of the signal  $s(t)$  where

$$P(t) = \frac{a(t)^2}{2} \quad (7)$$

Is a function of the signal amplitude (see Equation 4).

The quantities:

$$\langle P(N) \rangle = \frac{1}{N} \sum_{i=0}^{i=N} P(i) \quad (8)$$

and

$$\langle P^2(N) \rangle = \frac{1}{N} \sum_{i=0}^{i=N} P^2(i) \quad (9)$$

(also Equation 6), are average values evaluated from 1 minute long observation time periods for the I- and Q correlations respectively. They are calculated in loops over all satellites in view. The argument  $i$  indicates the observation epoch number within each 1 minute data interval, and  $N$  is number of available observations in the given minute.

### 3.1.2 Calibration of the S4 Index

As demonstrated by Van Dierendonck et al., (1993), the calculated signal power (Equations 4 and 6-9) “is measured in a way that its value does not fluctuate with noise power”. This is because of the thermal noise contributions  $\eta_I$  and  $\eta_Q$  (see Equations 5a and 5b).

For this reason the S4 values are calibrated against the ambient (thermal) noise, which can be estimated as the average SNR value over the same time span for which the signal power is averaged. The influence of the ambient noise on the S4 index can be obtained from the formula given by Van Dierendonck et al. (1993):

$$S4N_0 = \sqrt{\frac{100}{SNR} \left[ 1 + \frac{500}{19SNR} \right]} \quad (10)$$

The SNR quantity in the above equation is expressed in units of Watts. Now the calibrated S4 indices can be calculated as:

$$S4_{calibrates} = \sqrt{S4^2 - S4N_0^2} \quad (11)$$

In the absence of scintillations, the right hand side of Equation 10 can take negative values. In such a case the calibrated S4 value have to be set to the uncalibrated value.

#### 4 SELECTED PRELIMINARY RESULTS

The algorithm described above was used to analyse a single day of data collected at DLR Neustrelitz. The data was processed using the TUB ionospheric software tools to determine the ionospheric scintillation index S4 and the ambient noise components of the correction to the total value of S4. Selected time series of S4 and S4-corrected for SV26 are displayed in Fig. 4.1.

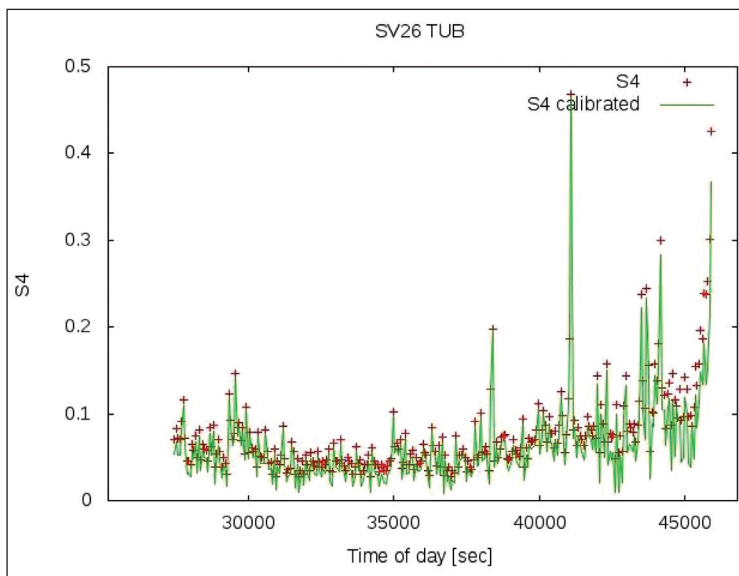


**Figure 4.1**  
Amplitude scintillation index S4 and its calibrated value calculated with the TUB software-tools

A comparison of Figures 4.1 and 4.2 shows that the TUB software generates identical numbers for the both quantities.

**Figure 4.2**

Amplitude scintillation indices S4 and its calibrated value calculated with the Septentrio's post-processing software "sbf2ismr".

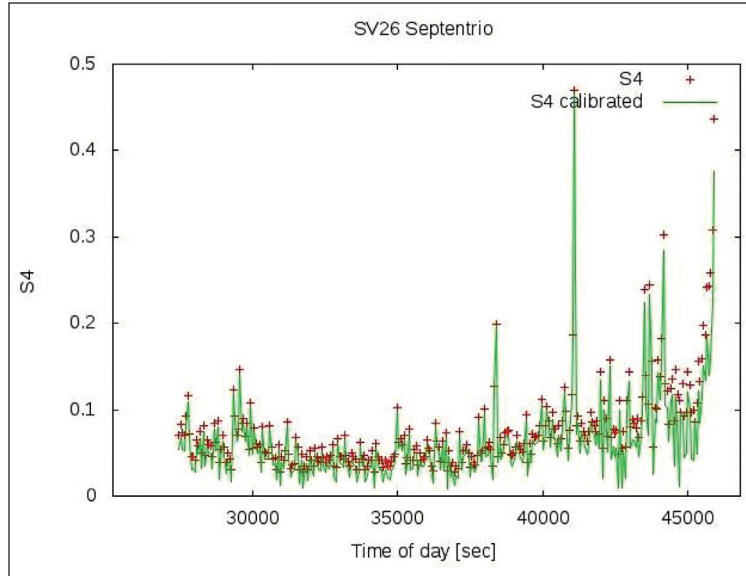
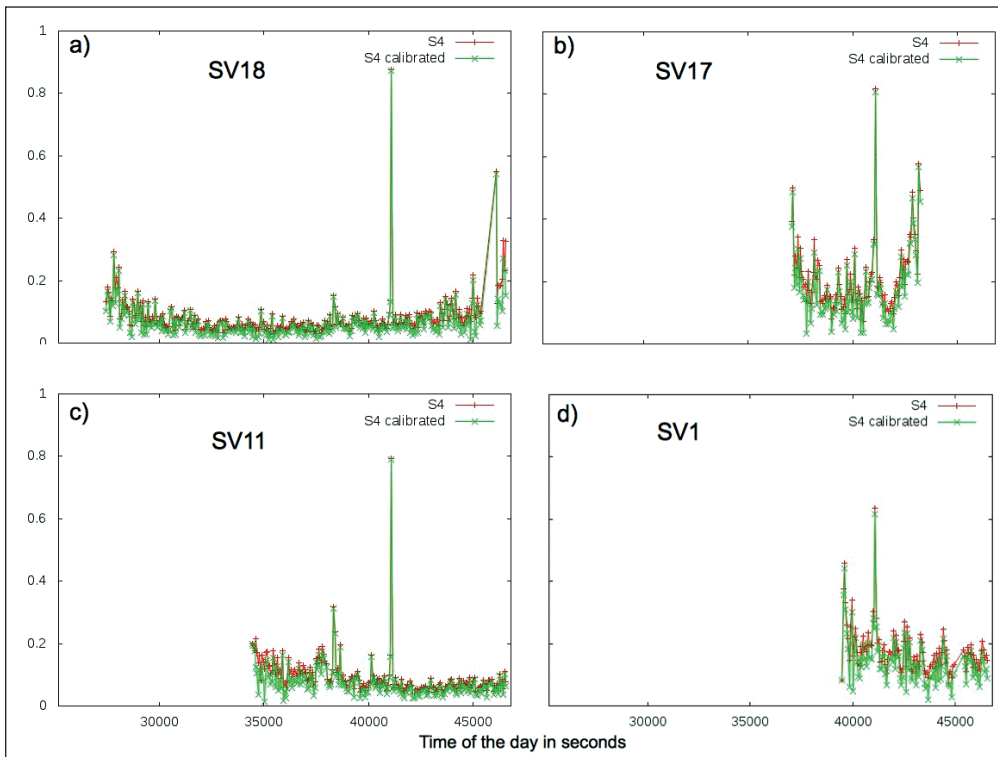


**Figure 4.3**

S4 and S4-calibrated for all visible satellites around observation epoch number 41100



The time series for both Septentrio's and TUB display some, not yet clear, irregularities, which appeared for all visible satellites at the same epoch number 41100 (see Fig. 4.3).

In the table 4.1 the azimuth and elevation angles for this selected epoch are given.

**Table 4.1**

Irregularity observed at the 41100 epoch

| SV PRN | Elevation angle<br>[°] | Azimuth angle<br>[°] | S4    | S4 calibrated |
|--------|------------------------|----------------------|-------|---------------|
| 8      | 3                      | 93                   | 0.472 | 0.473         |
| 11     | 4                      | 25                   | 0.818 | 0.807         |
| 1      | 5                      | 41                   | 0.635 | 0.617         |
| 22     | 14                     | 324                  | 0.491 | 0.482         |
| 12     | 16                     | 224                  | 0.420 | 0.415         |
| 28     | 38                     | 58                   | 0.875 | 0.874         |
| 17     | 39                     | 101                  | 0.792 | 0.790         |
| 9      | 52                     | 283                  | 0.393 | 0.394         |
| 15     | 65                     | 218                  | 0.372 | 0.371         |
| 27     | 72                     | 290                  | 0.368 | 0.367         |

## 5 CONCLUSIONS AND FORTHCOMING ACTIVITIES

Results obtained for both the Septentrio and TUB-NavigationSolutions programs show, that there are no significant differences between both software tools. Therefore, the TUB ionospheric tools can be used for the calculation of amplitude indices for any GNSS receiver providing In-phase and Quadrature correlations.

Currently the TUB ionospheric tools are being upgrade to support the calculation of the TEC and phase scintillation indices. The software will be equipped with a real time data streaming and near-real time data processing capacity. Further, influence of multipath effects onto scintillation indices will be investigated as well.

### Acknowledgements

The research in this paper is funded by the FP7 People Programme through the Marie Curie Initial Training Network TRANSMIT – Training Research and Applications Network to Support the Mitigation of Ionospheric Threats.

## REFERENCES

- [1] Beniguel Y. (2011). Global Ionospheric Scintillation Model. GISM Technical Manual.
- [2] Borre K., Akos D.M., Bertelsen N., Rinder P., Jensen S.H. (2007). A software- defined GPS and Galileo receiver- A single-frequency approach. Birkhäuser Boston 2007.
- [3] Galas R., Köhler W. (2001). A Binary Exchange Format for GPS Data. Phys. Chem. Earth, Vol. 26, No 6-8, pp 645-648.
- [4] Mushini S.C., Jayachadran P.T., Langley R.B., MacDougall J.W., Pokhotelov D. (2011). Improved amplitude- and phase- scintillation indices derived form wavelet detrended high-latitude GPS data”, GPS Solutions, DOI 10.1007/s10291-011-0238-4. Published online 18. August 2011.
- [5] Popugaev A.E., Wansch R., Urquijo S. (2007). “A novel high performance antenna for GNSS applications”. Fraunhofer Institute for Integrated Circuits IIS, Erlangen Germany. Proceedings of European Conference on “Antennas and Propagation, 2007.
- [6] Septentiro (2010). SBF Reference Guide. Version 1.9.0 July 16, 2010.
- [7] Van Dierendnock A.J., Klobuchar J., Quyena H. (1993). Ionospheric Scintillation Monitoring Using Commercial Single Frequency C/A Code Receivers. Proceedings on ION GPS-93, the 6th International Technical Meeting of the Satellite Division of the Institute of Navigation, Salt Lake City, Utah, pp 333-344.



Faculty of Maritime Studies  
University of Rijeka, Croatia



Royal Institute of Navigation  
Science · Technology · Practice



The University of  
Nottingham

**6<sup>th</sup> GNSS**  
Vulnerabilities  
and Solutions  
Conference

# A THEORETICAL FRAMEWORK FOR UNDERSTANDING RELATIONSHIP BETWEEN SPACE WEATHER INDICES AND GPS IONOSPHERIC DELAY

**Renato Filjar<sup>1</sup>, Serdjo Kos<sup>1</sup>, Tomislav Kos<sup>2</sup>**

<sup>1</sup> Faculty of Maritime Studies, University of Rijeka, Rijeka, Croatia  
Studentska ulica 2, 51000 Rijeka, Croatia  
E-mail: renato.filjar@gmail.com

<sup>2</sup> Faculty of Electrical Engineering and Computing, University of Zagreb,  
Croatia

**ABSTRACT.** *Space weather effects, and the ionospheric disturbances in particular, have been identified as the major single component of the GNSS error budget. For that reason, the research into the space weather-ionospheric coupling has become the major cornerstone in the development of mitigation techniques for the space weather-induced GNSS vulnerabilities and risks.*

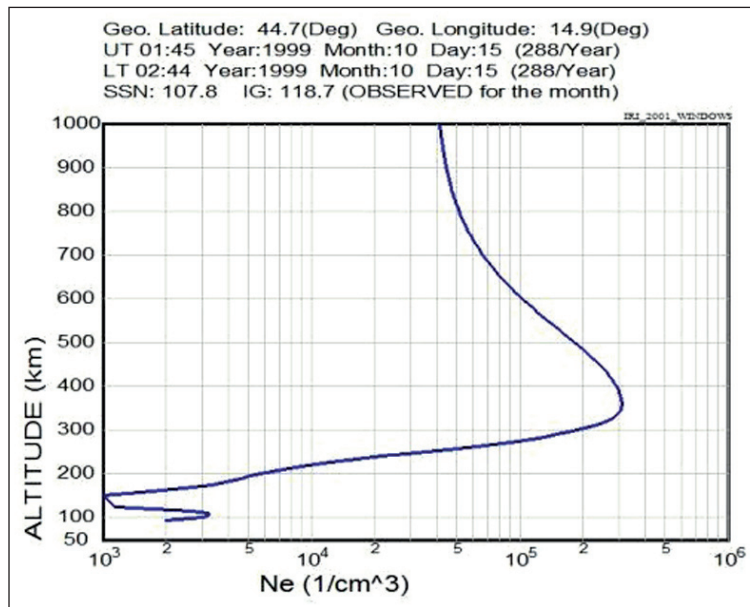
*Here we present a theoretical framework, based on Appleton-Hartree formula and experimental models, that relates the space weather (solar and geomagnetic) indices to the GNSS ionospheric delay, thus establishing a theoretical framework for establishing relationship between the space weather observables and the major source of GNSS positioning error.*

**KEY WORDS:** *GNSS ionospheric delay, ionospheric layer, theoretical framework, experimental models*

## 1 INTRODUCTION

A wide acceptance of satellite navigation, that results in increasing number of technology and socio-economic systems founded on GNSS utilisation, calls for systematic robust solution against various sources of GNSS vulnerabilities and risks (Thomas *et al*, 2011, Filjar and Huljenic, 2012). In many cases, this means assuring the provision and maintenance of a certain level of positioning accuracy, given the common ambiental conditions for GNSS-based positioning.

**Figure 1**  
Vertical ionospheric profile, as simulated using the International Reference Ionosphere IRI 2001



The GNSS ionospheric delay has been proven as the major single source of the GNSS positioning deterioration (Parkinson and Spilker, Jr, 1996, Klobuchar, 1987, Filjar, 2008, Filjar, Kos and Kos, 2009). Driven by solar activity and space weather disturbances, the Earth's ionospheric dynamics expresses itself in continuous stochastic variations of its electrical (conductive) parameters (Booker, 1954, Davis, 1990, Helliwell, 2006, Hunsucker and Hargreaves, 2007, McNamara, 1991). Resulting from the intrinsic instabilities in the Earth's vertical ionospheric profile (Fig 1), the GNSS ionospheric delay may cause severe, fast-changing and strong GNSS positioning error dynamics, thus determining the GNSS ionospheric delay (Davis, 1990, Klobuchar, 1987, Parkinson and Spilker, Jr, 1996, Filjar, 2006, Filjar, 2008).

Here we propose a theoretical framework for direct relation of the space weather indices with the GNSS ionospheric delay, thus presenting a contribution to better understanding of the relation between the space weather and GNSS positioning performance.

This paper is organised as follows. After providing the outline of the scientific background on radio propagation theory (Chapter 2), the nature of the GPS ionospheric delay (Chapter 3) and the characterisation of the space weather through the space weather indices (Chapter 4), a proposed theoretical framework is given (Chapter 5), that directly relates space weather indices with GPS ionospheric delay. Discussion (Chapter 6) addresses the methodology of development and limitations of the proposed framework. This paper concludes (Chapter 7) with the outline of the major achievements, and plans for the near-future research.

## 2 APPLETON-HARTREE FORMULA

The GPS ionospheric delay results from the nature of (GPS satellite) radio waves propagation in the ionised environment (Davis, 1990, Helliwell, 2006, Parkinson and Spilker, Jr, 1996, Hunsucker and Hargreaves, 2007).

Maxwell's equations (Hunsucker and Hargreaves, 2007):

$$\nabla \times \mathbf{E} = -\frac{\partial \mathbf{B}}{\partial t} \quad (1)$$

$$\nabla \times \mathbf{B} = \mu_0 \mathbf{J} \quad (2)$$

and Ohm's law (Hunsucker and Hargreaves, 2007):

$$\mathbf{J} = \sigma (\mathbf{E} + \mathbf{v} \times \mathbf{B}) \quad (3)$$

give the general theoretical description of radio wave propagation.

Setting the velocity  $\mathbf{v} = 0$ , and eliminating  $\mathbf{J}$  and  $\mathbf{E}$ , we obtain (Hunsucker and Hargreaves, 2007):

$$\frac{\partial \mathbf{B}}{\partial t} = \frac{\nabla^2 \mathbf{B}}{\mu_0 \sigma} = \epsilon_0 c^2 \frac{\nabla^2 \mathbf{B}}{\sigma} \quad (4)$$

The equation (4) is known as a diffusion equation, a governing model of plasma conditions in which electromagnetic waves propagate.

Propagation of radio waves in dispersive medium (i.e. where radio waves of different frequencies have different velocities) is defined by frequency-dependent refractive index  $n$  (Davis, 1990, Hunsucker and Hargreaves, 2007), as defined in (5).

$$n^2 = 1 - \frac{X}{1 - jZ - \left[ \frac{Y_T^2}{2(1-X-jZ)} \right] \pm \left[ \frac{Y_T^4}{4(1-X-jZ)^2} + Y_L^2 \right]} \quad (5)$$

with the parameters defined as follows:

$$\begin{aligned} X &= \frac{\omega_N^2}{\omega^2} \\ Y &= \frac{\omega_B}{\omega} \\ Y_L &= \frac{\omega_L}{\omega} \\ Y_T &= \frac{\omega_T}{\omega} \\ Z &= \frac{\nu}{\omega} \end{aligned} \quad (6)$$

and with the following descriptions:

$\omega_N$  ... angular plasma frequency

$\omega_B$  ... electron gyrofrequency

$\omega_L$  ... longitudinal component of  $\omega_B$  of direction of propagation

$\omega_T$  ... transversal component of  $\omega_B$  of direction of propagation

$\nu$  ... electron collision frequency

$\omega$  ... angular wave frequency

### 3 GPS IONOSPHERIC DELAY

After removing the negligible factors in (5), the index of GPS radio wave refraction can be given approximately by (7) (Davis, 1990, Parkinson and Spilker, Jr, 1996, Hunsucker and Hargreaves, 2007).

$$n^2 \approx 1 - X \quad (7)$$

Considering previously defined parameter  $X$  (Davis, 1990, Hunsucker and Hargreaves, 2007):

$$X = \frac{\omega_N^2}{\omega^2} = \frac{N(h)e^2}{\epsilon_0 m \omega} \quad (8)$$

with:

$N(h)$  ... vertical ionospheric profile

$e$  ... electron charge

$\epsilon_0$  ... permittivity of free space

$m$  ... rest mass of electron

$\omega$  ... angular wave frequency

the another approximation follows (Davis, 1990, Parkinson and Spilker, Jr, 1996, Hunsucker and Hargreaves, 2007):

$$n \approx 1 - \frac{X}{2} \quad (9)$$

The GPS ionospheric delay is defined, as follows (Davis, 1990, Parkinson and Spilker, Jr, 1996, Hunsucker and Hargreaves, 2007):

$$\Delta t = \frac{1}{c} \int (1 - n) dh \quad (10)$$

Combination of (9) and (10) yields:

$$\Delta t = \frac{1}{c} \int \frac{X}{2} dh \quad (11)$$

and:

$$\Delta t = \frac{1}{2c} \int \frac{N(h)e^2}{\epsilon_0 m \omega^2} dh = \frac{e^2 H}{2\epsilon_0 m \omega^2} c \int N(h) dh \quad (12)$$

Equation (12) can be rewritten in the following format, giving the GPS ionospheric time delay as:

$$\Delta t = \frac{40.3}{c f^2} \int N(h) dh \quad (13)$$

The equation (13) can be used to express the equivalent GPS ionospheric delay in the ranging unit, as follows:

$$\Delta \rho = \frac{40.3}{f^2} \int N(h) dh \quad (14)$$

The expression (15) defines a new parameter Total Electron Content ( *TEC*), as follows (Davis, 1990, Parkinson and Spilker, Jr, 1996, Klobuchar, 1987):

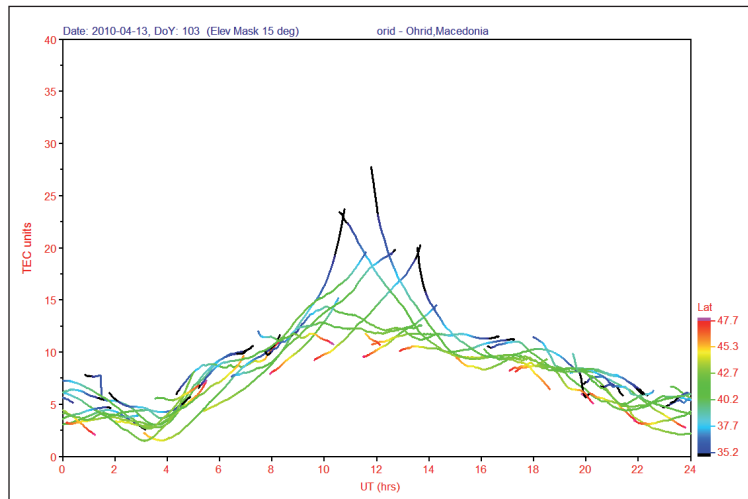
$$TEC = \int N(h) dh \quad (15)$$

thus allowing for the equivalent GPS ionospheric ranging delay to be expressed as in (16).

$$\Delta \rho = \kappa \cdot TEC \quad (16)$$

Expression (16) directly relates GPS ionospheric delay with the vertical ionospheric profile.

**Figure 2**  
Actual GPS ionospheric delays/TECs as observed by different GPS satellite dual-frequency measurements at the reference station Ohrid, Macedonia on 13 April, 2010



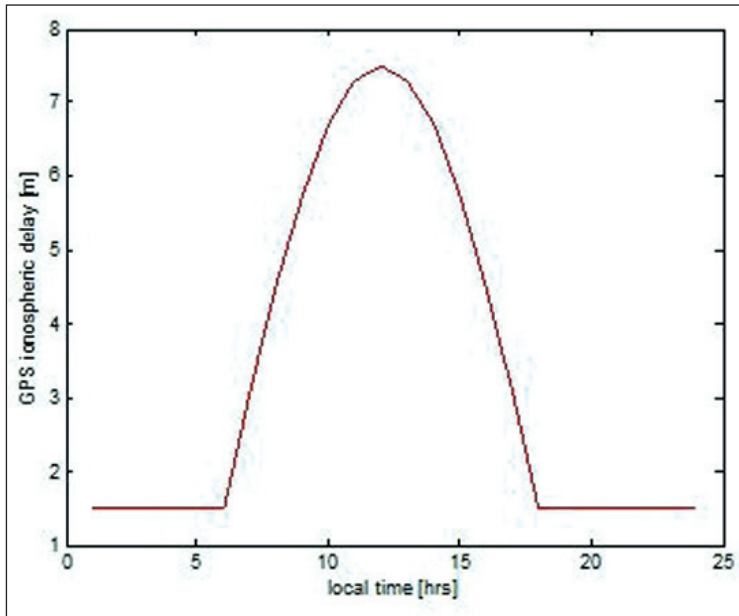


**Figure 3**  
A characteristic daily variation of the GPS ionospheric delay

Modified by numerous processes, the Earth's ionosphere undergoes numerous and mostly unpredictable dynamics (Fig 2), despite several already identified patterns of behaviour, such as regular daily (Fig 3) or seasonal variations.

#### 4 SPACE WEATHER INDICES

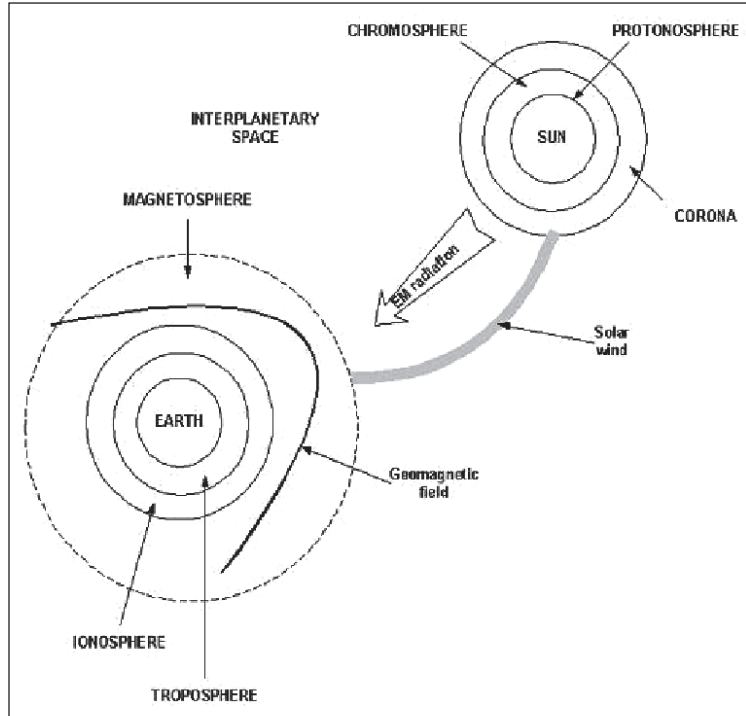
Space weather (Fig 4) is a common name for a group of processes involved in transmission of energy and high-energy particles from the Sun to neighbouring space (Davis, 1990). Resulting from the solar activity, the energy and particles are sent into space in a form of a so-called solar wind. Depending on the nature and position of local solar activities, the solar wind can be directed towards the Earth, causing minor to severe disturbances of the Earth's magnetic (geomagnetic) field and ionosphere (Davis, 1990, Helliwell, 2006).

The solar activity is usually described by parameters summarised in Table 1, and measured in a continuous fashion.

**Table 1**

| Parameter of solar activity | Abbreviation | Sampling frequency                                    |
|-----------------------------|--------------|---|
| sunspot number              | SSN          | once a day  |
| solar flux at 2800 MHz      | FLUX         | once a day (terrestrial),<br>continuously (satellite) |

**Figure 4**  
Sun – Earth environment in which space weather processes occur



Disturbances of the geomagnetic field are expressed using the geomagnetic indices, the most important of them outlined in Table 2.

**Table 2**

| Geomagnetic index  | Abbreviation | Sampling frequency |
|--|--------------|--------------------|
| Planetary K index of disturbances in horizontal component of geomagnetic field   | Kp           | 3 hours            |
| Daily planetary average of geomagnetic field variations  | Ap           | daily              |
| Dst index of magnetic activity derived from the observables taken by network of near- equatorial observing stations, measuring the intensity of the globally symmetrical equatorial electro jet. | Dst          | hourly             |

Description of the ionospheric status is generally given by the vertical ionospheric profile  $N(h)$ , relating the free electron density with the height above the Earth’s surface. The vertical ionospheric profile can be modelled in various

ways. For this discussion of GPS ionospheric delay and TEC, the most suitable is the ionospheric description using geometrical description of the ionospheric layers contributing to the TEC formation, as depicted on Fig 5.

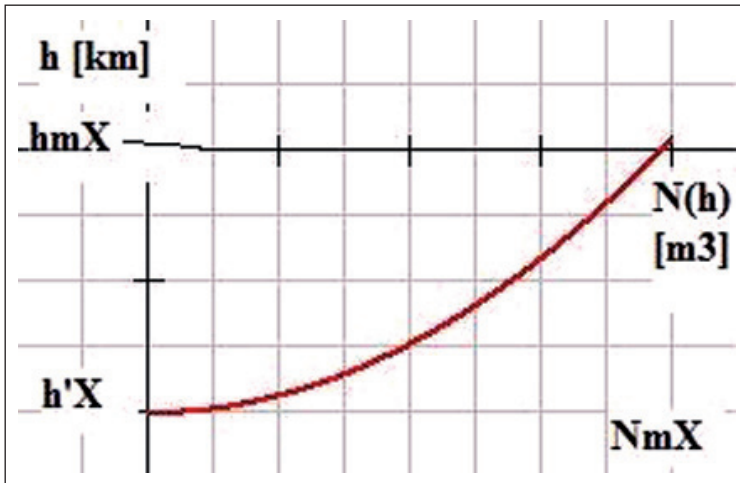


**Figure 5**

The approximation of an ionospheric layer

Every relevant ionospheric layer is determined by upper  $hm$  and lower  $h'$  limit of the layer, minimum and maximum  $Nm$  values of the free electron densities, and the layer's critical frequency  $f_0$ .

According to [Bent, 1971], the E and F2 layers, the main contributors to TEC, can be modelled using the parabolic model (Fig 5)(Davis, 1990), as follows:

$$N(h) = NmF2 \left[ 1 - \left( \frac{h - hmF2}{hm - h'} \right)^2 \right] \quad (8)$$

The other contributing ionospheric layer, F1, mostly active daily, can be modelled by a simple linear model.

Long-term continuous experimental monitoring have revealed the firm correspondence between TEC and critical frequency's time series (Lilensten, Pibaret and Lemieux-Dudon, 2004), with conclusion that TEC and (especially  $f_0F2$ ) critical frequencies dynamics can be governed by the same process. This provides us with the key milestone in establishing the theoretical framework for relation the GPS ionospheric delay and TEC to the space weather indices.

## 5 PROPOSED THEORETICAL FRAMEWORK

The process of free electron generation in the mid-ionospheric layers is governed by the continuity equation (Davis, 1990, Hunsucker and Hargreaves, 2007), as follows:

$$\frac{dN_e}{dt} = q - \frac{\beta \alpha N_e^2}{\beta + \alpha N_e} \quad (9)$$

where:

$\alpha$  ... mean dissociative recombination coefficient

$\beta$  ... parameter determined by molecular density

$N_e$  ... the free electrons concentration

At the higher ionospheric layer, the rate of the increase of free electron concentration is modelled as follows:

$$\frac{dN_e}{dt} = q - \beta N_e \quad (10)$$

where:

$$q = \frac{\Phi(\infty) \eta}{H_p \epsilon} \quad (11)$$

$$H_p = \frac{KT}{\bar{m} g} \quad (12)$$

with:

$K$  ... Boltzman constant

$T$  ... absolute temperature at the height  $h$   $m$  ... average molecular mass

$g$  ... gravitational acceleration

$\eta$  ... number of ionised particles pairs generated by a single photon

$\Phi(\infty)$  ... solar flux above the atmosphere, expressed as  $\left[ \frac{\text{photons}}{m_2} \right]$

The absolute temperature of the ionospheric layer at the height  $h$  can be expressed as (Davis, 1990):

$$T = T_{\infty} - (T_{\infty} - T_{120}) e^{-s(h-120)} \quad (13)$$

where:

$$T = T(h)$$

$T_{\infty}$  ... exosphere temperature ( $T(h \rightarrow \infty)$ )

$h$  ... height

$s$  ... coefficient dependent on the exosphere temperature

Exosphere temperature can be related to solar flux using the experimentally devised expressions (Davis, 1990), as follows:

$$T_{\infty - min} = 379 + 3.24 \bar{F} + 1.3(F - \bar{F}) \quad (14)$$

where:

$F$  ... actual value of solar flux for the time of  $T_{\infty}$  estimation

$\bar{F}$  ... solar flux average during a longer period of observation

Another experimental model relates the exosphere temperature increase to planetary Kp index (Davis, 1990), as follows:

$$\Delta T_{\infty} = 28 Kp + 0.03 e^{Kp} \quad (15)$$

With (14) and (15) relating the exosphere temperature to indices of solar and geomagnetic activities, the generation of free electrons in the upper atmosphere, vertical ionospheric profile and, consequently, TEC and GPS ionospheric delay are related to the space weather indices.

Furthermore, as (Lilensten, Pibaret and Lemieux-Dudon, 2004) reported the correlation between time series of TEC values and critical frequencies of the ionospheric layers, it is worth noting the experimentally identified models of dependences of the critical frequencies of E and F1 layers, respectively, on the twelve months-average sunspot number R12 as follows ( $\chi$  is the solar zenith angle):

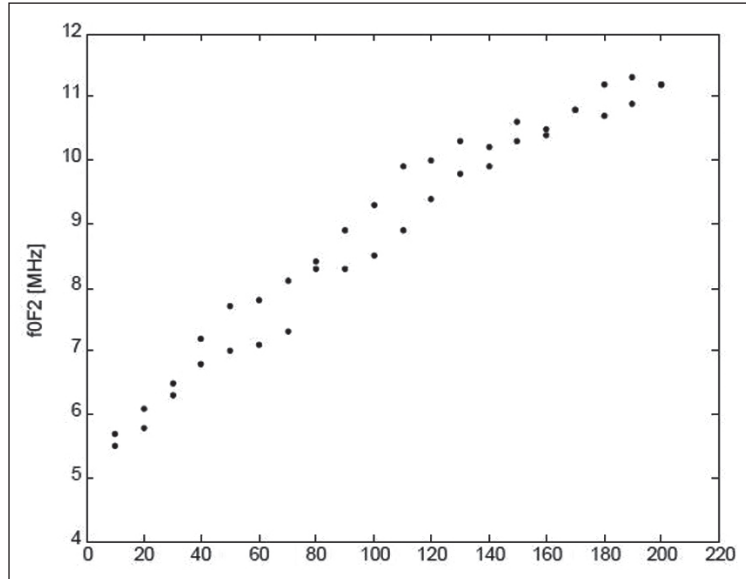
$$f_0 E(\text{daily}) = 0.9 \cdot [(180 + 1.44 \cdot R_{12}) \cdot \cos \chi]^{\alpha} \quad (16)$$

$$f_0 E(\text{midnight}) = 0.36 \cdot (1 + 0.098 \cdot R_{12})^{0.5} \quad (17)$$

$$f_0 E(\text{sunrise, sunset})=1.05 \cdot (1+0.008 \cdot R_{12})^{0.5} \quad (18)$$

$$f_0 F1=(4.3+0.01 \cdot R_{12}) \cdot \cos^{0.2} \chi \quad (19)$$

**Figure 6**  
Non-linear  
relationship between  
f0F2 parameter  
(vertical axis, in  
[MHz]) and sunspot  
number (horizontal  
axis, unit-less)



However, the dynamics of the critical frequency of F2 layer f0F2 shows more complex relation to the space weather parameters (Fig 6) that cannot be modelled as easily as it is the case with E and F1 layers.

## 6 DISCUSSION

The proposed theoretical framework combines space weather, geomagnetic and ionospheric activities with the emphasis on the identification of the effects affecting satellite navigation.

The established experimental models determine the relation between the exosphere temperature, the main driver of the ionospheric layer generation, and the space weather indices (solar flux and K index).

Experimental models relate the vertical geometrical shape of the ionospheric layers with space weather indices, thus allowing for TEC, and therefore the GPS ionospheric delay as well, to be analytically determined by space weather, geomagnetic and ionospheric conditions.

Proposed theoretical framework has a potentially limited accuracy of real-time TEC/GPS ionospheric delay estimation caused by utilisation of averaged values of space weather parameters. The extent of this limitation is to be proven with further experimental studies.

## 7 CONCLUSION

Space weather affects GPS ionospheric delay in a complex non-linear fashion. A theoretical model that relates the common space weather indices with the GPS ionospheric delay was presented.

Future work is to be focused on improved modelling of sudden ionospheric disturbances and the effects of local ionospheric disturbance on a single frequency GNSS ionospheric delay, experimental assessment of the framework's accuracy in real-time estimation of GPS ionospheric delay as well as on correlation between TEC and f0F2 dynamics.

## REFERENCE

- [1] Booker, H. G. (1954). Morphology of Ionospheric Storms. *Proc. NAS*, 40, pp 931–943.
- [2] Davis, K. (1990). *Ionospheric Radio*. Peter Peregrinus Ltd. London, UK.
- [3] Filjar, R and D Huljenic. (2012). The importance of mitigation of GNSS vulnerabilities and risks. *Coordinates*, 8(5), 14-16. Available at: <http://bit.ly/Mv4QSc>, accessed on 10 July, 2012.
- [4] Filjar, R., T. Kos, S. Kos. (2009). Klobuchar-Like Local Model of Quiet Space Weather GPS Ionospheric Delay for Northern Adriatic. *Journal of Navigation*, 62, 543–554.
- [5] Filjar, R. (2008). A Study of Direct Severe Space Weather Effects on GPS Ionospheric Delay. *Journal of Navigation*, 61, 115–128.
- [6] Filjar, R., T. Kos. (2006). GPS Positioning Accuracy in Croatia during the Extreme Space Weather Conditions in September 2005. *Proc European Navigation Conference ENC 2006*. Manchester, UK.
- [7] Filjar, R. (2001). Horizontal GPS Positioning Accuracy During the 1999 Solar Eclipse. *J of Navigation*, 54, 293–296. Cambridge University Press.
- [8] Helliwell, R. (2006). *Whistlers and Related Ionospheric Phenomena* (2nd ed.). Dover Publishing. Mineola, NY.
- [9] Hunsucker, R D, J K Hargreaves. (2007). *The High-Latitude Ionosphere and its Effects on Radio Propagation*. Cambridge University Press. Cambridge, UK.
- [10] Klobuchar, J. A. (1987). Ionospheric Time-Delay Algorithm for Single-Frequency GPS Users. *IEEE Trans on Aerospace and Electronic Systems*, 23(3), 325–331.
- [11] Liliensten, J., B. Pibaret, B. Lemieux-Dudon. (2004). A morphological study of the Integrated Total Electron Content and F region parameters using EISCAT in the frame of

Space Weather. EISCAT Technical Report 04/54. EISCAT Scientific Association. Kiruna, Sweden.

- [12] Lockwood, M. et al. (1999). Predicting Solar Disturbance Effects on Navigation Systems. *J of Navigation*, **52**, 203–216. McNamara, L. F. (1991). *Ionosphere: Communications, Surveillance and Direction Finding*. Krieger Publishing.
- [13] Malabar, FL. Parkinson, B. W., J. J. Spilker, Jr. (editors). (1996). *Global Positioning System: Theory and Applications (Vol. I)*. AIAA. Washington, DC.
- [14] Sandford, W. H. (1999). The Impact on Solar Winds on Navigation Aids. *J of Navigation*, **52**, 42–46.
- [15] Thomas, M et al. (2011). *Global Navigation Space Systems: reliance and vulnerabilities*. The Royal Academy of Engineering. London, UK. Available at: <http://bit.ly/feFB2i>.



Faculty of Maritime Studies  
University of Rijeka, Croatia



Royal Institute of Navigation  
Science Technology Practice



The University of  
Nottingham

**6<sup>th</sup> GNSS**  
Vulnerabilities  
and Solutions  
Conference

# A PROPOSAL FOR A GNSS FAILURE LEGAL LIABILITIES SCHEME

**Renato Filjar, Axel Luttenberger, Serdjo Kos**

Faculty of Maritime Studies, University of Rijeka, Rijeka, Croatia  
Studentska ulica 2, 51000 Rijeka, Croatia  
E-mail: renato.filjar@gmail.com

**ABSTRACT.** *The proper scheme of legal liability for the management of legal consequences of a GNSS failure has become an important GNSS utilisation issue for some time. As the GNSS has become both the enabling and the underlying foundation to a growing number of systems and services, the quest of legal liability emerges as an important component of the establishment of the GNSS business environment. Considering the current state of the art, the GNSS should be considered a component of the national infrastructure, along with the systems such as those for power distribution or the national airspace.*

*Here we present a proposal for a legal liability scheme in the case of the GNSS failure, which is based on the spatial, technology and business environment shared liability. Reflecting the GNSS utilisation from the service provision perspective, this proposal requests the GNSS risks assessment, and mitigation plan to be prepared by the GNSS business environment stakeholders. Under the proposed scheme, the national regulatory agency and the service providers should take a portion of legal responsibility for provision of the guaranteed level of the GNSS positioning and timing service, thus allowing for sustained provision of the GNSS performance and the quality of GNSS-based services.*

**KEY WORDS:** *GNSS failure, liability scheme, GNSS-based services, legal framework*

## 1 INTRODUCTION

The widespread utilisation of the satellite navigation technologies allow more people to use GNSS either directly or embedded within complex technological and socio-economic systems. Satellite navigation applications range from navigation, through transport-, financial- and telecommunications-related services, to national security and public safety, thus establishing the GNSS as a component of national infrastructure.

The GNSS utilisation in various technological and socio-economic systems means that GNSS will be increasingly used mostly by users with poor GNSS education and interest in technology, and in challenging positioning environments with natural and artificial threats to GNSS integrity and performance. Operators of satellite navigation systems can guarantee the GNSS service performance only in favourable positioning environments that are completely opposite to the environments in which majority of GNSS users utilise the technology. The growing number of GNSS-based services ask for the establishment of the GNSS failure legal liabilities scheme for the cases of damages to property, health and life. After establishing the framework for its deployment, we propose the appropriate GNSS failure legal liability scheme based on shared responsibility between the stakeholders of GNSS-based services business environment.

## 2 GNSS AS A COMPONENT OF NATIONAL INFRASTRUCTURE

Human population can be considered navigation oriented, with a number of individual and common societal activities (such as economy and transport) being firmly navigation-oriented. Satellite navigation has brought unprecedented enhancement in ability to accurately and robustly estimate one's position in space. With a growing number of technology and socio-economic applications, satellite navigation systems have matured to the level of being considered a public goods. Embedded in numerous technological and socio-economic systems, GNSS has become a component of national infrastructure in a way that its performance and operation should be sustained for the benefits on the national level. While the GNSS supports provision of fundamental, regulated and commercial (private) services, the satellite navigation technology can be found in national, as well as in regulated and commercial (private) infrastructure. GNSS failure, caused by either operational failure, or a failure to sustain the expected positioning, navigation and timing (PNT) performance will inevitably



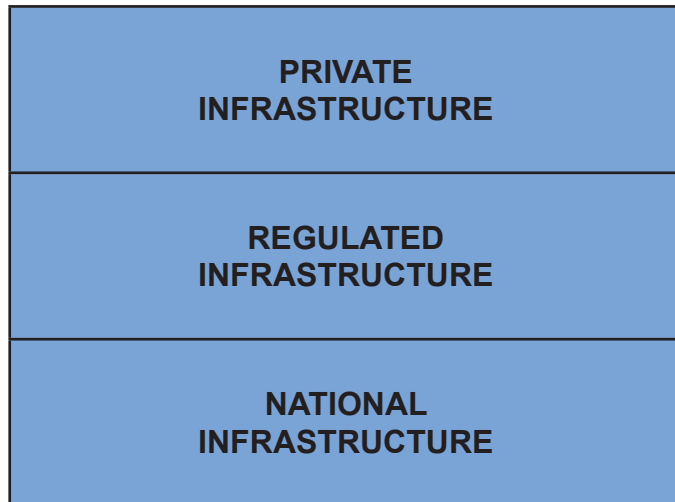
**Figure 1**  
GNSS improves services and processes in various segments of transport (in the air, on the sea and on land), but increasingly extends its reach to non-navigation disciplines



lead to considerable deterioration or even temporal suspension of a wide variety of services.

Sustained PNT GNSS services provision is therefore essential for economic growth, safety and security, and receives the nation-wide sustainability and protection priority. This applies to both navigation-related and non-navigation applications of GNSS.

**Figure 2**  
All three layers of infrastructure in support of a wide variety of services available nation-wide utilise GNSS



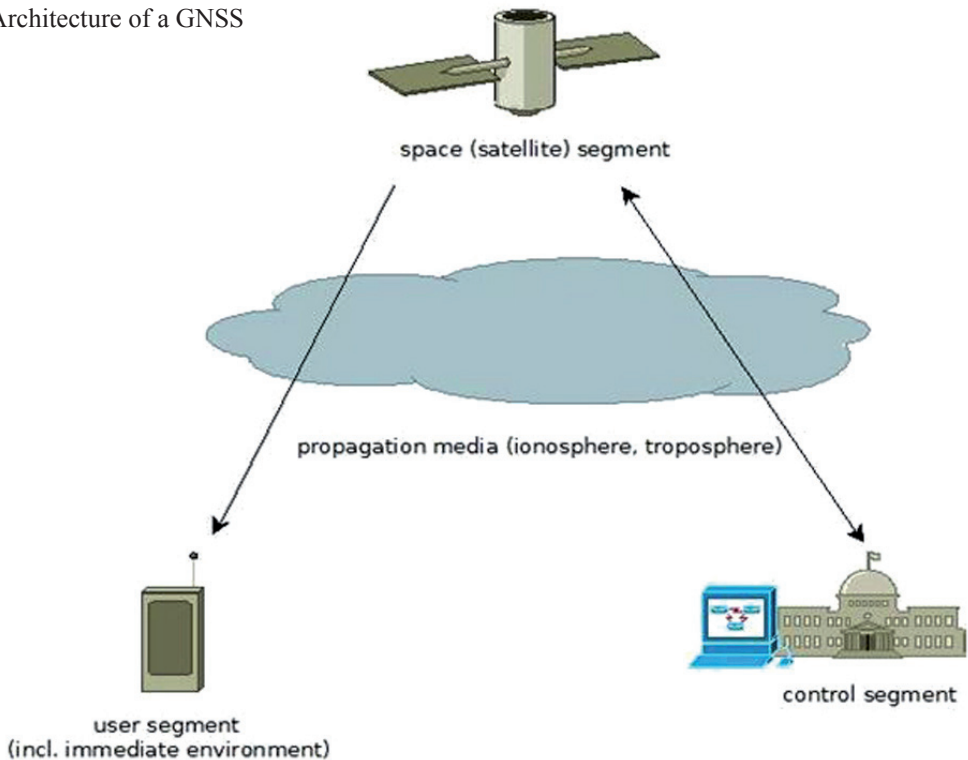
### 3 CORE GNSS VULNERABILITIES AND RISKS

Core GNSS vulnerabilities and risks arise as the effects of both natural and artificial (man-made) sources. Those can ignite the GNSS vulnerabilities and risks by either affecting the positioning estimation errors, or reducing the availability of the PNT services. The vulnerabilities and risks of satellite navigation systems' usage emerge as result of the core nature of the GNSS operation, its architecture, and the environment in which the GNSS operations are performed, as depicted on Fig 3.

Comprising four essential components, the GNSS architecture does not allow for complete control of the system's operation and performance by any single stakeholder (system's operator, regulator, end-user or any other). Thus online a limited assurances can be offered in regard to the quality of system performance and operation, although it is kept at every high level.

**Figure 3**

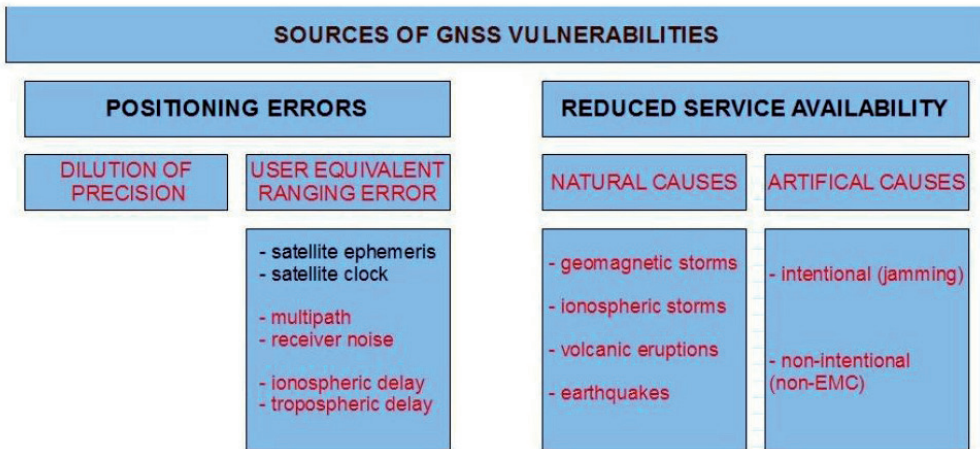
Architecture of a GNSS



The errors in positioning estimation result in combined effects of Dilution of Precision (DOP) and User Equivalent Ranging Errors (UERE), where the ionospheric delay and multipath emerge as the most influential sources. A proper modelling and forecasting of the ionospheric dynamics (for GNSS ionospheric delay) and hardware, software and operational solutions (for multipath-caused errors) can successfully mitigate the positioning errors as a source of GNSS vulnerabilities and risks for a wide range of GNSS applications, at least to a bearable levels. Mitigation of causes of reduced PNT service availability is much harder to overcome. The effects of some natural causes of GNSS vulnerabilities and risks may be identified or forecast relatively easily, but the transfer of this knowledge to community of GNSS users still seems to be a daunting task. For the rest, it is the quest for continuous monitoring of geophysical processes on the local scale and learn of the mechanism and patterns that will lead to establishment of new prediction models related to effects on GNSS PNT performance and system's operation. On the other side, the effects of the artificial sources of disruptions and deteriorations of GNSS PNT services have become increasingly

**Figure 4**

Sources of GNSS vulnerabilities



frequent and disastrous. The abundance of low-cost low-priced GNSS jamming equipment raises concerns of potentially devastating effects on GNSS-based systems and services.

## 4 GNSS RESILIENCE SCHEME

In its essence, satellite navigation technology was not designed to satisfy all the demands of modern GNSS-based systems and services. Still, the freely globally available (i. e. non-royalty) PNT service has attracted a huge attention at both commercial and non-commercial (incl. governments and science) communities, raising the quest on how to properly address the GNSS vulnerabilities and risks problems in a system with distributed (i. e. non-centralised) control.

These authors have proposed a GNSS resilience scheme, depicted on Fig 5, aimed at solution of the problem of curbing the GNSS vulnerabilities and risks problem. The main actions comprised by the proposed GNSS resilience scheme include the following operation segments:

- preparatory segment (particular threats identification, individual risk assessment for every GNSS-based system or service user),
- monitoring segment (continuous monitoring of relevant parameters that indicate the time of appearance and nature of the known threats),
- operational segment (comprising activities following the identification of the threat, such as: alerting targeted group of GNSS users, corrective

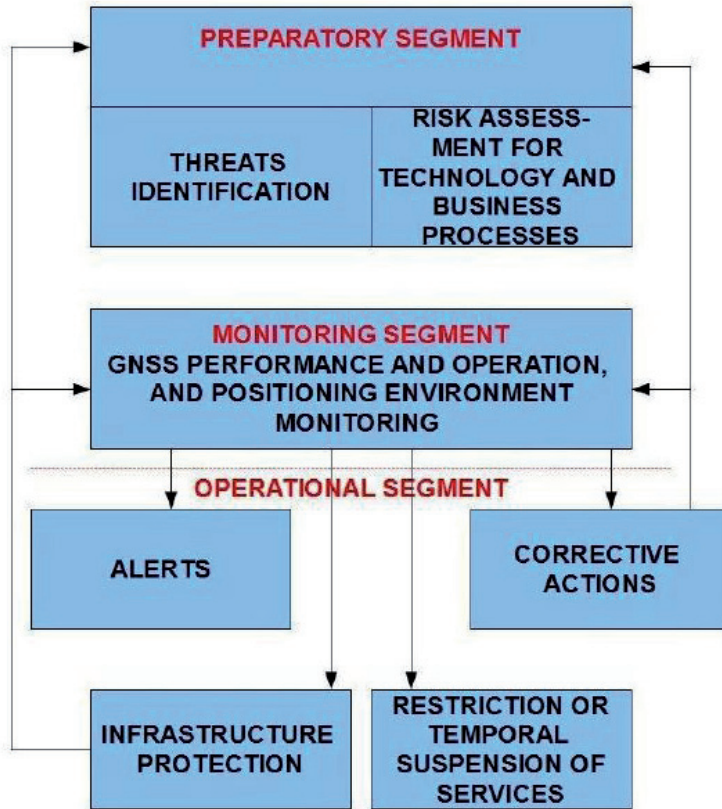


**Figure 5**  
GNSS resilience  
scheme

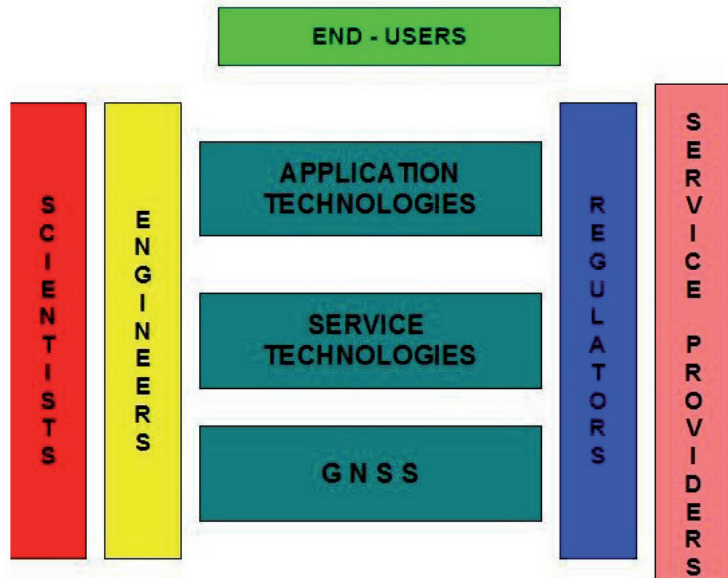
actions deployment, suspension of GNSS-based services and protection of the infrastructure).

## 5 BUSINESS ENVIRONMENT FOR GNSS-BASED SERVICES

Satellite navigation is a fundamental technology, utilised to provide a plethora of commercial and non-commercial services. End-users use services through interaction with the related applications.

The establishment of technologies-services-applications hierarchy is a task conducted by a number of stakeholders (scientists, engineers, regulators, service and content providers, technology operators and en-users), as presented on Fig 6. The engagement of every stakeholder within the business environment for GNSS-based systems and services means that relations between them has been established, and that every stakeholder influences not only the business balance, but also the essential balance of system and services performance and operation.

**Figure 6**  
Business environment  
for GNSS-based  
systems and services



## 6 PROPOSAL FOR GNSS FAILURE LEGAL LIABILITIES SCHEME

Considering the role of the GNSS within the national infrastructure (Chapter 2), the complexities of core GNSS vulnerabilities and risks (Chapter 3) and the business environment for GNSS systems and services (Chapter 5) and the need for utilisation of the GNSS resilience scheme (Chapter 4) for the purpose of curbing the GNSS vulnerabilities and risks, here we propose the scheme for identification of legal liabilities due to the GNSS failure to provide expected performance of PNT service. Assuming that in certain cases the failure in provision of expected GNSS PNT service can lead to material and financial damage, and/or injuries or loss of life, our proposal attempts to fill in the gap of defining the legal liability for cases in question.

Our proposal for the GNSS failure legal liability scheme is based on the shared liability concept, instead of the sole liability of the GNSS operator, that comprise all stakeholders of the GNSS business environment within the limits of their effects and contributions to GNSS business and technology environment (Fig 7, Table 1).

Furthermore, our proposal calls for joint effort of all GNSS-related stakeholders in provisioning reasonable alerts of misused utilisation of satellite navigation-based systems and services, and of alerting on deteriorating conditions for GNSS utilisation.



**Figure 7**  
Concept of the shared liability for GNSS failures

**Table 1**

| Legally liable subject       | Causes of loss   |
|------------------------------|--|
| GNSS operators               | Core system failure, failure in global GNSS assistance and augmentation provision, failure in provision of alerts on global ionospheric and the other global natural effects   |
| National regulators          | Failure in GNSS signal and spectrum protection on national level, failure in combating local jamming and spoofing, failure in regulating GNSS-based service provisioning   |
| GNSS-based service providers | Failure in advising and fostering the proper use of robust standardised equipment, failure in combating user-initiated jamming, failure in provision of targeted GNSS performance deterioration alerts, failure in robust provisioning of GNSS-based services, failure in conducting the risk assessment |
| End-users                    | All remaining failures, including misconducts, and equipment misuse and unlicensed modifications.  |

## 7 DISCUSSION

GNSS failure may cause loss of life, injuries, material and financial damage. Since the GNSS failure legal liability has not regulated at the international level, this paper attempts to clarify the situation and propose the shared liability concept based on the areas of reasonable impact on GNSS-based services and systems.

Present view on the problem assumes the GNSS operator’s responsibility. We argue that national regulators, service providers and end-users should be engaged

in the scheme, accepting responsibilities for their actions and legal liabilities for the failures in their respective areas of operation. Within the proposed scheme, we call for proper risk assessment, preparations of corrective actions, and their operational status in case of particular threats to GNSS performance and operations.

Finally, we emphasise the request for co-ordinated efforts between GNSS operators, national authorities and service providers in establishment and operation of the GNSS resilience scheme on the national level.

## 8 CONCLUSION

Raising number of GNSS-based services and systems accentuate the importance of the establishment of the GNSS failure legal liability scheme. We presented a proposal for such a scheme, based on understanding of sources of GNSS vulnerabilities and risks, and GNSS applications business environment, GNSS resilience scheme, and the fact that GNSS has become a component of national infrastructure. Based on shared responsibility concept, the proposed GNSS failure legal liability scheme defines clear legal liability for every stakeholder and fosters the implementation of GNSS resilience scheme as nation-wide contribution to provision of sustained GNSS performance to the end-users.

## REFERENCE

- [1] Bollweg, H-G. (2008). Initial Considerations regarding the Feasibility of an International UNIDROIT Instrument to Cover Liability for Damage Caused by Malfunctions in Global (Navigation) Satellite Systems. International Institute for the Unification of Private Law (UNIDROIT). Rome, Italy. Available at: <http://bit.ly/s7dlb8>, accessed on: 2 January, 2012.
- [2] Carbone, S M, M E De Maestri. (2009). The Rationale for an International Convention on Third Party Liability for Satellite Navigation Signals. International Institute for the Unification of Private Law (UNIDROIT). Rome, Italy. Available at: <http://bit.ly/s3DfB2>, accessed on 2 January, 2012.
- [3] Filjar, R, H Gold, I Markežić. (2011). GNSS – the risk of the underlying technology. *Proc of 5th GNSS Vulnerabilities and Solutions Conference*. Baska, Krk Island, Croatia.
- [4] Filjar, R, K Vidovic, P Britvic. (2011). Scenarios of critical GPS positioning performance for eCall (4 pages). *Proc of 5th GNSS Vulnerabilities and Solutions Conference*. Baska, Krk Island, Croatia.
- [5] Filjar, R, S Kos, K Vidović. (2010). Global Navigation Satellite System as a Component of National Infrastructure. *UN/Moldova/US Workshop on GNSS Applications*. Kishinev, Moldova.

- 
- [6] Filjar, R. (2009). Satellite navigation as a component of national infrastructure. *53rd European Organization for Quality Annual Congress*. Cavtat/Dubrovnik, Croatia.
  - [7] UNIDROIT Secretariat. (2010). An instrument on third party liability for Global Navigation Satellite System (GNSS) services: a preliminary study. International Institute for the Unification of Private Law (UNIDROIT). Rome, Italy. Available at: <http://bit.ly/vCUJDQ>, accessed on 2 January, 2012.





Faculty of Maritime Studies  
University of Rijeka, Croatia



Royal Institute of Navigation  
Science Technology Practice



The University of  
Nottingham

**6<sup>th</sup> GNSS**  
Vulnerabilities  
and Solutions  
Conference

## SCINTILLATION ASSESSMENT TOOLS

*Tools to assess the influence of scintillation on  
positioning quality*

**Peter Kieft**

Marie Curie Fellow at University of Nottingham  
University Park, Nottingham, NG7 2RD, UK  
E-mail: Peter.Kieft@nottingham.ac.uk

**ABSTRACT.** *Scintillations are rapid fluctuations of the phase and amplitude of satellite radio signals travelling through the ionosphere, caused by time varying electron density irregularities. Scintillations can have a considerable effect on the performance (e.g. Positioning Quality) of Global Satellite Navigation Systems (GNSS) as they may reduce the accuracy of the pseudo-range and phase measurements and can even cause a loss of lock on the signal.*

*The paper will discuss some tools which are under development to monitor the occurrence of scintillation and to assess the impact on the final positioning quality through Fugro's worldwide network of GNSS stations and a network of stations operated by the University of Nottingham.*

**KEY WORDS:** *GNSS, scintillations, assessment tools*

## 1 INTRODUCTION

The adopted strategy to investigate and develop real time and post mission mitigation tools against effects of scintillations on GNSS positioning (author's task within TRANSMIT work package 4.1) is to start off with the development of some initial tools to monitor scintillation events and assess their impact on the position quality. Two mailing services have been setup, the first one in collaboration with Fugro Intersite, monitoring Fugro's worldwide network of GNSS receivers for possible scintillation related effects. The second mailing service uses the scintillation monitoring receivers operated by the University of Nottingham to inform about scintillation events.

A separate more in depth windows program (Scintillation Assessment Tool) is being developed to further assess the occurrence of scintillation and to perform a position calculation on the data to see the impact of scintillation on the position quality.

## 2 MAILING SERVICES

The mailing services aim to inform about possible significant scintillation events and hence make event selection for further analyses easier. The Fugro mailing service is able to give a worldwide overview of possible scintillation occurrence using loss of lock indicators as it uses geodetic grade receivers and not scintillation receivers. The Nottingham scintillation service is limited in coverage but since it uses scintillation monitoring receivers it can provide much more detail on scintillation events and can more easily differentiate between scintillation, interference and obstructions.

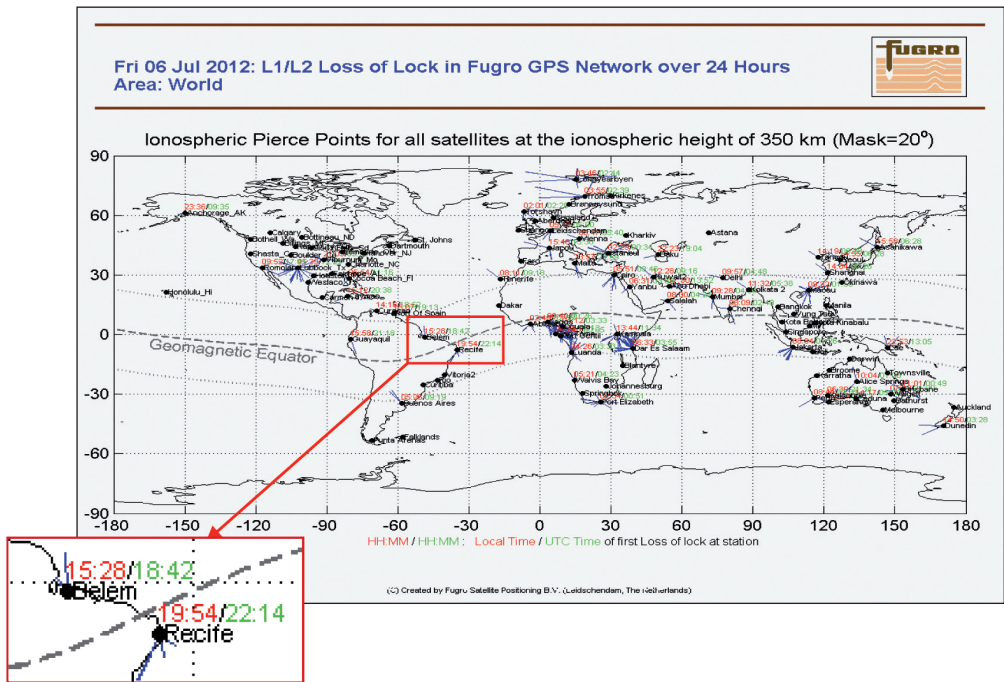
### 2.1 Fugro mailing service

The Fugro mailing service has been developed in cooperation with Fugro Intersite. Fugro Intersite is a Research and Development company within the Fugro group. Fugro Intersite's objective within the group is to develop software and solutions aiding the operations and products from other companies within the Fugro group. Part of their work is to deliver a quality control service from a positioning service user perspective. In order to do so it utilizes the data from the worldwide Fugro network of receivers as sent to the users via geostationary satellite(s) or other means of communication. The Fugro mailing service can be set up through an initialisation file to define the regional maps and for which stations an azimuth/elevation and local time/elevation plot has to be included.

### 2.1.1 Worldwide and regional scintillation maps

The world map (see Figure 1) shows a daily overview of all losses of lock on all GPS satellites. A loss of lock can occur because of scintillation but also because of interference or signal blockage. The blue lines in the graph present the satellite – receiver links mapped to the ionospheric pierce point above a set elevation mask (20 degrees). The elevation mask can be set to take out low elevation signal blockage. The times in red and green present the first loss of lock of the day in local and UTC time, respectively. The local time can indicate interference when a loss of lock occurs frequently over successive days at the same local time.

**Figure 1**  
World overview of losses of lock



A more detailed view can be obtained looking at the regional plots (see Figure 2). The satellite receiver links are now presented by coloured lines (PRN colour scheme) again mapped to the ionospheric pierce point. Blue dots show the missing epochs after a loss of lock has occurred. A mini histogram per affected station presents the relative occurrence of the losses of lock over the day in local time. Around the magnetic equator one would expect the histogram to show that most losses of lock happen after sunset.

**Figure 2a**  
Regional overview losses of lock and missing epochs

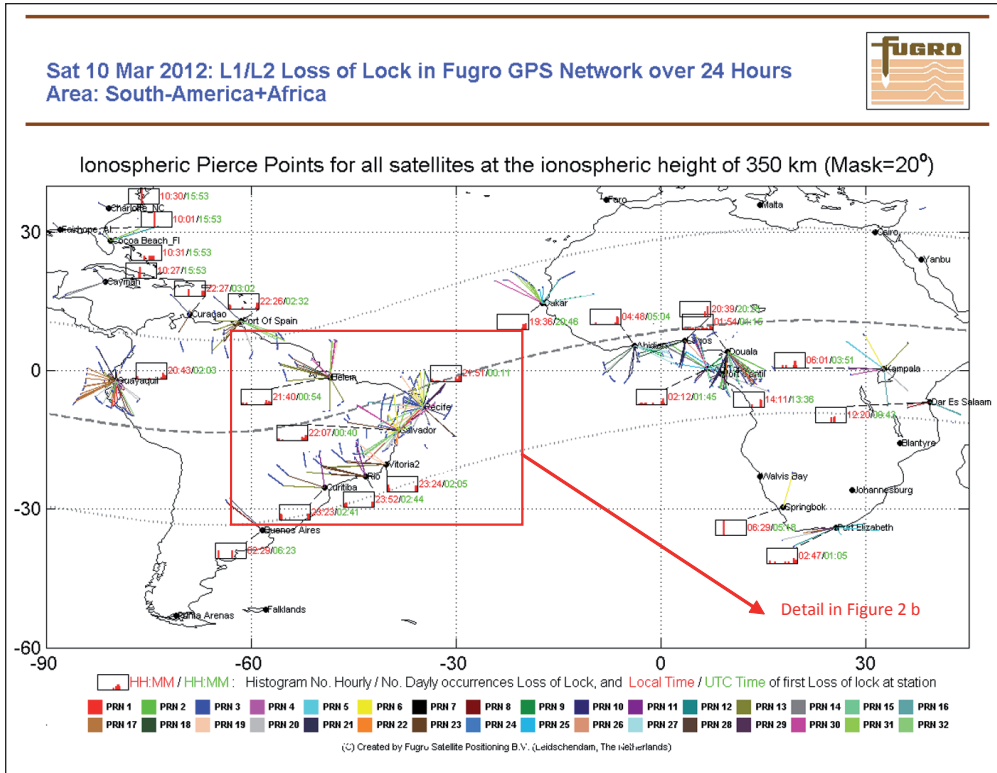
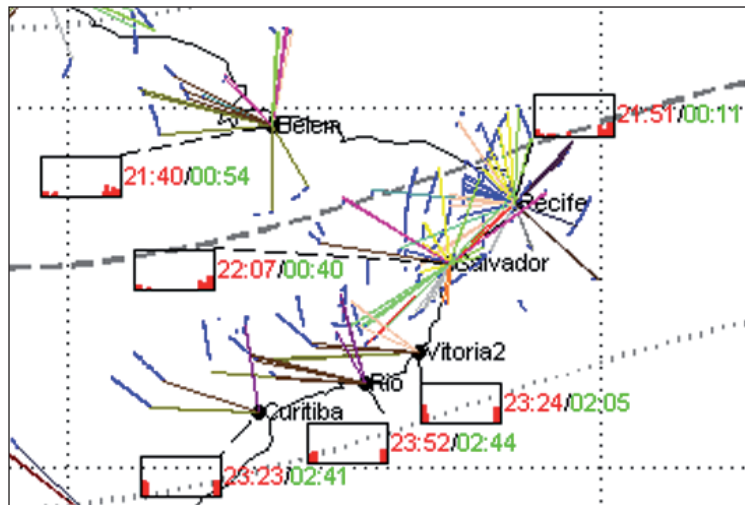


**Figure 2b**  
Detail Figure 2a showing stations in Brazil

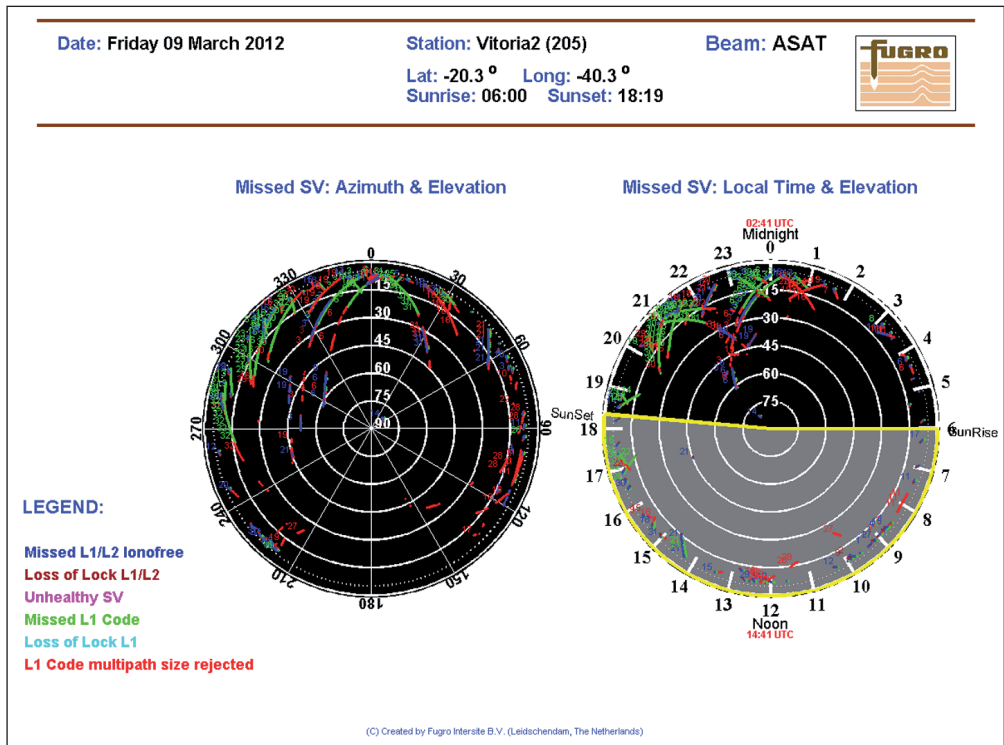


### 2.1.2 Azimuth vs. elevation and local time vs. elevation graphs

The mailing service also allows including stations for more in depth analyses through azimuth/ elevation and local time/elevation plots (see Figure 3). The azimuth/elevation plot makes it possible to easily distinguish between local blockage and possible scintillation. All indicators in Fugro’s propriety format are presented. Most important are the loss of lock L1/L2 indicator and successive missed L1/L2 measurements. The local time/elevation plot shows the same data but in Local Time (depending on the longitude of the station) and makes it easy to find correlation between losses of lock and the local time of the day. Typically at low latitudes the losses of lock, if caused by scintillation, will fall after sunset, which is indicated by sunset and sunrise in the plot.

**Figure 3**

Fugro Mailing Service Station Sky plots

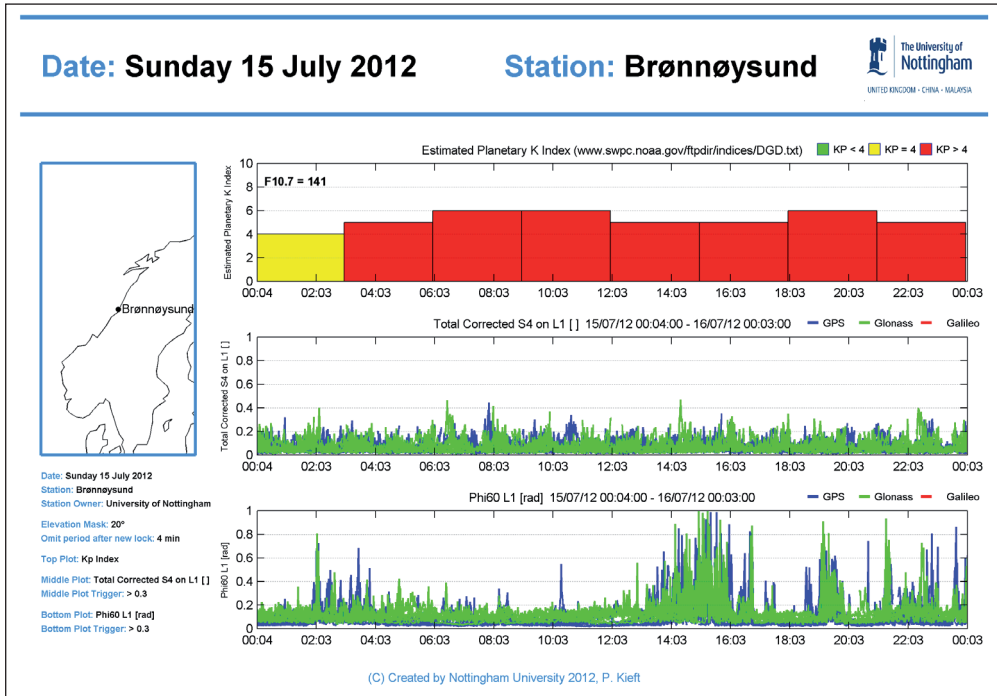


### 2.2 University of Nottingham Scintillation Mailing service

The University of Nottingham Scintillation Mailing service is another initialisation file driven script running on a university server. The initialisation script allows setting various parameters which shape the outcome of the script. A

**Figure 4**

University of Nottingham Scintillation Mailing Service



typical setup (see Figure 4) shows a map with the location of the scintillation monitoring receiver, the Planetary K index over the day, the F10.7 index for the day, the Total Corrected S4 amplitude scintillation index and the Phi60 Phase scintillation index for the day.

Through the initialisation script it is possible to set trigger values for the indices, so only to send the email containing the plot when the scintillation index exceeds the trigger value at any point during the day.

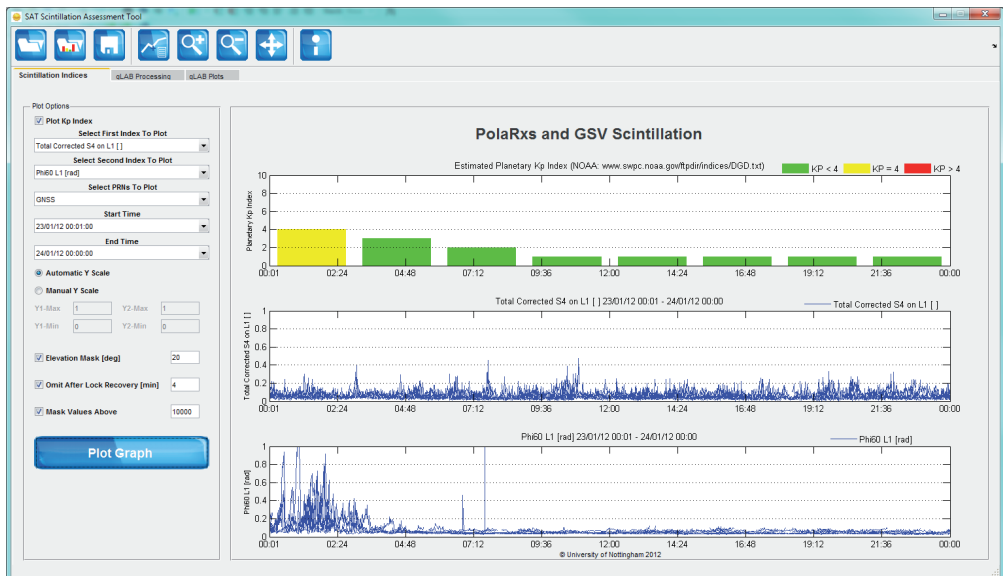
### 3 SCINTILLATION ASSESSMENT TOOL (SAT)

The Scintillation Assessment Tool is a Windows based application serving as a more in depth tool to assess the impact of scintillation. The first tab of the program offers the loading of scintillation data logged by scintillation receivers. Scintillation receivers in use by the University of Nottingham are the PolarXs from Septentrio (www.septentrio.com) and the GSV4004B from Novatel (www.novatel.com), which are capable to calculate and store various ionospheric (e.g. TEC and vTEC) and scintillation (e.g. S4 and SigmaPhi) parameters. SAT can

read the various scintillation file formats and all data (e.g. S4, Phi, TEC, DTEC, etc.) stored in these files can be presented to the user through the graphs in the ‘Scintillation Indices’ tab of the program (see Figure 5). The program incorporates the utilities provided by Septentrio (Septentrio, 2011a, Septentrio, 2011b) and Novatel (Novatel, 2010) for the conversion of file formats. The presented graphs can be exported to a picture file for later use. The planetary K index can be plotted to investigate possible correlation between geomagnetic activity and scintillation, and can be automatically downloaded from the internet. This downloading is done using wget (GNU, 2011).

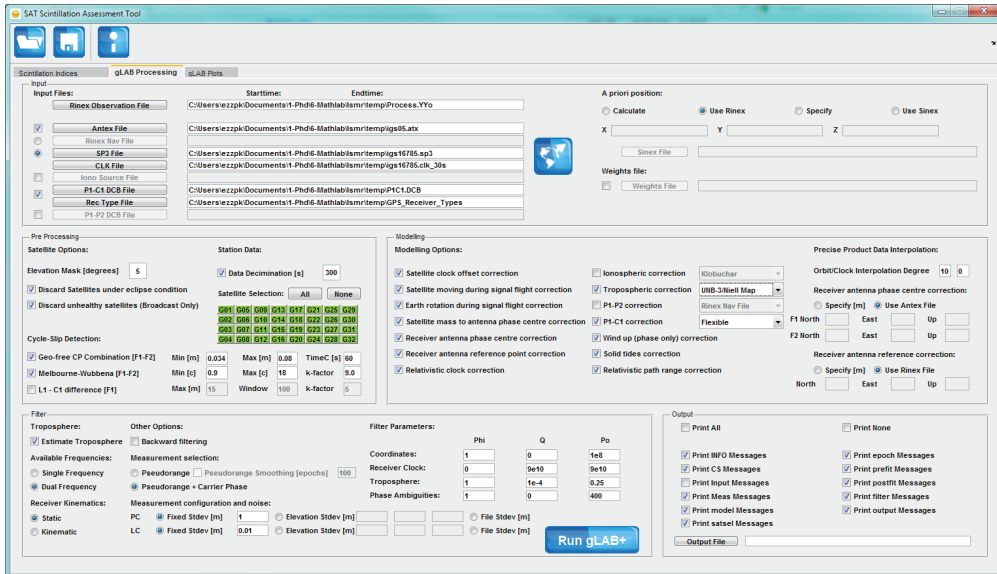
**Figure 5**

SAT, Scintillation Indices



The second tab of the programming is a user interface to the gLAB program (gACE/UPC, 2010). gLAB is a software tool suite developed under an European Space Agency (ESA) contract by the research group of Astronomy and Geomatics (gAGE) from the Universitat Politècnica de Catalunya (UPC). It is an interactive educational multipurpose package to process (Single Point Positioning and Precise Point Positioning) and analyse GNSS data (more info on gLAB and gLAB downloads at [www.gage.upc.edu/gLAB](http://www.gage.upc.edu/gLAB)). The user interface of the tab is very similar to the graphical user interface provided with gLAB but with extensions and various automated tasks (see Figure 6).

**Figure 6**  
SAT, gLAB processing

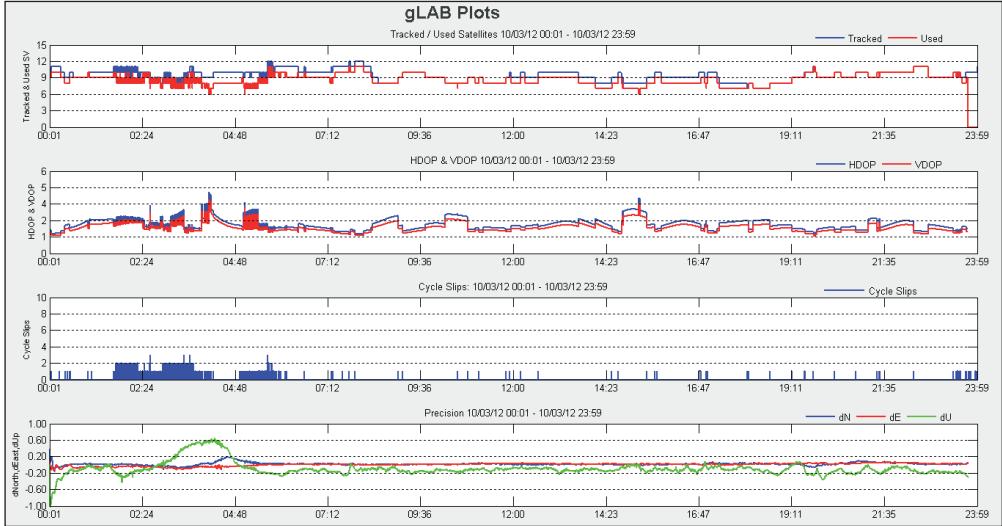


For instance, it is possible to automatically download all dependency files to a selected RINEX or receiver proprietary format (precise ephemeris and clock files, hardware delays, etc.) incorporated by using wget (GNU, 2011). When all input is set SAT will start the gLAB program and let it perform the position calculation. The gLAB program called can either be the default or an adjusted version of gLAB including the new options of the user interface of the SAT program.

The third tab (see Figure 7) allows the plotting of the results from gLAB. Possible plots are: tracked and used satellites, HDOP and VDOP, Cycle slips and positioning accuracy represented by the deviations in Easting, Northing and height from a given 'ground truth'.

**Figure 7**

gLAB plots, with tracked/used SV, HDOP/VDOP, Cycle Slips, and Precision



### 4 EXAMPLE RESULTS WITH SAT

On the 9<sup>th</sup> of March 2012 an ionospheric storm occurred, with Planetary K index values reaching as high as 7 (see Figure 8). Phase and amplitude scintillations were not present during that day but could be observed at a scintillation

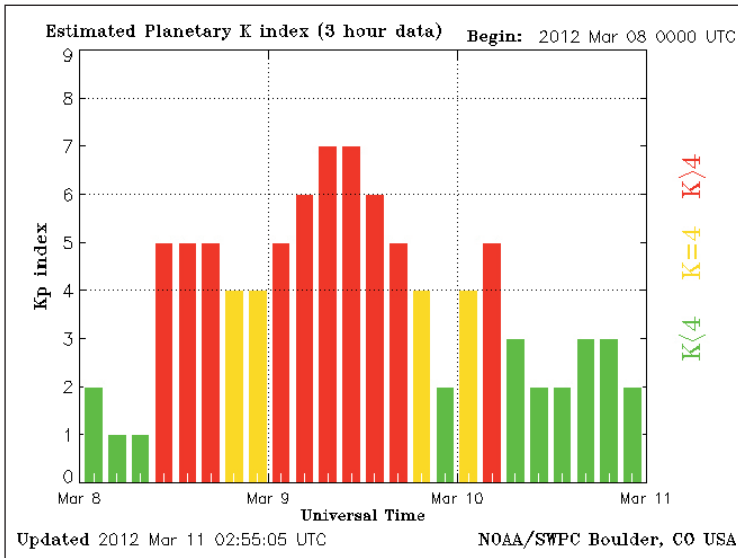


**Figure 8**  
Estimated Planetary K index for 08 – 10 March 2012

monitoring receiver at Presidente Prudente (See Figure 9, Data Source: GSA/FP7 CIGALA project, through UNESP) the next day between 02:00h – 05:00h (See Figure 10), when  $K_p$  reached a value of 5. At equatorial latitudes there is not always a clear relationship between the  $K_p$  index and the observed scintillation, and hence, this example just demonstrates the impact of the occurring scintillation on the position calculation.

### Figure 9

Presidente Prudente and Curitiba Stations in Brazil



Although Fugro's Curitiba station is situated approximately 420 kilometres south - east to Presidente Prudente (See figure 9), it is possible to correlate results for the former with scintillation observed at latter. When Curitiba station data is processed with gLAB, results show that, although enough GPS satellites are available to calculate a position, there is correlation between the cycle slips observed, tracked and used satellites, the precision of the computation result and the period of scintillation observed at Prudente (See Figure 11).

**Figure 10**

Kp, Total corrected S4 and Phi60 for Presidente Prudente on 10/03/2012 (1 day after geomagnetic storm)

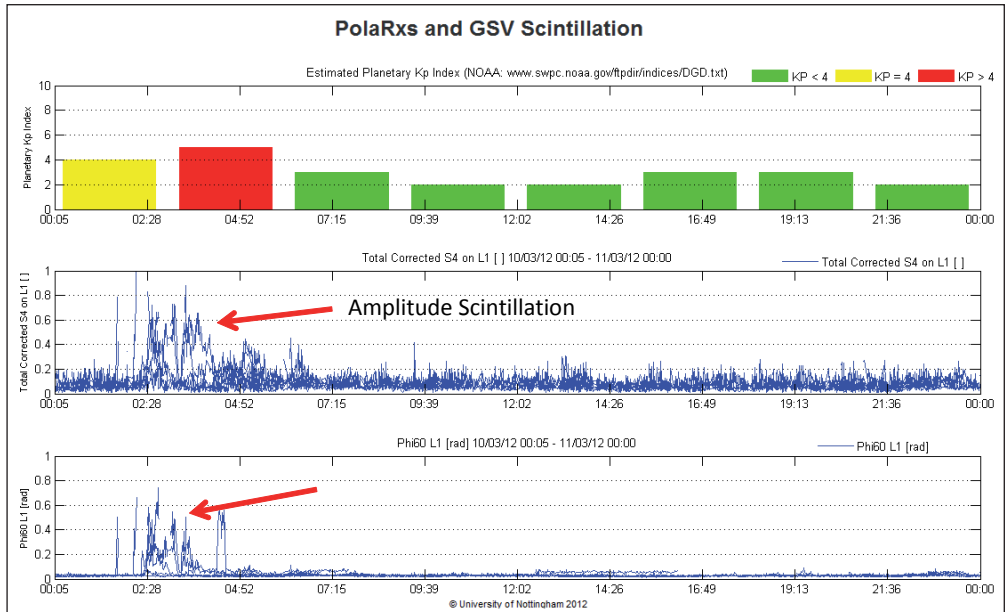
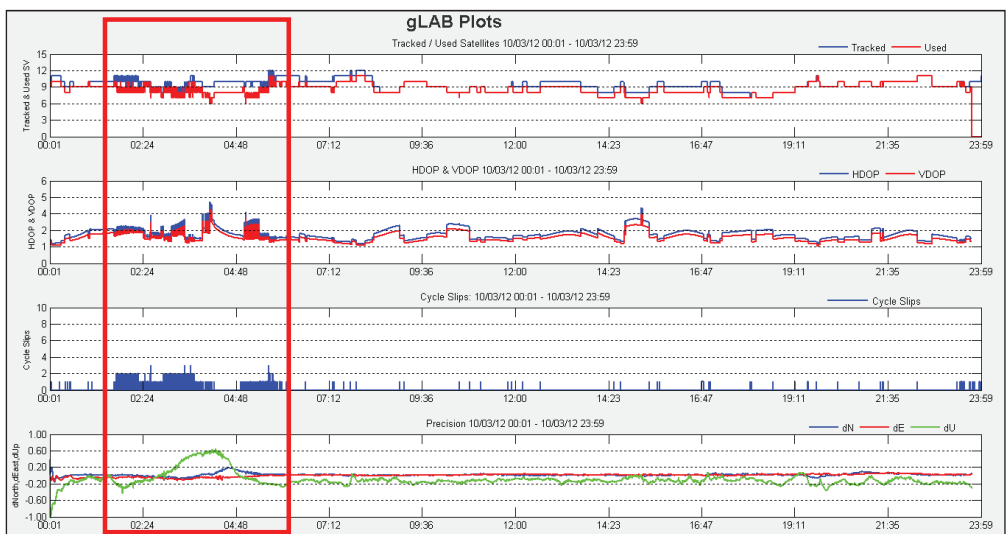


**Figure 11**

Curitiba Kinematic gLAB result



## 5 FUTURE WORK

### 5.1 Mailing Services

The Fugro scintillation tools will be updated to try to improve their capability to distinguish between scintillation, interference and signal blockage. One possibility would be to include more days of data in the program to allow analyses over a longer period. For example, interference could have a daily signature reoccurring at a certain local time, whereas blockage (multipath) will reoccur 4 minutes later with GPS on successive days.

The figures produced with the University of Nottingham mailing tool are planned to also be presented as a web based service on the TRANSMIT website ([www.transmit-ionsphere.net](http://www.transmit-ionsphere.net)). More stations from cooperating universities could be later included in the service.

### 5.2 Scintillation Assessment Tool

The scintillation assessment tool will be further developed and used to assess new and updated positioning algorithms implemented in gLAB and later on in other processing software. A starting point for this will be to incorporate the estimation of tracking errors into gLAB, initially using the Conker model (Conker et al., 2003), in order to introduce a weighting scheme on the satellite – receiver links, according to the method described in (Aquino et al., 2009). The plotting of the results will be further improved, e.g. to include available satellites calculated from the ephemeris data.

#### 5.2.1 *Introducing a modified weight matrix in gLAB*

The idea behind this weighting scheme is to reduce the weights of satellite links that are still tracked by the receiver in correspondence with the prevailing scintillation conditions. This will be achieved by using an input file with weights which are inversely proportional to the tracking error variances, initially based on the Conker model. The Conker model can be used to calculate the tracking error variance for the phase (PLL tracking jitter variance) and for the code measurements (DLL tracking jitter variance) for each satellite/receiver link. The Conker model however can only be applied for S4 index values lower than 0.7 (values of S4 above 0.7 result in a singularity in the model), limiting its use at lower latitudes, where the S4 index will frequently exceed this value. Part of the TRANSMIT project is to improve the tracking of satellite/receiver links under strong scintillation and to estimate the error of the tracked signal, which could then be used as an input for the proposed weighting scheme.

## 6 SUMMARY

This paper has presented the initial tools developed by the author under the TRANSMIT ITN project, in particular in order to investigate novel methods to mitigate the impact of scintillation on the accuracy of GNSS positioning. The aim of these initial tools is monitoring and selecting relevant scintillation events, and assessing the impact of scintillation through a Windows based tool incorporating the gLAB PPP software. Future updates will introduce new features, like a web based monitoring service and the introduction of new algorithms and positioning (sub) programs in the Scintillation Assessment tool.

## ACKNOWLEDGMENTS

The author would like to thank the European Commission for their FP7 Marie Curie ITN program which gives excellent opportunities for researchers in the early stage of their career. Furthermore the author would like to thank his supervisors, Marcio Aquino and Alan Dodson for their input and support and Hans Visser, Yahya Memarzadeh and Kees de Jong from Fugro Intersite for the great opportunity they provided to learn from and work with them. Finally the author would like to thank João F. Galera Monico from UNESP (Universidade Estadual Paulista in Brazil) for making the Presidente Prudente data available through the CIGALA project (<http://cigala.galileoic.org/>).

## REFERENCES

- [1] AQUINO, M., MONICO, J. F. G., DODSON, A. H., MARQUES, H., DE FRANCESCHI, G., ALFONSI, L., ROMANO, V. & ANDREOTTI, M. 2009. Improving the GNSS positioning stochastic model in the presence of ionospheric scintillation. *Journal of Geodesy*, 83, 953-966.
- [2] CONKER, R. S., EL-ARINI, M. B., HEGARTY, C. J. & HSIAO, T. 2003. Modeling the effects of ionospheric scintillation on GPS/Satellite-Based Augmentation System availability. *Radio Science*, 38.
- [3] GACE/UPC 2010. gLAB. 2.0.0 ed.
- [4] GNU 2011. wget. 1.11.4 ed.
- [5] NOVATEL 2010. convert4.
- [6] SEPTENTRIO 2011a. sbf2ismr. 3.2.0 ed.
- [7] SEPTENTRIO 2011b. sbf2rin. 6.1.0 ed.





Faculty of Maritime Studies  
University of Rijeka, Croatia



Royal Institute of Navigation  
Science Technology Practice



The University of  
Nottingham

**6<sup>th</sup> GNSS**  
Vulnerabilities  
and Solutions  
Conference

# INFLUENCE OF SUDDEN IONOSPHERE DISTURBANCES ON VLF COMMUNICATIONS

**Martina Kunšтовиć<sup>1</sup>, Krešimir Malarić<sup>1</sup>, Dragan Roša<sup>2</sup>**

<sup>1</sup> Department of Wireless Communications,  
Faculty of Electrical Engineering and Computing, Zagreb, Croatia  
Zavod za telekomunikacije, Unska 3, 10 000 Zagreb, Croatia  
E-mail: martina.kunstovic@gmail.com

<sup>2</sup> Zagreb Astronomical Observatory, Zagreb, Croatia

**ABSTRACT.** *This paper gives the review on the term Space weather. After defining Space weather, its causes and impacts, Sudden Ionosphere Disturbances (SID) on VLF communications are described. To detect solar events, SID monitor that operates in the VLF range is needed. This paper includes the measurements that were performed with SUPER SID monitor at Zagreb Astronomical Observatory showing one day when there was registered some solar flares captured from four different VLF stations that transmit radio waves in that frequency range. The paper concludes with the interpretation of the measurements.*

**KEY WORDS:** *Space weather, Sudden Ionosphere Disturbances, VLF, SOHO*

## 1 INTRODUCTION

Space weather is a term that represents sum of physical and chemical processes created in area between the Sun and the Earth. Therefore it is defined as: „*Conditions on the Sun and in the solar wind, magnetosphere, ionosphere, and thermosphere that can influence the performance and the reliability of space – borne and ground – based technological systems and can endanger human life or health.*“ – US National Space Weather Programme.

The solar activity can modify the conditions of the solar wind, magnetosphere and atmosphere influencing the radiation and particle output of the Sun, producing corresponding changes in the near Earth space environment, as well as at Earth's surface [1]. The condition of the Sun has a major impact on the Ionosphere propagation for two way radio communications, mobile radio communications and point to point radio communications, satellite communications as well as radio broadcasting. Impacts of Space weather can be divided into impacts on Space Technology, Terrestrial Technology and Living Organisms.

A good understanding of solar physics and solar activity can help understand the Space weather effects and the possibility to avoid them. Solar and Heliospheric Observatory (SOHO) and Advanced Composition Explorer (ACE) are main observations acquired by space missions and have purpose in observing the Sun and Space weather for better understanding of Space weather and implications related to geomagnetic disturbances [2]. In this work, we analyse the influence of Sudden Ionosphere Disturbances (SID) on VLF communications by monitoring the strength of VLF radio waves using SuperSID monitor on Zagreb Astronomical Observatory [3]. First, we discuss Space weather, its definition, causes and consequences (Sec.II) and also present how EM waves propagate through Earth's ionosphere and how SID affect VLF communications (Sec. III). Following that, we show the results of SuperSID MONITOR measurements taken at Zagreb Astronomical Observatory from four VLF stations. Section IV interprets those measurements and concludes this paper.

## 2 SPACE WEATHER

Sun is the main source of Space weather on Earth. It is composed mainly of hydrogen (about 92.1%) and helium (7.8%) together with small traces of heavier elements. The Sun is structured roughly with the core, the radiation layer, and the convective layer. The core is the source of the Sun's energy and has the highest temperature and density and it is the site of thermonuclear fusion. This

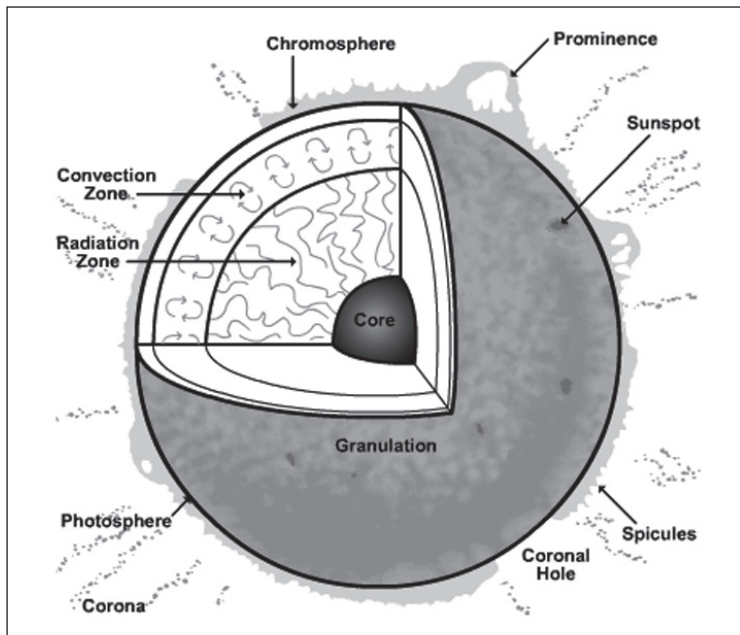


**Figure 1**  
Structure of the Sun

energy is carried to the surface – photosphere [4]. The solar corona is the outermost atmosphere of the Sun (Fig. 1).

Sunspots are regions in the solar photosphere with a magnetic field stronger than the average ( $\Delta \approx 0.4 \text{ nT}$ ). They occur in elaborate groups and each one last from less than one hour to half a year and vary in size from 300 km to 100000 km. The number of sunspots varies with 11 year cycle and they are good indicators of solar activity. Sun's activity cycles last between 8 and 15 years and are numbered. Numbering began in 1755. (Current cycle, 24<sup>th</sup>, began in January 2008). Sunspots contains vast amounts of energy that can be released at certain moments and can result in Coronal Mass Ejection – CME, and be result of solar flares, which can affect the Earth.

CMEs consists of very large structures containing plasma and magnetic fields that are expelled from the Sun into the Heliosphere and can produce disturbances that strike the Earth with sometimes catastrophic results. Travel time is approximately 42 hours to Earth orbit.

Solar flare is defined as electromagnetic radiations – explosions on the surface of the Sun from radio waves to X-rays and gamma-rays. They can be classified as X-class, M-class and C-class from more to less energetic and each class has nine subdivisions ranging. The main effect felt on Earth is an increase in the level of solar radiation and affects radio propagation and radio communications on Earth.

Solar wind originates in corona and streams from the Sun in all directions at speeds of about 400 km/s (about 1 million miles per hour).

It is an expanding coronal gas that fills interplanetary space. The Earth's magnetic field is affected by relatively strong solar winds which compress it on the sun side and on the night side creates a long magnetic tail (comet like) because solar wind contains and conducts the magnetic field due to its high electrical conductivity (Fig 2). This phenomenon is called magnetic reconnection. Solar wind creates heliosphere – bubble that contains our solar system (Fig 3).

**Figure 2**  
Solar wind

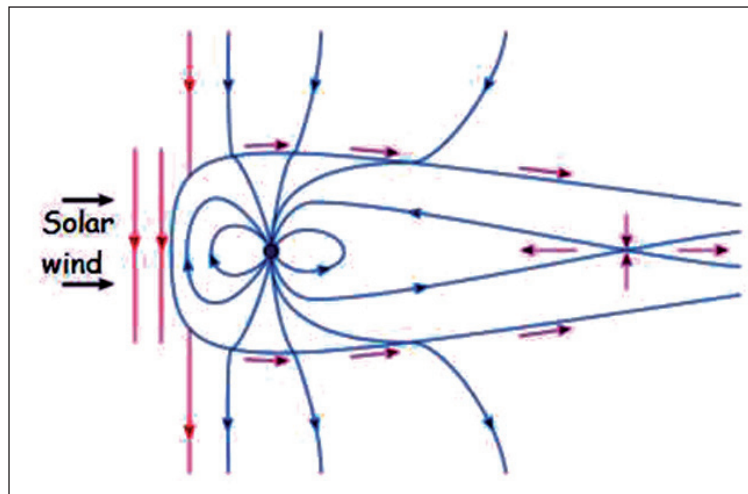
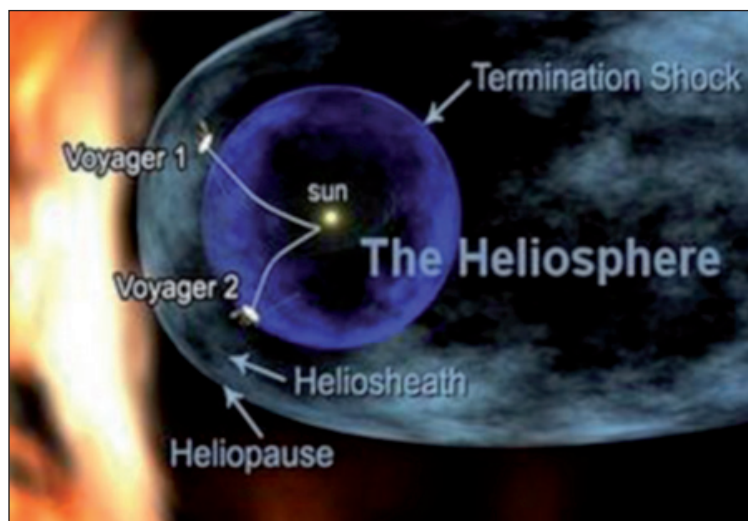


**Figure 3**  
Structure of the Sun



### 3 EM WAVE PROPAGATION THROUGH EARTH'S IONOSPHERE

The ionosphere is the ionized part of the upper atmosphere (60-1000 km) which contains significant numbers of free electrons and positive ions. This is a very important layer for EM wave propagation where increased height increases the concentration of ionized particles. The level of ionization also changes with time. It varies with the time of day, time of year, and according to many other external influences. There are three regions of ionosphere which are shown in Fig. 4. (D layer, E layer and F layer [5]). The intensity of ionizing radiation varies with elevation of the Sun and further affecting the electron density. At night electron density decays because there is no radiation source (Fig. 5.)

#### A. Sudden Ionosphere Disturbances on VLF communications

Sudden ionosphere disturbances or SIDs are the result of high energy electrons that slam into the Earth's ionosphere and influence on ionosphere radio propagation. SID is caused by large solar flares and CMEs. SID has its effects on VLF radio waves [6].

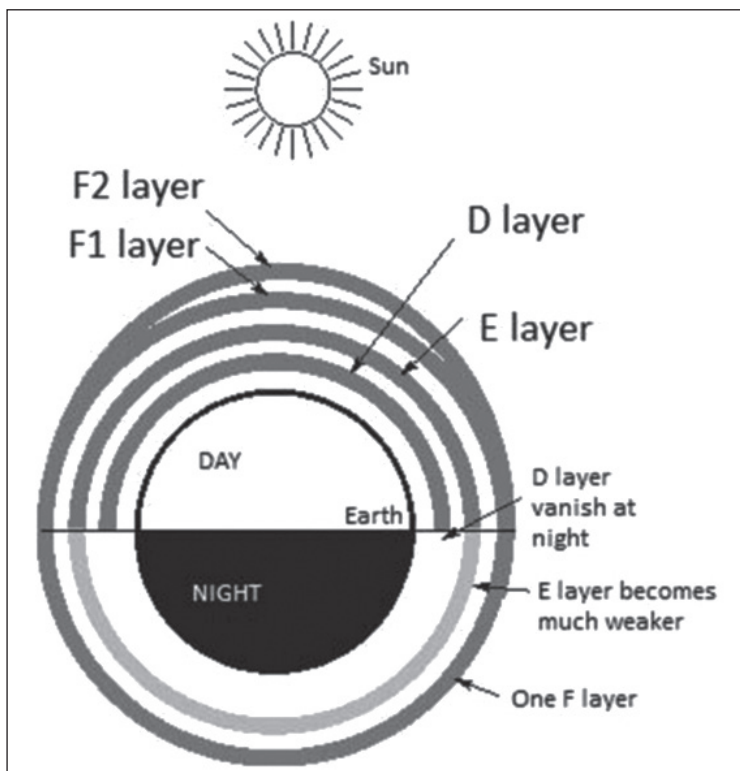
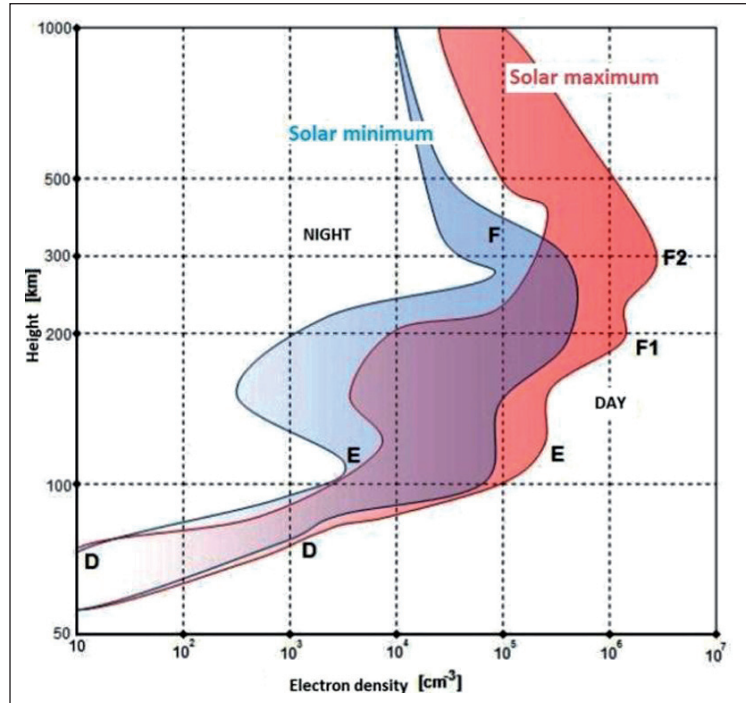


**Figure 4**  
Ionosphere layers by day and night

**Figure 5**  
Electron density in  
correlation to  
atmospheric altitude



These waves are partially reflected and partially absorbed by the lowest region of the ionosphere (the D-layer), which begins at about 60 km and ends at about 90 km above Earth's surface. The strength of these radio waves depends on ionization of ionosphere [7]. Since ionosphere reflects VLF waves we use them to observe solar activity and SIDs by monitoring the strength of VLF radio waves. There are some very high powered stations all over the world transmitting in VLF band for long range communications with submarines. SuperSID monitor (graphical application), PC sound card and some wire loop antenna can record VLF radio waves that are emitted from transmitter stations [8], [9]. By plotting the signal strengths over time it is shown when there was a solar flare on the Sun.

## B. Overview of the results

SuperSID monitor records 24 hours a day signal strength every 5 seconds in .csv format (Fig. 6). It also records signal strength from more than one station in the same time.

| T1 |                                       | f <sub>z</sub> |   |   |   |
|----|---------------------------------------|----------------|---|---|---|
|    | A                                     | B              | C | D | E |
| 1  | # Site = Croatia                      |                |   |   |   |
| 2  | # Longitude = 15.97                   |                |   |   |   |
| 3  | # Latitude = 45.82                    |                |   |   |   |
| 4  | #                                     |                |   |   |   |
| 5  | # UTC_Offset = -23                    |                |   |   |   |
| 6  | # TimeZone = central european time    |                |   |   |   |
| 7  | #                                     |                |   |   |   |
| 8  | # UTC_StartTime = 2011-08-11 00:00:00 |                |   |   |   |
| 9  | # StationID = DHO                     |                |   |   |   |
| 10 | # Frequency = 23400                   |                |   |   |   |
| 11 | # MonitorID = 0219                    |                |   |   |   |
| 12 | # SampleRate = 5                      |                |   |   |   |
| 13 | 2011-08-11 00:00:00, 687.546150778    |                |   |   |   |
| 14 | 2011-08-11 00:00:05, 686.476474389    |                |   |   |   |
| 15 | 2011-08-11 00:00:10, 685.406798       |                |   |   |   |
| 16 | 2011-08-11 00:00:15, 680.747858417    |                |   |   |   |
| 17 | 2011-08-11 00:00:20, 676.088918833    |                |   |   |   |
| 18 | 2011-08-11 00:00:25, 671.42997925     |                |   |   |   |
| 19 | 2011-08-11 00:00:30, 666.771039666    |                |   |   |   |
| 20 | 2011-08-11 00:00:35, 662.112100082    |                |   |   |   |
| 21 | 2011-08-11 00:00:40, 657.453160499    |                |   |   |   |
| 22 | 2011-08-11 00:00:45, 652.794220915    |                |   |   |   |
| 23 | 2011-08-11 00:00:50, 648.135281331    |                |   |   |   |
| 24 | 2011-08-11 00:00:55, 644.546018137    |                |   |   |   |
| 25 | 2011-08-11 00:01:00, 640.956754942    |                |   |   |   |
| 26 | 2011-08-11 00:01:05, 637.367491747    |                |   |   |   |
| 27 | 2011-08-11 00:01:10, 633.778228552    |                |   |   |   |
| 28 | 2011-08-11 00:01:15, 631.901794657    |                |   |   |   |
| 29 | 2011-08-11 00:01:20, 633.614623956    |                |   |   |   |
| 30 | 2011-08-11 00:01:25, 635.327453255    |                |   |   |   |
| 31 | 2011-08-11 00:01:30, 637.040282554    |                |   |   |   |

**Figure 6**

Example of .csv  
format file  
(11.08.2011, Zagreb,  
Croatia)

The signal strengths of the radio stations appear as vertical spikes standing in the noise floor (Fig. 7). These spikes slowly rise at night and lower to a stable level during the day. Around sunrise and sunset the graphs have large spikes because of the sudden change in ionization. During the nighttime the signal was high, but the signal strength also varied from night to night. After the sunrise the signals begin to drop in strength. This is the transition between E layer sky wave propagation and D layer propagation due to the Sun's ionizing effect on the Ionosphere. During daylight and quiet solar periods the plots will appear as a straight line. If there was a solar flare of sufficient size during the daylight hours, the plot would show a sharp rise in the signal strength of the VLF station and then a slow decay back down to the previous level.

**Figure 7**  
Graphical representation of VLF spectrum on SuperSID monitor with signal strength of more than one station

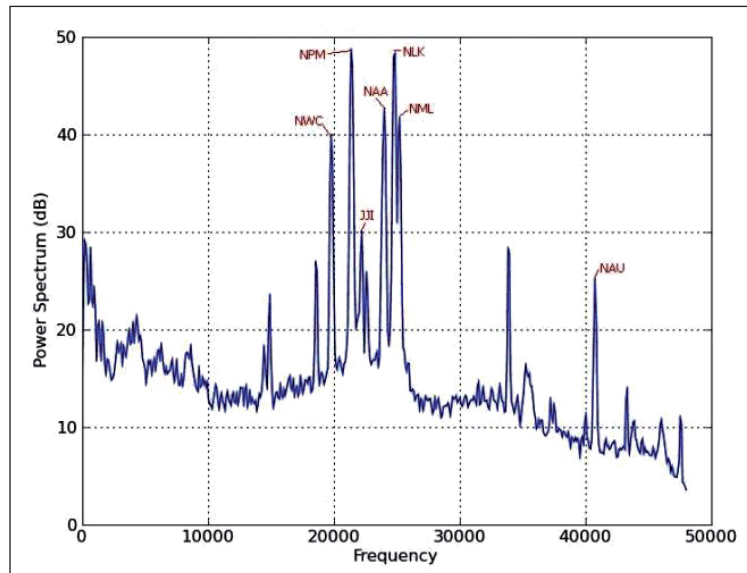
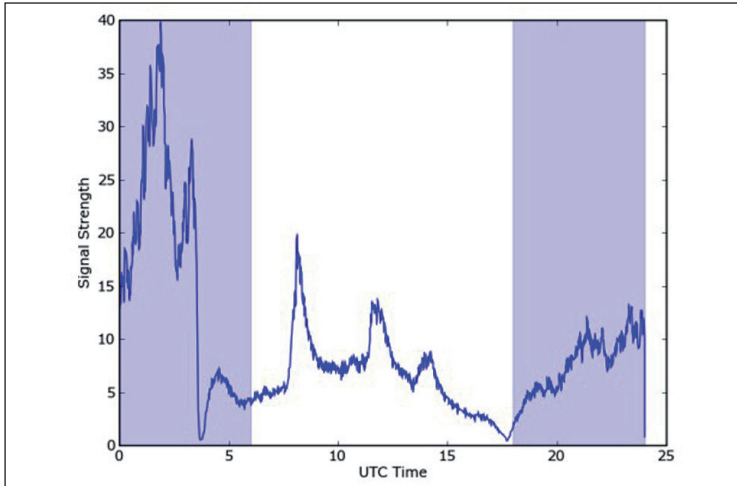
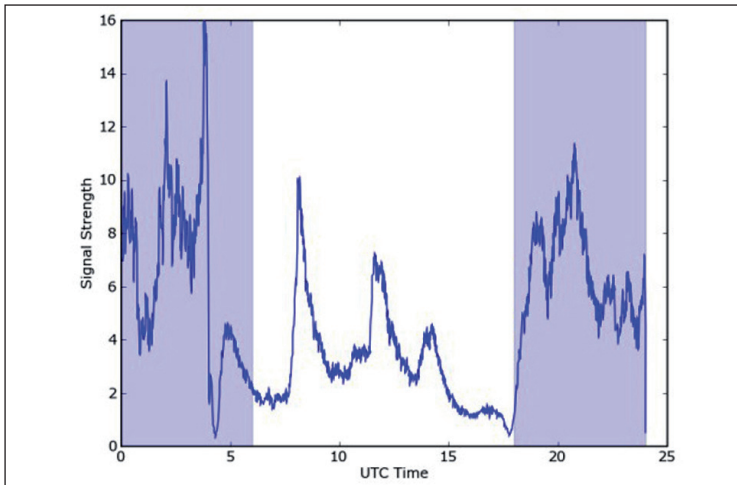


Fig. 8, 9, 10 and 11 is a sample of SID data graph from four different VLF stations on the same day and there are also shown 3 visible solar flares captured from all four stations. It's possible to tell how strong the solar flare was just by looking at how much the signal increased before going back down again.



**Figure 8**  
TBB station  
(5.9.2011, Zagreb,  
Croatia)



**Figure 9**  
NSY station  
(5.9.2011, Zagreb,  
Croatia)

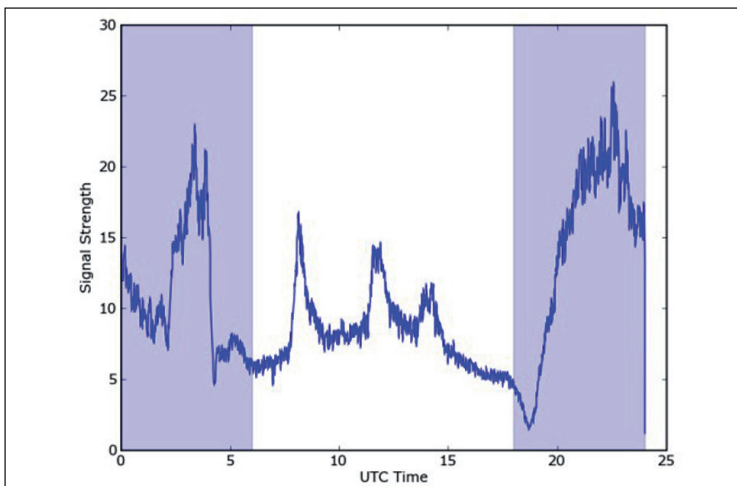
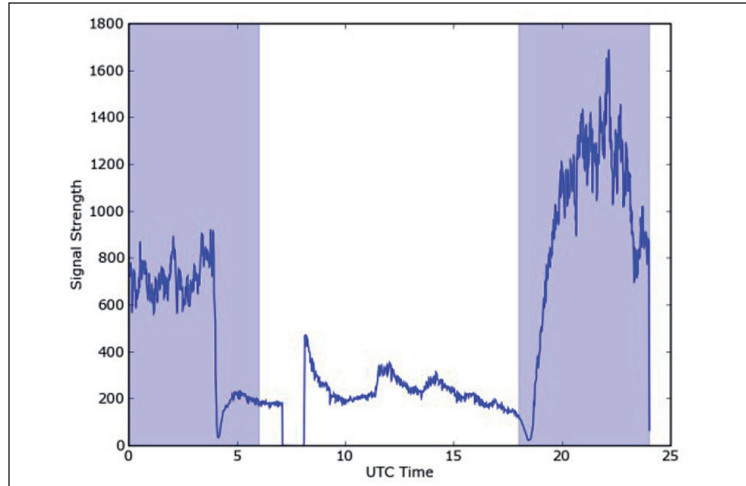


**Figure 10**  
FTA station  
(5.9.2011, Zagreb,  
Croatia)

**Figure 11**  
DHO station  
(5.9.2011, Zagreb,  
Croatia)



## 4 CONCLUSION

The goal of this paper was to understand how sudden ionosphere disturbances can affect the Earth's ionosphere and to observe how radiation from the Sun affects the strength of VLF radio waves on Earth.

The radiation from the Sun caused by the flare is able to penetrate through the D layer of the ionosphere and cause high ionization in the D region. VLFs are affected first and an increase in radiation from a flare can cause much higher frequencies to be affected. The results of these observations, taken from the Zagreb Astronomical Observatory, showed that radiation from the Sun disturbs VLF waves that are reflected by the ionosphere. Since the years 2011 and 2012 are predicted to be in the solar maximum of this 24-year cycle,

we were able to capture a solar flare, which is shown in the results. Also, it is shown how sunrise and sunset suddenly change the signal strength of VLF radio waves because of variations in the ionization of the ionosphere from the Sun. The signal strength of the VLF wave is stronger at night than in the daytime because during the night VLF waves have to travel 90 km to reach the E layer before they return to Earth, and during the day VLF radio waves must first travel through the D layer and thus lose some of their energy.

Solar activity, the ionosphere, and VLF radio waves are all interrelated. Observations of the ionosphere and the Sun in their correlation can be very useful in understanding the impact on radio wave technology that relies on the ionosphere.

---

## REFERENCES

- [1] D. Roša, “Methods of astronomical research”, Zagreb, 2010.
- [2] Solar and heliospheric observatory, SOHO, URL:<http://sohowww.nascom.nasa.gov/>
- [3] Zagreb Astronomical Observatory, URL:<http://www.zvjezdarnica.hr/index.php?lang=english>
- [4] Structure of the Sun, 20 Jul. 2011. Anjung Sains Makmal 3, URL: <http://anjungainsmks.wordpress.com/2011/07/20/699/>
- [5] About the Ionosphere, 21 Jan. 2003. HAARP, URL: <http://www.haarp.alaska.edu/haarp/ion1.html>
- [6] Antennas and propagation, Radio-electronics, Resources and analysis for electronics engineers, URL: <http://www.radio-electronics.com/>
- [7] A. P. Mitra, “Ionospheric effects of Solar flares”, D. Reidl Publishing Company, Boston-U.S.A.
- [8] Space Weather Monitors, Stanford SOLAR Center, URL: <http://sid.stanford.edu/>
- [9] Sudden Ionospheric Disturbances Monitoring Station A11 website, URL: <http://sidstation.loudet.org/home-en.xhtml>



## COMPARISON OF TEC MODELS

**Pavel Najman<sup>1</sup>, Tomislav Kos<sup>1</sup>, Norbert Jakowski<sup>2</sup>**

<sup>1</sup> University of Zagreb, Faculty of Electrical Engineering and Computing  
Zavod za telekomunikacije, Unska 3, 10 000 Zagreb, Croatia  
E-mail: pavel.najman@fer.hr

<sup>2</sup> German Aerospace Center, Institute for Communication and Navigation

**ABSTRACT.** *Demands from civil and army sector on precision of Global Navigation Satellite Systems (GNSS) are continuously rising. However, there are several factors which can introduce a positioning error. Particularly ionospheric error can cause one of the biggest errors (10-100m) when not properly mitigated. A significant part of the error can be easily removed using two or more frequencies due to the dispersive nature of the ionosphere. However, as most of GNSS receivers are still single frequency receivers, they have to use a ionospheric model to mitigate ionospheric errors. Although there are several models of the ionosphere, they are not thoroughly efficient under all conditions. Therefore, further study of ways how to improve existing ionospheric models is required, especially now, when the Sun's activity peak is anticipated.*

*Training Research and Application Networks to Support a Mitigation of Ionospheric Threats (TRANSMIT) is a project focused on variable topics dealing with the influence of the ionosphere on GNSS performance. Our research is inquired into ionospheric single frequency mitigation techniques during different space weather conditions. This paper will present the results of the comparison between the global TEC (Total Electron Content) map provided by Space Weather Application Center – Ionosphere (SWACI) of German Aerospace Center (DLR) and the values modelled using the new DLR ionospheric model NTCM, models IRI 2011 and NeQuick2 and data of F10.7 solar flux during the year 2011.*

**KEY WORDS:** *IRI 2012, NeQuick2, SWACI, NTCM*

## 1 INTRODUCTION

Every global navigation satellite system (GNSS) signal used for positioning purposes passes the ionosphere on its way from a satellite to a receiver. GNSS uses L-band signals which are able to pass through the ionosphere, however, their propagation is still affected by mutual interaction. When passing through the ionosphere, every signal encounters certain amount of electrons which changes its speed and trajectory. Thus, the amount of time which the signal needs for passing the ionosphere is higher than the amount needed for passing the same distance in vacuum. Such time delay is called *ionospheric error*.

Since the ionosphere is a disperse medium, two signals with different frequency carriers transmitted on the same path experience two different time delays. Therefore, using multi-frequency communication, the first order of error can be easily mitigated by linear combination. However, most of the commercial GNSS receivers are still single frequency receivers and are not able to benefit from dual frequency transmission. Instead, they rely on ionospheric models implemented in the receivers. Ionospheric model inside a receiver makes an assumption of ionosphere condition above the receiver and the ionospheric error is calculated accordingly. The second option how to mitigate ionospheric error is by using satellite-based augmentation systems such as EGNOS (European Geostationary Navigation Overlay Service) or WASS (Wide Area Augmentation System), which estimate ionospheric delay from dual frequency measurements by a network of reference stations. In this case, the system sends the information about the ionospheric delays of the reference stations to the receiver. The receiver then interpolates its ionospheric delay according the data of the nearest reference stations.

There are several models available which can be used for mitigation of the first order of the ionospheric error. The most widely used is the Klobuchar model which is implemented in GPS (Global Positioning System) receivers. This model is able to reduce ionospheric error on 50% in average. Another available model which is going to be used in GNSS Galileo is the NeQuick. Even though a great deal of work was done in developing ionospheric models, their performance is not satisfactory every time. Because the knowledge of solar-terrestrial environment is continuously improving, it is reasonable to improve ionospheric modelling as well. What is more, in the year 2013 and 2014 the solar activity maximum is anticipated which will bring more solar flares and coronal mass ejections (CMEs). Therefore, more disruptions of the ionosphere can be anticipated. The models should be improved so that they would perform more effectively in such disruptive events.

## 2 IONOSPHERIC ERROR

Ionospheric error is caused when a signal transmitted by a satellite is passing through the ionosphere. Such error is proportional to the total number of electrons which the signal encounters during its travel. The integration of the electrons along the signal trajectory is called *total electron content* (TEC) (Soicher, 1977).

$$TEC = \int N dl \quad (1)$$

where  $N$  is electron density in  $m^{-3}$  and  $l$  is length of signal path. Range error  $\Delta R$  caused by a certain TEC value can be easily calculated according to the following formula:

$$\Delta R = \frac{40.3}{f^2} TEC \quad (2)$$

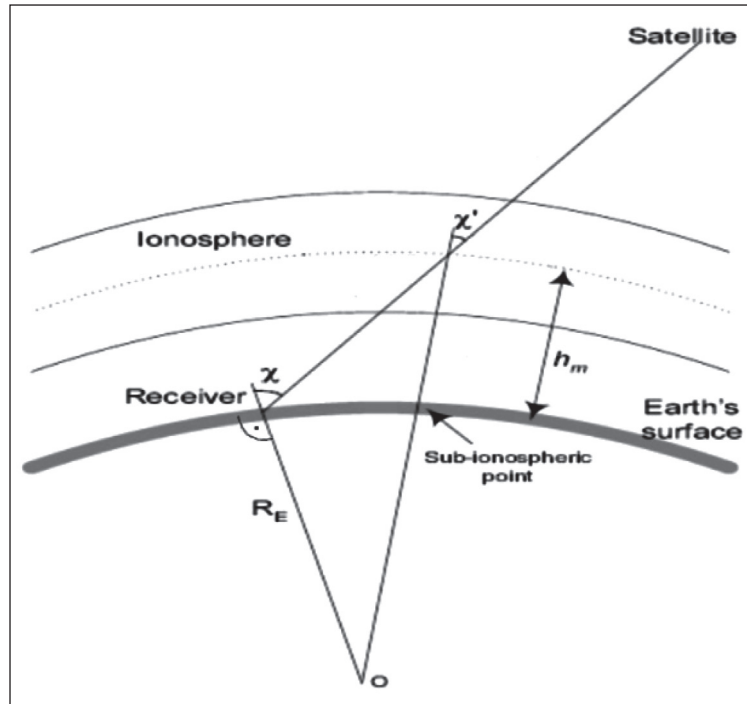
If a value of total electron content which affects a signal is used, it is most of the time referred to slant TEC (sTEC), the total electron content from the point of a receiver towards the direction of a satellite. However, if a ionosphere situation in a region is described, it is often referred to as *vertical TEC* values (vTEC), which are slant TEC with elevation angle of  $90^\circ$ . Mapping functions are used to convert slant values to vertical values or vice versa. One very common mapping function is Single layer mapping function where the ionosphere is approximated as a single layer with zero thickness:

$$vTEC = sTEC \sqrt{1 - (\sin \chi')^2} \quad (3)$$

$$\sin \chi' = \frac{Re}{(Re + h_m)} \sin \chi \quad (4)$$

where  $Re$  is the effective earth radius,  $h_m$  is the height of the single layer and  $\chi$  is the angle between the receiver zenith angle and the direction towards the satellite (Figure 1).

**Figure 1**  
Geometry of Single  
layer ionosphere  
approximation  
(Norsuzila et al.,  
2007).



Electron density of the ionosphere varies in time and space. Therefore, continuous monitoring of the ionosphere is required and functions approximating time variation of electron density in models have to be implemented.

### 3 IONOSPHERIC MODELS

Several models used for estimating ionospheric error or total electron content are currently available. The most widely used model is the Klobuchar model implemented in GPS. The model approximates the diurnal TEC variation as a cosine function with its maximum at 14:00 local time. During night time, the ionospheric delay is approximated as a constant of 5 ns. The cosine part is modelled as third-order polynomials whose eight coefficients are broadcasted in GPS navigation message. According to the approximate position of the receiver, the Klobuchar model estimates the magnetic latitude and longitude of the piercing point and the slant factor for the elevation angle. The Klobuchar model is very fast and simple, however, as a global model, not taking into account any local anomalies, it is capable of reducing the ionospheric error of only 50% at average (Klobuchar, 1987).

A model which will be used by the new GNSS Galileo to mitigate the ionospheric error is the NeQuick, based on the model introduced by Di Giovanni and Radicella. The NeQuick model use sum of Epstein layers to obtain vertical profile of electron density distribution in the ionosphere. The model, developed as a quick-run model for trans-ionospheric application, enables to calculate electron density in any given location in the ionosphere, and therefore also total electron content along the ray-path between any two given points. The version of the NeQuick model used for the data analysis was obtain at Seminar on Development and Use of the Ionospheric NeQuick Model at the International Centre for Theoretical Physics in Trieste in April 2012. The model is driven by foF2 and M3000 parameters or 10.7 cm solar flux values (Radicella and Nava, 2010).

Another empirical model, which is often used for estimating TEC, is the International Reference Ionosphere (IRI) currently freely available on National Aeronautics and Space Administration (NASA) webpage in 2012 version (<http://nssdcftp.gsfc.nasa.gov/models/ionospheric/iri/>). The IRI serves as an international standard for climatological specifications of ionospheric parameters such as ionospheric density, temperatures and chemical content [International Reference Ionosphere 2007: Improvements and new parameters]. The IRI is able to compute TEC values in zenith angle only with the integration height up to 1500km. The electrons above this border are not included and so a slightly undervaluation can be expected (Bilitza and Reinisch, 2008).

At Deutsches Zentrum für Luft-und Raumfahrt (DLR) Neustrelitz, GNSS-based ionospheric monitoring has been carried out since 1995. Recently, they have developed a simple global ionospheric model NTCM which should provide a simple way to obtain the value of vertical TEC (vTEC) at any given time and location. The model requires 12 coefficients and value of solar radio flux and can be autonomously used for a full solar cycle. The model does not use any integration of electron density profiles and is therefore very simple and fast (Jakowski, Mayer, Hoque and Wilken, 2011). The code of the model was obtained at DLR. All the formulas of the code are written in (Jakowski, Hoque and Mayer, 2011).

## 4 COMPARISON METHODOLOGY

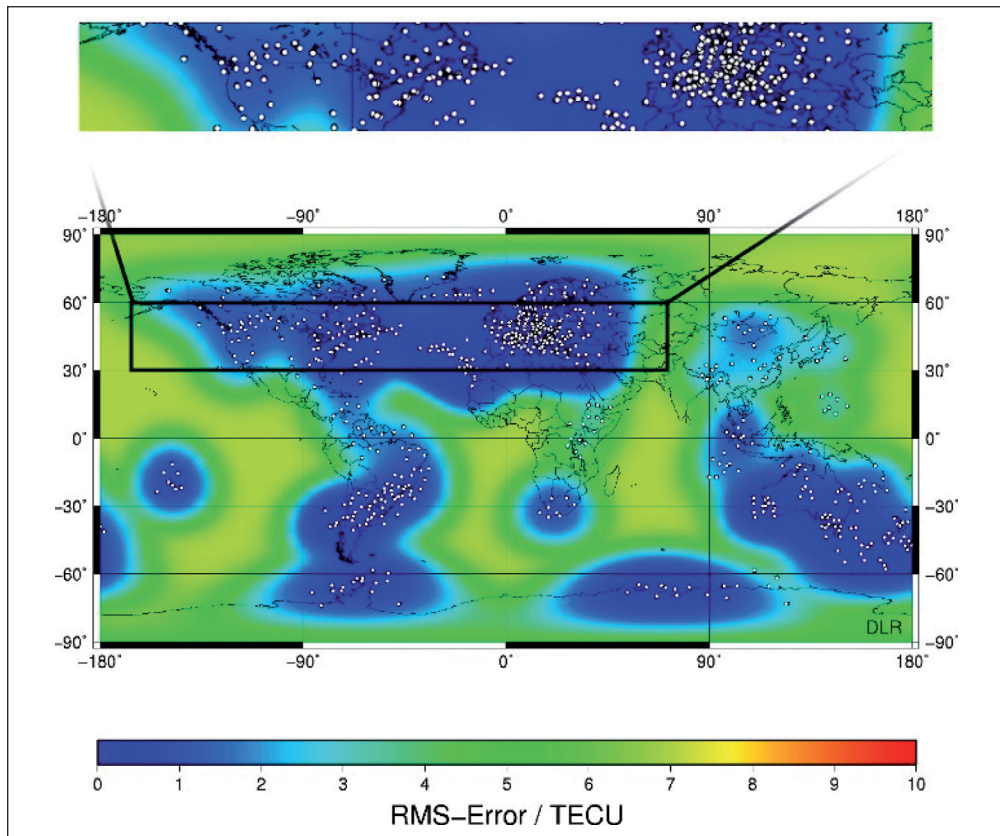
The ionospheric total electron contents computed by the models were compared with the results of satellite-based augmentation system called Space Weather Application Center –ionosphere (SWACI) developed in DLR. First, the system's background model produces a global TEC map, then the TEC map is adjusted

according to measurements from double-frequency stations around the Earth (Figure 2). The SWACI uses GPS measurements by various GNSS networks such as IGS (International GNSS Service), EUREF (Reference Frame Sub-Commission for Europe), BKG Frankfurt (Bundesamt für Kartographie und Geodäsie), SAPOS (Satellitenpositionierungsdienst der deutschen Landesvermessung) and IGS-RTTP (IGS Real-time Pilot Project) and creates a TEC map every 5 minutes.

To minimize the influence of the SWACI background model on final results, the area between  $170^{\circ}\text{W} - 80^{\circ}\text{E}$  and  $60^{\circ}\text{N} - 30^{\circ}\text{N}$  was chosen. This area has a good coverage by ground stations, therefore the average difference between the SWACI results and reality is around 1 TECU (TECU; 1 TECU = 1016 electrons/m<sup>2</sup>). What is more, there are no equatorial or polar ionospheric anomalies in mid-latitude regions. Since the grid map of the SWACI has  $5^{\circ}$  step in longitude and  $2, 5^{\circ}$  step in latitude, the ionosphere was modelled also exactly in these points.

### Figure 2

Distribution of stations used by the SWACI system (SWACI, 2012).



Two types of model comparisons were done. Vertical TEC values vary in different time of a day and in days of a year. The Day of a Year analysis is divided into 3 subgraphs: one for day time (10-16 hours local time), one for night time (22-04 hours local time) and one for sunset and sunrise together (5-9 and 17-21 hours local time). The comparison was carried out for 3 separate day intervals, because sun radiation influence differs in the periods. During day time, the Sun shines directly on the surface of the Earth and the ionization the highest. One the other hand, the ionization is very low during night time, as there is no direct Sun radiation. The sunset and sunrise periods are typical for both their weakening and rising levels of ionization. Mean values for diurnal variation were obtained according to the formula

$$vTEC_{mean} = \frac{1}{n} \sum_{k=1}^n \left( \frac{1}{m} \sum_{l=1}^m vTEC_{kl} \right) \quad (5)$$

where  $n$  is the number of days included in computation and  $m$  is the number of grid vTEC map points. Mean values for daily variation were obtained according to the formula

$$vTEC_{mean} = \frac{1}{p} \sum_{j=1}^p \left( \frac{1}{m} \sum_{l=1}^m vTEC_{jl} \right) \quad (6)$$

where  $p$  is the number of hours included in computation and  $m$  is again the number of grid vTEC map points.

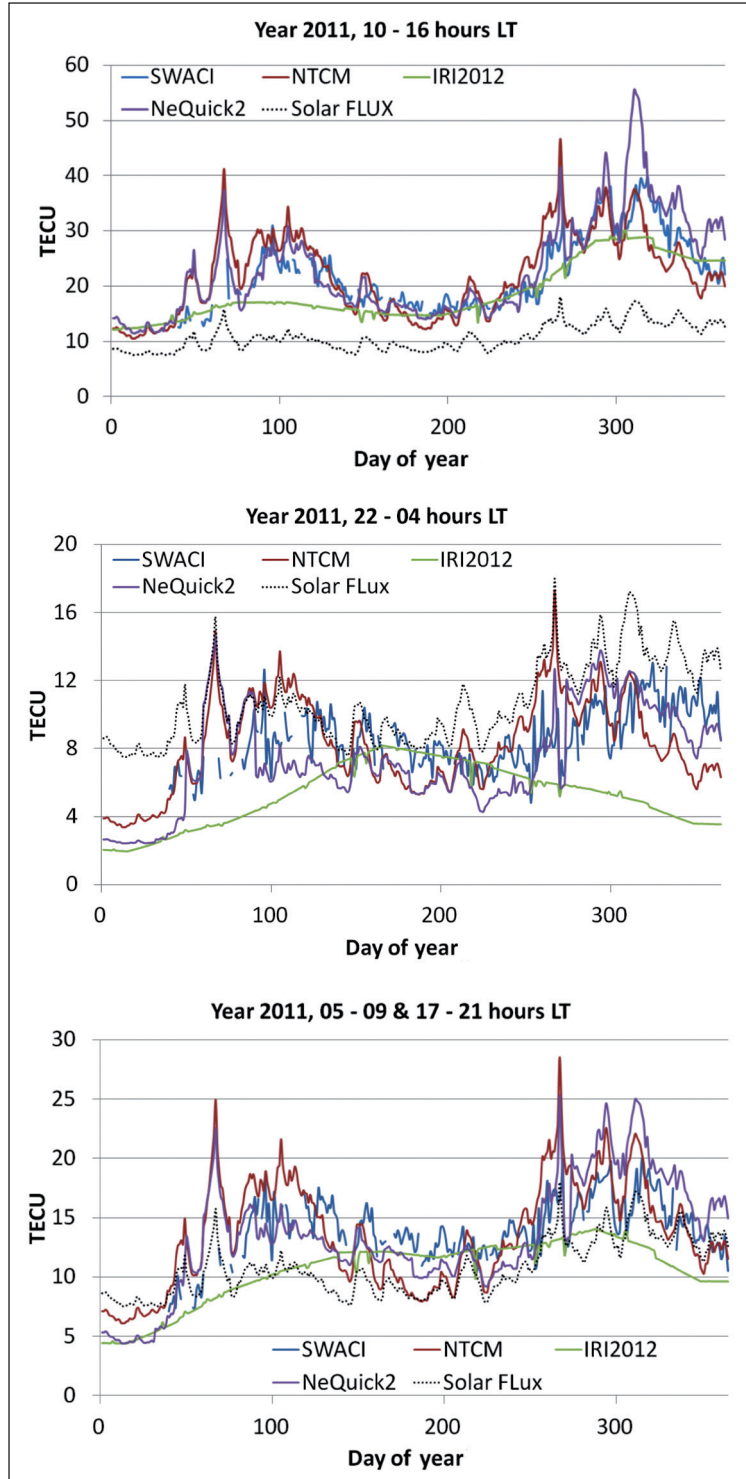
Values of observed solar radio flux with the wavelength 10.7 cm were taken from the National Oceanic and Atmosphere Administration (NOAA) site, National Geophysical Data Center (NGDC) section. The geomagnetic activity data input file for IRI computation was obtained directly from IRI developers.

## 5 RESULTS

The obtained SWACI database covers data for the year 2011 except some days especially in the beginning of the year. The database consists of global  $5 \times 2.5^\circ$  grid TEC maps stored hourly. At first, similar vTEC maps for mid-latitude regions were created by the models, then data in the TEC maps were compared.

The vertical TEC variation according to day of a year for the year 2011 is shown in Figure 3. The gaps in the blue curve indicated that SWACI data were not

**Figure 3**  
vTEC variation in day of year 2011; results for day (upper graph), night (middle graph), sunrise and sunset (bottom graph).



available. The NTCM, as well as the NeQuick model, follows the curve of radio the flux since these models are driven by it. This behavior is significant especially during the day period. The IRI model shows the seasonal dependence of the  $vTEC$  values. However, this seasonal dependence completely changes during the night time period where, especially in the winter period, it makes bigger errors.

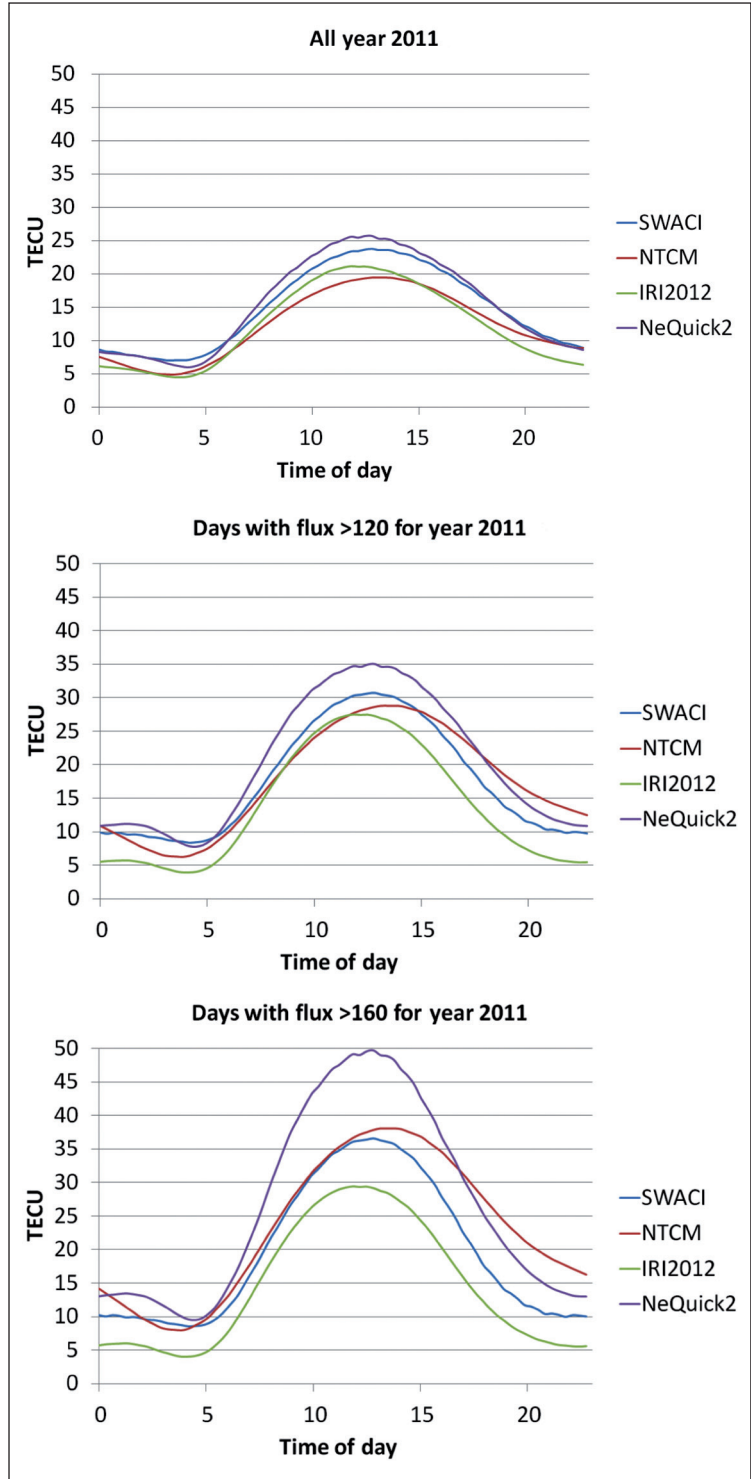
The second comparison of the models was done in diurnal dependence. Figure 4 shows how the models computed  $vTEC$  variation during the day. The comparison of the SWACI measurements with the NTCM, NeQuick and IRI model was done just in the days of the year 2011 during which SWACI data were available. The first graph shows the variation of mean vertical TEC value of all days in the year 2011. The mean value for solar flux in the year 2011 was 113.4. The second and the third graph include all days in 2011 which have their flux ratio higher than 120 and 160 respectively. We can see, that the higher the mean value of solar flux is, the less accurate ionospheric models perform. The statistical values are presented in Table 1.

**Table 1**

Statistical results of model comparison with the SWACI, the  $\Delta$  refers to a difference between the modelled  $vTEC$  values and the  $vTEC$  values of the SWACI data

| Model name | $\Delta$ for day of year [TECU] |          |          | $\Delta$ for time of day [TECU] |       |                    |
|------------|---------------------------------|----------|----------|---------------------------------|-------|--------------------|
|            | all year                        | flux 120 | flux 160 | day                             | night | sunrise and sunset |
| NeQuick2   | 0.92                            | 2.88     | 6.84     | 3.25                            | 1.93  | 2.67               |
| NTCM       | 2.69                            | 2.21     | 3.68     | 3.80                            | 2.12  | 2.71               |
| IRI 2012   | 2.78                            | 3.70     | 5.19     | 3.40                            | 3.06  | 2.46               |

**Figure 4**  
vTEC variation in time of a day; results for all days in 2011 (upper graph), days with solar flux higher than 120 (middle graph), days with solar flux higher than 160 (bottom graph).



## 6 CONCLUSION

Since each compared model computes the vertical total electron content by different approaches, each of them shows different performance efficiency under the different circumstances. There were time periods with quite and as well with disturbed ionosphere in the year 2011. The fact that predictive ionospheric models lost their accuracy and that variability of the ionosphere is not well correlated with variation in the flux is known (Langley and Brunswick, 2000). In this paper, in agreement with previous assumption, the performance of all of the analyzed models is decreasing as the high solar activity is increasing. Especially, the NeQuick model shows very good performance all over the year but tends to overestimate electron density in the ionosphere during the day with solar flux value of more than 160. Another noticeable issue is that not in all days with high electron density ionosphere a high solar flux ratio was observed (14th May) therefore models performs significantly worse. On the other hand, not every time high solar flux leads to high electron density in the ionosphere (17th October). In such periods the models tend to overestimate the the ionospheric condition what also lets to degradation of their performance. It can be therefore said that even-thought models driven by 10.7cm wavelength parameter model daily ionosphere condition better, there are other factors which can significantly influence the real state of ionosphere, and therefore, produce errors in ionospheric error estimation.

Future research will be focused on even more detailed analyses in order to obtain correlations between various solar-terrestrial indices and ionosphere behavior in different day and year periods.

## ACKNOWLEDGMENT

Pavel Najman's research work is undertaken in the scope of the TRANSMIT ITN ([www.transmit-ionosphere.net](http://www.transmit-ionosphere.net)), funded by the Research Executive Agency within the 7th Framework Program of the European Commission, People Program, Initial Training Network, Marie Curie Actions - GA no 264476.

## REFERENCES

- [1] Bilitza, D. and Reinisch, B. (2008), 'International Reference Ionosphere 2007: Improvements and new parameters', *Advances in Space Research* **42**(4), 599–609.
- [2] Jakowski, N., Hoque, M. M. and Mayer, C. (2011), 'A new global TEC model for estimating transionospheric radio wave propagation errors', *Journal of Geodesy* **85**(12).
- [3] Jakowski, N., Mayer, C., Hoque, M. M. and Wilken, V. (2011), 'Total electron content models and their use in ionosphere monitoring', *Radio Science* **46**(5), 1–11.

- [4] Klobuchar, J. A. (1987), ‘Ionospheric Time-Delay Algorithm for Single-Frequency GPS Users’, *IEEE Transactions on Antennas and Propagation* **AP-35**(3), 325–331.
- [5] Langley, R. B. and Brunswick, N. (2000), ‘GPS, the Ionosphere, and the’, *GPS world*.
- [6] Norsuzila, Y., Ismail, M. and Abdullah, M. (2007), ‘Investigation of the GPS signals ionospheric correction: Ionospheric TEC prediction over equatorial’, *2007 IEEE International Conference on Telecommunications and Malaysia International Conference on Communications* (May), 294–298.
- [7] Radicella, S. M. and Nava, B. (2010), ‘NeQuick model: Origin and evolution’, *Proceedings of the 9th International Symposium on Antennas, Propagation and EM Theory* **2**(4), 422–425.
- [8] Soicher, H. (1977), ‘Ionospheric and Plasmaspheric Effects in Satellite Navigation Systems’, *IEEE Transactions on Antennas and Propagation* **AP-25**, 705–708.
- [9] SWACI (2012), ‘Space Weather Application Center - Ionosphere (SWACI)’. **URL:** <http://swaciweb.dlr.de/>



Faculty of Maritime Studies  
University of Rijeka, Croatia



Royal Institute of Navigation  
Science Technology Practice



The University of  
Nottingham

**6<sup>th</sup> GNSS**

Vulnerabilities  
and Solutions  
Conference

# VARIATION IN THE IONOSPHERIC SCINTILLATION INDEX WITH ELEVATION ANGLE

**S. Priyadarshi, A.W. Wernik**

Space Research Centre, Polish Academy of Sciences  
Ul. Bartycka 18A, 00-716 Warsaw, Poland  
E-mail: s.priyadarshi@cbk.waw.pl, aww@cbk.waw.pl

**ABSTRACT.** *We have analyzed GPS data from 2007-2011 to determine the nature of variation of scintillation index with elevation angle and azimuth of the direction of propagation at an observing point Warsaw, Poland and Hornsund, Svalbard. We have found that the scintillation intensity dependence on the secant of the elevation angle  $E$  is of the power-law type  $(\sin E)^m$ , where the index  $m$  is a function of the spectral index  $p$  and shape of the irregularities responsible for scintillation. After correcting for the elevation angle dependence we produced the maps of the scintillation index  $S_4$  in the coordinates: corrected magnetic latitude-corrected local magnetic time, separately for low ( $K_p < 3$ ) and high ( $K_p > 3$ ) magnetic activity, and for summer and winter.*

**KEY WORDS:** *GPS, scintillation index, elevation angle, azimuth.*

## 1 INTRODUCTION

The amplitude and phase scintillation depends on many factors such as the distance and thickness of the layer containing irregularity, size and degree of anisotropy of the average, statistical irregularity, variance of the electron density, frequency of signals etc. (Wernik et al., 2007). One of the most characteristic features of scintillations is the variation of scintillation intensity with the change of elevation angle of the wave source. However, for the scintillation modeling the data should be independent of the geometrical effects. In order to make scintillation data independent of geometrical effects a detailed knowledge of variation of scintillation with geometry is required.

We have analyzed GPS data from 2007-2011 to determine the nature of variation of scintillation index with the elevation angle of the direction of propagation at an observing point Warsaw, Poland and Hornsund, Svalbard. To compare with the theory the intensity scintillation index is simulated as a function of elevation angle, azimuth, magnetic field inclination, and shape of irregularities using the phase screen model of scintillation as formulated by (Rino, 1979). Comparison of data and theory let us to estimate certain parameters describing the irregular structure of the ionosphere.

## 2 THEORY, OBSERVATION AND RESULT

It is known that with a decrease of the elevation angle the length of the ray-path through irregular layer increases (Singleton et al., 1970). Simultaneously the distance to the irregular layer increases. These changes cause an increase of the scintillation intensity with the decrease in elevation angle. The scintillation theory predicts such increase and it is interesting to compare the theoretical, simulated, and experimental  $S_4$  dependence on the elevation angle.

We started our simulation assuming the phase screen model of scintillation (Rino, 1979). For the amplitude scintillation index we used the formula

$$S_4^2 = (r_e \lambda)^2 L \csc EC_s Z^{p/2} \frac{\Gamma(1-p/4)}{\pi^{1/2} \Gamma(p/4+0.5) p} F(a,b) \quad (1)$$

where

$$Z = \frac{\lambda z_R \dot{\theta} E}{4\pi} \quad (2)$$

Here  $E$  is the elevation angle of the satellite,  $a$  is the elongation parameter along the geomagnetic field lines,  $b$  is the elongation parameter transverse to the geomagnetic field lines and  $p$  the electron density fluctuations spectral index (as measured in situ along the satellite path).  $F(a,b)$  is the geometry-dependent Fresnel filter factor defined in equation (34) of (Rino 1979).  $r_e$  is the classical electron radius;  $\lambda$  is the signal wavelength,  $L$  is the irregularity layer thickness, and  $C_s$  represents turbulence strength parameter. Amplitude scintillation index also depends on the factor  $Z$  which is again a function of the elevation angle  $E$  and  $z_R = z z_s / (z + z_s)$ , where  $z$  and  $z_s$  are distances to the screen and source, respectively. Therefore we get

$$S_4 \sim (\csc E)^{(p+2)/4} F(a, b) \tag{3}$$

Thus explicitly  $S_4$  is a power-law function of the cosecant of the elevation angle with the power dependent on the spectral index  $p$ . However, since the filter

**Figure 1**

Log log plot of  $S_4$  Vs  $\sin$  of corrected elevation angle  $E'$  for Warsaw, Poland

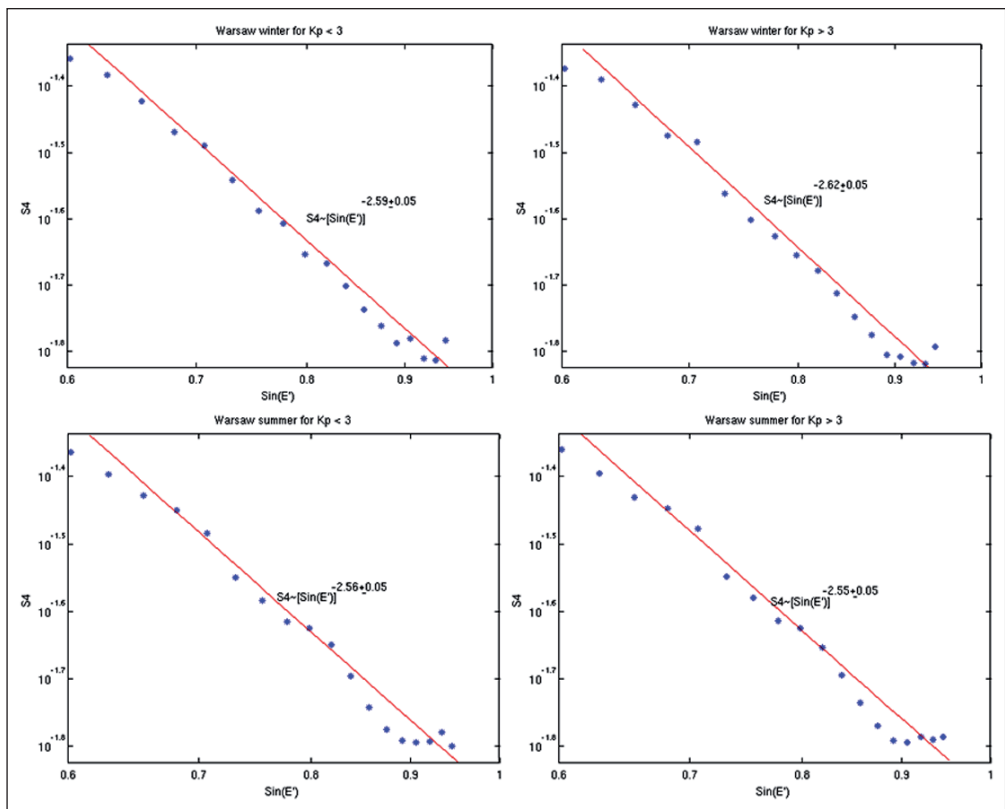
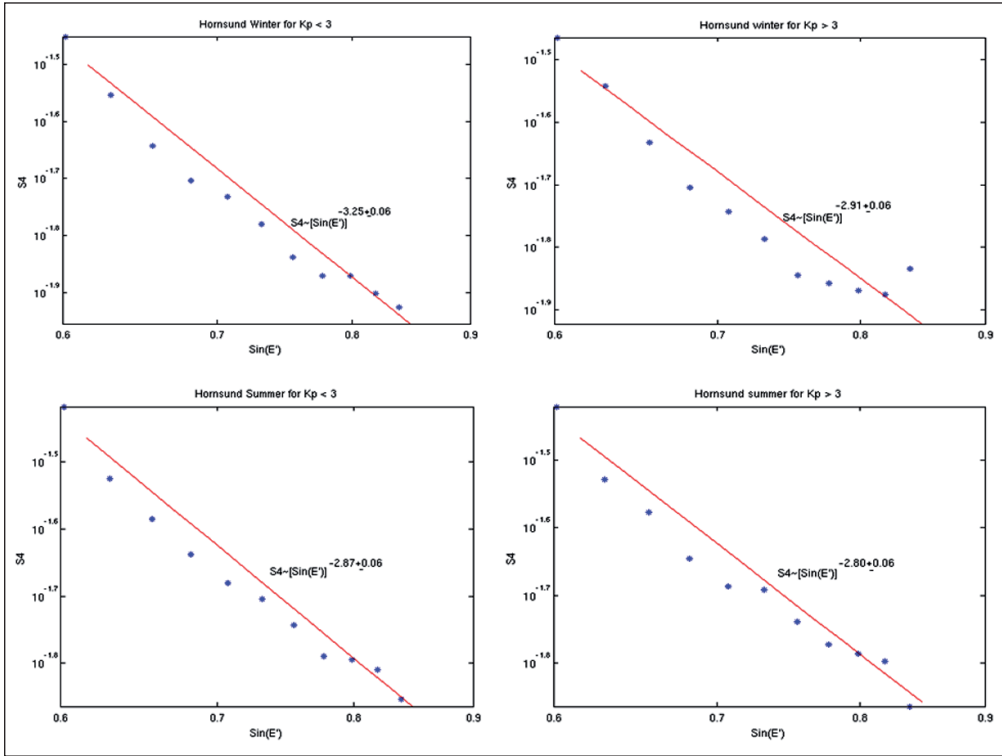


**Figure 2**

Log log plot of  $S_4$  Vs  $\sin$  of corrected elevation angle  $E'$  for Hornsund, Svalbard



factor  $F(a,b)$  is also dependent on  $E$ , the overall dependence on the elevation angle is more complicated.

$$S_4 \sim (\sin E')^{-\mu} \tag{4}$$

where the index  $\mu$  is parametrized with the spectral index  $p$ .

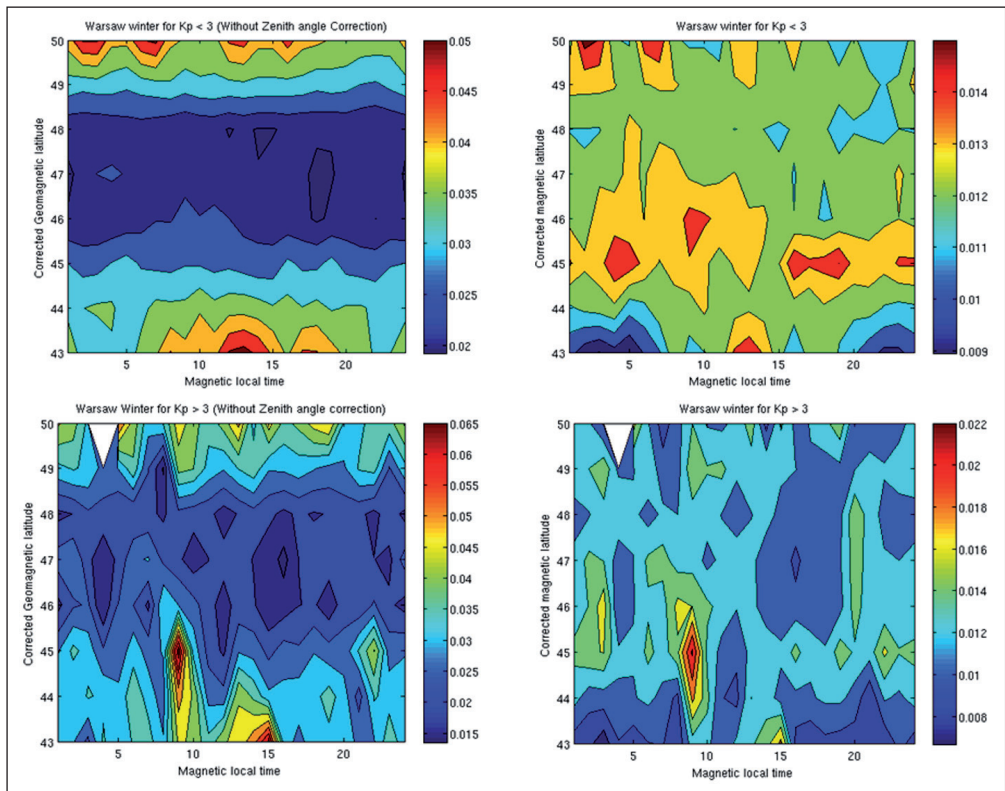
For a typical value of  $p=1.6$  (Wernik et al. 2007) the index  $\mu=(p+2)/4=0.9$ . To test this relationship we fitted a linear function to the log-log dependence of  $S_4$  vs.  $\sin(E')$ .  $E'$  is the elevation angle at the pierce point and it is related to the local elevation angle  $E$  at the receiver. In the real calculations we have fitted a line to  $S_4$  binned according to the elevation angle. In this way we saved a computer time. We have derived the index  $\mu$  for Warsaw, Poland (Figure 1) as well as for Hornsund, Svalbard (Figure 2) for summer and winter with high and low geomagnetic conditions. Our results show that the index  $\mu$  is different from the predicted 0.9, namely it is approximately equal 2.5 and 2.9 for Warsaw and

Hornsund, respectively. We also have found that  $\mu$  is practically independent on the season and magnetic activity.

The observed scintillation indices corrected for the elevation angle according to (4) have been used to generate maps in corrected geomagnetic latitude – magnetic local time coordinates, for varying geomagnetic conditions, for Warsaw, Poland (Figure 3 and 4) as well as Hornsund, Svalbard. Left part of the both the figure 3 and 4 shows the scintillation index without elevation angle correction derived from our observation while right part shows the scintillation index with elevation angle correction. On the left maps the most noticeable feature is a minimum of scintillation intensity near the latitude of the receiving station. Apparently this minimum is related to the propagation geometry and has nothing to do with the real distribution of scintillation. After applying the correction for elevation the distribution of scintillation changes significantly. The distribution so obtained can be considered as reflecting the distribution of electron density fluctuations.

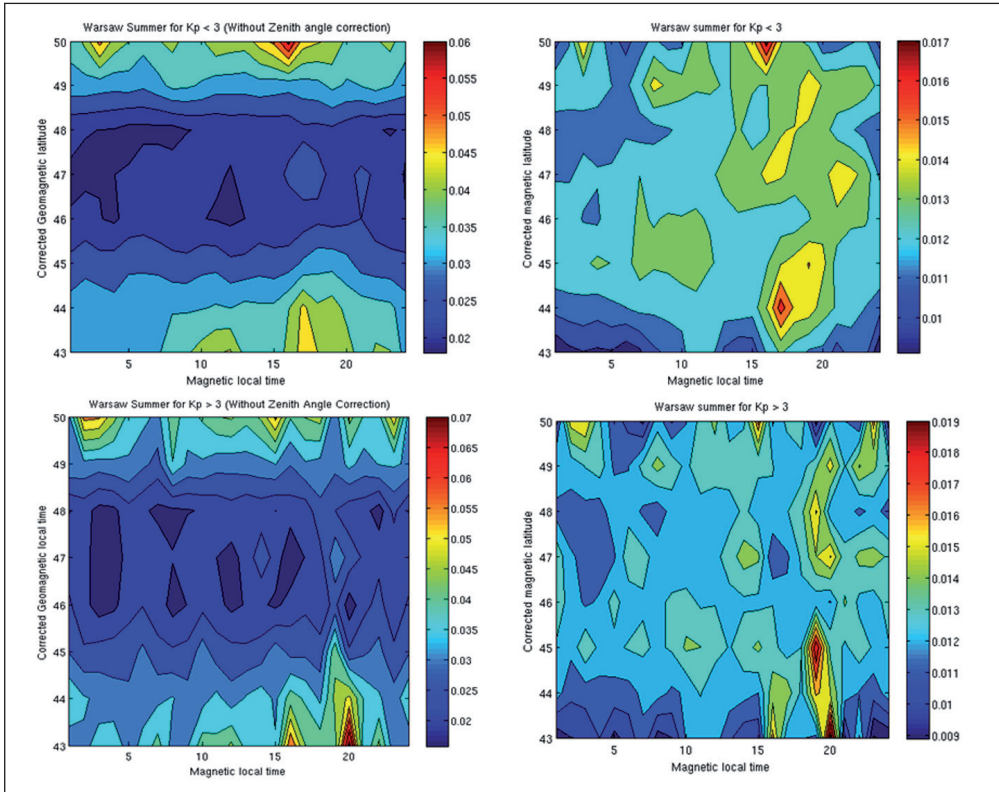
**Figure 3**

CGM latitude Vs. Magnetic local time maps during quiet and disturbed day during winter for Warsaw, Poland.



**Figure 4**

CGM latitude Vs. Magnetic local time maps during quiet and disturbed day during summer for Warsaw, Poland

**3 CONCLUSION**

This study is concluded with the following points:

1. Elevation angle variations of the scintillation index  $S_4$  index depend not only on the spectral index  $p$  but also on the irregularities form i.e. elongation in the direction of geomagnetic field lines or flattening across the magnetic field.
2. The data analysis shows that  $S_4$  is a power-law function of the cosecant of elevation angle  $E$ :  $S_4 \sim (\csc E)^m$  and that the index  $\mu$  is different from the theoretically predicted.
3. Not only at high- but also at mid-latitude station, such as Warsaw, the scintillation level depends magnetic activity.

---

## ACKNOWLEDGEMENT

Shishir Priyadarshi's research work is undertaken in the scope of the TRANSMIT ITN ([www.transmit-ionosphere.net](http://www.transmit-ionosphere.net)), funded by the Research Executive Agency within the 7th Framework Program of the European Commission, People Program, Initial Training Network, Marie Curie Actions - GA no 264476.

## REFERENCES

- [1] Rino, C. L. (1979). A power law phase screen model for ionospheric scintillation 1. Weak scatter. *Radio Science*, 14, 1135-1145.
- [2] Singleton, D. G. (1970). Dependence of satellite scintillations on elevation angle and azimuth. *Journal of Atmospheric and Terrestrial Physics*, 32, 789–803.
- [3] Wernik, A. W., Alfonsi, L. And Materassi, M. (2007). Scintillation modeling using in situ data. *Radio Science*, 42, doi:10.1029/2006RS003512.





Faculty of Maritime Studies  
University of Rijeka, Croatia



Royal Institute of Navigation  
Science Technology Practice



The University of  
Nottingham

**6<sup>th</sup> GNSS**  
Vulnerabilities  
and Solutions  
Conference

# LAW ENFORCEMENT AUTHORITIES' SPECIAL REQUIREMENTS FOR GNSS

**Jyri Rajamäki, Jouni Viitanen**

Laurea University of Applied Sciences  
Ratatie 22, 01300 Vantaa, Finland  
E-mail: Jyri.Rajamaki@laurea.fi

**ABSTRACT.** *Organised crime is a real threat in Europe with the emergence of international warehouses of crime. For improving their evidence-gathering abilities, law enforcement authorities (LEAs) are constantly seeking new technological recording, retrieving and monitoring solutions that would facilitate their combat against criminal organisations. The criminals' counter measure activities, such as electronic counter-surveillance, jamming and constant changes in behaviour for preventing eavesdropping or physical surveillance are continuously increasing. The pressure to find new intelligent technologies, which are harder to detect, more strongly encrypted, longer-lasting, quicker to install and more adaptive, is emerging and is a high-priority task. With regard to the global navigation satellite systems (GNSS), LEAs have five operational and technological challenges: (1) commercial GNSS sensors do not fulfil the needs of LEAs; (2) cross-border operations are difficult because criminal nature has internationalised but LEAs are national organisations; (3) secure mobile communications is more and more important in all operations; (4) the surveillance data that LEAs collect should be valid in the court; and (5) LEAs' operations should be transparent ensuring sufficient privacy safeguards for the public.*

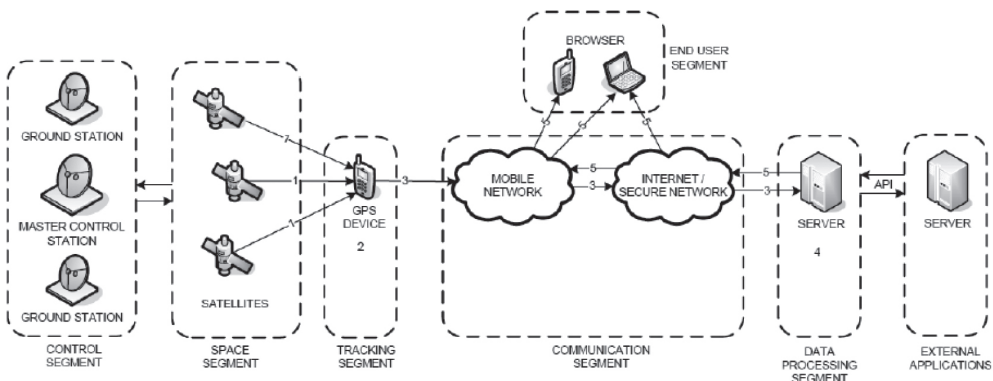
**KEY WORDS:** *GNSS, law enforcement, law enforcement authority, legality control, technical surveillance, tracking*

## 1 INTRODUCTION

Satellite-based navigation and tracking have become routine features of modern society and everyday life. Their use is still growing—a recent market research report predicts that the Global Navigation Satellite System (GNSS) market will likely double by 2016. The European Commission launched its first two operational satellites for the Galileo positioning system in October 2011. A modern satellite-based tracking system combines navigation and telecommunications technologies. The system is complicated and it consists of many technical segments, including the control segment, space segment, tracking segment, communication segment, data processing segment, application interface for external applications and end-user segment. The basic principle is that a tracked device is positioned by GNSS and positioning data is delivered for post-processing via mobile networks, the Internet or a secure network as shown in Figure 1 (Kämpfi and Guinness, 2010). The system is complex and vulnerable of several kinds of cyber-attacks (Kämpfi et al., 2009).

**Figure 1**

Principle of a satellite-based tracking system



GNSS-based tracking devices are able to calculate and deliver position information for post processing. Today many mobile phones include Global Positioning System (GPS) receivers, and phones are easy to turn into tracking devices by client software. For professional services and public authorities, TETRA clients and tracking-only clients (without communications functionality) are available. New positioning devices will support several systems, such as GPS, GLObalnaja NAVigatsionnaja Sputnikovaja Sistema (GLONASS) and Galileo, so that several techniques can be used simultaneously to guarantee better positioning accuracy and availability. GNSS-based tracking is used in

many applications, e.g. in logistics, fleet management, road tolls, traffic signal management. Also, Law Enforcement Authorities (LEAs) are using them e.g. for tracking suspects.

Professional criminals are aware that LEAs are gathering information about them, their actions and whereabouts. They have learned to find a tailing car among other traffic. GNSS-based tracking is a good tool for LEAs, because a small device under the car is harder to find than a tailing car. But criminals are learning, they have learned to check their vehicles and use other countermeasures. Therefore, LEAs need new tracking sensors which are resilient to these countermeasures.

European LEAs' GNSS-based tracking sensors are based on GPS. U.S. Department of Defense operates the GPS systems, but they cannot guarantee to maintain global uninterrupted service. If GPS signals were switched off in Europe tomorrow LEAs efficiency would suffer heavily jeopardizing the public safety.

This article has five sections. The second section briefly introduces the empirical case, the SATERISK research project, in which the results and findings of this paper are based on. The third section shows the operational environment where LEAs apply GNSS-based tracking. The fourth section presents the findings with regard to the tracking challenges that LEAs have. The last section discusses the future role of GNSS-based tracking in LEAs' operations and presents future research topics.

## **2 ANALYTICAL FRAMEWORK AND METHODS**

### **2.1 The SATERISK Research Project**

Often new technologies will present opportunities for increased safety and security—and this is certainly true with satellite-based navigation and tracking—but they can also create new risks. It is important for the technology developers, end-users, and authorities to clearly understand these risks and take steps to mitigate them. Amongst all of the developments within navigation and tracking issues, Laurea University of Applied Sciences led a research project to investigate the risks associated with satellite-based tracking. The SATERISK (SATEllite positioning RISKS) project started in September 2008 and ended in December 2011. It aimed to answer the following questions:

- Does satellite-based navigation and tracking involve risks?
- Do we know what the risks are now and what they will be in the future?

The SATERISK project also aimed to bring new know-how to the European field of security. The project created new methods and development paths for positioning and tracking systems that address the risks and limitations that had already been discovered. These include methods related to information security, signal interference, and legal restrictions on tracking. A special emphasis had been placed on the use of satellite-based tracking amongst security professionals—both in the public and private sectors—where the risks could be high if they were not properly addressed. (Rajamäki et al., 2012.)

The SATERISK project had partners and other participants from the whole value-chain of satellite-based tracking; starting from the network operators like Cassidian Finland to companies that offer information-gathering devices and tracking software, and finally to the users of these tracking systems, such as Finnish Customs. The legal aspects of satellite-based tracking were studied at the University of Lapland in its own SATERISK co-project (Viikari, 2011).

## 2.2 Research Methodology

Neither computer science alone with its technical solutions nor psychology or other behavioural disciplines is able to address the challenges of today's security problems in a sufficiently integrated way. If we put innovative artefacts into action and analyse how they are used and how they perform, we will see things that cannot be seen in the lab. (Nunamaker, 2010.) Management information systems (MIS) involve three primary resources: people, technology, and information. The SATERISK project follows the basic development research in the MIS wheel diagram, first published by Nunamaker, Chan and Purdin (1991). In the concept of Development Research (DR), the continuum of scientific method using each aspect to inform system design as Design Science Research (DSR) choices and using systems technology to inform the science (March and Smith, 1995; Van Aken, 2004; Hevner et al., 2004). DR and DSR are research approaches that can be combined with other social science methods, such as the grounded theory or action research as well as case study research.

According to Nunamaker's (2010) "going the last mile" approach, the starting point of research should be a real problem for real people. In the SATERISK project, this real problem came from Law Enforcement Authorities who had exploited GNSS-based tracking but who had fretted about how it had been used. Nunamaker continues that the creation of innovative artefacts includes three phases: proof of concept (POC), proof of value (POV) and proof of use (POU). This means that a designed artefact is not really understood and cannot really be evaluated before it is actually implemented. In addition to POC and POV, they should also strive for POU. The SATERISK project integrates science both in

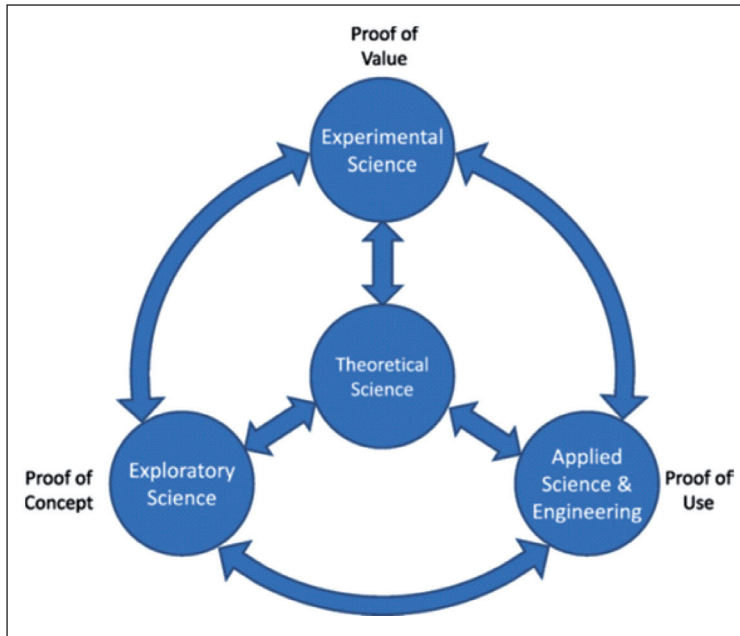


**Figure 2**  
Integrated,  
multidisciplinary,  
multi methodological  
development research

the lab and in the field (see Figure 2), including the theory, prototype and validation by experiments or field study.

The SATERISK project has widely studied technical, operational and legislative risks from different points of view. All end-users of tracking devices and systems face some risks when they use tracking; also being tracked by someone else is a problematic issue. This paper presents the SATERISK project's main results with regard to the risks that law enforcement authorities face when they exploit tracking.

### 3 OPERATIONAL ENVIRONMENT

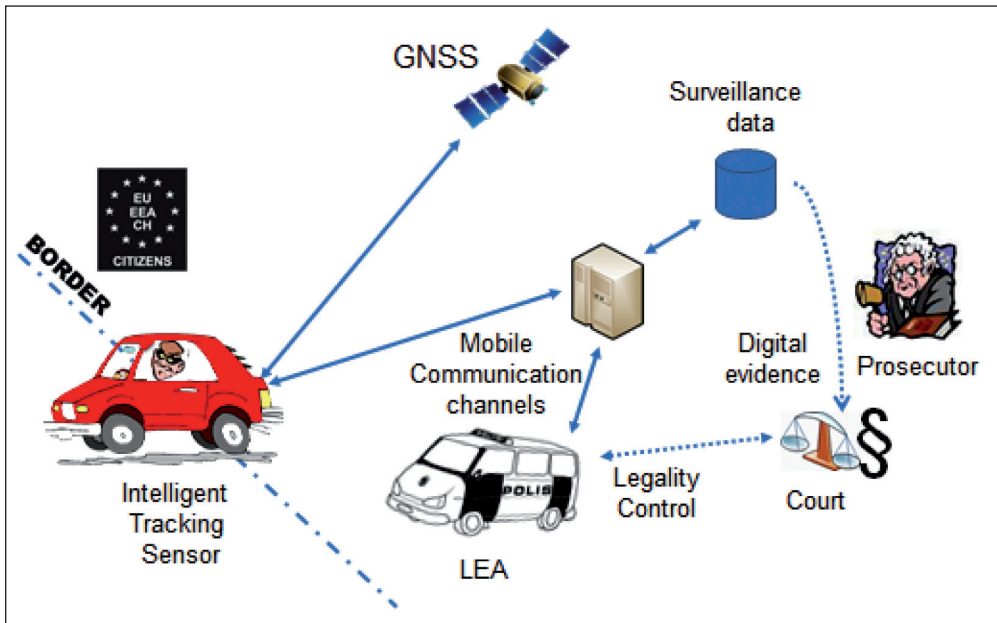
Organized crime is a real threat in Europe with the emergence of international warehouses of crime. For improving their evidence-gathering abilities, the law enforcement authorities are constantly seeking new technological recording, retrieving and monitoring solutions that would facilitate their combat against criminal organizations. The criminals' counter measure activities like electronic counter-surveillance, jamming and constant changes in behaviour for preventing eavesdropping or physical surveillance are continuously increasing. The pressure to find new, harder to detect, more strongly encrypted, longer-lasting and quicker to install and more adaptive intelligent technologies, is emerging and a high priority task. Respecting the accountability and integrity requirements and

smooth utilization of data in different phases of chains-of-custody is of utmost importance. In the current situation the chain of custody is difficult to maintain due to different techniques that operate on their own and are connected to different monitoring systems. This makes LEA work very labour-intensive so the use of new state-of-the-art technologies should enable the optimization of the use of human resources.

Figure 3 shows the operational environment where LEAs use tracking.

**Figure 3**

Operational environment



For pinpointing the major deficiencies in existing surveillance technologies, in the discussions between researchers and industrial and LEA experts, the following major needs or gaps related to everyday investigation and monitoring technologies and the context they are deployed were highlighted:

- Current tracking and monitoring systems are lacking in performance, old equipment is too big in size, hard to disguise and energy consuming.
- Most devices produced for LEAs take account their needs, but commercial interests are sometimes stronger incentive. This situation means that the best solutions are not always for sale and the manufacturers sell out the first generation products before bringing the next generation. This means that LEAs end up with having several inefficient systems lacking integration. This

requires a lot of support and logistics. The open IT solutions launched on the markets should be adaptable with new (experimental) sensors.

- Counter measures by criminals are posing new challenges as criminals use advanced detection and signal jamming technologies. Because of this the technologies used by LEAs have to be concealed in better ways, e.g. by size and appearance and have the jamming detection capabilities.
- Operational models of LEAs' information gathering do not comply with the legal and societal requirements and expectations in the needed level, neither with the possibilities the modern technology would allow. Harmonizing by implementing legal requirements into a new system that is useful for all LEAs in Europe is a first step.
- Safety, encryption and access control are very important. For investigation data has to be protected so that no unpermitted access will be possible and the content will not be revealed. Encryption safeguards privacy; tampering will be recognized and encrypted files will guarantee a strong chain of custody.
- New alternative positioning system is required; Galileo becoming operative will give new interdependence possibilities and advantages for tracking.

#### **4 TRACKING CHALLENGES FOR LEAS**

LEA officers need to have an easier access to all investigation data, independently from place and time and attention has to be paid to public awareness and concern on the use of surveillance equipment. However, legal recording, retrieving and monitoring of criminal activities in a safe and unnoticed way raise two problems: (a) how to ensure the accountability of law enforcement officers making use of such intrusive techniques and (b) how to ensure that sufficient privacy safeguards are implemented to ensure that these measures are used exclusively when overriding interests prevail and in a proportionate way.

Based on the identified deficiencies in the existing solutions, operational scenarios defined by the consortium LEAs and considerations of future challenges and issues that would be the most influential in European and international context, SATERISK has found to follow five main operational and technological challenges.

1. GNSS sensors; commercial sensor do not fulfil the needs of LEAs.
2. Cross-border operations; criminal nature has internationalised but LEAs are national organisations.
3. Secure mobile communications is more and more important in all operations.

4. Digital evidence; surveillance data LEAs collect should be valid in the court.
5. Legality control; LEAs' operations should be transparent.

#### 4.1 GNSS Sensors

With regard to tracking operations, the LEAs have the following problems: The size of available equipment is too big which restricts concealment possibilities. Power consumption is too high (maintaining of devices during the operation brings risks of being exposed etc.), there is scalability but low power options mean lower data quality so alternatives should be found. The systems are GPS and GSM dependent for positioning and communications; there are no cross-over possibilities, e.g. positioning could be based on using different satellite systems, known WLAN networks, mobile phone cell location, RF/DF etc. Also, intelligence is lacking from the systems; they can be commanded but they do not have the capability of self-reacting and alerting. Furthermore, available commercial products are vulnerable to jamming without jamming detection possibilities.

A new tracking sensor system, which has multi GNSS capability (Galileo, GPS, CLONASS) should be developed. Because the battery is the biggest part of these sensors, miniaturizing will mainly be achieved by optimizing sensor's power consumption, and utilizing energy harvesting and new high energy rechargeable battery technologies, For easy concealment, recharging will be wireless. For improving legal, policy and social acceptance issues, tracking sensors should need authenticated permission token to operate. Encryption should be done in the first possible phase, so that there will be no plain information stored in the system. Self-protection and counter measure protection as well as jamming detection should be included.

European LEAs can only be independent if their tracking is based on Galileo, the only European global navigation satellite system Galileo will allow positions to be determined accurately even in high-rise cities, where buildings obscure signals from today's satellites. Galileo will also offer several signal enhancements making the signal more easy to track and acquire and more resistant against interference and reflections. European GNSS will deliver much more precise and much more reliable services than the American and Russian systems. By placing satellites in orbits at a greater inclination to the equatorial plane, Galileo will also achieve better coverage at high latitudes, making it particularly suitable for operation over northern Europe, an area not well covered by GPS<sup>1</sup>.

---

<sup>1</sup> <http://www.gsa.europa.eu/go/galileo/why-galileo>

Many companies are developing tracking sensors and miniaturizing them; some are even considering the power consumption. However, most are concentrating only to hardware size. Military equipment are very sophisticated but use too much energy, because their main interest is Blue Force Tracking (tracking for own vehicles and people) and not for the enemy tracking. This means that energy consumption is not a big problem, because tracking sensors are in your possession; it is easy to change batteries or use other power sources from the car etc. Big part of the power consumption is how you use the equipment. Today already, the actual hardware is usually smaller than the battery back, smaller hardware size with no reduction in battery consumption helps only marginally. Figure 4 shows all relevant miniaturizing levels. Also, energy harvesting methods could be used; energy from ambient vibrations, wind, heat or light could enable smart sensors to be functional indefinitely.

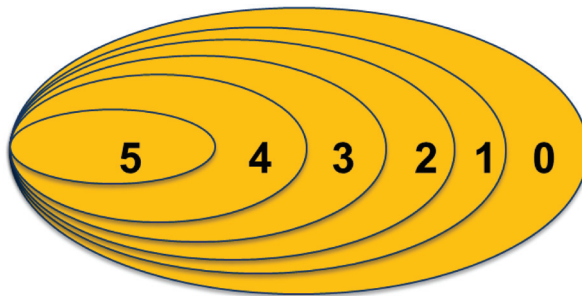


**Figure 4**

Miniaturizing levels in tracking sensor development

- 0 – Starting point: sensors and battery now;
- 1 – Add: Optimizing the use with AI;
- 2 – Add: Better sensor software;
- 3 – Add: New battery or other power source technology;
- 4 – ADD: Lower hardware power consumption;
- 5 – ADD: Smaller hardware size

On batteries new technology is based on the elements of lithium and sulphur. These two combine to yield a battery system with the highest theoretical gravimetric and volumetric energy densities of any known useful battery couple. This will enable many new LEA applications. The difference with Lithium-Ion is that the cell voltage is not anymore 3.6 V but varies nonlinearly in the range 2.5-1.7 V during discharge.

## 4.2 Cross-border LEA Operations

Organized criminality does not respect national borderlines and international warehouses of crime involved in smuggling, drug and human trafficking and terrorism are becoming a stronger threat to the European security. Following this, there is an increased need for European collaboration and information sharing related to the investigation technologies; cross-border usability and interoperability of investigation tools have to be guaranteed. However, joint

cross-border investigations are challenging as the LEA practices and technologies used in technical operations and legal procedures have big differences and incompatibilities. This leads to e.g. to slow or even hindered information exchange, endangering the success of entire investigations.

Viitanen et al. (2010) focus on cross-border surveillance operations dealing with time critical data communication between multinational organizations. This problem is common between the LEAs. Criminals are working more often abroad due the European integration, but LEAs do not have common protocols and procedures, how to pass information between each other. Especially machine to machine (M2M) communication is not researched yet.

### 4.3 Secure Mobile Communications

Secure, uninterrupted communication is a pre-requisite in critical environments, for example in public safety applications and critical infrastructure telemetry. General purpose IP based communication links may not be adequate and sufficient. For example, capacity of communication links and cyber warfare may present problems. Methods for ensuring constant connectivity and maintaining unbroken communication in all circumstances are needed. Traffic engineering and multichannel communication may mitigate the aforementioned problems. The DSiP solution (Distributed Systems intercommunication Protocol ®) enables parallel use of different network technologies in a consistent and transparent way enabling communications services platforms to be created. For example in cross-border operations, this is a huge advantage (Rajamäki et al., 2010).

Information security has at least five dimensions: Availability, authenticity, confidentiality, integrity and non-repudiation. Violating any of these may cause considerable harm or even damage. Identifying issues related to information security in satellite-based tracking systems is a huge topic. Kämppi et al. (2009) open this playground in the SATERISK project introducing the technical architecture and data flow in General Packet Radio Service (GPRS) and points out vulnerabilities and unknown issues in information security. They conclude that applicable security solutions or satellite-based tracking systems are, however, available. The study also describes major technical vulnerabilities of such systems. The field is divided into four segments: the satellite and tracking segment, the communication segment, the data-processing segment and the end-user segment. Each of these segments has its own set of risks and threats, which can be reduced to an acceptable level. Preserving the confidentiality of data is seen as the most important issue.

#### 4.4 Digital evidence

Remote operation is the control and operation of a system or equipment from a remote location. In systems engineering, monitoring means a process within a distributed system for collecting and storing state data. LEA monitoring station is a workstation or a place in which sensor information accumulates for end-users how needs it. There must be a central control station, which collects and stores all the information according to the rules and provides also legality control. The real time information will be sent on demand to the end-user where ever he or she is. In many cases, the users of information are not in the office but in the field using portable devices. This is called front deployed knowledge. Monitoring systems should be able to combine multiple forms of information, temporal, spatial, audio and visual, etc. However, combining information from many sources is technically, operationally and legally difficult task and analysing is suffering from it.

At present many LEAs are still using point to point investigation tools and tracking systems, where the information is transmitted from the sensor to e.g. a laptop of the surveillance team for monitoring. These old-fashioned stand-alone systems create neither watermarks nor log file marks; the system only retrieves the information and stores it locally. For that reason neither chain-of-custody nor social acceptance by transparency comes true. (Viitanen et al., 2011.)

The gathering, conservation, communication and presentation of the computer - derived evidence must fulfil legal requirements with regard to the admissibility of the evidence; they should be admissible, authentic, complete, reliable and believable. Electronic evidence not gathered in accordance with the law will be inadmissible and be ruled out of court. Today's main evidence authentication system is the hash value calculated from the retrieved information. With hash value you can prove that the data is the original and no one has tampered with it. The problem is that systems like hashing are incapable to fully expose when, where and by whom data is produced.

#### 4.5 Legality control

For example in Finland, the oversight of police's coercive measures is based on a file system SALPA run by National Bureau of Investigation. The SALPA system guides how to make applications and notifications in the correct manner. The question then is, can this system alone be a sufficient legality control system, if the information that police officers write down are not based on actual log files. These non-transparent systems might be handicaps to LEAs (Tuohimaa et al. 2011). LEAs may also act according to the law but they are not able to prove it because methods cannot be audited by an outsider. The current state of affairs

is neither efficient nor transparent. More advanced monitoring system is needed to provide faultless control of the surveillance equipment and procedure all the time. At present no process or instance is able to present publicly accepted proof of correct use of these equipment as long as there are no a publicly proven technical control methods involved in the chain.

## 5 DISCUSSION AND CONCLUSIONS

In order to bringing about the LEAs' special requirements for GNSS, technological and socio-technical research and development work is needed. Development of novel monitoring systems and miniaturized sensors improves LEAs' evidence-gathering abilities while respecting legal and ethical expectations of society. The over-all development target will be accomplished through the following specific objectives:

- 1) to enable new operational models for investigation for LEAs
  - by improving existing technology and developing new integrated digital systems for tracking and audio and video retrieving and monitoring
  - to achieve next level in digital miniaturization and state of the art development including: a) easy usability; equipment can be handled under difficult situations; b) long life-time; extended to several months or even over an year; c) (self-) protection; applying artificial intelligence, the sensor is capable of monitoring its surroundings and can change its operation model autonomously for its own safety, d) data securement by deep encrypting
- 2) to develop methods of working that are legally binding and social acceptable
  - information gathered is legally binding and court proof developed technology will enable audit trail, accountability and further societal acceptance
- 3) to support wider European goals
  - to recognize needs for regulation and harmonisation
  - to promote use of other European technologies like Galileo and create needed interfaces.

## REFERENCE

- [1] Hevner, A., March, S., Park, J. & Ram, S. (2004). Design science in information systems research. *MIS Quarterly* 28, No 1.
- [2] Kämppe, P. and Guinness, R (2010) Technical Risk Analysis for Satellite Based Tracking Systems. *Proceedings of the Integrated Communications Navigation and Surveillance Conference*, Herndon, VA, USA, May, M3-1 - M3-16.
- [3] Kämppe, P. Rajamäki, J. and Guinness, R. (2009) Information security risks for satellite tracking systems. *International Journal of Computers and Communications*, Issue 1, Volume 3.
- [4] March, S. & Smith, G. (1995). Design and natural science research on information technology, *Decision Support Systems* 15.
- [5] Nunamaker (2010). Interview with Jay F. Nunamaker, Jr. on “Toward a Broader Vision of IS Research”. *Business & Information Systems Engineering*, Issue 5.
- [6] Nunamaker, J., Chan, M. & Purdin, T. (1991). Systems Development in Information Systems Research. *Journal of Management Information Systems*. Vol. 7, No. 3.
- [7] Rajamäki, J., Pirinen, R. & Knuutila, J. (eds.) (2012). *SATERISK Risks of Satellite Based Tracking. Sample of Evidence Series: Volume (2)*. Edita Prima Oy, Helsinki.
- [8] Rajamäki, J., Holmström, J. & Knuutila, J. (2010). Robust Mobile Multichannel Data Communication for Rescue and Law Enforcement Authorities. *Proceedings of the 17th IEEE Symposium on Communications and Vehicular Technology in the Benelux (SCVT)*, Twente, The Netherlands Nov. 24–25 and IEEE Xplore.
- [9] Tuohimaa, T., Tikanmäki, I., Rajamäki, J., Viitanen, J., Patama, P., Knuutila, J. & Ruoslahti, H. (2011). Is Big Brother Watching You? *International Journal of Systems Engineering, Applications and Development*, Issue 5, Volume 5, 602–609.
- [10] Van Aken, J. (2004). Management research based on the paradigm of the design sciences: The quest for field-tested and grounded technological rules. *Journal of Management Studies* 41, No 2.
- [11] Viikari, L. (ed.) (2011). *SATERISK: Tutkimusraportti 2008-2011*. University of Lapland. Lapin yliopistopaino (in Finnish).
- [12] Viitanen, J., Happonen, M. Patama, P. & Rajamäki, J. (2010). Near Border Procedures for Tracking Information. *WSEAS TRANSACTIONS on SYSTEMS*. Issue 3. Volume 9. pp. 223–232.
- [13] Viitanen, J., Patama, P., Rajamäki, J., Knuutila, J., Ruoslahti, H., Tuohimaa, T. & Tikanmäki, I. (2011). How to Create Oversight in Intelligence Surveillance. *Proceedings of 9th WSEAS International Conference on Applied Electromagnetics, Wireless and Optical Communications*, March 24-26, Meloneras, Gran Canaria, 52–56.





Faculty of Maritime Studies  
University of Rijeka, Croatia



Royal Institute of Navigation  
Science Technology Practice



The University of  
Nottingham

**6<sup>th</sup> GNSS**  
Vulnerabilities  
and Solutions  
Conference

# EFFECTS OF GNSS PERFORMANCE DETERIORATION ON PRECISION AGRICULTURE

**Tomislav Ratajec<sup>1</sup>, Renato Filjar<sup>1,2</sup>, Hrvoje Gold<sup>3</sup>,  
Zoran Vrhovski<sup>1</sup>**

<sup>1</sup> University College of Applied Sciences, Bjelovar, Croatia  
A. B. Šimića 1, 43 000 Bjelovar, Croatia  
E-mail: renato.filjar@gmail.com

<sup>2</sup> Faculty of Maritime Studies, University of Rijeka, Croatia

<sup>3</sup> Faculty of Traffic and Transport Sciences, University of Zagreb, Croatia

**ABSTRACT.** *Precision agriculture is a new discipline aimed to provide a framework for optimal crops yield soil management. Satellite navigation plays an essential role in precision agriculture, providing the most accurate position estimate for various sensors deployed in order to survey both the soil characteristics and the crops yield. Since the sensor readings serve as an input to the advanced agricultural geostatistics algorithms, the quality of positioning estimation is essential for optimal planning of soil treatment activities. Here we demonstrate the importance of high-quality position estimation for precision agriculture based on a real case-study, and present an assessment of potential drawbacks in soil treatment planning, caused by GNSS performance deterioration. This paper concludes with an outline of mitigation techniques and proposals for further development.*

**KEY WORDS:** *GNSS, performance deterioration, vulnerabilities, precision agriculture*

## 1 INTRODUCTION

Due to increased availability and ease of use, reliance on high precision GNSS technologies has risen sharply in recent years (Filjar *et al*, 2011, Filjar *et al*, 2010). A large number of public and industrial services now depend on the continued functioning and reliability of GNSS and new applications are being implemented at high frequency (Filjar *et al*, 2010, ICG, 2011). Due to this fact it has become a necessity, to examine, predict, and eliminate or mitigate the inherent vulnerabilities of GNSS and also to research and develop possible alternatives to serve as contingencies in the event of failure (Thomas *et al*, 2011).

An emerging industrial application of GNSS is *Precision Agriculture*, an agricultural production management concept aiming to increase production efficiency, product quality and economic effectiveness while minimizing environmental impacts through the use of modern satellite navigation, information and automation technologies (Hengl, 2009).

In precision agriculture, GNSS is employed in a variety of applications including guidance, parcel measurement, mapping of soil properties and topographic mapping, all of which require reliable high accuracy positioning. In order to make the prospect of widespread implementation of precision agriculture feasible in the future it is imperative to ensure that these requirements are met in a continuous manner (Hengl, 2009, ICG, 2011, Thomas *et al*, 2011).

This paper will attempt to analyze the possible effects of GNSS performance deterioration on precision agriculture systems and propose measures to mitigate these vulnerabilities.

The purpose of this paper is to show the effect of GNSS positioning errors on the process of soil sampling and the spatial prediction of soil acidity (pH) values through interpolation since these measurements directly influence the subsequent treatment of the soil through variable rate liming.

## 2 GNSS AND PRECISION AGRICULTURE

### 2.1 A brief introduction to precision agriculture

Through most of agricultural history, agronomic practices and recommendations have been implemented on a field-basis with resources and farming practices such as tilling, liming, fertilizer, sowing and pest control treatment being applied uniformly at the field-scale. It has however been found that conditions on farm

fields display considerable variation in crop yield and soil properties at comparatively short spacial scales.

Since a uniform approach inherently ignores within-field variation, it is likely that certain parts of the field will be under-treated, while others will be over-treated resulting in economic and environmental issues due to inefficient resource allocation. An impetus to address these issues led to the development Precision Agriculture (PA), a farming management concept intent on matching resource application and farming practices to localized conditions within fields by recording and responding to the spatial and temporal variability of the various parameters that affect product yield and quality, thereby reducing expenses and environmental impact through increased efficiency.

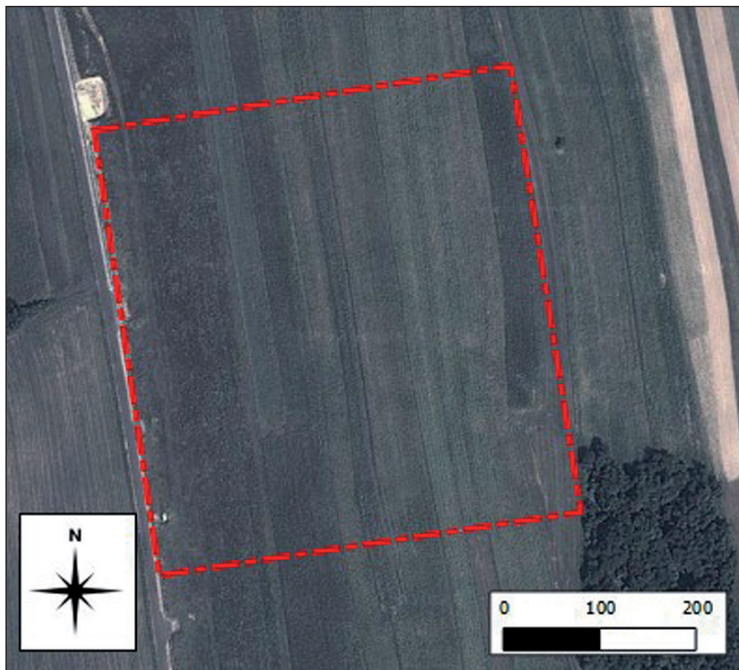
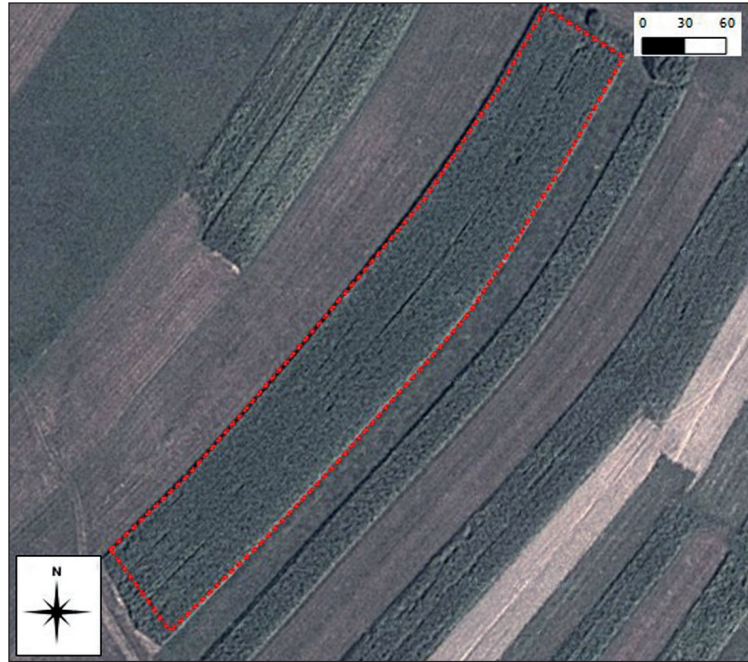


**Figure 1**  
10 ha-field in Velika  
Pisanica  
(Lat: 17.087990,  
Lon:45.797480 -  
WGS84)

The practices that are nowadays identified with the term *Precision Agriculture*, emerged first during the the 1980's when initial experiments using yield monitoring devices were performed to manually define localized yield variation within wheat fields. While this offered a first insight into spatial variation, which was shown to be considerable, there was still no means for commercial farmers to bring this data to bear on management decisions (Hengl, 2009).

**Figure 2**  
1 ha-field in Velika  
Pisanica  
(Lat: 17.031321,  
Lon:45.810211 -  
WGS84)



With the advent of GNSS in 1990 and the subsequent improvements in positional accuracy through the introduction of differential corrections (DGPS) in 1995 and the removal of selective availability of GPS by US Department of Defence in 2000, yield and soil mapping became a more accessible practice to farmers world-wide and this in turn prompted further development. With high-accuracy position data being widely available, it was now possible to not only record the spatial variation of yield and other relevant parameters but also to use the recorded data guide management decisions and to control GNSS equipped machinery through the use of digital maps, computers and electronic controllers.

## 2.2 Variable Rate Application

The *Variable Rate Technologies (VRT)* or *Variable Rate Applicators (VRA)* are used to vary the rate of application of seed, nutrients, and soil amendments within the field for the purpose of optimizing resource allocation. Variable rate drills and planters, fertilizer spreaders, sprayers and irrigation systems are also being used. Farm machinery equipped with VRA micro-controllers typically use differentially corrected satellite navigation (*DGNSS*) to identify the precise location of spatial variability in the field and automatically control the rate of application based on digital input prescription maps. These maps can be derived by either local sensing using sensors mounted on farm machinery,

remote sensing using multi-spectral aerial and satellite imagery or direct soil sampling.

### 3 RESEARCH METHODOLOGY

#### 3.1 Data description

Soil samples were taken from 2 agricultural fields (figs 1 and 2) located in the village of Velika Pisanica, Bjelovar-Bilogora County. A total of 54 soil samples were taken on a 50x50m grid from a 10ha field and 20 samples were taken from a 1ha field at a spacing of 20m. All samples were geolocated using differentially corrected GNSS positioning with sub-meter accuracy. Subsequently, the samples were analyzed in a laboratory setting, where pH values were measured individually in a solution of soil and water. The results for each sample were stored in digital form and combined with the previously recorded location data into a data frame. *The Coordinate System Reference (CRS)* used was *HTRS96/Croatia TM (EPSG:3765)*, a transverse mercator projection which is the official CRS for Croatia.

#### 3.2 Experiment design

For the purpose of analyzing the effect of GNSS performance deterioration on the spatial prediction of soil pH through interpolation (Hengl, 2009, Pebesma, 2011), the initially recorded positions were assumed to be completely accurate, i.e. the original sub-meter error was ignored and new error values were simulated using a computer program, written using the statistical programming language R. A horizontal positional error was introduced to the recorded positions and new point patterns were created based on the original measurements, each with a different, randomly generated error value corresponding to statistical data describing the positional accuracy of the GPS Standard Positioning Service (SPS), taken from multiple sources.

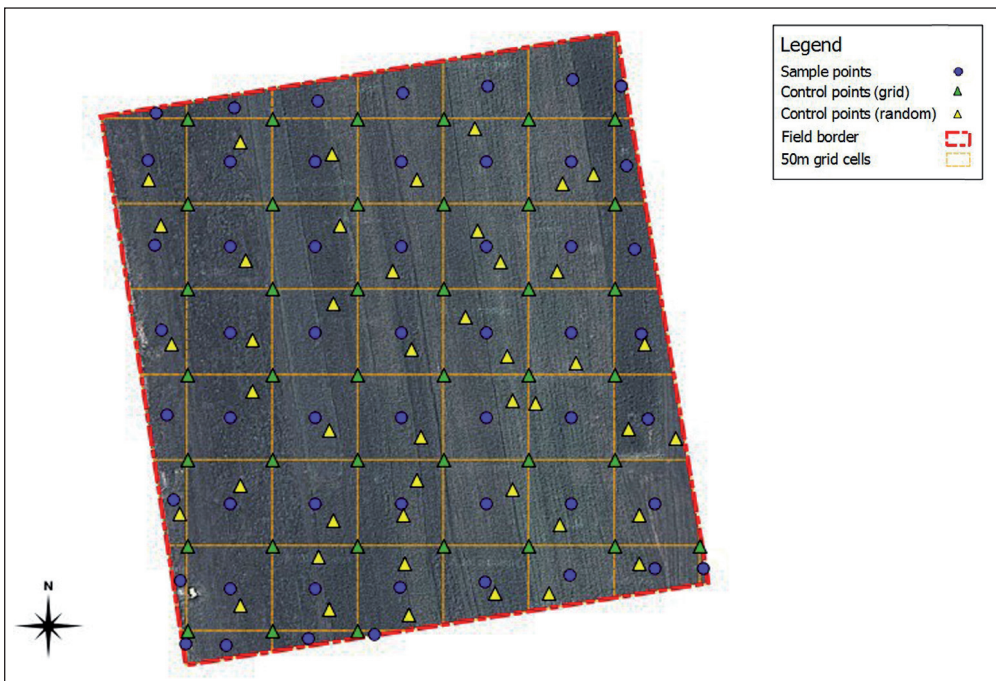
Two case studies were carried out, with the purpose being to show the overall effect of GNSS positional errors on the spatial prediction of soil pH values by comparing the spatial distribution of soil pH derived from point sample values through interpolation by inverse distance weighting (IDW). In order to be deemed acceptable, pH values predicted for the simulated point patterns should fall within 0.2 pH units of the values predicted using the original point pattern, which as mentioned shall be assumed accurate.

### 3.3 Case study 1 (Fig 3)

A total of 8 cases was examined, each with different error values. The simulated error consisted of two components, a randomly generated horizontal distance value conforming to a normal distribution with a  $1-\sigma$  value of 6.4 m, derived from statistical data and an angle, also randomly generated but with a uniform distribution. Assuming that during the sampling process, the time between each sample taken amounted to 5 minutes, the error value at each point was subject to temporal variation based on data from (*M.Olynik et al, 2001*) from which a measure of variation was derived.

**Figure 3**

Sampling and control point patterns for Field 1



In 6 of the cases, conditions were assumed to be generally favorable and the error was generated to fall within 12.8 m, 95% percent of the time, which corresponds to the official GPS SPS performance standard regardless of the age of ephemeris data (AOD). This value includes the User Equivalent Ranging Error (consisting of satellite clock, ephemeris data and atmospheric delay errors) and Dillution of Precision (DOP) due to satellite geometry.

In the remaining 2 cases, an error of up to 30 m was introduced to account for worst-case scenario. All resulting point patterns were interpolated over the 10 ha area of the sampled field using the inverse distance weighting technique with a standard power parameter  $p=2$  (Fig 4). The resulting maps were compared to the original map (assumed accurate) at a total of 85 control points, 40 of which were located at the intersections of the 50x50 m grid cells, and the remaining 45 points were distributed randomly across the field. Subsequently, histograms and basic statistical parameters were calculated for each case and compared.

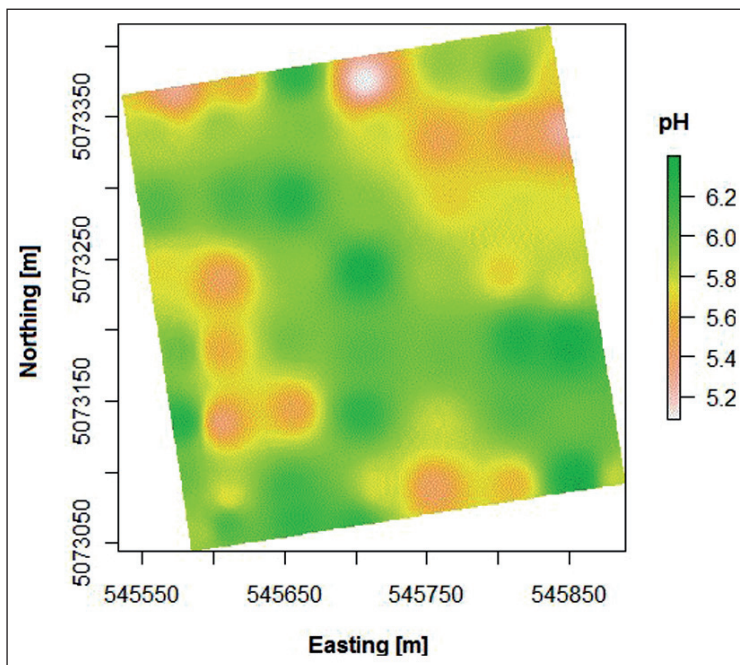


**Figure 4**

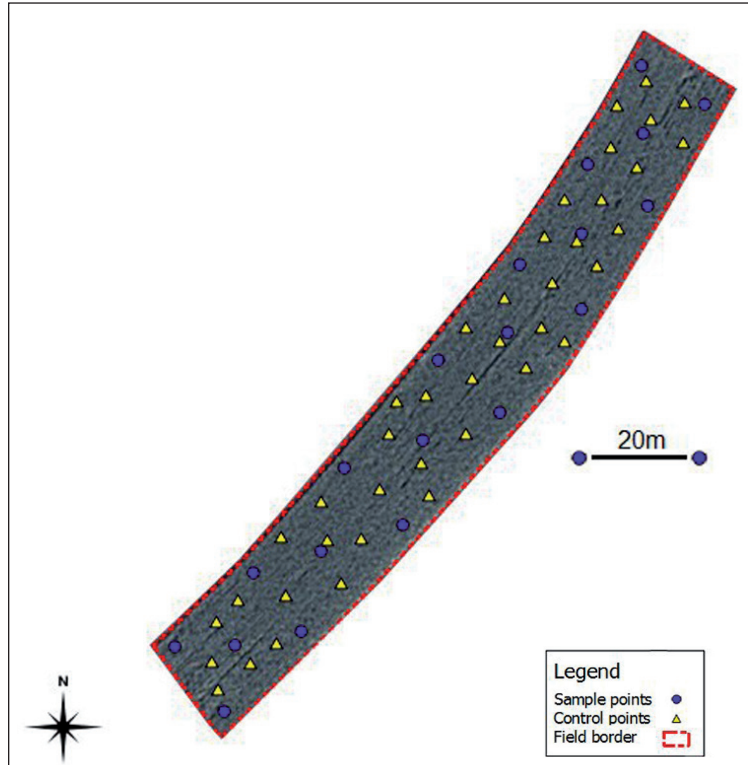
An example of interpolated spatial distribution of pH

### 3.4 Case study 2 (Fig 5)

The same process used in Case Study 1 was applied to the second sampled field. The goal was to show how much the smaller size and irregular shape of the field, as well as a denser sampling interval of 20 m between each point will change the effect of GNSS positioning error on the spatial prediction of soil pH values.

Once again, a total of 8 cases were examined, using approximately the same mean error values as were used in the prior study, for later reference in the first 6 cases. The remaining two cases were simulated with lower error values (2.2 m-3.2 m) to illustrate a best case scenario. Using inverse distance weighting, pH values were interpolated across the 1 ha area of the field and the resulting maps were compared to the original at a total of 40 randomly placed control points.

**Figure 5**  
Sampling and control  
point patterns for  
Field 2



## 4 DISCUSSION

### 4.1 Case study 1

In the first 6 cases, where positional errors ranged from 4.2 m to a maximum of 13.8 m it was found that the impact on the spatial prediction through IDW was relatively small. The maximum deviation of predicted values in the case of a 13.4 m meter mean error (Case 4) amounted to 0.28 pH units and in all cases, the 95-percentile value was within the tolerance.

In the worst cases (Cases 7 & 8) where the mean positional errors amounted to 22.11 m and 17.05 m respectively, the 95-percentile value exceeded the recommended tolerance and the maximum prediction error for Case 7 amounted to 0.57 pH units, which can be seen as a considerable deviation.

To conclude, in all but two cases, which represented worst-case scenarios, the results showed that standard GNSS positioning without the use of differential corrections would perform adequately given a zonal sampling approach on large field plots.

4.2 *Case study 2.* The first 6 cases yielded generally unfavorable results, with the maximum prediction error value going from 0.31 pH units in Case 3 with an average positional error of 4.68 m and reaching 0.67 pH units in Case 1 with an error of 10 m. The 95-percentile values were outside the 0.2 pH tolerance in all of the first 6 cases.

The remaining 2 cases were simulated with mean positional errors of 2.32 and 3.19, respectively. These cases represent a best case scenario where all conditions are favorable (clear sky, low DOP, no additional error sources). In both cases, the mean and 95-percentile values were well within the specified tolerance.

**Table 1**

A summary of results for Case Study 1

| Case | Mean Positional Error | Max. Prediction Error | Mean Prediction Error | 95%     |
|------|-----------------------|-----------------------|-----------------------|---------|
| 1    | 6,16980               | 0,24963               | 0,03951               | 0,13284 |
| 2    | 10,58073              | 0,20152               | 0,04863               | 0,14827 |
| 3    | 4,57256               | 0,16233               | 0,03519               | 0,09197 |
| 4    | 13,46016              | 0,28000               | 0,06230               | 0,17496 |
| 5    | 8,34538               | 0,20525               | 0,04807               | 0,14818 |
| 6    | 9,96606               | 0,23296               | 0,05146               | 0,14082 |
| 7    | 22,11840              | 0,52847               | 0,10510               | 0,28405 |
| 8    | 17,05542              | 0,27493               | 0,06943               | 0,22091 |

**Table 2**

A summary of results for Case Study 2

| Case | Mean Positional Error | Max. Prediction Error | Mean Prediction Error | 95%     |
|------|-----------------------|-----------------------|-----------------------|---------|
| 1    | 6,16980               | 0,67438               | 0,10891               | 0,29106 |
| 2    | 10,59678              | 0,63209               | 0,14400               | 0,45214 |
| 3    | 4,68678               | 0,30875               | 0,07947               | 0,24601 |
| 4    | 13,47342              | 0,40776               | 0,14829               | 0,36647 |
| 5    | 8,35662               | 0,55321               | 0,12122               | 0,32877 |
| 6    | 9,90013               | 0,49909               | 0,16383               | 0,43648 |
| 7    | 2,32060               | 0,20123               | 0,03856               | 0,12390 |
| 8    | 3,19884               | 0,18764               | 0,06064               | 0,14970 |

## 5 CONCLUSION

As it was shown in Case Study 1, the uncorrected GNSS positioning can offer sufficient accuracy for large fields if the sampling is done using a grid based approach, provided the grid cells are of a certain size and the spatial interval between sample points is larger than the positional error itself. However, if the sampling is done at shorter intervals and on smaller fields, the effect of positional errors becomes far greater and errors beyond 3-4 m result in a significant misrepresentation of a variable's spatial distribution as was demonstrated in Case Study 2.

## REFERENCE

- [1] Filjar, R, H Gold, I Markežić. (2011). GNSS: the risk of the underlying technology. *Proc of 5th GNSS Vulnerabilities and Solutions Conference*. Baska, Krk Island, Croatia.
- [2] Filjar, R., S. Kos, R. Mohovic. (2010). Global Navigation Satellite System as a Component of National Infrastructure (7 pages). *UN/Moldova/US Workshop on GNSS Applications*. Kishinev, Moldova.
- [3] Hengl, T. (2009). A practical guide to geostatistical mapping. Tomislav Hengl. Amsterdam, the Netherlands. Available at: <http://bit.ly/vsDWn2>, accessed on 2 January, 2012.
- [4] ICG. (2011). Current and Planned Global and Regional Navigation Satellite Systems and Satellite-based Augmentations Systems. International Committee on Global Navigation Satellite Systems, Office for Outer Space Affairs, United Nations. Vienna, Austria. Available at: <http://bit.ly/bDHbZd>, accessed on 13 October 2011.
- [5] Pebesma, E. (2011). Spatio-temporal geostatistics using *gstat*. Institute for Geoinformatics, University of Muenster, Germany. Available at: <http://bit.ly/vyUARw>, accessed on 2 January, 2012.
- [6] Thomas, M *et al.* (2011). Global Navigation Space Systems: resilience and vulnerabilities. The Royal Academy of Engineering. London, UK. Available at: <http://bit.ly/feFB2i>, accessed on 13 October 2011.



# IONOSPHERIC SCINTILLATION EFFECTS ON THE TRACKING LOOP OF A GPS SOFTWARE RECEIVER

Melania Susi<sup>1</sup>, M. Andreotti<sup>2</sup>, M. Aquino<sup>1</sup>, A. Dodson<sup>1</sup>

<sup>1</sup> Nottingham Geospatial Institute, University of Nottingham, UK  
Triumph Road, Nottingham, NG7 2TU, UK  
E-mail: Melania.Susi@nottingham.ac.uk

<sup>2</sup> NovAtel Inc., Canada

**ABSTRACT.** *GNSS (Global Navigation Satellite Systems) signals traversing small scale irregularities in the ionosphere can experience sudden fluctuations of their amplitude and phase. This phenomenon, known as scintillation, is able to produce serious effects on GNSS, starting from a degradation of the final solution's accuracy up to a total loss of signal lock. During severe scintillation, required levels of accuracy, availability and therefore continuity of GNSS are not met, thus compromising commercial operations, such as maritime navigation, geophysical exploration and airplane navigation during airport precision approach. TRANSMIT (Training Research and Applications Network to Support the Mitigation of Ionospheric Threats) is an Initial Training Network (ITN) funded by the European Commission, whose purpose is to carry out research training aiming to investigate and find solutions to ionospheric related issues potentially affecting GNSS operations. One particular sub-project within the TRANSMIT ITN, entitled "Improved receiver tracking models and GNSS scintillation simulation tool", has the aim to study the problems faced by GNSS receivers under scintillation. First investigations and outcomes of this project are illustrated in this paper.*

**KEY WORDS:** *scintillation, GNSS, software receiver, PLL*

## 1 INTRODUCTION

Due to small scale irregularities in the ionosphere's electron density, transionospheric signals are subjected to fast and unpredictable variations of phase and amplitude known as scintillation. This event can strongly impact the performance of GNSS receivers degrading the final GNSS solution, inducing cycle slips or, in the worst case scenario, preventing the signal tracking. The ionosphere's composition is conditioned by factors of both spatial, i.e. the geographical location, and temporal nature, i.e. seasons, day time, and solar cycle (Gherm et al., 2005). Indeed, ionospheric scintillation events are more likely in the equatorial and high latitude regions, although scintillation characteristics are different for these two regions. In fact high latitude scintillation shows strong phase fluctuations and weak amplitude fades. Conversely, at equatorial latitudes scintillation is characterized by weak phase fluctuations and strong amplitude fades.

Furthermore scintillation occurrence is positively correlated with solar activity, and, consequently its negative impact for GNSS users is expected to be more significant during the years around the next solar maximum, predicted for 2013. Therefore, great is the attention now on ionospheric related issues and on their effects on GNSS systems. To this concern the European Commission has funded a Training Research and Applications Network to Support the Mitigation of Ionospheric Threats (TRANSMIT) , led by the University of Nottingham and involving many universities and institutions in Europe, Canada and Brazil. In this context a sub-project, entitled "Improved receiver tracking models and GNSS scintillation simulation tool", has been defined. The main objective of this sub-project is to investigate scintillation effects at the GNSS receiver level and to mitigate such effects through advanced tracking schemes. In this paper first analysis and results of this sub-project are exposed.

This paper is organized as follows. In Section II possible approaches to model scintillation and test GNSS receivers are discussed. In Section III the software receiver approach is presented. Then, Section IV introduces the implemented Fast Adaptive Tracking scheme, while in Section V results are discussed. Finally, in Section 6 some conclusions are drawn.

## 2 TESTING GNSS RECEIVERS BY MODELING SCINTILLATION

In order to test receiver performance under scintillation both real and simulated data can be used. The main advantage of using simulated data is the possibility to control the different parameters characterizing scintillation and to reproduce

identical scenarios in different times. This aspect is quite appealing for the evaluation of GNSS receivers since, for example, it ensures that the performance of different receivers can be compared under the same conditions. However, simulated scintillation should ideally reproduce realistic scenarios as much as possible. To pursue this objective, different scintillation models can be used. For example, a physical model taking into account the specific structure of the ionosphere for a specific location and time could be adopted. This approach enables reproducing different scintillation scenarios, enriching the possible applications. However, physical models require a high number of input parameter and generally high computation cost. Another possible approach is to implement the random screen theory which requires the availability of experimental data. Indeed random screen theory's parameters are selected in order to fit the real data (Gherm et al., 2005). Finally, statistical models have been largely used in view of their simplicity.

In particular the Cornell scintillation model (Hinks et al., 2008), a statistical model able to model equatorial scintillation, has been used for receiver testing in view of its simplicity. The model is based on the assumption that the Probability Distribution Function (PDF) of amplitude scintillation is well approximated by a Rice distribution while the power spectrum of phase scintillation can be approximated by the response of a second order Butterworth filter. This model is particularly suitable for testing GNSS receivers since it characterizes the scintillation features which are more challenging for the GPS (Global Positioning System) receiver's signal processing components. Once scintillation histories have been created they can then be used to perturb a clean GPS signal.

Indeed, a GPS signal affected by scintillation can be expressed in its complex form as:

$$s = A(\Delta A)e^{j(\phi + \Delta\phi)} \quad (1)$$

where

- $A$  is the signal amplitude and  $\Delta A$  is the variation in amplitude due to scintillation
- $\phi$  is the signal phase and  $\Delta\phi$  is the variation in phase due to scintillation.

### 3 GPS SOFTWARE RECEIVER

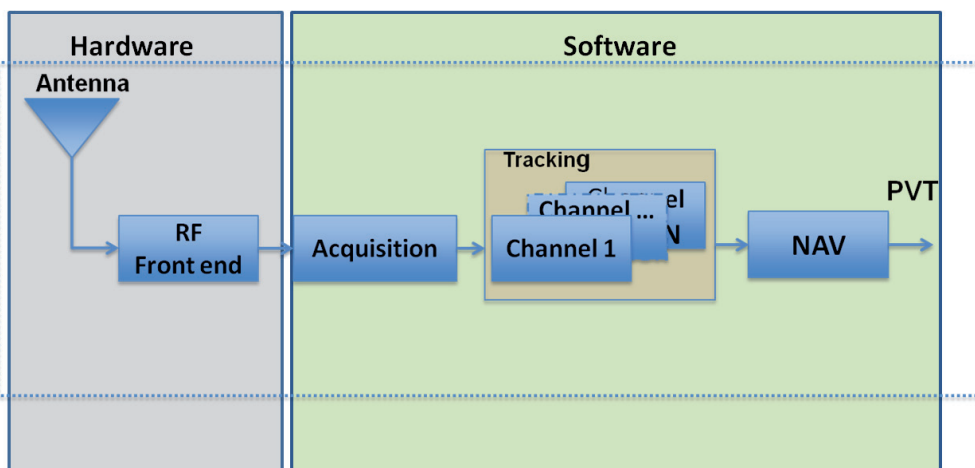
Working with GPS (Global Positioning System) receivers at hardware level to analyze various parts of the signal processing in the GPS processing chain is not always feasible. Most of the processing is done inside specific electronics chips

(so called ASICs, or ‘Application Specific Integrated Circuits’), and therefore it is not possible sometimes to access results from intermediate steps as the GPS signal is processed inside the receiver. One way around this is to make use of a software based approach, which reproduces the GPS processing that takes place inside of ASICs.

A popular open source GPS L1 software receiver developed by K. Borre et al. (2007) has been used for the analysis described in this paper. Software receivers are very powerful tools for investigating receiver performance since they offer many advantages; they are flexible, reconfigurable and low cost. A GPS receiver, whose general structure is reported in Figure 1, is composed of different blocks, each with a specific function. Antenna and front end are the only hardware components used in this research work. All the other blocks represented in Figure 1 and included in the green box are implemented in the software receiver.

As shown in Figure 1, the first receiver element is the antenna that receives the signal coming from the satellite. Since the signal arriving at the antenna is very weak the front end has the purpose to filter, amplify, and down convert it to an intermediate frequency (IF) that can be processed by the following blocks. After that, the acquisition block checks all satellites in view and provides a rough estimate of code delay and Doppler frequency for each channel. It is worth pointing out that the acquisition’s outcome is not precise enough to be used for computing the navigation solution. For this reason the rough estimate provided by the acquisition block has to be refined. This is the task of the tracking stage. Specifically, the tracking loop evaluates the refined code delay and the Doppler

**Figure 1**  
GNSS receiver’s scheme.

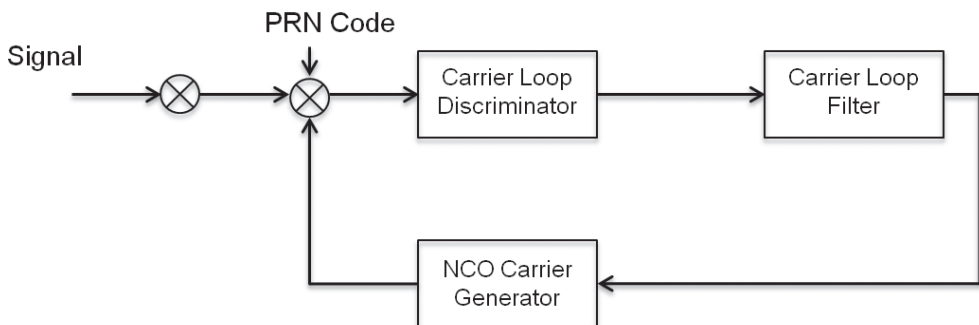


frequency along with the carrier phase. Then, these measurements are exploited by the navigation block to compute the final navigation solution.

More in detail, the tracking stage of GPS receivers is composed of two concatenated loops, namely the PLL (Phase Lock Loop) and the DLL (Delay Lock Loop) that estimate, respectively, the carrier phase and the code measurements. The PLL, which is the focus of this paper, is particularly sensitive to the deep fading and phase variations of the input signal that can be caused by ionospheric scintillation. For this reason, specific countermeasures have to be adopted to render this stage more robust to scintillation. In Figure 2 the general scheme of a PLL is represented. In a PLL the input signal is correlated with the Pseudo Random Noise (PRN) code evaluated by the DLL and then correlated with a local carrier produced by the Numerical Controlled Oscillator (NCO). After that, the carrier loop discriminator evaluates the phase error between local and input carrier. Finally, the loop filter refines the error's estimation and its output is used to tune the NCO, therefore closing the loop.

**Figure 2**

PLL structure



The order of the loop filter is indicative of the PLL's capability to react to signal dynamics. Since scintillation events can produce high signal dynamics, a third order loop filter has been implemented in this work, replacing the original second order loop filter of the used software receiver. The transfer function of the loop filter can be expressed in the  $z$  domain by the following expression:

$$D(z) = \frac{\sum_{n=0}^{N-1} b_n z^{n-1}}{(1-z^{-1})^{N-1}} \quad (2)$$

with  $N$  representing the order of the tracking loop. Furthermore, the optimum coefficients ( $b_0, b_1, b_2$ ) for a third order loop are so expressed (Kaplan, 2006):

$$b_0 = \frac{T_{coh}^2 \omega^3}{4} + \frac{a^{(0)}_3 \omega^2 T_{coh}}{2} + b_3^{(0)} \omega_0 \quad (3)$$

$$b_1 = \frac{T_{coh}^2 \omega^3}{2} - 2b_3^{(0)} \omega_0 \quad (4)$$

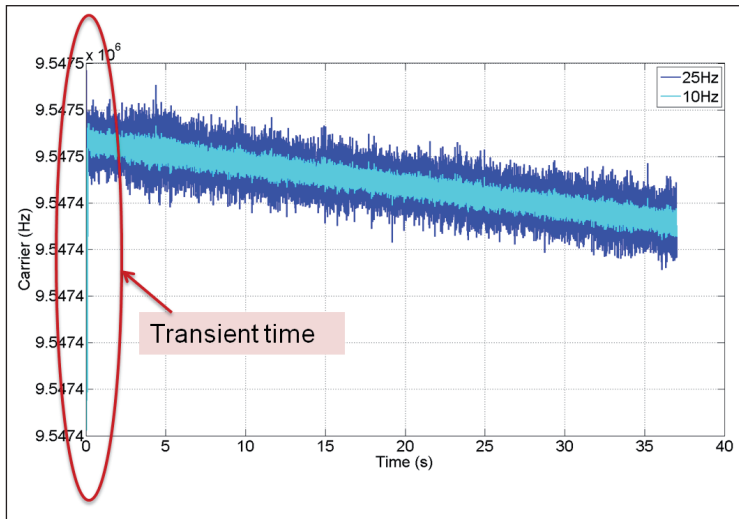
$$b_2 = \frac{T_{coh}^2 \omega^3}{4} - \frac{a^{(0)}_3 \omega^2 T_{coh}}{2} + b_3^{(0)} \omega_0 \quad (5)$$

where

- $a_3 = 1.1$  and  $b_3 = 2.4$  as in Kaplan et al (1996)
- $T_{coh}$  is the pre-integration time
- $\omega_0$  is the natural frequency related to the carrier loop noise bandwidth (Kaplan, 2006) according to the expression  $\omega_0 = B_n / 0.7845$ .

Another key parameter for the design of the loop filter is the bandwidth. The filter bandwidth is responsible for the amount of noise transferred from the input to the estimated phase in the output. Lower PLL bandwidth values allow rejecting a larger amount of noise. Scintillation, especially the equatorial type, is characterized by abrupt fluctuations in the signal intensity, and therefore degrading the signal to noise ratio, or  $C/N_0$ . Consequently, a narrower bandwidth would be preferred. On the other side, a loop filter with narrower bandwidth values requires a longer transition time. This contradiction becomes clear by observing Figure 3, where the carrier response for two bandwidth values is reported. Here, using the 25 Hz bandwidth produces a noisier output, but a faster response on the abrupt signal variation at the beginning, whereas using the 10 Hz PLL filter bandwidth produces a less noisy output, but slower response at abrupt signal variations. This aspect is particularly critical in presence of high dynamics as the ones produced by strong scintillation events.

For this reason, in case of strong scintillations, higher PLL bandwidth values are expected to improve the tracking loop performance but also to increase the noise level of the GPS phase measurement. Consequently, in absence of scintillation, or for low scintillation levels, the selection of a high bandwidth value could be a

**Figure 3**

Carrier response for two PLL loop filter's bandwidth values

suboptimum choice. These considerations suggest the use of an Adaptive Bandwidth tracking scheme enabling the optimum bandwidth selection for each specific case. In fact this approach allows tuning the PLL bandwidth according to the experienced signal dynamics and, subsequently, to the experienced scintillation level. To evaluate the optimum bandwidth the method adopted in (Mao et al., 2005) is here used and briefly described in the following section.

#### 4 ADAPTIVE BANDWIDTH PLL

The adaptive bandwidth PLL in (Mao et al. 2010, Skone et al. 2005) evaluates the optimum bandwidth value starting from the assumption that the main contribution to the PLL phase error is given by the phase jitter and the dynamic stress. Furthermore, by rule of thumb (Kaplan, 1996) the PLL total phase error should be less than  $15^\circ$

$$\sigma_{t,PLL} + \frac{\vartheta_e}{3} < \lambda \quad (6)$$

where

- $\sigma_{t,PLL}$  is the thermal noise
- $\vartheta_e$  is the dynamic error
- $\lambda$  is the error threshold set to 15 Hz as previously mentioned.

The thermal noise error is evaluated by the following:

$$\sigma_{i,PLL} = \frac{360}{2\pi} \sqrt{\frac{B_n}{C/N_0} \left( 1 + \frac{1}{2T_{coh}/N_0} \right)} \quad (7)$$

where  $B_n$  is the loop bandwidth,  $C/N_0$  is the carrier to noise ratio and  $T_{coh}$  is the coherent integration time

The dynamic error for the third order loops case is so defined:

$$\vartheta_e = 0.4828 \frac{d^3R}{B_n^3} \quad (8)$$

Where  $d^3R/dt^3$  is the Line Of Sight (LOS) jerk. To evaluate the jerk noisy data are accumulated for 200 ms following the approach adopted in Mao et al. (2010).

$$Accel(k) = \lambda_{L1} K_0 \sum_{i=0}^2 b_i B_n^3 \sum_{n=1}^N \theta_e(\infty)_n T_{coh} \quad (9)$$

where

- $N = 200 \text{ ms}/T_{coh}$
- $b_i$  are the coefficients of the third order loop filter
- $\theta_e(\infty)$  refers to the measurement from the PLL discriminator,
- $B_n$  is the loop bandwidth
- $\lambda_{L1}$  is the wavelength of GPS L1

Then the jerk for a specific instant  $k$  is computed as a derivative of the acceleration as follows

$$\left. \frac{d^3R}{dt^3} \right|_{t=k} = \frac{Accel(k) - Accel(k-i)}{iT} \quad (10)$$

Finally, knowing the dynamic stress and the thermal noise the optimum bandwidth value can be found by iterating the (6).

## 5 EXPERIMENTAL TEST

In order to simulate a GPS L1 signal the GSS8000 Spirent signal simulator, available at the University of Nottingham, has been used. The Radio Frequency (RF) measurements are collected by using a Universal Software Radio Peripheral (USRP) front end. An external Low Noise Amplifier (LNA) with tuning gain is also connected between the simulator and the front-end. The characteristics of the collected data are reported in Table 1. Finally, the collected data have been input into the GPS software receiver, as shown in Figure 4. For these tests, the amplitude perturbations have been synthetically added to the clean signal generated by the hardware simulator assuming a Rice distribution of the perturbation as in (Hinks et al., 2008).

**Figure 4**

Experimental test set-up

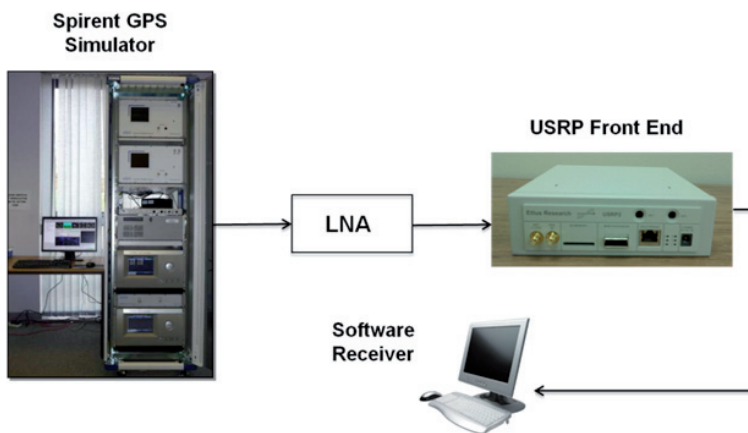


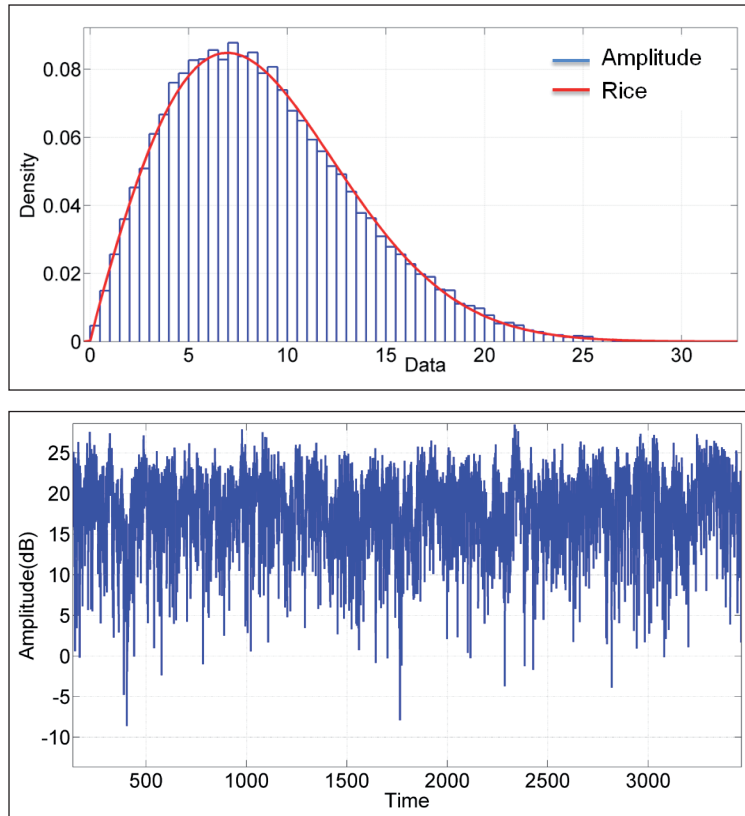
**Table 1**

Details of collected GPS signals

| Parameters             | Value            |
|------------------------|------------------|
| Sampling Frequency     | $f_s = 8$ MHz    |
| Intermediate Frequency | $f_{IF} = 0$ MHz |
| Sampling               | Complex          |

In Figure 5 (upper) the Rice distribution of the generated scintillation amplitude is reported while in Figure 5 (down) the generated data affected by scintillation are shown.

**Figure 5**  
 (Upper) amplitude scintillation distribution;  
 (Down) Signal affected by simulated amplitude scintillation



The standard deviation of the received signal power normalized by the average signal power is conventionally used to indicate the level of scintillation amplitude. This parameter, known as  $S_4$ , is normally used to characterise different levels of amplitude scintillation. In Figure 6 the real part of the correlator output is represented for the fixed and adaptive bandwidth cases when  $S_4$  is equal to 0.6 which corresponds to a quite strong level of amplitude scintillation. From Figure 6 it is clear that the adaptive tracking scheme outperforms the fixed PLL bandwidth. Indeed, in the adaptive case it is still possible to identify the bits without ambiguity while in the fixed case the bits are corrupted in correspondence of high values of  $S_4$ .

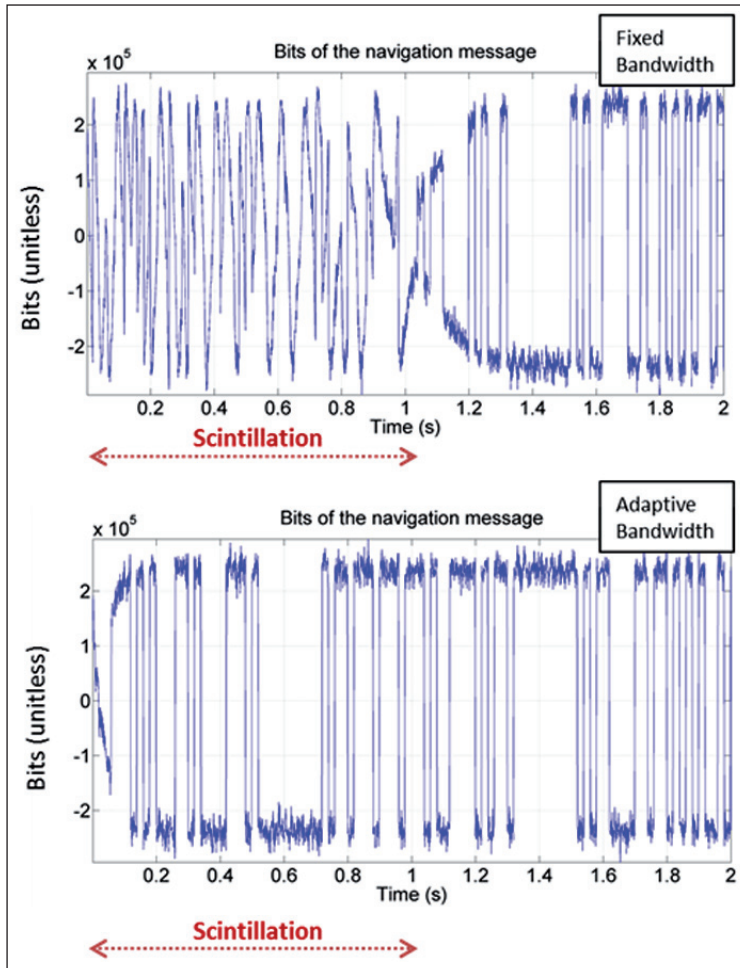


**Figure 6**  
 (Upper) Bits of the navigation message for the fixed bandwidth PLL ( $B = 15$  Hz);  
 (Down) Bits of the navigation message for the adaptive bandwidth PLL

## 6 CONCLUSION AND FUTURE WORKS

In this paper the effects of signal amplitude variations on the PLL of a software receiver have been investigated. The effects of ionospheric scintillation on GPS receivers have been presented with attention to the PLL block on the GPS signal processing chain, which is the part of the receiver most sensitive to signal variations. The impact of different bandwidths on the PLL loop filter was demonstrated and an adaptive approach for the filter has been tested using a GPS software receiver. The use of an adaptive bandwidth tracking loop seems to improve the performance in the case of strong amplitude variations as can be the case under scintillation. Further studies will be performed to investigate the effects of phase variations on the adaptive bandwidth PLL.

Work is ongoing for testing the adaptive tracking scheme by using also a physics based model (Gherm et al., 2005). Although physical models increase the computational cost, they allow recreating a large variety of scenarios, including high latitude and very strong scintillation cases ( $S_4 > 1$ ), which cannot be modelled by using the Cornell scintillation model.

## REFERENCE

- [1] Gherm, V. E., N. N. Zernov, and H. J. Strangeways (2005). Propagation model for transionospheric fluctuational paths of propagation: Simulator of the transionospheric channel, *Radio Sci.*, 40, RS1003, doi: 10.1029/2004RS003097.
- [2] Hinks, J.C., T.E. Humphreys, B.W. O'Hanlon, M.L. Psiaki, P.M. Kintner, Jr. (2008). "Evaluating GPS Receiver Robustness to Ionospheric Scintillation", *Proceedings of ION GNSS*, The Institute of Navigation, Savannah, Georgia,
- [3] Borre, K., Akos, D. M., Bertelsen, N., Rinder, P., Jensen S. H. (2007). *A Software-Defined GPS and Galileo Receiver*, Birkhäuser, Boston, 176p.
- [4] Kaplan, E. D. (1996). *Understanding GPS: Principles and Applications*, Artech House Publishers, 1996.
- [5] Mao, X., Morton, Y.T., Zhang, L., Kou, Y., (2010). "GPS Carrier Signal Parameters Estimation Under Ionosphere Scintillation," *Proceedings of the 23rd International Technical Meeting of The Satellite Division of the Institute of Navigation (ION GNSS 2010)*, Portland, OR, September, pp. 3277-3283.
- [6] Skone, S., G. Lachapelle, D. Yao, W. Yu, and R. Watson (2005) "Investigating the Impact of Ionospheric Scintillation using a Software Receiver," in *Proceedings of ION GPS/GNSS*, 13-16 Sept, Long Beach CA, pp 1126-1137.



Faculty of Maritime Studies  
University of Rijeka, Croatia



Royal Institute of Navigation  
Science Technology Practice



The University of  
Nottingham

**6<sup>th</sup> GNSS**

Vulnerabilities  
and Solutions  
Conference

# GPS RECEIVER POSITIONING PERFORMANCE

**Josip Vuković, Tomislav Kos, Pavel Najman**

University of Zagreb, Faculty of Electrical Engineering and Computing,  
Department of Wireless Communications  
Unska 3, 10 000 Zagreb, Croatia  
E-mail: josip.vukovic@fer.hr

**ABSTRACT.** *NMEA sequences of three consumer grade GPS receivers of different age and prices were recorded. GPS signal obtained through a fixed, roof-mounted antenna was fed to the receivers in the lab. Their performance in quiet space weather and tropospheric weather conditions is compared. Positioning drifts caused by a solar storm and a snow storm are examined. Other positioning anomalies are described, especially diurnal height variation and constellation related effects. Overall consumer grade receiver positioning performance is evaluated.*

**KEY WORDS:** *consumer grade GPS receiver, height fluctuation, ionospheric error, tropospheric error*

## 1 INTRODUCTION

In GNSS systems there are different positioning errors, such as ionospheric error, tropospheric error, multipath propagation error and clock biases. Ionospheric error is the most important cause of accuracy degradation in the estimation of the propagation time and consequently, in the position calculation. This is particularly significant in periods of high solar activity, which occur every eleven years and will have the peak in the year 2013. Influence of the ionosphere on high end, precise GPS receivers is usually observed. However, its influence on low end devices is not fully depicted. Other error causes which do not affect positioning performance on advanced devices as much as ionospheric error can have strong impact on less expensive and less sophisticated GPS receivers.

## 2 TEST SYSTEM SETUP

In the beginning of the measurements, test system consisted of a roof mounted Huber+Suhner 1315.17.0013 antenna and a consumer grade single-frequency Garmin III Plus GPS receiver, connected to the computer which was recording NMEA sequence for later analysis. NMEA sequence was recorded by VisualGPS 4.2 software. The environment of the antenna had minimal multipath probability and open view to the entire sky, constantly providing high number of visible satellites. After unusual measurements results with diurnal height variation were noticed, additional receivers needed to be introduced for validation of the obtained results. Sheng Jay Automation Bluetooth GPS Receiver SJ-5286AIII and i-gotU GPS Travel Logger GT-200 were available for the measurements. Those receivers are newer than Garmin III Plus and use more sophisticated SiRFstarIII microcontroller chip, but also cost significantly less than Garmin in the time of acquisition, a decade ago.

These receivers have no option for connecting an external antenna so measurement system had to be rearranged. The roof-mounted antenna was connected through a splitter to a DC power supply for the antenna amplifier and to a simple GPS antenna situated in the laboratory, which retransmitted the received signal. All used receivers were placed under this antenna, having receiving conditions as if they were on the roof. In comparison with the receiver connected directly to the roof-mounted antenna, signal strength on the Garmin receiver in this system setup was on average 1 dB lower. The difference is minor so usage of this system setup with two additional receivers is valid. Recorded NMEA sequences allow analysis of GPS positioning performance over longer period and receiver performance comparison. Test system collected data for several weeks.

### 3 MEASUREMENT

The Garmin receiver calculates position every two seconds and the other two receivers calculate it every second. Latitude and longitude on i-gotU and Bluetooth receivers are calculated with one digit more than on the Garmin receiver, providing better precision. I-gotU receiver software uses averaging, which does not take into account small changes in latitude, longitude and height. It keeps previously calculated values instead, until the change is significant enough to be shown as a different positioning point. Bluetooth receiver demonstrates the same problem, but with less position deviation flattening. In quiet solar and tropospheric weather conditions, the Garmin receiver positioning performance was better than other receiver performance in spite of the lack of one digit in latitude and longitude calculation, as Table 1 shows.

**Table 1**

Positioning statistics for week 16-23 March 2012

|                        | Garmin III+ | i-gotU GT-200 | Bluetooth   |
|------------------------|-------------|---------------|-------------|
| <b>Height [m]</b>      |             |               |             |
| Mean                   | 178.42056   | 177.7940761   | 170.7990984 |
| Median                 | 178.4       | 177.7         | 171.3       |
| Standard deviation     | 3.90016243  | 8.66160904    | 4.710422778 |
| Minimum                | 160.5       | 151.1         | 117.8       |
| Maximum                | 194.4       | 206.4         | 204.2       |
| <b>Longitude [° E]</b> |             |               |             |
| Mean                   | 15.97085328 | 15.97086029   | 15.97084906 |
| Median                 | 15.97085    | 15.97086167   | 15.97085    |
| Standard deviation     | 1.72369E-05 | 6.69469E-05   | 2.04105E-05 |
| Minimum                | 15.97078333 | 15.97066333   | 15.97073833 |
| Maximum                | 15.97096667 | 15.97101833   | 15.97096167 |
| <b>Latitude [° N]</b>  |             |               |             |
| Mean                   | 45.80154349 | 45.80154679   | 45.80154741 |
| Median                 | 45.80155    | 45.80154833   | 45.80154667 |
| Standard deviation     | 1.70912E-05 | 6.81261E-05   | 2.0077E-05  |
| Minimum                | 45.80146667 | 45.80131667   | 45.80137333 |
| Maximum                | 45.80165    | 45.80178      | 45.80169333 |

**Figure 1**  
 Height measurement  
 in week 16-23 March  
 2012 for  
 (a) Garmin;  
 (b) i-gotU;  
 (c) Bluetooth receiver

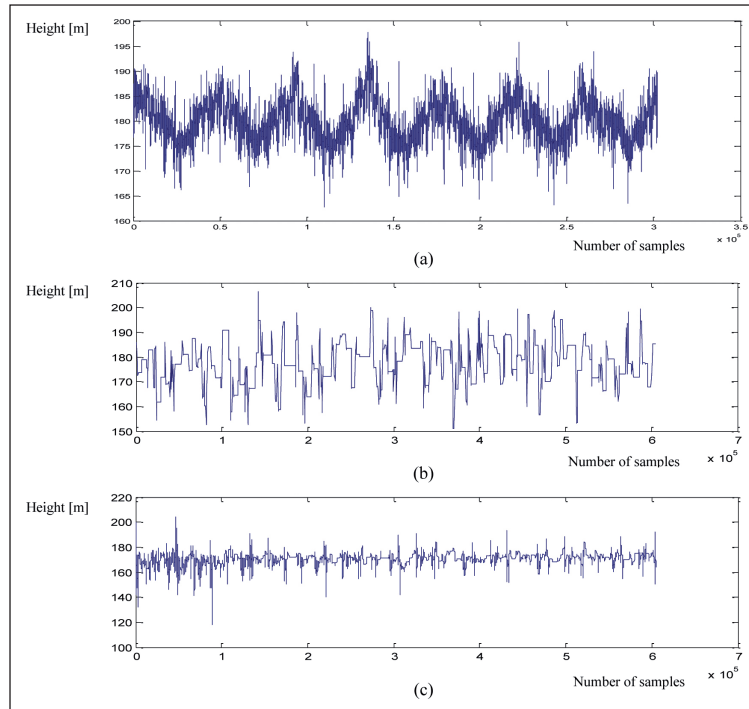
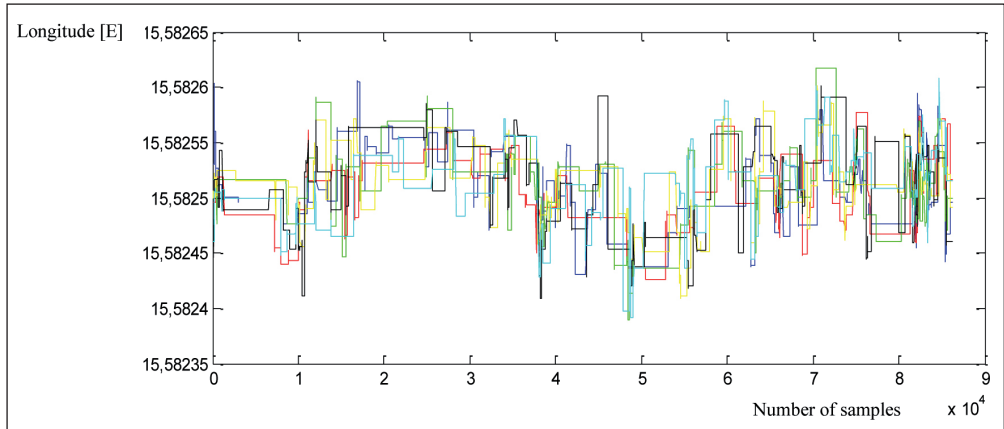


Figure 1 shows height measured in one week by all three receivers, with time on  $x$  axis, represented by the number of samples. Garmin vertical positioning shows diurnally periodic fluctuation. Fluctuation reaches maximal measured height around 13:00 hours and minimal height around 3:00 hours every day. Height difference between those extremes is 10 meters on average. The other two receivers do not produce this anomaly, which means it is Garmin specific. The anomaly does not match GPS constellation repeat time of 23 hours and 56 minutes, but repeats every 24 hours. This points out that the cause of Garmin diurnal height variation is software based, specifically related with the time of day. Figure 1 also demonstrates consequences of the averaging procedures on i-gotU.

Longitude calculation on the i-gotU receiver displays slow fluctuation, following the satellite constellation repeat time. Figure 2 shows longitude calculated in six consecutive satellite repeat time cycles, with calculation of each 23:56 h section represented by different colour. In the morning and in the afternoon position is calculated more to the east, while around the noon and in the early morning, calculation results in a position more to the west.

In periods of disturbed tropospheric weather, impact on positioning performance was higher than expected. Snow storm that occurred on 21 January 2012 and

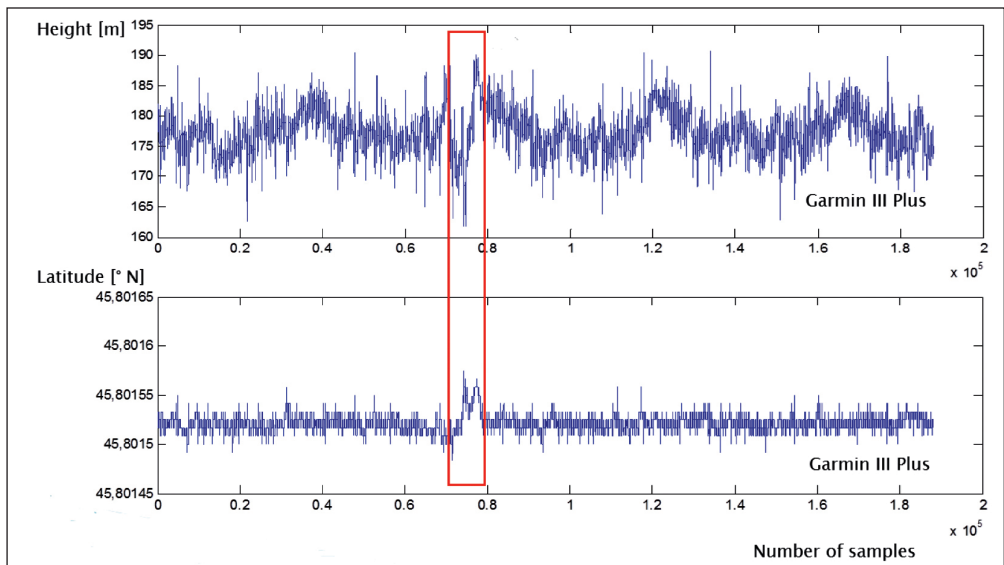
**Figure 2**  
i-gotU longitude fluctuation



lasted for several hours caused positioning error of 25 m in height and 7 m in latitude and longitude on Garmin (Figure 3). Other receivers were not yet introduced at the time of this occurrence.

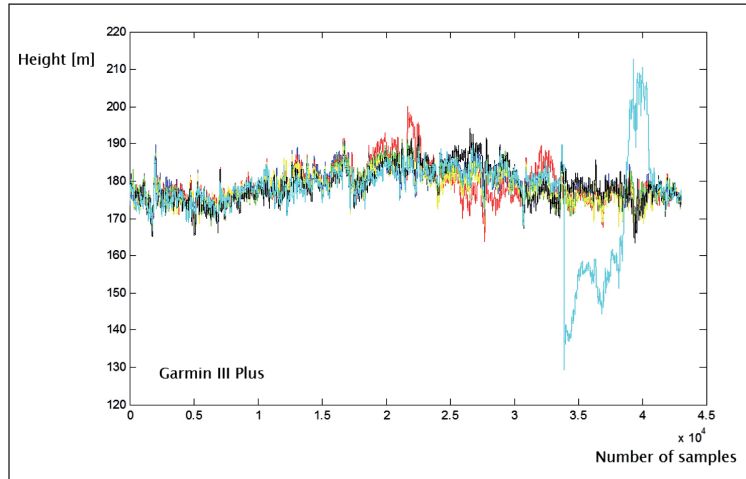
Considering an increase of the solar activity because of the nearing 11-year maximum, it was expected that ionospheric storms might appear. Strong solar

**Figure 3**  
21 January 2012 snow storm positioning impact



flares occurred between 7 March and 13 March 2012 (NOAA readings). All the receivers were recording data at that time, but only Garmin experienced difficulties in positioning. Figure 4 shows daily height measurement of 7-14 March 2012, overlapped on top of each other. Red and cyan lines show deflection from usual daily measurements, red representing 9 March and cyan representing 13 March. The height reached minimum at 129.3 m and maximum at 212.7 m. This level of error is significant even to less demanding applications of GPS.

**Figure 4**  
Height measurement  
in period of high solar  
activity



The last positioning anomaly, observed on all three receivers' latitude and longitude measurement, was constellation related. It appeared in different periods and with different intensity for every receiver. Characteristic spikes in positioning performance appeared 4 minutes earlier every day, corresponding to the constellation repeat time. These biases did not have high amplitude and lasted from several minutes to couple of hours. Constellation arrangements in periods of these events will be further analysed.

## 4 CONCLUSION

Influence of sudden tropospheric and ionospheric disorders on consumer grade GPS receiver positioning performance, along with anomalies observed in quiet weather conditions were analysed. Even in ideal atmospheric conditions, consumer receivers produced noticeable positioning error. Height calculation appeared to vary the most, showing vulnerability in case of both, quiet and disturbed ionosphere. Every tested receiver had some downsides in its regular

performance. These receivers can face significant positioning discrepancies caused by tropospheric and ionospheric disorders or by buildings obstructing and reflecting satellite signals. Receiver movement additionally increases the problems. Single frequency receivers with no SBAS facility are wide spread and cost less and less. These devices can be successfully used in numerous situations, but users should be aware of the level of their positioning accuracy.

## ACKNOWLEDGEMENT

The work described in this paper was conducted under the research project: “Environment for Satellite Positioning” (036-0361630-1634), supported by the Ministry of Science, Education and Sport of the Republic of Croatia.

## REFERENCES

- [1] Bilitza, D., (2006). The international reference ionosphere – climatological standars for the ionosphere, *Characterising the Ionosphere*, pp. 32-1 – 32-12, Meeting Proceedings RTO-MP-IST-056.
- [2] Filjar, R., (2007). Ionospheric component of satellite positioning error due to extreme space weather disturbances (Pogreška satelitskog određivanja položaja zbog ekstremnih ionosferskih poremećaja), PhD thesis, University of Zagreb, Faculty of Electrical Engineering and Computing.
- [3] NOAA / Space Weather Prediction Center, Today's Space Weather, <http://www.swpc.noaa.gov/today.html>, accessed in March 2012.
- [4] Samama, N., (2008). *Global Positioning: Technologies and Performance*, Wiley Interscience.
- [5] Schüler T., (2001). *On Ground-Based GPS Tropospheric Delay Estimation*, PhD thesis, Universität der Bundeswehr, Munich.
- [6] Xinlong, W., Jiaying, J., Yafeng, L., (2009). The applicability analysis of troposphere delay error model in GPS positioning, *Aircraft Engineering and Aerospace Technology*, **81**, Iss: 5, pp.445-451.
- [7] Wing, M.G., Eklund, A., Kellogg L.D. (2005). Consumer grade global positioning system (GPS) accuracy and reliability. *Journal of Forestry*, **103**, 169-173.





Faculty of Maritime Studies  
University of Rijeka, Croatia



Royal Institute of Navigation  
Science Technology Practice



The University of  
Nottingham

**6<sup>th</sup> GNSS**  
Vulnerabilities  
and Solutions  
Conference

# PROGRESS OF BEIDOU NAVIGATION SATELLITE SYSTEM AND GNSS EDUCATION

Jingnong Weng<sup>1</sup>, Jun Lu<sup>2</sup>, Dongkai Yang<sup>1</sup>, Min Zhang<sup>1</sup>

<sup>1</sup> Beihang University, Beijing, China 100191  
XueYuan Road No.37, HaiDian District, BeiJing, China  
E-mail: wengjn@buaa.edu.cn

<sup>2</sup> China Satellite Navigation Office, Beijing, China 10083

**ABSTRACT.** *The construction of BeiDou System goes smoothly with 13 satellites launched and the initial service was released on December 27, 2011. As an essential element of GNSS, BeiDou will further enhance compatibility and interoperability with other GNSS through international cooperation, promote monitoring and evaluation of GNSS open services, as well as accelerate the demonstration application of BeiDou/GNSS. China has already promoted the demonstration of application programs in Asia-Pacific area. Up to now, domestic users can evaluate the system performance through pilot operation. Since 2003, the demonstration system has been widely used in many fields and brought remarkable social and economic benefits. Adhering to the policy of opening up to the outside world, and actively engaging in international space exchanges and cooperation, China supports all activities that utilize outer space for peaceful purposes. With the demands of United Nations International Committee on Global navigation satellite system for GNSS education and training, particularly in the promotion of GNSS applications in the developing nations, China, as one of GNSS providers has dedicated to the development of GNSS research and education. In this paper, Beidou system and its latest development and activities on GNSS education and training will be introduced.*

**KEY WORDS:** *BeiDou, progress, GNSS education*

## 1 DEVELOPMENT PLAN

As a global navigation satellite system compatible with other navigation satellite systems worldwide, the BeiDou system is independently established and operated by China. Here will briefly describe the roadmap of the BeiDou system.

### A. System description

The BeiDou system is comprised of three main components: space constellation, ground control segment and user terminals.

- The space constellation consists of 5 GEO satellites and 30 non-GEO satellites (include 27 MEO satellites and 3 IGSO satellites).
- The Ground Control Segment consists of several Master Control Stations (MCS), Upload Stations (US), and a network of globally distributed Monitor Stations (MS).
- The User Terminals include various BeiDou user terminals, and terminals compatible with other navigation satellite systems, to meet different application requirements from different fields and industries.

### B. System planning

According to development principle of “independency, openness, compatibility and gradualness”, and following the general guideline of starting with regional services and then expanding to global services, the BeiDou system is steadily accelerating the construction based on a “three-step” development strategy, as shown in figure 1.

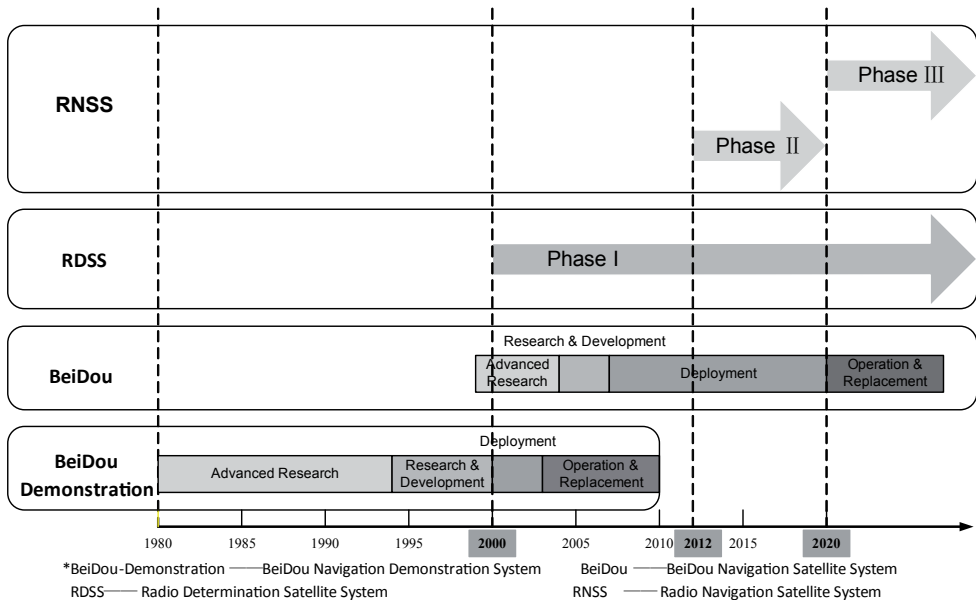
#### *Step 1: BeiDou navigation satellite demonstration system*

In early 1980s, China began to actively study the navigation satellite system in line with China’s conditions. In 1994, China started construction of BeiDou navigation satellite demonstration system. In 2000, two BeiDou navigation experiment satellites were launched, and BeiDou navigation demonstration system is basically established. In 2003, the third BeiDou navigation experiment satellite was launched, further enhancing the performance of BeiDou navigation demonstration system.

#### *Step 2: BeiDou navigation satellite (regional) system*

In 2004, China started construction of BeiDou navigation satellite system. In 2007, the first satellite, a round medium earth orbit satellite was launched. By

**Figure 1**  
BeiDou system roadmap



the end of 2012, the BeiDou system will consist of 14 satellites, including five GEO satellites, five IGSO satellites (two in-orbit spares), and four MEO satellites.

***Step 3: BeiDou navigation satellite system with global coverage will completely be established by 2020.***

BeiDou demonstration system uses the radio determination satellite system (RDSS), which only needs two geostationary satellites, and completes the distance measurement and position calculation by the central control system based on user responses. Therefore, BeiDou demonstration system is an active positioning system. It has the dual role of positioning and communications, and promotes the start of China’s navigation satellite system with a smaller price.

BeiDou navigation satellite system uses the integrated system of radio determination satellite system (RDSS) and radio navigation satellite system (RNSS), not only provide users with radio navigation satellite service, just like GPS, GLONASS, GALILEO, but also provide position reporting and short-message communication function.

### C. Service performance

Form December 27<sup>th</sup> 2011, BeiDou system provides Initial Operational Capability (IOC) of regional services. The main service performances are as follows:

- Service Coverage Area: From 84°E to 160°E; from 55°S to 55°N
- Positioning Accuracy: Horizontally 25meters, Vertically 30 meters
- Velocity Accuracy: 0.4m/s
- Timing Accuracy: 50 ns

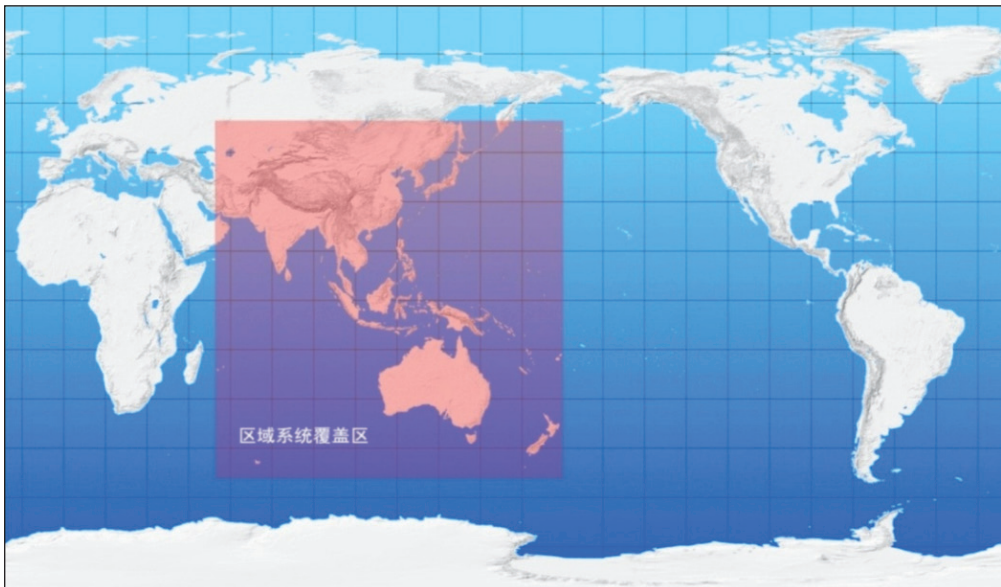
By the end of 2012, BeiDou system will achieve full Operational Capability (FOC) of regional services. The main service performances are as follows:

- Service Coverage Area: From 84°E to 160°E; from 55°S to 55°N
- Positioning Accuracy: 20 meters
- Velocity Accuracy: 0.2m/s
- Timing Accuracy: 20 ns

By 2020, BeiDou system will achieve full Operational Capability (FOC) of global services. The main service performances are as follows:

#### Figure 2

Regional Service Coverage Areas



- Service Coverage Area: Global
- Positioning Accuracy: <10 meters
- Velocity Accuracy: <0.2m/s
- Timing Accuracy: <20 ns

## 2 CURRENT PROGRESS

The construction of BeiDou System goes smoothly with 10 satellites launched. In December 27<sup>th</sup>, 2011, initial operational service provision was announced. Along with the release of initial service, two documents were also published: Interface Control Document (ICD) of BeiDou Navigation Satellite System (test version), Development of BeiDou Navigation Satellite System (V1.0).

By the end of April 2012, 13 BeiDou satellites have been launched and already formed the basic system. It retains the active positioning and short message services from BeiDou Navigation Satellite Demonstration System, and provides Initial Operational services to China and most parts of its surrounding areas, including continuous passive positioning, navigation and time services.

Based on the launching plan, 3 more satellites will be launched in 2012 to further expand service area, to improve performances and to provide services for more parts of Asia-Pacific region. The following tables list the launch record of BeiDou Satellites.

**Table 1**

Launch Record of BeiDou Satellites before Nov 2011

| Date       | Type | Launch Site | Launch Vehicle | Satellite Platform | Orbit                     |
|------------|------|-------------|----------------|--------------------|---------------------------|
| 2007.04.14 | MEO  | Xichang     | CZ-3A          | DFH-3              | ~21,500 km                |
| 2009.04.15 | GEO  | Xichang     | CZ-3C          | DFH-3              | In-orbit maintenance      |
| 2010.01.17 | GEO  | Xichang     | CZ-3C          | DFH-3              | 144.5° E                  |
| 2010.06.02 | GEO  | Xichang     | CZ-3C          | DFH-3              | 84° E                     |
| 2010.08.01 | IGSO | Xichang     | CZ-3A          | DFH-3              | Intersection node: 118° E |
| 2010.11.01 | GEO  | Xichang     | CZ-3C          | DFH-3              | 160° E                    |
| 2010.12.18 | IGSO | Xichang     | CZ-3A          | DFH-3              | Intersection node: 118° E |
| 2011.04.10 | IGSO | Xichang     | CZ-3A          | DFH-3              | Intersection node: 118° E |
| 2011.07.27 | IGSO | Xichang     | CZ-3A          | DFH-3              | Intersection node: 95° E  |

**Table 2**

Newly Launched satellites After Nov 2011

| Date       | Type | Launch Site | Launch Vehicle | Satellite Platform | Orbit                    |
|------------|------|-------------|----------------|--------------------|--------------------------|
| 2011.12.02 | IGSO | Xichang     | CZ-3A          | DFH-3              | Intersection node: 95° E |
| 2012.02.25 | GSO  | Xichang     | CZ-3C          | DFH-3              | 58.75 E                  |
| 2012.04.30 | MEO  | Xichang     | CZ-3A          | DFH-3              | MEO                      |
| 2012.04.30 | MEO  | Xichang     | CZ-3A          | DFH-3              | MEO                      |

### 3 SYSTEM APPLICATIONS

Since the BeiDou navigation satellite demonstration system began to provide services in 2003, considerable progress has been made in the field of theoretical research, technology R & D, receiver production, application and service development. BeiDou system has been widely used in many fields, such as transportation, marine fishery, water conservancy, weather forecast, forest fire prevention, telecommunication and timing, electric power control and disaster mitigation, etc. It has brought remarkable economic and social benefits, especially has played an important role in the South China frozen disaster, Wenchuan and Yushu earthquakes, the Beijing Olympic Games and Shanghai World Expo.

- In the field of Chips and Terminals R&D, Bayou/GPS dual-mode chip has been developed, and been applied in vehicle terminals.
- In the field of Civil Aviation, BeiDou system is in the phase of airborne test, which focuses on reliability and safety. This will promote the BeiDou system into the framework of the ICAO standards.
- In the field of Transportation, the BeiDou navigation satellite system has been widely used in many different areas such as transportation monitoring & management demonstration system, including:
  - Collecting traffic information
  - Preventing fatigue driving
  - Monitoring dangerous goods
  - Ensuring safety
  - Improving service efficiency
- In the field of Surveying & Mapping, we have developed high-precision receiver to improve precision, and carried out tests on B1/B2 dual-frequency RTK.

- In the field of Meteorology, a series of BeiDou terminal equipments have been developed for weather forecast, “demonstration application of monitoring & warning in atmosphere, ocean , and space” has started, this system include:
  - High altitude detecting balloon
  - Ionosphere and water vapour monitoring
  - Sea wind and waves
  - Meteorological disaster early warning and information dissemination
  - Occultation satellite

#### 4 INTERNATIONAL COOPERATION

Upon the basis of the principles of equality, mutual benefit, peaceful utilization of outer space and common development, China has been committed to international exchange and cooperation in the field of satellite navigation; various forms of activities have been carried out with extensive outcome. The BeiDou Navigation Satellite System adheres to the policy of opening up to the outside world, and has already carried out extensive exchanges and consultation with countries that possess navigation satellite systems, to promote compatibility and interoperability between GNSS. Meanwhile, we extensively exchange and cooperate with countries that do not have navigation satellite system, to share the benefits of navigation satellites with them.

As an important member of International Committee on Global Navigation Satellite System (ICG), China has participated in all each ICG General Assembly Meeting and ICG Providers Forum. In 2007, China became one of the four core providers designated by organization. In the sixth meeting of ICG, China has launched initiatives of International GNSS Monitoring & Assessment Service for Open Service (iGMAS) and BeiDou Application Demonstration & Experience Campaign (BADEC), dominated the establishment of iGMAS sub-working group and application sub-working group, and served as Co-Chair. The main tasks of BADEC include:

- Introduce the development, progress and application of BeiDou System, firstly in the Asia – Pacific region
- Help people to know more about M-GNSS’s knowledge, applications and benefits by the application demonstration
- Let international users experience the BeiDou/GNSS
- Promote new multi-GNSS applications

The main tasks of iGMAS include:

- Setup a global monitoring and assessment network through international cooperation
- A information service platform of data collection, storage, analyze, management, issuance
- Monitor Multi-GNSS open signal and service performance
- Serve GNSS world with data, products, information
- Be able to promote service assurance and improve service performance
- Beneficial to technology experiment, science research and applications, and compatibility & interoperability

As an essential element of GNSS, BeiDou system will further enhance compatibility and interoperability with other GNSS through international cooperation, promote monitoring and evaluations of GNSS open services, as well as accelerate the demonstration application of BeiDou/GNSS. The seventh meeting of ICG will be organized by Chinese government in Beijing from November 4<sup>th</sup> to 9<sup>th</sup>, 2012. Currently, China is comprehensively preparing for the meeting and arranging all routine activities.

## **5 GNSS EDUCATION AND TRAINING**

In 1968, the first United Nations conference on Exploration and Peaceful Use of Outer Space (UNISPACE) took place in Vienna, Austria. United Nations Office for Outer Space Affairs (UNOOSA), in accordance with the conference decisions, proposed the Programme on Space Applications in 1971. According to the suggestions of UNOOSA, Chinese government has shown active avocations of Asia-Pacific Multilateral Cooperation in Space Technology and Applications (AP-MCSTA) and substantial steps have been taken since 1992. The latest progress in education program and training activities on GNSS in China, include the MASTA program, GNSS curriculum development, GNSS summer school and the international center for GNSS Science, Technology and Education, will be discussed below.

### **A. MASTA Program**

In order to translate the recommendation of the United Nations Program on Space Applications (UN-PSA) into an operational program, Beihang University has initiated the Master program on Space Technology Applications (MASTA)

especially for Asia-Pacific applicants in 2006 and they have held fourth successfully up to now.

MASTA (Master Program on Space Technology Applications) is an elaborately designed and intensive Master program for students who are interested in exploring the mysterious universe. It focuses on both knowledge acquisition and operational training, and is an application-oriented program. It provides a powerful platform for scholars and professionals to obtain more opportunities for communicating and experiencing the space technology practice in China.

MASTA is designed to give participants a competitive edge by:

- Broadening their knowledge on space-related issues and activities and encouraging participants to use acquired knowledge and skills through practical, hands-on experience
- Developing the skills necessary for working effectively with colleagues from a diverse range of disciplines and cultures
- Placing the participants at the frontier of the industry through contact with space professionals
- Compiled with international conventions
- Modularized curricula design
- Flexible study modes

In October, 2004, Master degree program in Space Technology and Applications (MASTA) at Beihang University was authorized by the Minister of Education, China. The faculty for MASTA consists of leading professors, chief experts and senior engineers from Beihang University as well as from other famous institutes and Academies. The facilities include Ground Receiving Station, RS & GIS Teaching and Practice Lab, and GNSS Teaching and Practice Lab, etc.

Up to now, 40 participants from 8 countries have been graduated and 36 participants are studying at Beihang University.

## **B. GNSS Curriculum**

The education curriculum of MASTA adopts module pattern. Courses are organized into three modules:

Module I is 7 weeks and designed as Platform Course. The purpose of this module is to strengthen the participants' fundamental knowledge, help them to study the followed specialty courses smoothly, and know about the new trends of technologies and applications in Space. This Module is compulsory for all the academic areas of MASTA.

Module II is designed as Specialty Curriculum of 6 months, while Module III is a pilot project of 16 weeks' Beihang University will undertake Master Degree Program on GNSS 2012 in this September. The core courses of 9 months GNSS curriculum is below:

**Table 3**

Module II-1 Major Basic Courses (8 weeks)

| Code  | Title  | Class Hr's | Credits | Remark     |
|-------|--|------------|---------|------------|
| MC1-1 | GNSS Reference System                                      | 18         | 1       | Compulsory |
| MC1-2 | Principle of Global Navigation Satellite Systems           | 32         | 2       | Compulsory |
| MC1-3 | Navigation Signal Simulation and Test Technologies         | 32         | 2       | Compulsory |
| MC1-4 | GNSS Receiver Principles and Design                        | 32         | 2       | Compulsory |
| MC1-5 | GNSS/INS Integration Navigation Principle and Technologies | 32         | 2       | Compulsory |

**Table 4**

Module II-2 Major Core Courses and Major Electives (6 weeks)

| Code   | Title                                  | Class Hr's | Credits | Remark     |
|--------|--|------------|---------|------------|
| MC1-6  | Satellite Navigation Applications      | 32         | 2       | Compulsory |
| MC1-7  | Satellite Navigation Data Processing   | 32         | 2       | Compulsory |
| MC1-8  | GNSS Experiment                        | 18         | 1       | Compulsory |
| MC1-9  | GNSS New Technologies and Applications | 12         | 1       | Compulsory |
| MC1-10 | GNSS Applications in Timing            | 6          | 1       |            |
| MC1-11 | GNSS New Technologies and Applications | 12         | 1       |            |

### C. GNSS Summer School on GNSS Frontier Technology

The GNSS Summer School on GNSS Frontier Technology is part of International Committee on GNSS (ICG) educational program, aiming to promote training of early career researchers and professionals involving research and development and application of Global Navigation Satellite System and BeiDou technologies. It is recognized that there is a significant shortage of well-educated and highly-skilled professionals in GNSS and related fields in the Asia-Pacific region.

The first GNSS Summer School on GNSS Frontier Technology will be held on 25-31 August, 2012, Beihang University, China. The objective of the one-week intensive program is to provide a comprehensive overview on selected areas of GNSS theory, hardware, software and applications. The program is open to postgraduates, PhD students, and early career professionals who wish to broaden their GNSS knowledge and discuss with renowned experts in their research directions and their research problems.

Internationally renowned experts are invited to give lectures on several selected topics, covering receiver design, ground-based and space-based augmentation, user precise positioning and integrity algorithms, and processing of multiple GNSS and multi-frequency data. In addition to the overview of state-art advances, each lecture will also introduce their contribution to the field and provide perspectives on research challenges, trend and tangible research topics.

#### **D. International Centre for GNSS Science, Technology and Education**

The increasingly important role of GNSS science, technology and education called for the establishment of an international centre for GNSS science, technology and education. The United Nations International Meeting on the Applications of Global Navigation Satellite Systems, held in Vienna from 12 to 16 December 2011 concluded to establish such kind centre. That conclusion was underscored by the 10 years of achievement of the United Nations on GNSS.

This Centre should grow into a network of national and regional centers, focusing on space weather, around the world – all dedicated to advancement of GNSS research and education.

The Centre would provide capacity building and technical guidance to nations that wish to engage in space weather science and education. Capacity building consists of three main components:

1. Laboratories on GNSS.
2. Distant learning/video conference system/environment.
3. Education/training on GNSS technology and application.

Research and education is the domain of advanced research institutions and universities. The Centre, recommended in this “Vienna GNSS Resolution” must be part of such an advanced research institution or university. Moreover, a proven record of capacity building is an essential prerequisite for this Centre.

The Centre is an institution with a proven record in organizing international activities. These activities include GNSS schools, GNSS workshops, GNSS Seminars, and observation campaigns, installation of instruments in different regions of the world, training of instrument host staff and students, and

international outreach programmes. The Centre must possess experience in promoting and supporting international programmes such as ISWI.

The Centre would cooperate with the UN-affiliated Regional Centres for Space Science and Technology Education, located in India, Mexico/Brazil, Morocco, and Nigeria (<http://www.unoosa.org/oosa/en/SAP/centres/index.html>), and other centres of excellence in space science and technology education.

## 6 CONCLUSIONS

The construction of BeiDou Navigation Satellite System goes smoothly, and the initial operational service has been provided from December, 2011. Up to now, 13 satellites have been launched, and with the launch of new satellite performance will be enhanced.

China will promote the construction and application of BeiDou as planned, continue making contributions to GNSS Science, Technology and education.

## REFERENCES

- [1] GNSS Master Degree Curriculum, International School, Beihang University, 2012.
- [2] Introduction to the summer school on GNSS Technology Frontier, Beihang University, 2012.
- [3] Investigation Report to the Regional Centres for Space Science and Technology Education, International School, Beihang University, 2011.
- [4] Report on the Development of BeiDou Navigation Satellite System (V2.0), China Satellite Navigation Office, 2012.
- [5] Report on the United Nations International Meeting on the Applications of Global Navigation Satellite Systems, Committee on the Peaceful Uses of Outer Space, Fifty-fifth session, Vienna, 6-15 June 2012.



# MODELLING OF THE DYNAMIC CHANGES OF COORDINATES GPS-STATION TO PREDICT THE IONOSPHERIC EFFECTS

**Liubov Yankiv-Vitkovska<sup>1</sup>,  
Oksana Grynshyna-Poliuga<sup>2</sup>**

<sup>1</sup> National University “Lviv Polytechnic”, Lviv, Ukraine

<sup>2</sup> Space Research Centre PAS, Warsaw, Poland  
18A Bartycka Street, 00-716 Warsaw, Poland  
E-mails: luba\_y@ukr.net, ogp@cbk.waw.pl

**ABSTRACT.** *Temporal variations of coordinates permanent station display complex and unknown processes related to Earth physics, tectonic motion, and ionospheric effect etc. Thus, it is a very important to use information obtained during the monitoring of coordinates GPS station to experimental verification of quantitative theory related to the many phenomena that deal with satellite method of the ground coordinates determination. We suggest to use macro-modelling approach to monitoring the temporal change of coordinates, in particular, for example, the changes of coordinates GPS-permanent station JOSE (Poland). Macromodelling method introduces the increases of the results efficiency. It also helps to predict target values, and make it possible to compare the results of calculations with experimental results. This method is aimed to identify the physical influence (ionosphere effects) on the observing position of GPS-station.*

*The correlation between the values of geodetic coordinates obtained using GPS-observations and data that describe the local state of the Earth's surface and near-Earth space was researched. We calculate autocorrelation and cross-correlation integrals of integrals of functions for a given period of time to identify the possible connection between the oscillating components of the geodetic coordinates and parameters that describe geo-seismic and solar activity.*

*The value of geodetic coordinates obtained from GPS-observations depends on external influences, which are deterministic frequency, but to test this requires more research, particularly through the methods described in literature. Coordinates are dependent on each other and depend on the influence of solar activity. The reason for this relationship may be changing the state of the ionosphere, in some cases – gravitational effects of matter in the solar wind space technology that is used to determine the geodetic coordinates. To clarify this assumption is suitable methods of dynamic macro-modeling.*

*To confirm our assumptions should explore the relationship between small changes in geodetic coordinates and solar activity for a network of many GPS-stations in the period of high geo-seismic and solar activity.*

**KEY WORDS:** *macromodelling method, geodetic coordinates, seismic activity*

## 1 INTRODUCTION

The definition of coordinates and velocity of GNSS-stations from satellite observations is currently one of the methods of establishing coordinate of national references system and the main method of practical recreation. Holds the task of creating such reference systems that are not inferior in accuracy of the international system ITRF, that a few millimeters in view of determining their error velocities. Such precise characteristics can be achieved by improving the equipment and methods of observations, as well as algorithms and software for data processing. The new trend in the development of software for processing the results of GNSS-observations – consideration of more delicate reductions that can simulate the movement of stations to within 1 mm and above. Unfortunately, while still processing the data cannot always take into account the effects of natural environment (solar activity, seismic processes, atmospheric phenomena, etc.) that can cause change of coordinates stations a few centimeters.

For the detailed study of influence of chaotic dynamic processes on the systematic errors of the satellite measuring it is possible to use the different methods of mathematical design, including “macromodeling” method of the dynamic systems, in which for the prognosis model estimation of exactness of coordinate determinations apply “macromodeling” renewal of the system of ordinary differential equalizations which describe dependence of measuring error on time [1].

Conceptual supposition is – that tectonic motion is represented in measuring of geodesic coordinates, by a direct component, and systematic error – by some casual vibrations. In this approach it is ignored seismic vibrations which arise up, for example, during earthquakes. Consideration of these issues devoted to this article.

The introduction of the technique used macromodeling in GPS – measurement increases efficiency of intermediate processing results of observations gives a means of forecasting their values, and – to perform computational experiments with the results of measurements designed for the detection certain physical effects (ionospheric effects) on the observed position of permanent GPS station. For a detailed study of the influence of chaotic dynamical processes of the systematic errors of satellite measurements may be used various methods of mathematical modelling, including the method macromodeling dynamic systems in which the predictive model to assess the accuracy of coordinate definitions used macromodel recovery system of ordinary differential equations describing the dependence of measurement error from time to time.

The conceptual assumption that tectonic movement is reflected in the data space geodetic coordinates measuring aperiodic component and the systematic error – some random fluctuations. That is mean, this approach ignored seismic vibrations that appear, such as during Earthquakes.

For disclosure regularities of aperiodic and tectonic vibrational motion is taken coordinate SULP-station measured during 1137 – 1495 weeks of GPS-measurements [2]. Experimentally measured coordinates, which corresponds to the designation in geodesy coordinates for  $i$ -th station (SULP):

$$x_i^E(t_k), y_i^E(t_k), z_i^E(t_k); k = \overline{1, m_i}; i = \overline{1, n} \quad (1)$$

where,  $n$  – number of stations;  $m_i$  – number of discrete measurements of coordinates for the  $i$ -station;  $t_k$  – time measurement.

Knowing the constant component of geodetic coordinates of points

$$\begin{aligned} x_i^C &= \acute{e} \acute{a} x_i^E(t_k), k \in \check{S}, m_i \acute{C} \\ y_i^C &= \acute{e} \acute{a} y_i^E(t_k), k \in \check{S}, m_i \acute{C} \\ z_i^C &= \acute{e} \acute{a} z_i^E(t_k), k \in \check{S}, m_i \acute{C} \\ i &= \overline{1, n}, \end{aligned} \quad (2)$$

To have found their variable components:

$$\begin{aligned} x_i(t_k) &= x_i^E(t_k) - x_i^C; k = \overline{1, m_i}; \\ y_i(t_k) &= y_i^E(t_k) - y_i^C; k = \overline{1, m_i}; \\ z_i(t_k) &= z_i^E(t_k) - z_i^C; k = \overline{1, m_i}; \\ i &= \overline{1, n}. \end{aligned} \quad (3)$$

A priori known that the radio-electronic space geodetic equipment are often the weak external influences (e.g. – local moving vortices in the ionosphere during the passage through the radio waves), and rarely are strong external influences (such as ionization disturbances caused by the solar activity). Antialiasing values (3) drive to the branch `small movements represented in these values, and leave them significant (longer and more intense) movements. So in some parameters of antialiasing values (3) of them received “substantial oscillating and aperiodic components.” A priori nature of these components is unknown. That is, it is unknown whether they are caused by seismic movement, great or disturbing influences on the measuring equipment.

Proceeding from this assumption, based on the variable component (3) the experimentally determined coordinates of the station identified smoothed values of their coordinates.

$$\check{y}_i(t_k), \check{y}_p(t_k), \check{y}_o(t_k); k = \overline{1, m}; i = \overline{1, n} \quad (4)$$

For calculation of the smoothed values used methods of spline approximation. The values (4) were obtained at different parameters of antialiasing – beginning from weak and strong finishing antialiasing (which provides conditional tectonic drift). Additional for indirect evidence for the assumption of the existence of tectonic oscillations detected according to (4), performed a computational experiment based on macromodeling techniques.

## 2 OVERVIEW OF PREVIOUS RESEARCH AND PUBLICATIONS

The improvement of equipment for determining the spatial coordinates, the development of physical facilities for monitoring the earth's surface and near-space allowed accumulating a variety of experimental data. Therefore, faced the task to develop a standardized method for predictive modeling of changes of coordinates. To solve this problem it used macro-modeling method. In work [1] it is proved that the experimentally measured discrete functional relationship the (vector) input  $u(t)$  and output  $y(t)$

$$u(t_k), y(t_k) \quad (k = \overline{1, m}) \quad (5)$$

modeling system of ordinary differential equations

$$\begin{aligned} \frac{dy_i}{dt} &= y_{i+1}; \quad (i = \overline{0, n-1}) \\ \frac{dy_n}{dt} &= P(y_0, \dots, y_n; u^{(0)}, \dots, u^{(p)}), \end{aligned} \quad (6)$$

where,  $t_k$  – times of measurement,  $m$  – number of measurements,  $P$  – polynomial of many arguments,  $n$  – number of equations,  $p$  – highest order derivative of  $u(t)$ .

The variable  $y_0$  approximately equal output  $y_0(t) \approx y(t)$ , if the initial conditions  $y_i^0$  ( $i = \overline{0, n}$ ) system (2) select derivatives  $y_i^0 = y^{(i)}(t_0)$  ( $i = \overline{0, n}$ ) of  $y(t_k)$  ( $k = \overline{1, m}$ ) on  $t_0 \in \check{S}_1, t_m \check{C}$ , and arguments  $u^{(i)}$  ( $i = \overline{0, p}$ ) to derivatives of  $u(t_k)$  ( $k = \overline{1, m}$ ) on  $t \in \check{S}_1, t_m \check{C}$ .

The power-law polynomial

$$P(\mu_0, \dots, \mu_n; \eta_0, \dots, \eta_p) = \sum_I c_I (\mu_0)^{i_0} \cdot \dots \cdot (\mu_n)^{i_n} \cdot (\eta_0)^{j_0} \cdot \dots \cdot (\eta_p)^{j_p} \quad (7)$$

has coefficients  $c_I$  of multi indexes  $I = (i_0 \dots i_n j_0 \dots j_p)$  which meet the requirements  $i_0 + \dots + i_n + j_0 + \dots + j_p < r$ , where  $r$  – is a positive integer.

The algorithm for the identification model (6) described in to (5). The model used for modeling of radio devices, systems and processes of different nature, making it possible to improve the algorithms and their application to characterize other processes.

### 3 FORMULATION OF THE PROBLEM AND THE MAIN PROBLEMS

We know that the coordinates of GNSS-stations containing quick-specific component that is associated with an error of measurement. For improve the coordinates, it is important to understand how their changes affect the physical processes occurring in near space. In this regard, was tasked to build a macro-model impact of solar activity and geo seismic processes in the small change of coordinates that are regularly determined by GNSS-stations.

For the solution of this problem we decided to investigate the changes of coordinates of Polish GNSS-station JOZE for 1999, which took place during the typical changes in solar activity and the rare event of a major change in local geometry of seismic activity and infrasound earth's surface (i.e. earthquake of this year) [2] .

For our researches have been selected years set of coordinates of permanent GNSS-station JOZE:

$$\bar{x}(t_k), \bar{y}(t_k), \bar{z}(t_k) \quad (k = \overline{1, \bar{m}}) \quad (8)$$

where,  $m$  – number of values,  $t_k$  – times of measurement that meet the daily value. Select a station has been connected with the fact that it at this time worked for 4 years, and its coordinates, and especially the speed of the changes were sufficiently reliably determined.

For describe the impact of geo seismic processes have been taken value of the indicator geo seismic activity  $g(t)$  and infrasound Earth's surface  $v(t)$ :

$$\bar{g}(t_k), \bar{v}(t_k) \quad (k = \overline{1, \bar{m}}) \quad (9)$$

measured at the same moments of time.

The influence of solar activity described by the daily number of flares on the Sun:

$$\bar{s}(t_k) \quad (k = \overline{1, \bar{m}}) \quad (10)$$

On the basis of daily values (8)-(10) by spline approximation to calculate the smoothed hourly values:

$$x(t_k), y(t_k), z(t_k), s(t_k), g(t_k), v(t_k) \quad (k = \overline{1, m}),$$

where,  $m$  – number of hourly values.

For the modeling of processes in near-Earth space on accuracy of coordinates developed macro-model with this structure:

$$\begin{aligned} x'_i &= x_{i+1}; \quad (i = \overline{0, 2}); \\ x'_3 &= P_x(x_0, x_1, x_2, x_3, y_2, y_3, z_2, z_3, s, s', g, g', v, v'); \\ y'_i &= y_{i+1}; \quad (i = \overline{0, 2}); \\ y'_3 &= P_y(x_2, x_3, y_0, y_1, y_2, y_3, z_2, z_3, s, s', g, g', v, v'); \\ z'_i &= z_{i+1}; \quad (i = \overline{0, 2}); \\ z'_3 &= P_z(x_2, x_3, y_2, y_3, z_0, z_1, z_2, z_3, s, s', g, g', v, v'), \end{aligned} \quad (11)$$

where,  $P_x, P_y, P_z$  – polynomials on a number of reasons, chosen to reflect the impact of external factors on the coordinates. The parameters of the polynomials found with the identification of the expression:

$$\dot{\hat{c}}_{i\xi} \left( \sum_{k=1}^m [\xi^{(4)}(t_k) - S_\xi(t_k)]^2 + \alpha_\xi \sum_{l_\xi} c_{l_\xi}^2 \right) \quad (\xi = x, y, z) \quad (12)$$

where,  $\alpha_x, \alpha_y, \alpha_z$  – regularization parameters. The symbols  $S_x(t), S_y(t), S_z(t)$  are indicated:

$$S_x(t) = P_x(x_0(t), x_1(t), x_2(t), x_3(t), y_2(t), y_3(t), z_2(t), z_3(t), s(t), s'(t), g(t), g'(t), v(t), v'(t));$$

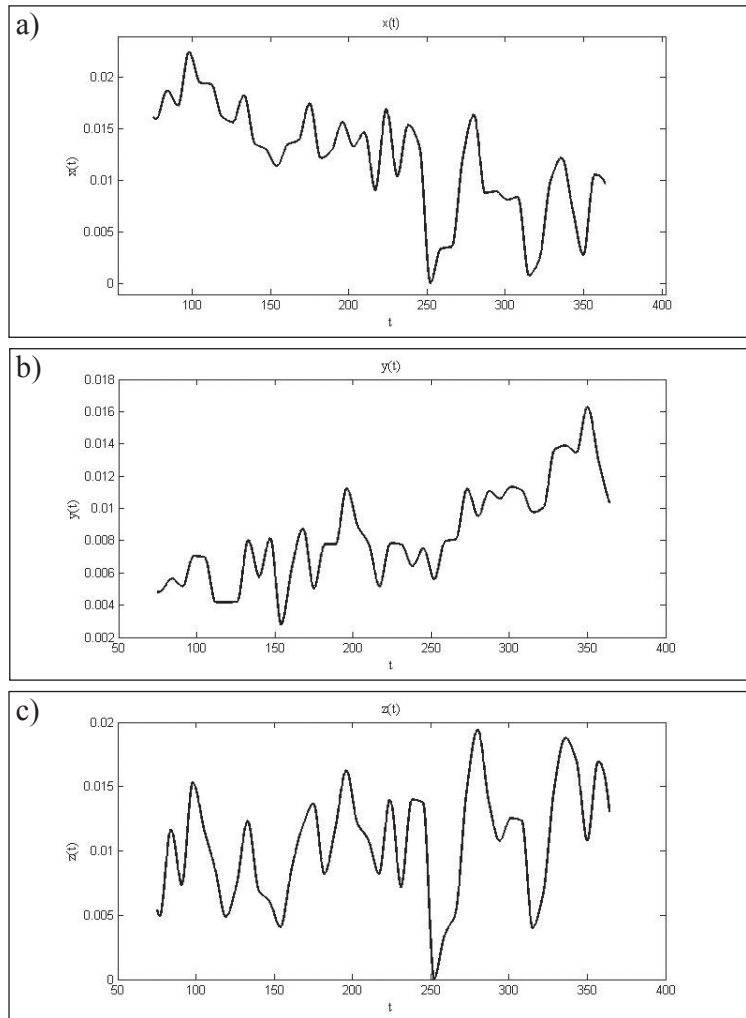
$$S_y(t) = P_y(x_2(t), x_3(t), y_0(t), y_1(t), y_2(t), y_3(t), z_2(t), z_3(t), s(t), s'(t), g(t), g'(t), v(t), v'(t));$$

$$S_z(t) = P_z(x_2(t), x_3(t), y_2(t), y_3(t), z_0(t), z_1(t), z_2(t), z_3(t), s(t), s'(t), g(t), g'(t), v(t), v'(t)).$$

To identify the possible connection between the values calculated autocorrelation integrals and mutual correlation integrals of functions respectively the first and last (365-th) day in 1999.

**Figure 1**

The charts of variable components of coordinates  $x(t)$  (a),  $y(t)$  (b),  $z(t)$  (c) station JOZE, 1999.



The charts of the autocorrelation integrals researched functions have central peaks. These integrals are functions symmetrical about the line of the central maximum. The width of central peak functions researched reflects the approximate length of time interval, train appropriate physical process occurs as determined. Figures 2-3 characteristic time for the reflected process is deterministic, indicated  $\tau$ .

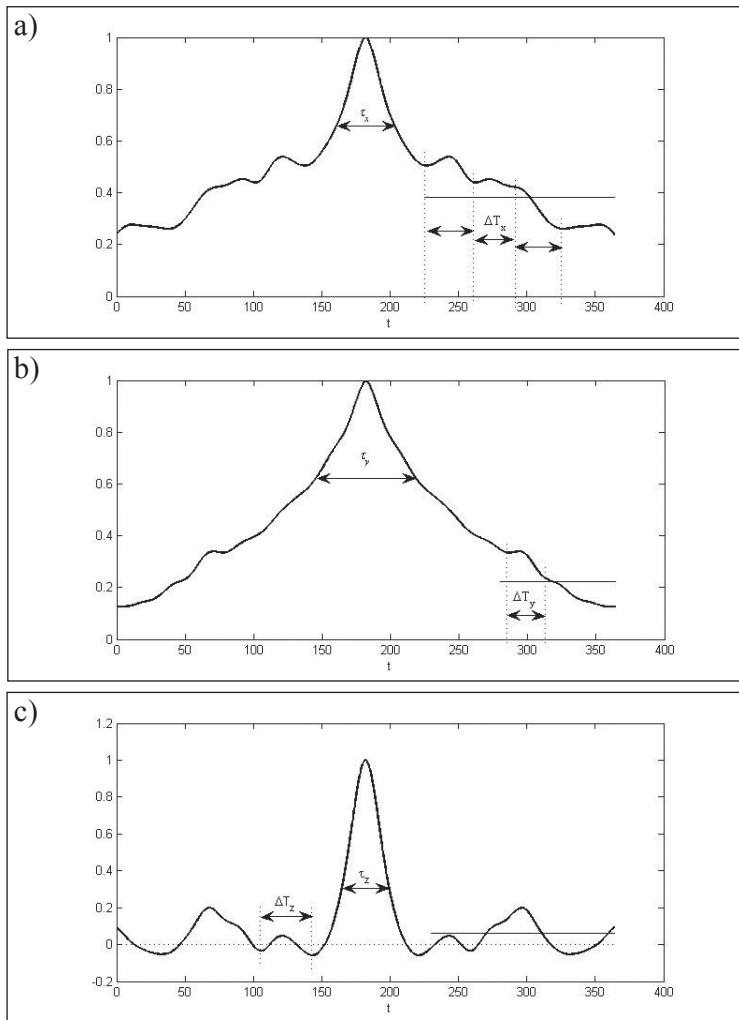


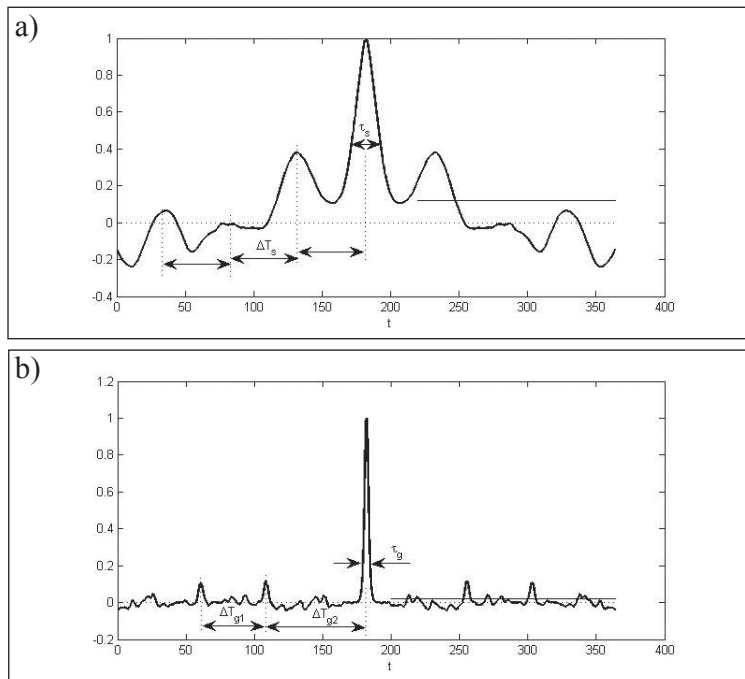
**Figure 2**  
The charts of the autocorrelation integrals of variable components of the coordinates  $x(t)$  (a),  $y(t)$  (b),  $z(t)$  (c) station JOZE 1999.

The integrals of autocorrelation functions  $x(t)$ ,  $z(t)$ ,  $s(t)$ , with a maximum of about average width. The width of the maxima for the coordinates  $x(t)$ ,  $z(t)$ , and solar activity  $s(t)$  levels respectively  $\tau_x = 38$ ,  $\tau_z = 36$ ,  $\tau_s = 38$  (hereinafter – the time in Earth days). During these periods the processes of change  $x(t)$ ,  $z(t)$ ,  $s(t)$ ,

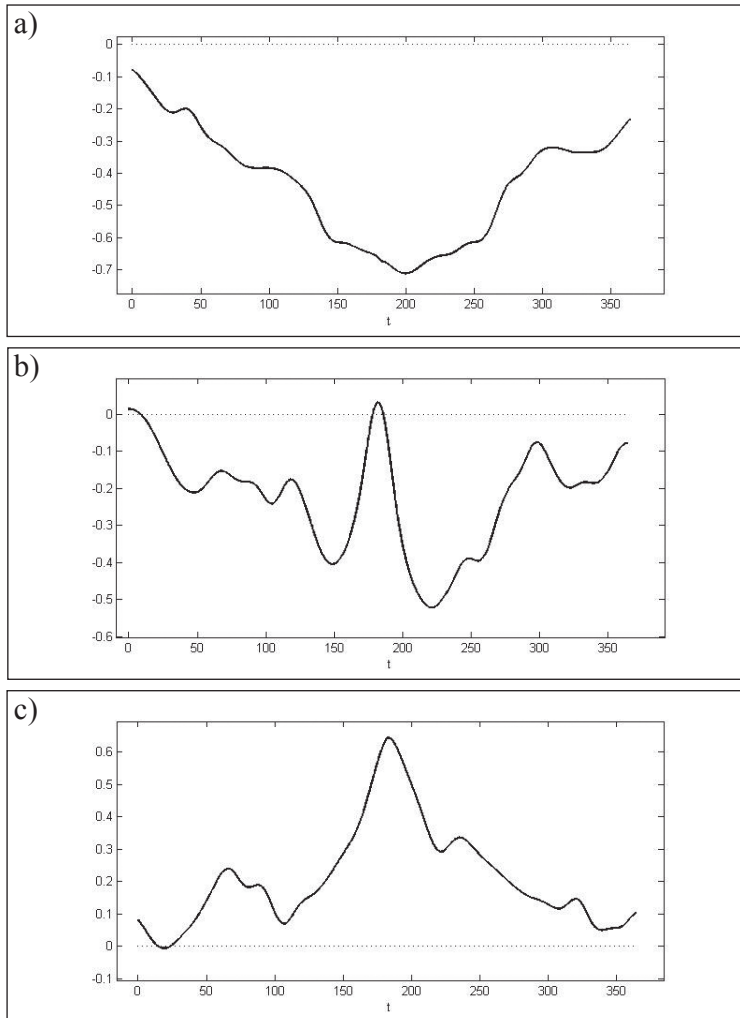
had evidence of “a strong dependence on previous values” This allows to select the named characteristic time as a parameter that describes the processes of change  $x(t)$ ,  $z(t)$ ,  $s(t)$ .

The graph of the autocorrelation integral function (see Fig. 3, b) does not have a characteristic maximum. This means that during the whole period of observation coordinates change occurred “with little influence of random processes.” The graphs of the autocorrelation functions (see Fig. 2-3) shows local “side” highs. The distance between these maxima shows that over periods of time value of strongly depends on past values. Figures 2 and 3 of these time periods indicated.

**Figure 3**  
The charts  
autocorrelation  
integrals of solar  
activity  
(a) seismic activity  
(b) for 1999 station  
JOSE.



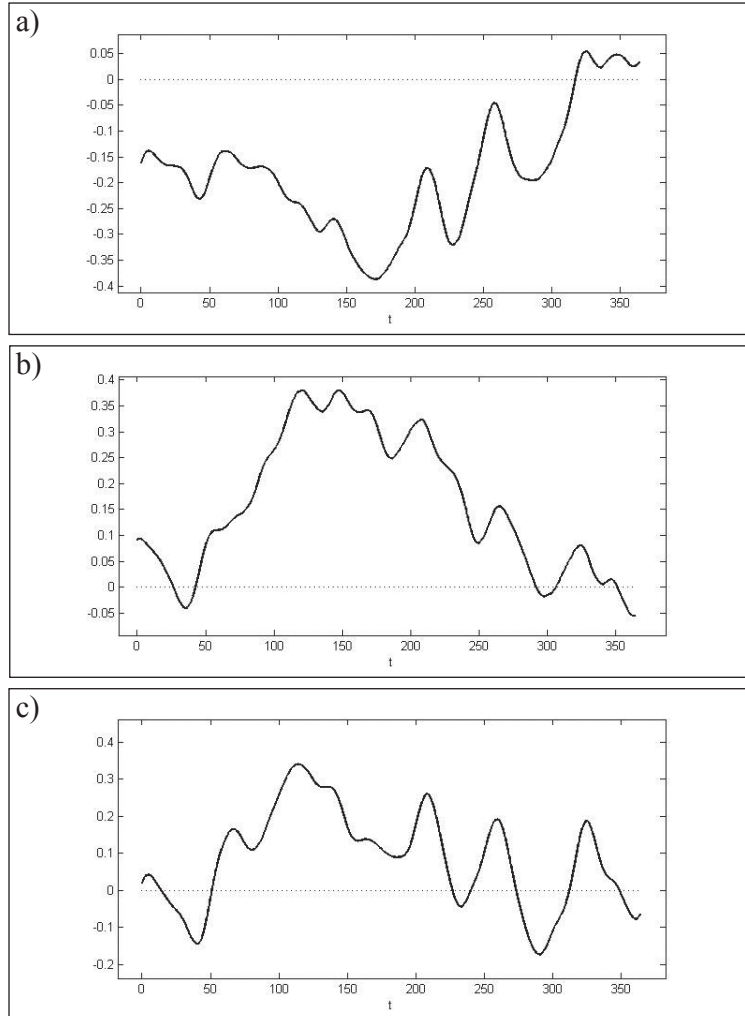
Charts mutual correlation integrals calculated for pairs of coordinates is presented in Figure 4. The value of the correlation integrals has some highs and some points in time up 0.7. This means that at different times with different values of the level of statistical dependence. Such dependence is typical for dynamic values, which reflect the same dynamic process.

**Figure 4**

The charts of the correlation integrals deductions between variable components of the coordinates  $x(t)$ ,  $y(t)$  (a),  $x(t)$ ,  $z(t)$  (b),  $y(t)$ ,  $z(t)$  (c) station JOZE, 1999.

The charts mutual correlation integrals between solar activity and geodetic coordinates (Fig. 5) qualitatively similar to the graphs of the correlation integrals between the coordinates (see Fig. 4). It follows the assumption that the coordinates are dependent on each other and depend on Solar activity. The reason for this dependence may be disturbances in the ionosphere, in some cases – gravitational influence of solar wind material on the equipment that is used to determine the geodetic coordinates. To clarify this assumption is suitable methods of dynamic macromodeling [2].

**Figure 5**  
The charts of the correlation integrals deductions between solar activity  $s(t)$  and variable components of the coordinates  $x(t)$  (a),  $y(t)$  (b),  $z(t)$  (c) station JOZE, 1999



The correlation integral between seismic activity and coordinate is not lying in the range up to 0.1 (Fig. 6). Less than a value (in comparison with the correlation integrals for pairs  $(x,g)$ ,  $(z,g)$ ) may be associated with the manifestation of the rotational motion of the Earth around its axis. The value of the mutual correlation integral order of 0.1 does not exclude a nonlinear relationship between the pairs  $(x,g)$ ,  $(y,g)$ ,  $(z,g)$ .

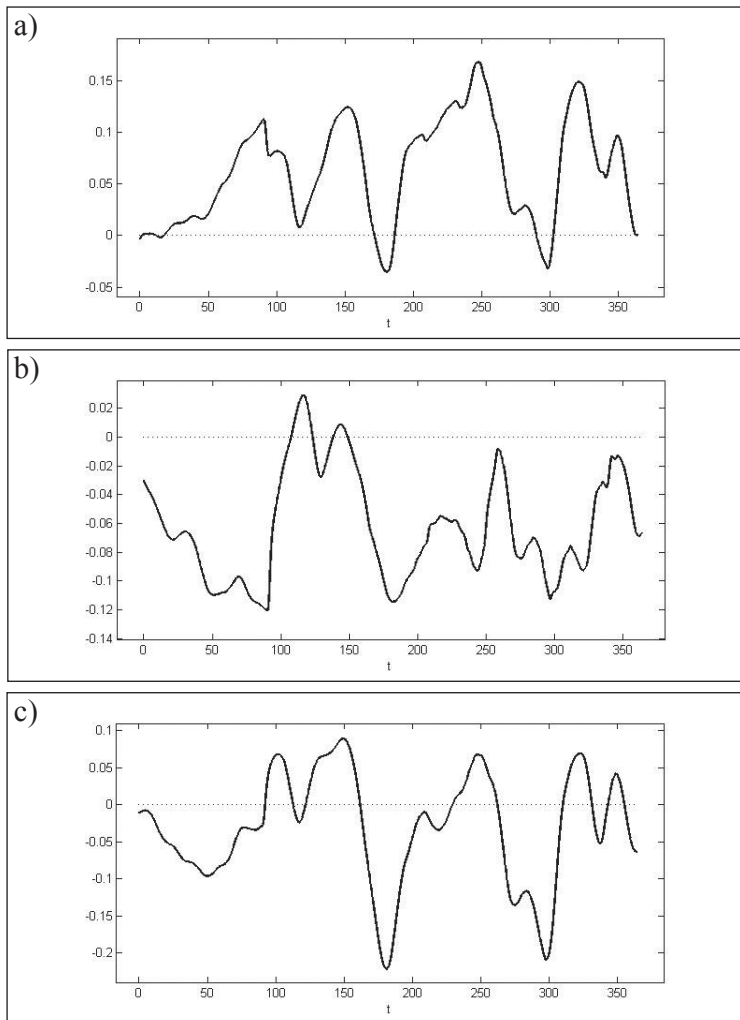


**Figure 6**  
The charts of the correlation integrals deductions between seismic activity  $g(t)$  and variable components of the coordinates  $x(t)$  (a),  $y(t)$  (b),  $z(t)$  (c) station JOZE, 1999

## 4 CONCLUSION

1. The coordinates are dependent on each other and depend on the influence of solar activity. The reason for this relationship may be changing the state of the ionosphere, in some cases – the gravitational effects of matter of solar wind on the space equipment that is used to determine the geodetic coordinates. To clarify this assumption is suitable methods of dynamic macromodeling.
2. The data infrasound monitoring the Earth's surface can be used in modeling the dynamics of geodetic coordinates only for relatively short periods of time.

3. To confirm our assumptions should explore the relationship between small changes geodetic coordinates and solar activity for a network of many GPS-stations in the period of high seismic and solar activity.

## ACKNOWLEDGEMENT

Oksana Grynshyna-Poliuga's research work is undertaken in the scope of the TRANSMIT ITN ([www.transmit-ionosphere.net](http://www.transmit-ionosphere.net)), funded by the Research Executive Agency within the 7th Framework Program of the European Commission, People Program, Initial Training Network, Marie Curie Actions – GA no 264476. Liubov Yankiv-Vitkovska is associate professor of National University "Lviv Polytechnic".

## REFERENCES

- [1] *Матвійчук Я.М.* Математичне макромодельовання динамічних систем: Теорія і практика/Я.М. Матвійчук. - Львів: Вид-во ЛНУ, 2000., с. 214.
- [2] *Янків-Вітковська Л.М.* Дослідження динаміки змін координат перманентних GPS станцій/Л.М Янків-Вітковська, С.Г. Савчук, В.К. Паучок // Вісник геодезії і картографії. – Київ. – №1, 2008, с. 7-12.
- [1] *Matviychuk Ya.M* The mathematical macromodeling dynamic systems: Theory and Practice/Ya.M. Matviychuk. Lviv: Type-in LNU, 2000., p. 214.
- [2] *Yankiv-Vitkovska LM.* The investigation of the changes the coordinates of permanent GPS stations/L. M. Yankiv-Vitkovska, S. G. Savchuk, V. K. Pauchok // Bulletin of Geodesy and Cartography. – Kyiv. – № 1, 2008, p. 7-12.

ISBN 978-953-165-109-7



9 789531 651097

